UNIVERSIDAD DE CANTABRIA

ESCUELA DE DOCTORADO DE LA UNIVERSIDAD DE CANTABRIA
DOCTORADO EN INGENIERÍA QUÍMICA DE LA ENERGÍA Y DE PROCESOS

DESIGN AND OPTIMIZATION OF PROPYLENE PURIFICATION PROCESSES USING HIGH PERFORMANCE PVDF-HFP/BMImBF$_4$/AgBF$_4$ MEMBRANES

Diseño y optimización de procesos de purificación de propileno mediante membranas de alto rendimiento PVDF-HFP/BMImBF$_4$/AgBF$_4$

Memoria de tesis doctoral presentada para optar al título de Doctor por la Universidad de Cantabria

Presentada por:

Raúl Zarca Lago

Dirigida por:

Prof. Dra. Inmaculada Ortiz Uribe

Dr. Alfredo Ortiz Sainz de Aja

Santander, 2018

Programa de Doctorado en Ingeniería Química, de la Energía y de Procesos (BOE núm. 16, de 19 de enero de 2015. RUCT: 5601000)

The research described in this thesis has been conducted at the Advanced Separation Processes (ASP) Research Group of the Department of Chemical and Biomolecular Engineering of the University of Cantabria.

This research has been financially supported by the Spanish Ministry of Economy and Competitiveness and the European Regional Development Fund through the projects: CTQ2012-31639 (MINECO-FEDER, UE), “New separation processes with kinetic control based on the use of functionalized materials”; CTQ2015-66078-R (MINECO-FEDER, UE), “Advanced separation applications. Modeling and experimental validation”; CTQ2016-75158-R (MINECO-FEDER, UE), “Composite selective membranes and their implementation in microfluidic devices”.

Raúl Zarca also would like to express his gratitude to the University of Cantabria for the postgraduate fellowship (B.O.C. 13 mayo 2015) and the financial support to conduct a short research stay at the Department of Chemical and Biomolecular Engineering, National University of Singapore, (September-December 2016) under the supervision of Prof. Chung Tai-Shung.

This PhD thesis document has been performed as a compendium of interrelated scientific publications. The scientific articles that enable this dissertation modality are published in international journals indexed in the Journal Citation Reports (JCR):

- **R. Zarca**, A. Ortiz, D. Gorri, I. Ortiz, A practical approach to fixed-site-carrier facilitated transport modeling for the separation of propylene/propane mixtures through silver-containing polymeric membranes, *Sep. Purif. Technol.* 180 (2017) 82-89.

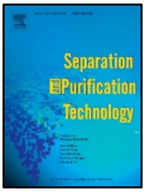
Separation
Purification
Technology

- **R. Zarca**, A. Ortiz, D. Gorri, I. Ortiz, Generalized predictive modeling for facilitated transport membranes accounting for fixed and mobile carriers, *J. Memb. Sci.* 542 (2017) 168–176.

journal of
MEMBRANE
SCIENCE

- **R. Zarca**, A. Ortiz, D. Gorri, L.T. Biegler, I. Ortiz, Optimized distillation coupled with state-of-the-art membranes for propylene purification, *J. Memb. Sci.* 556 (2018) 321–328.

journal of
MEMBRANE
SCIENCE

Table of Contents

Summary / Resumen ***ix***

Chapter 1. Introduction ***1***

1.1. Propylene industrial relevance 2
1.2. Propane/propylene separation. Traditional methods and membrane technology. 6
1.3. Facilitated transport modelling 12
1.4. Facilitated transport membrane processes. Design and optimization. 14
1.5. Background and scope 17
1.6. References 19

Chapter 2. Experimental and modeling methods ***27***

2.1. Experimental Methods 28
2.2. Facilitated transport modeling 38
2.3. Modeling and optimization of hybrid and multistage membrane processes 44
2.4. References. 57

Chapter 3. Results summary ***61***

3.1. Membrane characterization 62
3.2. Gas permeation and mathematical modeling 70
3.3. Process design and optimization 79
3.4. References. 91

Chapter 4. General conclusions and prospective view Conclusiones generales y perspectivas *93*

4.1. Membrane characterization 94
4.2. Recommendations for future research 97
4.3. Conclusiones generales 98
4.4. Recomendaciones para investigación futura 102

Chapter 5. Scientific publications *103*

5.1. JCR Scientific publications 104

Appendices *131*

A.1. List of additional scientific publications 132
A.2. Contributions to scientific meetings 201
A.3. GAMS program used for hybrid process optimization 203
A.4. GAMS program used for multistage process optimization (two-and-one-half-stages) 216

Summary

The separation of propane/propylene gaseous mixtures entails great challenges from the point of view of the economic and environmental sustainability of the manufacture processes of propylene and its derivative products. These challenges arise, on the one hand, from the large energy and capital intensity of the current separation processes, mainly based on cryogenic and high pressure distillations, and caused by the similar physico-chemical properties of both substances. On the other hand, environmental considerations dictate that propylene-containing purge and vent streams from polypropylene reactors and polymer facilities, which were traditionally flared, must be recycled and recovered. For these reasons, the need for process intensification by means of efficient and cost-effective technologies has led to a growing research activity on alternative materials and processes. In this regard, membrane-based gas and vapor separation has consolidated during the last thirty years into an important unit operation of the chemical industry with great potential for process intensification. However, the efficiency of this technology strongly relies on the physico-chemical properties and the transport mechanisms featured by the selected membrane materials.

In view of the above, this thesis aims at the synthesis and development of innovative membrane materials and the assessment of their separation performance when implemented in alternative membrane-based processes. For this purpose, the facilitated transport of propylene by means of π-complexation with silver cations has been studied; with this promising transport mechanism high permeability and selectivity towards the olefin

have been reached. The separation is achieved through the synthesis of novel dense polymeric membranes integrating the use of a high performance fluoropolymer (PVDF-HFP), an imidazolium-based ionic liquid (IL) as a non-volatile additive ($BMImBF_4$) and the silver salt that provides the silver cations upon dissociation inside the membrane ($AgBF_4$).

The complexity of the resultant structure requires a thorough characterization work in order to identify the interactions between the membrane constituents. This characterization has been supported by spectroscopic, thermogravimetric and microscopy techniques and the results confirm the existence of the chemical species and interactions required to yield the fixed-site and mobile carrier transport mechanisms.

Afterwards, the separation performance of the synthesized membranes has been assessed through gas permeation experiments. First, the pure gas diffusivity and solubility of propane and propylene in the PVDF-HFP and PVDF-HFP/$BMImBF_4$ matrices have been calculated through the time-lag technique. Then, the mixed-gas separation performance of the PVDF-HFP/$BMImBF_4$/$AgBF_4$ composite membranes under several operating conditions, namely feed pressure, temperature and membrane composition, has been analyzed using the continuous-flow permeation technique. The experimental data obtained are later used for the development of a semi-predictive mathematical model able to describe the propylene transmembrane flux in the studied range of the operating variables.

Additional permeation experiments reveal the influence of silver degradation during long-term permeation and the effect of feed humidity on the membrane performance. Eventually, real gas mixtures provided by a petrochemical company have been tested to assess the effect of potential trace contaminant on the membrane stability.

In further pursuit of the main objective of this thesis, the industrial applicability of the developed membranes has been explored through design and optimization of membrane-based separation processes. First, the retrofitting of an existing distillation process with a membrane stage has been proposed, quantifying the potential operating costs reduction achieved compared with the distillation base-case. Several membrane materials including the proposed facilitated transport membranes are considered for this optimization, which provides a wider insight into the state-of-the-art of propylene-selective membranes. Lastly, multistage membrane processes implementing the PVDF-HFP/$BMImBF_4$/$AgBF_4$ system have been studied to determine the feasibility of a complete distillation replacement. In this case-study, the previously developed mathematical model accounting for the gas transport mechanisms has been introduced in the optimization, which allows a simultaneous optimization of the membrane process and the membrane material.

Resumen

La separación de mezclas gaseosas propano/propileno entraña grandes retos desde el punto de vista de la sostenibilidad económica y medioambiental de los procesos de fabricación de propileno y sus productos derivados. Estos retos surgen, por un lado, de la elevada intensidad energética y de capital de los actuales procesos de separación, principalmente basados en destilaciones criogénicas o a alta presión, y causada por las similares propiedades fisicoquímicas de ambas sustancias. Y, por el otro lado, las nuevas consideraciones medioambientales dictan que las corrientes de purga y venteo de los reactores de polimerización y fábricas de polímeros que contienen propileno, tradicionalmente quemadas, deben ser recicladas y recuperadas. Por ello, la necesidad de alcanzar la intensificación de procesos por medio de tecnologías eficientes y rentables ha dado lugar a una creciente actividad de investigación sobre materiales y procesos alternativos. En este sentido, la separación de gas y vapor basada en membranas se ha consolidado en los últimos treinta años como una importante operación unitaria de la industria química con un gran potencial para la intensificación de procesos. Sin embargo, la eficiencia de esta tecnología depende enormemente de las propiedades fisicoquímicas y de los mecanismos de transporte presentados por los materiales de membrana seleccionados.

En vista de lo anterior, esta tesis tiene como objetivo la síntesis y el desarrollo de materiales de membrana innovadores y el estudio de su capacidad de separación cuando se implementan en procesos alternativos de separación basados en membranas. Para este propósito, se ha estudiado

el transporte facilitado de propileno por medio de complejación π con cationes de plata; con este prometedor mecanismo de transporte se han obtenido elevados valores de permeabilidad y selectividad hacia la olefina. La separación se consigue mediante la síntesis de novedosas membranas densas poliméricas que integran el uso de un fluoropolímero (PVDF-HFP), un líquido iónico (IL) basado en el imidazol como aditivo no-volátil ($BMImBF_4$) y una sal de plata que provee los cationes plata tras su disociación en el interior de la membrana ($AgBF_4$).

La complejidad de la estructura resultante requiere un exhaustivo trabajo de caracterización para identificar las interacciones entre los componentes de la membrana. Esta caracterización se ha soportado en técnicas espectroscópicas, termogravimétricas y de microscopía y los resultados confirman la existencia de las especies químicas y las interacciones necesarias para dar lugar a los mecanismos de transporte por carrier fijo y móvil.

Posteriormente, la capacidad de separación de las membranas sintetizadas se ha analizado mediante experimentos de permeación. Primero, la difusividad y solubilidad de propano y propileno en las matrices de PVDF-HFP y PVDF-HFP/$BMImBF_4$ se ha calculado mediante la técnica de time-lag con gases puros. Luego, la capacidad de separación de mezclas gaseosas de la membrana compuesta PVDF-HFP/$BMImBF_4$/$AgBF_4$ bajo diferentes condiciones de operación, principalmente presión de alimentación, temperatura y composición de la membrana, se ha analizado usando la técnica de permeación de flujo en continuo. Los datos experimentales obtenidos son usados posteriormente para el desarrollo de un modelo matemático semipredictivo capaz de describir el flujo transmembranal de propileno en el rango estudiado de las variables de operación.

Experimentos de permeación adicionales revelan la influencia de la degradación de la plata durante la permeación en períodos prolongados y el efecto de la humedad de la corriente de alimentación en el desempeño de la membrana. Finalmente, mezclas reales suministradas por una compañía petroquímica han sido empleadas para analizar el efecto de potenciales contaminantes minoritarios en la estabilidad de la membrana.

Continuando con el objetivo principal de esta tesis, la aplicabilidad industrial de las membranas desarrolladas se ha analizado mediante el diseño y la optimización de procesos de separación basados en estas membranas. Primero, se propone el reacondicionamiento de una columna de destilación existente por medio de una etapa previa de membranas, cuantificando los potenciales ahorros en los costes de operación logrados en comparación con el caso base, esto es, cuando solo se emplea la columna. Para esta optimización se consideran diferentes materiales de membrana, incluyendo las membranas desarrolladas durante esta tesis, lo que da una visión más amplia del estado del arte de las membranas selectivas al propileno. Finalmente, se han estudiado procesos de membrana de múltiples etapas implementando el sistema PVDF-HFP/$BMImBF_4$/$AgBF_4$ para determinar la viabilidad de un sustitución completa de la destilación. En este caso de estudio se ha introducido en la optimización el modelo matemático previamente desarrollado, lo que ha permitido una optimización simultánea del proceso y el material.

Chapter 1

Introduction

Abstract

Propylene (C_3H_6) is the second-largest-volume chemical produced globally, mainly driven by the production of polypropylene resins. The impact of this commodity chemical in the world's economy has been growing in the last decades and the notable importance of its wide list of derivative products guarantees that this trend will continue. This introductory chapter offers a general overview of the propylene industrial relevance, as well as the current production methods and the issues concerning the separation of propylene/propane mixtures. Then, membrane technology for propylene purification is introduced, emphasizing the facilitated transport membrane technology and the use of ionic liquids as novel additives. Moreover, a brief review on mathematical modeling and process design and optimization of membrane processes is presented. Finally, the background and scope of this thesis is summarized.

1.1. Propylene industrial relevance

Propylene is one of the most important building blocks in the petrochemical industry. Its global annual demand is estimated at, roughly, 90 million tonnes, only exceeded by ethylene, the other major light olefin [1]. Nonetheless, propylene shows a greater diversity of derivatives. The major derivative produced from propylene is polypropylene, the second most produced thermoplastic material, with a market share of 26% among all thermoplastics [2]. But other specialized products derived from propylene include the cumene value chain (phenol, acetone, bisphenol A, polycarbonate), epoxies, propylene oxide, phenol-formaldehyde resins, acrylic acid, acrylonitrile, *n*-butyl alcohol, isopropyl alcohol and 2-ethylhexanol. Figure 1.1 depicts the propylene demand contribution of each derivative.

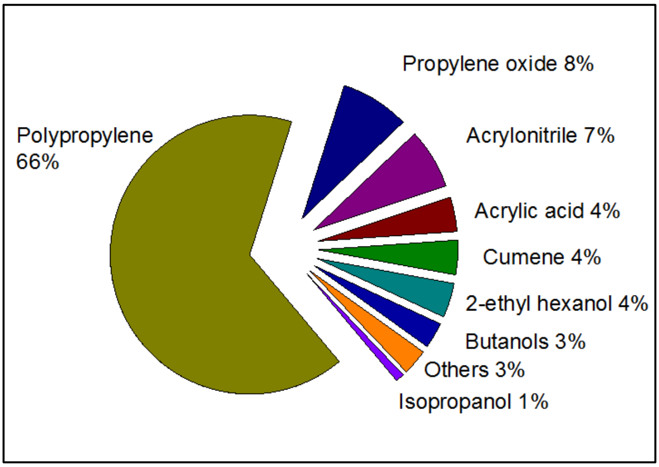

Figure. 1.1. Propylene demand.

Propylene has been traditionally manufactured as a coproduct in the steam cracking (SC) of naphthas and in the refinery fluid catalytic cracking (FCC) of heavier hydrocarbons. However, steam crackers produce a variety of other coproducts in larger quantities than propylene, typically ethylene, hydrogen and methane. Likewise, in the FCC units where heavy gas oil is converted to gasoline and light gas oil, propylene is usually a minor by-product [3]. Despite this, by controlling the feedstocks and the operating conditions in these two processes it is possible to increase the propylene yield to approach propylene-oriented processes. However, in the last few years, the change in the steam cracking feedstocks to favor the ethylene production and a growing demand of propylene for new applications have resulted in a "propylene gap" between production and demand, Figure 1.2.

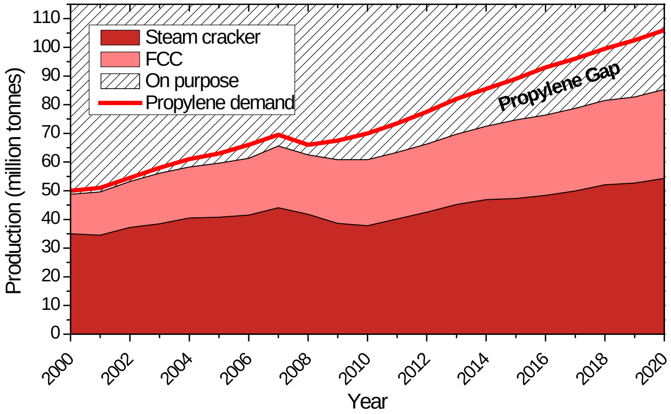

Figure. 1.2. Propylene production and production-demand gap [4]**.**

Recently, a third category of industrial processes, exclusively conceived to produce propylene has emerged to fill the gap and is gradually gaining importance among the production processes. These so called "on-purpose" processes, include propane dehydrogenation, olefin metathesis and methanol-to-olefins process (MTO). Figure 1.3 summarizes the propylene production routes.

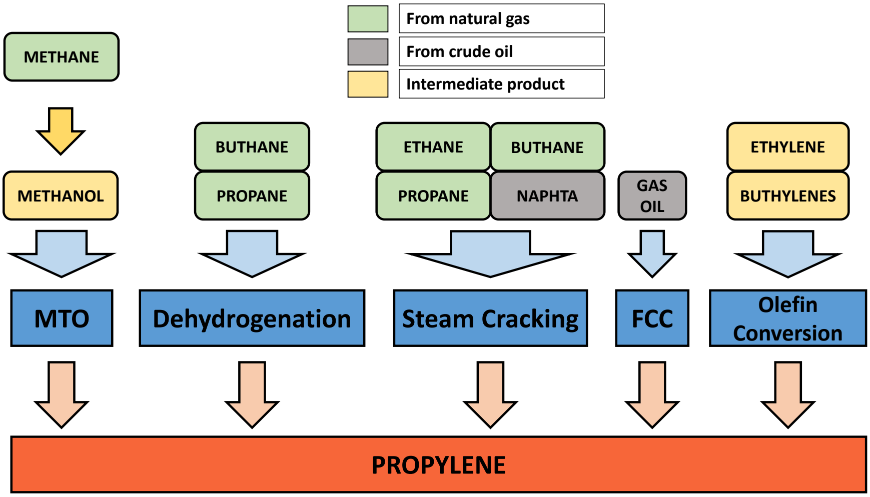
From natural gas
From crude oil
Intermediate product
METHANE
METHANOL
BUTHANE
PROPANE
ETHANE
BUTHANE
PROPANE
NAPHTA
GAS OIL
ETHYLENE
BUTHYLENES
MTO
Dehydrogenation
Steam Cracking
FCC
Olefin Conversion
PROPYLENE

Figure. 1.3. Propylene production routes.

After the cracking processes, sequential distillation columns are used to split each fraction of the resulting gas stream. In this way, after separating the C_1 and C_2 fractions in the so called deethanizer column, a depropanizer is used to split the C_3 fraction from C_{4+} products. Figure 1.4 schematizes the distillation sequence.

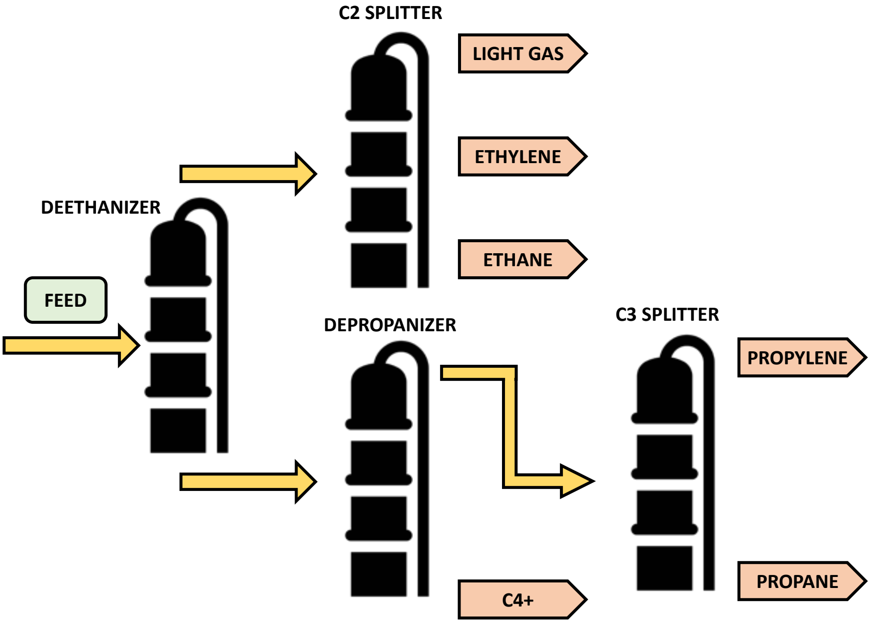
C2 SPLITTER
LIGHT GAS
ETHYLENE
ETHANE
DEETHANIZER
FEED
DEPROPANIZER
C3 SPLITTER
PROPYLENE
PROPANE
C4+

Figure. 1.4. Post-cracking separation sequence.

Typical product specification for propylene is divided into two categories: the high-pure polymer-grade, dedicated to the polypropylene industry, and the less pure chemical-grade, further used in most of the derivatives industry [3]. Table 1.1 displays the product specifications of each grade.

The polymerization reactions that take place during the polypropylene production require high propylene purity with propane concentrations typically below 0.5 mol.%, along with a complete removal of minor contaminants, such as carbonyl sulfide, which can poison the polymerization catalysts.

Table 1.1. Propylene most common product specification.

	Chemical grade	*Polymer grade*
Propene, mol. %	92-95	99.5-99.8
Acetylene, ppm	<10	<2
Ethylene, ppm	<20	<20
Ethane, ppm	<2000	<100
Propyne, ppm	<20	<5
Propadiene, ppm	<20	<5
C_{4+},ppm	<1000	<10
Hydrogen, ppm	<10	<10
Nitrogen, ppm	<50	<50
Oxygen, ppm	<5	<5
Carbon monoxide, ppm	<5	<5
Carbon dioxide, ppm	<5	<5
Sulfur, mass ppm	<5	<1
Water, mol. ppm	<25	<10
Propane	remainder	remainder

Given that the C_3 fraction from the depropanizer head stream contains both the olefin and its homologous paraffin (i.e. propane), effective separation methods are required to produce a propylene product in the specified purities.

1.2. Propane/propylene separation. Traditional methods and membrane technology.

The propane and propylene molecules show very similar physicochemical properties, as shown in Table 1.2. For this reason, the industrial separation of propane/propylene mixtures has traditionally relied on cryogenic and high pressure distillation, exploiting the minor boiling point variation between these two components. Typically, the columns used in these distillation processes exceed 120 equilibrium stages to be able to deal with the boiling points proximity and reach the desired high propylene purity.

Table 1.2. Propylene and propane physicochemical properties.

	Propylene	*Propane*
Molecular formula	C_3H_6	C_3H_8
Molecular weight (g mol^{-1})	42.07	44.09
Melting point (K)	88.0	85.5
Normal boiling point (K)	225.6	231.1
Water solubility, k^o_H (mol kg^{-1} bar^{-1})^a	0.0048	0.0015
Liquid density (kg m^{-3})^b	613.9	582
Vapor pressure (bar)^c	10.3	8.7
Critical temperature (K)	364.15	369.75
Critical pressure (bar)	46.1	42.5
Gas density (kg m^{-3}) ^{b}	2.365	2.423
Specific gravity (air=1)^d	1.48	1.55

[a] at 298 K
[b] at boiling point and 1 bar
[c] at 293 K
[d] at 1 bar and 293 K

All these equilibrium stages require large distillation columns, usually higher than 90 meters, which involves major capital investments. Additionally, high pressure and cryogenic distillation generate large energy consumption. In this sense, the energy consumption for propylene and ethylene purification alone has been calculated at roughly 0.3% of the world total energy demand [5].

These drawbacks have encouraged the search for alternative separation methods capable of reducing both the capital and energy intensity of the purification step. Among the conventional processes, extractive distillation, physical adsorption and physical/chemical absorption are the most commonly studied [6–8]. However, the economic feasibility of the first two processes is hampered by solvent usage and capital costs, and, although chemical adsorption through transition metal complexation has proven certain competitiveness, it has not been widely introduced in the industry due to complex regeneration cycles and low olefin load capacities [9].

In the last few years, increasing attention has been paid to membrane technology, a compact, modular and energy efficient solution that allows process intensification by implementing: "*…more or less complex technologies that replace large, expensive, energy-intensive equipment or processes with ones that are smaller, less costly and more efficient…*" [10].

The synthesis of effective olefin/paraffin separation membranes has been approached exploring several transport phenomena. The simplest way is to exploit the intrinsic separation properties of dense polymers, based on the solution-diffusion theory [11]. In this way, the membrane can discriminate different molecules due to permeability and/or solubility differences. Dense polymeric membranes made of glassy, rubbery and cellulosic polymers have been reported, but they usually perform high propylene selectivity at the expense of low permeability [12–15].

Another widely reported approach contemplates the molecular sieving effect of some advanced materials. These materials feature a combination of micro and ultramicropores able to discriminate different molecules based on their molecular size [16]. Among these materials, polymers with intrinsic microscopy (PIMs) [17,18], metal organic frameworks (MOFs)

[19,20], carbon molecular sieves (CMSs) [21,22] and graphene-based membranes [23] are the most notable.

However, the intrinsic separation properties of polymers are vastly improved when the capability of some transition metals (i.e. copper and silver) to form olefin-metal complexes is exploited. This complexation phenomenon, explained through the Dewar-Chatt-Duncanson model (Figure 1.5), consists in a selective and reversible bonding caused by the donation of electrons from olefin to metal [24]. The use of this complexation mechanism has given rise to a new kind of membrane materials featuring facilitated transport mechanisms [25].

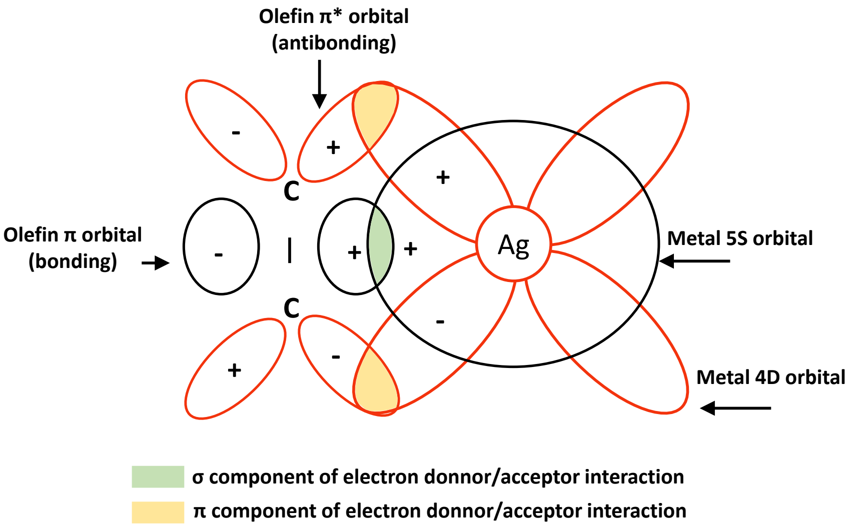
Olefin π* orbital (antibonding)
Olefin π orbital (bonding)
Metal 5S orbital
Metal 4D orbital
C
C
Ag
+
-
🟩 σ component of electron donnor/acceptor interaction
🟨 π component of electron donnor/acceptor interaction

Figure. 1.5. Dewar-Chatt-Duncanson model of π-complexation (adapted from [24]**).**

The first attempts to introduce facilitated transport in membrane technology involved the use of liquid membranes, most notably in the form of supported liquid membranes (SLM). In these membranes a liquid solvent containing the carrier (i.e. silver salt) is introduced into the pores of a polymeric support where the complexation reaction dramatically increases the olefin solubility. Due to the partial pressure gradient, the complex is transported to the permeate side, where decomplexation takes place. However, poor mechanical stability and solvent losses caused by evaporation and dragging prevent SLMs from becoming an industrial alternative [26–28].

Recently, researchers have tried to solve these drawbacks by replacing traditional organic solvents with novel room temperature ionic liquids (RTILs). These compounds are exclusively formed by ions. The relative size difference between the anion and the cation prevents these ionic substances from organizing in crystalline structures, which results in the liquid state at room temperature. Besides their negligible vapor pressure, ionic liquids are non-flammable excellent solvents whose chemical and physical properties can be tailored by a judicious selection of cation, anion, and substituents [29,30]. However, although their negligible vapor pressure eliminates the solvent evaporation issue, the introduction of RTILs cannot solve the other major issue of supported liquid membranes, which is the expelling out of solvent from the support pores due to the transmembrane pressure.

Advanced mechanical stability and separation performance can be achieved combining the properties of dense polymeric membranes with facilitated transport through the synthesis of polymer/salt systems. In these systems, the silver salt is dissolved along with the polymer and the membrane is then fabricated through solvent casting, which results in a dense facilitated transport membrane usually described as a polymer electrolyte [31,32]. In polymers containing electron donor heteroatoms such as oxygen or fluorine, the Pearson’s Hard-Soft–Acid-Base (HSAB) theory predicts the formation of weak interactions between the Ag^+ cations (soft acid) and the polymer heteroatoms (hard bases) [33]. These interactions are weak enough to still allow the π-complexation between the metal cation and the olefin. As a result, the silver cations remain “fixed” to the polymer backbone and the permeating olefin molecules follow a “hopping” pathway from active site to active site, this has come to be called “fixed site carrier transport mechanism” [34,35]. Figure 1.6 schematizes the fixed site carrier mechanism.

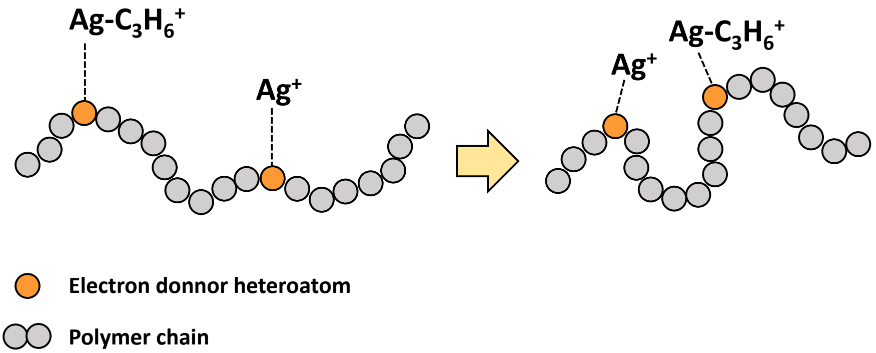

Figure. 1.6. Fixed site carrier transport mechanism.

Room temperature ionic liquids can be effectively implemented to improve the membrane performance of polymer electrolyte membranes. The presence of an ionic liquid within the free volume of the polymer promotes dissociation and mobility of the silver cations, which, after binding to the olefin, will diffuse through the membrane following a “mobile carrier” transport mechanism, similar to that of the facilitated transport liquid membranes [36].

Finally, the selection of the silver salt counterion plays a major role in the cation capability to dissociate and interact with the olefin. Low electronegative large anions such as BF_4^-, $CF_3SO_3^-$, and ClO_4^- form salts featuring a low lattice energy, whereas high electronegative small anions like F^-, Cl^- and NO_3^- form high lattice energy salts, hindering olefin-silver coordination and impeding facilitated transport [37,38].

Solid state facilitated transport membranes have proven promising potential for olefin/paraffin separation, thanks to their mechanical stability and remarkable performance. However, a future replacement of traditional distillation by facilitated transport membranes requires of rigorous process design and optimization based on comprehensive mathematical models able to predict the system response to a wide range of operational variables and parameters.

1.3. Facilitated transport modelling

Several approaches have been reported in the literature for the mathematical modeling of facilitated transport in solid membranes. The dual sorption model, originally developed to interpret gas sorption in glassy polymers, has been commonly used to explain facilitated transport due to its simplicity and conceptual analogy to the mass transport with fixed carrier membranes. However, this model does not predict facilitated transport without direct diffusion between carriers [39].

A more rigorous analysis of facilitated transport in solid membranes is achieved by introducing the “effective diffusion coefficient” between fixed site carriers. In this analysis, the concentration of unreacted fixed carrier is assumed to be constant, implying large excess of carrier. If the reaction rate is much faster than the diffusion rate, then the model is reduced to the dual sorption transport model at low partial pressure of the solute. But, at high solute partial pressures, the assumption of excess carrier is violated and the model stars to gradually deviate from experimental data [35,40].

Another interesting model proposed by Cussler et al. [34] introduces the concept of “limited mobility of chained carriers”. This model assumes fast reaction on the membrane surface, thus, no uncomplexed solute can exist within the membrane. The polymer chains rearrangement motion allows a complexed molecule to find another uncomplexed carrier in the vicinity, resulting in facilitated transport.

All these models explain facilitated transport considering only direct diffusion between carriers and such diffusion requires the distance between carriers to be shorter than the diffusional jump distance of a given gas/polymer pair. However, facilitated transport has been experimentally observed in membranes that do not satisfy this condition, suggesting that some sort of solute diffusion in uncomplexed state may also occur between fixed sites [41].

Finally, the “concentration fluctuation model”, a description of facilitated transport that does not consider solute “hopping” between fixed sites has been reported [42,43]. Apart from the thermodynamic constant, this model also considers the reaction kinetics. According to this model the facilitation effect is produced by the local fluctuation in the solute concentration along the membrane thickness due to complexation-decomplexation reactions. This fluctuation increases the chemical potential of the permeant species according to Cahn’s theory [44], which results in a higher driving force.

A good mathematical model capable of describing the solute transmembrane flux in the common operating conditions range can be decisive for the rigorous design and optimization of facilitated transport membrane processes.

1.4. Facilitated transport membrane processes. Design and optimization.

The complete replacement of traditional distillation by a single-stage membrane process capable of producing polymer grade propylene and fuel grade propane simultaneously is not feasible, due to the purity-recovery trade-off inherent in membrane operation and the industrially achievable pressure ratio [45]. Accordingly, alternative strategies should be considered to introduce membrane technology in the olefin/paraffin separation.

A first approach consists in the implementation of hybrid separation processes combining membrane and distillation technology [46,47]. Such processes can potentially reduce the energy intensity of the olefin/paraffin separation process by a factor of 2 or 3 [5]. The membrane/distillation hybrid processes comprise a limited number of arrangements, including one or more membrane stages [46,48,49]. Figure 1.7 shows commonly studied hybrid configurations. However, membranes become increasingly efficient as the product requirements are relaxed from 100% purity target, which means that they are very efficient concentrators [50]. For this reason, parallel configurations, whereby a membrane contactor is intended for the bulk separation and distillation is just left for the final product refining, are preferred. This approach allows maintaining the existing distillation columns by just retrofitting them with the new membrane stages [51–53].

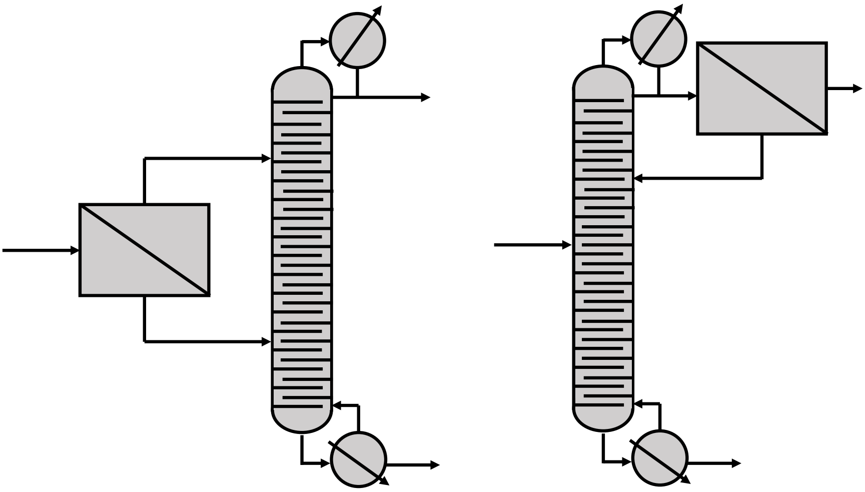

Figure. 1.7. Membrane/distillation hybrid processes.

According to the definition of a hybrid process by Lipnizki et al. [54], as *"…a process package consisting of generally different, unit operations, which are interlinked and optimized to achieve a predefined task."*, optimization is a key step in hybrid process design, which allows solving the trade-off between the membrane total cost and the column operating expenses.

On the other hand, complete replacement of distillation by membrane technology can be achieved by designing and optimizing appropriate multistage/multistep membrane processes [55,56]. Designing multistage membrane process based on facilitated transport membranes involves several trade-offs that should be balanced through optimization. In the first place, the total membrane area of each stage determines the flowrates and purities of the product streams of that stage. Thus, higher stage areas generate larger permeate flowrates at the expense of permeate purity. Additionally, the solute transmembrane flux by facilitated transport mechanisms is strongly dependent on the carrier loading, as evidenced from the experimental analysis and the mathematical models [57,58]. However, high carrier concentrations imply high membrane cost per unit area, which could affect the process economics. Finally, higher transmembrane pressures increase the driving force available for the permeation but at the expense of higher recompression requirements.

Unlike hybrid processes, membrane processes can be designed in many different configurations combining multiple stages, stages with multiple steps and recycle streams. Hence, optimization is crucial to determine the optimal layout for each specific separation. Although it is possible to expand the optimization to cover all configurations by building a complex superstructure that includes membranes, mixers, splitters and compressors, such optimization results in a complex mixed integer nonlinear programming problem (MINLP) [59]. MINLP problems are difficult to solve because they combine challenges of nonlinear and mixed integer programming, and require dedicated methods for its resolution [60]. Additionally, most studies dealing with superstructure optimization for gas separation conclude with a two-stage optimal configuration [61–64].

For this reason, selecting the most promising configurations based on the extensive literature seems to be the most efficient strategy. This allows solving less complex non-linear programming problems (NLP) and pay more attention to the facilitated transport particularities through the implementation of transport models in the optimization.

1.5. Background and scope

This thesis has been performed in the Advanced Separation Processes research group of the University of Cantabria. In previous works of this group, the propane and propylene solubility in RTIL/Ag$^+$ mixtures was studied, revealing the exothermic character of the complexation reaction and its reversibility through vigorous agitation and vacuum [65,66].

Subsequently, the reactive absorption kinetics of propylene in RTIL/Ag$^+$ media was assessed, determining the required physicochemical parameters to predict the absorption rates [67].

In order to study the industrial applicability of propylene reactive absorption in the proposed RTIL/Ag$^+$ media, several works reported the use of membrane contactors, assessing the influence of feed composition and silver loading [68]. Furthermore, supported ionic liquid membranes (SILMs) were also synthesized and tested [57].

During this period, the quantum chemical COSMO-RS method was applied to determine the most suitable system (ionic liquid/silver salt) to carry out the separation of propane/propylene gas mixtures by reactive absorption, concluding that the optimal medium should be based on an ionic liquid with the BF_4 anion and an ammonium or imidazolium-based cation and silver tetrafluoroborate ($AgBF_4$) as a silver salt.

Finally, a first study on polymer/ionic liquid composite membranes for propane/propylene separation was reported [69]. The use of ionic liquids as additives had previously proven certain advantages such as improved carrier stability and enhanced membrane permeability. In that study, PVDF-HFP/$BMImBF_4$ membranes were characterized through polarized light microscopy, gas permeation and tensile tests, concluding that the membrane with 80% polymer-20% IL w/w showed the best compromise between separation properties and mechanical resistance.

Based on the above-mentioned results, the main objective of this thesis is to assess the potential of the proposed facilitated transport membranes to offer a more efficient alternative to current propane/propylene separation processes. In the first place, this work contributes and makes progress to the fundamental knowledge of the phenomena involved in the propylene permeation in PVDF-HFP/$BMImBF_4$/$AgBF_4$ facilitated transport membranes. With this regard, a wide range of characterization techniques has been implemented to study the internal structure and the interactions between the membrane constituents. Additionally, time-lag and gas-mixture continuous-flow permeation techniques allowed determining the separation performance under different operating conditions, including changes in temperature, feed pressure, silver loading, feed humidity and feed composition. On the other hand, this work advances in the implementation of facilitated transport membranes in alternative separation processes. For this purpose and based on experimental data, a mathematical model able to describe the propylene permeation through carrier-mediated mechanisms under the previously studied operating conditions has been developed. Finally, based on process economics, hybrid membrane/distillation and multistage membrane processes have been proposed and optimized using computer aided process design. These studies predicted the economic savings that these membranes can potentially produce.

1.6. References

[1] J.S. Plotkin, The Propylene Gap: How can it be filled?, Am. Chem. Soc. (2015).

[2] C. Cathelin, M. Dorini, G. Mei, J. Pater, R. Rinaldi, Polypropylene, Kirk-Othmer Encycl. Chem. Technol. (2018) 27.

[3] H. Zimmermann, Propene, Ullmann’s Encycl. Ind. Chem. (n.d.) 2013.

[4] A. Akah, M. Al-Ghrami, Maximizing propylene production via FCC technology, Appl. Petrochemical Res. 5 (2015) 377–392.

[5] D.S. Sholl, R.P. Lively, Seven chemical separations to change the world, Nature. 532 (2016) 435–437.

[6] R. Kumar, J.M. Prausnitz, C.J. King, Process design considerations for extractive distillation: separation of propylene-propane, in: Dimitrios P. Tassios (Ed.), Extr. Azeotropic Distill., 1972: pp. 16–34.

[7] C.M. Shu, S. Kulvaranon, M.E. Findley, A.I. Liapis, Experimental and computational studies on propane-propylene separation by adsorption and variable-temperature stepwise desorption, Sep. Technol. 1 (1990) 18–28.

[8] R.T. Yang, pi-Complexation Sorbents and Applications, in: Adsorbents Fundam. Appl., John Wiley & Sons, Hoboken, NJ, 2003: p. 424.

[9] D.J. Safarik, R.B. Eldridge, Olefin/Paraffin Separations by Reactive Absorption: A Review, Ind. Eng. Chem. Res. 37 (1998) 2571–2581.

[10] J.C. Charpentier, In the frame of globalization and sustainability, process intensification, a path to the future of chemical and process engineering (molecules into money), Chem. Eng. J. 134 (2007) 84–

[11] J.G. Wijmans, R.W. Baker, The solution-diffusion model: a review, J. Memb. Sci. 107 (1995) 1–21.

[12] O.M. Ilinitch, G.L. Semin, M.V. Chertova, K.I. Zamaraev, Novel polymeric membranes for separation of hydrocarbons, J. Memb. Sci. 66 (1992) 1–8.

[13] K. Okamoto, A. Taguchi, J. Hao, K. Tanaka, H. Kita, Permeation and separation properties of polyimide membranes to olefins and paraffins, J. Memb. Sci. 121 (1996) 197–207.

[14] A. Ito, S.-T. Hwang, Permeation of propane and propylene through cellulosic polymer membranes, J. Appl. Polym. Sci. 38 (1989) 483–490.

[15] R. Faiz, K. Li, Polymeric membranes for light olefin/paraffin separation, Desalination. 287 (2012) 82–97.

[16] W.J. Koros, C. Zhang, Materials for next-generation molecularly selective synthetic membranes, Nat. Mater. 16 (2017) 289–297.

[17] R.J. Swaidan, X. Ma, E. Litwiller, I. Pinnau, Enhanced propylene/propane separation by thermal annealing of an intrinsically microporous hydroxyl-functionalized polyimide membrane, J. Memb. Sci. 495 (2015) 235–241.

[18] K.S. Liao, J.Y. Lai, T.S. Chung, Metal ion modified PIM-1 and its application for propylene/propane separation, J. Memb. Sci. 515 (2016) 36–44.

[19] V.F.D. Martins, A.M. Ribeiro, A. Ferreira, U.H. Lee, Y.K. Hwang, J.S. Chang, J.M. Loureiro, A.E. Rodrigues, Ethane/ethylene separation on a copper benzene-1,3,5-tricarboxylate MOF, Sep. Purif. Technol. 149 (2015) 445–456.

[20] M. Hartmann, U. Böhme, M. Hovestadt, C. Paula, Adsorptive Separation of Olefin/Paraffin Mixtures with ZIF-4, Langmuir. 31

(2015) 12382–12389.

[21] O. Salinas, X. Ma, Y. Wang, Y. Han, I. Pinnau, Carbon molecular sieve membrane from a microporous spirobisindane-based polyimide precursor with enhanced ethylene/ethane mixed-gas selectivity, RSC Adv. 7 (2017) 3265–3272.

[22] R.J. Swaidan, X. Ma, I. Pinnau, Spirobisindane-based polyimide as efficient precursor of thermally-rearranged and carbon molecular sieve membranes for enhanced propylene/propane separation, J. Memb. Sci. 520 (2016) 983–989.

[23] H.-X. Sun, B.-B. Yuan, P. Li, T. Wang, Y.-Y. Xu, Preparation of nanoporous graphene and the application of its nanocomposite membrane in propylene/propane separation, Funct. Mater. Lett. 08 (2015) 1550019.

[24] O.C.C.P.I.I. I, O.C. Compounds, P.I.I.I.I. Spectra, Olefin Co-ordination Compounds. Part I I I . 2939 586., (1952) 2939–2947.

[25] R. Faiz, K. Li, Olefin/paraffin separation using membrane based facilitated transport/chemical absorption techniques, Chem. Eng. Sci. 73 (2012) 261–284.

[26] M. Teramoto, H. Matsuyama, T. Yamashiro, Y. Katayama, Separation of Ethylene From Ethane By Supported Liquid Membranes Containing Silver-Nitrate As a Carrier, J. Chem. Eng. Japan. 19 (1986) 419–424.

[27] S. Duan, A. Ito, A. Ohkawa, Separation of propylene/propane mixture by a supported liquid membrane containing triethylene glycol and a silver salt, J. Memb. Sci. 215 (2003) 53–60.

[28] M.T. Ravanchi, T. Kaghazchi, A. Kargari, Supported liquid membrane separation of propylene-propane mixtures using a metal ion carrier, Desalination. 250 (2010) 130–135.

[29] T. Welton, Room-Temperature Ionic Liquids. Solvents for Synthesis and Catalysis, Chem. Rev. 99 (1999) 2071–2084.

[30] J.P. Hallett, T. Welton, Room-temperature ionic liquids: Solvents for synthesis and catalysis. 2, Chem. Rev. 111 (2011) 3508–3576.

[31] Y. Yoon, J. Won, Y.S. Kang, Polymer electrolyte membranes containing silver ion for facilitated olefin transport, Macromolecules. 33 (2000) 3185–3186.

[32] L. Liu, X. Feng, A. Chakma, Unusual behavior of poly(ethylene oxide)/AgBF4 polymer electrolyte membranes for olefin-paraffin separation, Sep. Purif. Technol. 38 (2004) 255–263.

[33] R.G. Pearson, Hard and Soft Acids and Bases, J. Am. Chem. Soc. 85 (1963) 3533–3539.

[34] E.L. Cussler, R. Aris, A. Bhown, On the limits of facilitated diffusion, J. Memb. Sci. 43 (1989) 149–164.

[35] R.D. Noble, Analysis of facilitated carrier membranes transport with fixed site, 50 (1990) 207–214.

[36] D.R. Smith, J.A. Quinn, The facilitated transport of carbon monoxide through cuprous chloride solutions, AIChE J. 26 (1980) 112–120.

[37] J.H. Kim, B.R. Min, J. Won, S.H. Joo, H.S. Kim, Y.S. Kang, Role of polymer matrix in polymer/silver complexes for structure, interactions, and facilitated olefin transport, Macromolecules. 36 (2003) 6183–6188.

[38] C.K. Kim, J. Won, H.S. Kim, Y.S. Kang, H.G. Li, C.K. Kim, Density functional theory studies on the dissociation energies of metallic salts: Relationship between lattice and dissociation energies, J. Comput. Chem. 22 (2001) 827–834.

[39] H. Nishide, M. Ohyanagi, O. Okada, E. Tsuchida, Dual-Mode

Transport of Molecular Oxygen in a Membrane Containing a Cobalt Porphyrin Complex as a Fixed Carrier, Macromolecules. 20 (1987) 417–422.

[40] R.D. Noble, Generalized microscopic mechanism of facilitated transport in fixed site carrier membranes, J. Memb. Sci. 75 (1992) 121–129.

[41] E. Tsuchida, H. Nishide, M. Ohyanagi, H. Kawakami, P. Chemistry, R. October, Facilitated Transport of Molecular Oxygen in the Membranes of Polymer-Coordinated Cobalt Schiff Base Complexes, (1987) 1907–1912.

[42] Y.S. Kang, J.M. Hong, J. Jang, U.Y. Kim, Analysis of facilitated transport in solid membranes with fixed site carriers: 1. Single RC circuit model, J. Memb. Sci. 109 (1996) 149–157.

[43] J.M. Hong, Y.S. Kang, J. Jang, U.Y. Kim, Analysis of facilitated transport in polymeric membrane with fixed site carrier: 2. Series RC circuit model, J. Memb. Sci. 109 (1996) 159–163.

[44] J.W. Cahn, Phase separation by spinodal decomposition in isotropic systems, J. Chem. Phys. 42 (1965) 93–99. doi:10.1063/1.1695731.

[45] H.B. Park, J. Kamcev, L.M. Robeson, M. Elimelech, B.D. Freeman, Maximizing the right stuff: The trade-off between membrane permeability and selectivity, Science (80-.). 356 (2017) 1138–1148.

[46] T.G. Pressly, K.M. Ng, A Break-Even Analysis of Distillation-Membrane Hybrids, AIChE J. 44 (1998) 93–105.

[47] A. Norkobilov, D. Gorri, I. Ortiz, Comparative study of conventional, reactive-distillation and pervaporation integrated hybrid process for ethyl tert-butyl ether production, Chem. Eng. Process. Process Intensif. 122 (2017) 434–446.

[48] W. Stephan, R.D. Noble, C.A. Koval, Design methodology for a membrane/distillation column hybrid process, J. Memb. Sci. 99 (1995) 259–272.

[49] T. Pettersen, A. Argo, R.D. Noble, C.A. Koval, Design of combined membrane and distillation processes, Sep. Technol. 6 (1996) 175–187.

[50] R. Spillman, Economics of gas separation membrane processes, in: R.D. Noble, S.A. Stern (Eds.), Membr. Sep. Technol. Princ. Appl., Elsevier Science, 1995.

[51] S. Moganti, R.D. Noble, C.A. Koval, Analysis of a membrane/distillation column hydrid process, J. Memb. Sci. 93 (1994) 31–44.

[52] J.A. Caballero, I.E. Grossmann, M. Keyvani, E.S. Lenz, N. Square, V. Pennsyl, Design of hybrid distillation - vapor membrane separation systems, Ind. Eng. Chem. Res. 48 (2009) 9151–9162.

[53] I.K. Kookos, Optimal Design of Membrane/Distillation Column Hybrid Processes, Ind. Eng. Chem. Res. 42 (2003) 1731–1738.

[54] F. Lipnizki, R.W. Field, P.-K. Ten, Pervaporation-based hybrid process: a review of process design, applications and economics, J. Memb. Sci. 153 (1999) 183–210.

[55] R.W. Baker, Membrane Technology and Applications, 3rd Editio, Wiley, Chichester, 2012.

[56] F. Ahmad, K.K. Lau, A.M. Shariff, G. Murshid, Process simulation and optimal design of membrane separation system for CO2capture from natural gas, Comput. Chem. Eng. 36 (2012) 119–128.

[57] M. Fallanza, A. Ortiz, D. Gorri, I. Ortiz, Experimental study of the separation of propane/propylene mixtures by supported ionic liquid membranes containing Ag+–RTILs as carrier, Sep. Purif. Technol.

97 (2012) 83–89.

[58] R. Zarca, A. Ortiz, D. Gorri, I. Ortiz, Generalized predictive modeling for facilitated transport membranes accounting for fixed and mobile carriers, J. Memb. Sci. 542 (2017) 168–176.

[59] R. Qi, M.A. Henson, Membrane system design for multicomponent gas mixtures via mixed-integer nonlinear programming, Comput. Chem. Eng. 24 (2000) 2719–2737.

[60] K. Zhou, X. Chen, Z. Shao, W. Wan, L.T. Biegler, Heterogeneous parallel method for mixed integer nonlinear programming, Comput. Chem. Eng. 66 (2014) 290-0300.

[61] B. Ohs, J. Lohaus, M. Wessling, Optimization of membrane based nitrogen removal from natural gas, J. Memb. Sci. 498 (2016) 291–301.

[62] C. Kunde, A. Kienle, Global optimization of multistage binary separation networks, Chem. Eng. Process. - Process Intensif. (2018).

[63] D.C. Nymeijer, T. Visser, R. Assen, M. Wessling, Composite hollow fiber gas-liquid membrane contactors for olefin/paraffin separation, Sep. Purif. Technol. 37 (2004) 209–220.

[64] A. Aliaga-Vicente, J.A. Caballero, M.J. Fernandez-Torres, Synthesis and Optimization of Membrane Cascade for Gas Separation via Mixed-Integer Nonlinear Programming, AIChE J. 63 (2017) 1989–2006.

[65] A. Ortiz, A. Ruiz, D. Gorri, I. Ortiz, Room temperature ionic liquid with silver salt as efficient reaction media for propylene/propane separation: Absorption equilibrium, Sep. Purif. Technol. 63 (2008) 311–318.

[66] A. Ortiz, L. Galán, D. Gorri, B. De Haan, I. Ortiz, Reactive Ionic

Liquid Media for the Separation of Propylene / Propane Gaseous Mixtures, Ind. Eng. Chem. Res. 49 (2010) 7227–7233.

[67] A. Ortiz, L.M. Galán, D. Gorri, A.B. De Haan, I. Ortiz, Kinetics of reactive absorption of propylene in RTIL-Ag+ media, Sep. Purif. Technol. 73 (2010) 106–113.

[68] A. Ortiz, D. Gorri, Á. Irabien, I. Ortiz, Separation of propylene/propane mixtures using Ag+-RTIL solutions. Evaluation and comparison of the performance of gas-liquid contactors, J. Memb. Sci. 360 (2010) 130–141.

[69] M. Fallanza, A. Ortiz, D. Gorri, I. Ortiz, Polymer-ionic liquid composite membranes for propane/propylene separation by facilitated transport, J. Memb. Sci. 444 (2013) 164–172.

Chapter 2

Experimental and modeling methods

Abstract

In this chapter, the materials and the experimental and modeling procedures used during this thesis are summarized. First, the materials and the experimental methods regarding membrane synthesis, characterization of the membrane structure and determination of the separation performance are presented. Next, the modeling methodology used to develop a mathematical description of the propylene transmembrane flux through facilitated transport mechanisms is described. Finally, the design and optimization strategies used to assess the facilitated transport membranes industrial applicability are discussed.

2.1. Experimental Methods

This section presents the materials and methods used for membrane synthesis, followed by a brief presentation of the membrane characterization techniques and a more detailed description of the gas permeation set-ups and methodologies.

2.1.1. Chemicals

Propylene and propane gases were supplied by Praxair with a purity of 99.5%. Poly(vinylidene fluoride-co-hexafluoropropylene) (PVDF-HFP) was purchased from Sigma Aldrich. 1-Butyl-3-methylimidazolium tetrafluoroborate ($BMImBF_4$) with a minimum purity of 99% and halide content of less than 500 ppm was supplied by Iolitec. Silver tetrafluoroborate ($AgBF_4$) with a minimum purity of 99% was supplied by Apollo Scientific Ltd. Tetrahydrofuran (THF) purchased from Panreac was used as solvent for membrane synthesis. The industrial propane/propylene gas mixture was kindly provided by Petronor S.A., Table 2.1 shows the industrial mixture composition. All chemicals were used as received without further purification.

2.1.2. Membrane synthesis

The proposed membranes for propane/propylene separation are composed of a polymer, an ionic liquid and a silver salt. Poly(vinylidene fluoride-co-hexafluoropropylene) (PVDF-HFP) is a high performance fluoropolymer featuring high thermal, chemical and mechanical stability, and is used to form the polymeric dense matrix. Based on previous results of the research group, the ionic liquid used in this work has been 1- butyl3-methylimidazolium tetrafluoroborate ($BMImBF_4$) since it provided the best results in terms of separation selectivity and propylene solubility and presents good miscibility with both the PVDF-HFP and the silver salt. Finally, silver tetrafluoroborate ($AgBF_4$) provides the silver cations upon dissociation inside the membrane thanks to the low lattice energy provided by the anion [1].

Table 2.1. Industrial gas mixture composition.

Component	*Concentration (mol.%)*
Methane	0.0034
Ethane	0.1503
Ethylene	0.0099
Propane	24.8837
Propylene	74.7208
Isobutane	0.1872
N-butane	0.0016
Trans-butene	0.0214
Iso-butene	0.0218
Hydrogen sulfide	< 0.2 ppm
Acetylene	< 0.2 ppm
Hydrogen	< 0.2 ppm

All the studied membranes were prepared by the solvent casting method. The desired amount of PVDF-HFP was dissolved in THF using a 10 ml sealed glass vial to avoid solvent losses by evaporation. The content was stirred during 24 h at room temperature. To achieve complete dissolution of the polymer, the mixture was subjected to a heating step at

50 °C during 5 min. After that, the selected amounts of ionic liquid and silver salt were added to the solution and the whole mixture was stirred at room temperature during 15 min. The membrane precursor was poured in a glass petri dish and then introduced in a vacuum oven overnight at 800 mbar and 25 °C. Finally, a more severe evaporation step at full vacuum (~1 mbar) during 1 h was performed for further solvent removal. Light exposure was avoided during the whole synthesis process to prevent silver reduction. The thickness of the synthesized membranes ranged from 40 to 100 µm depending on the specific composition. For calculation purposes, the real membrane thickness was measured using a digital micrometer Mitutoyo Digimatic MDC-25SX (accuracy±0.001 mm).

2.1.3. Characterization techniques

The cross-section and surface morphology of the membranes were observed using scanning electron microscopy (Carl Zeiss EVO MA 15). The samples were prepared by immersing and fracturing the membranes in liquid nitrogen followed by gold sputtering with a Balzers Union SCD040 sputter coating system.

Further knowledge on membrane structure can be extracted from the energy dispersive X-ray spectroscopy (EDX). EDX makes use of x-ray spectrum emitted by the solid sample bombarded with a focused beam of electrons to obtain a localized chemical analysis. When the sample is hit by the electron beam, electrons are ejected from the atoms of the sample's surface. The resulting electron vacancies are filled by electrons from a higher energy state, and an x-ray is emitted to balance the energy difference between the two electrons' states. The x-ray energy is characteristic of the element from which it was emitted. EDX was used in conjunction with

SEM to obtain scan-lines and plot-mapping patterns of elemental silver on cross-sectional images of the composite membrane.

Thermogravimetric analyses were performed using a TG-DTA 60H Shimadzu thermobalance to assess the potential water uptake of the studied membranes under humid feed conditions.

The interactions between the Ag^+ cations and the fluorine atoms of the polymer chains were studied through Fourier transform infrared spectroscopy (FTIR) analyzing the polymer CF_2 symmetrical stretching mode. FTIR spectra were recorded using a Perkin Elmer Spectrum Two spectrometer

Better insight on the $AgBF_4$ dissociation behavior was achieved using Raman spectroscopy to analyze the regions of the BF_4^- stretching bands in the pure $AgBF_4$ and the silver-containing membranes. Raman spectroscopy was carried out using a Horiba T64000 triple spectrometer equipped with a confocal microscope and a Jobin Yvon Symphony CCD detector cooled with liquid nitrogen. A 488 nm beam from a Kr-Ar ion laser was focused through a 100x objective, using 2 mW laser power in all measurements. The spectral curves were fitted using Lorentzian functions.

X-ray photoelectron spectroscopy (XPS) was used to expand the knowledge on membrane structure and silver degradation though the analysis of the silver oxidation states. Additionally, the Ag 3d regions of the XPS spectra can confirm the interactions between the silver cations and the polymer fluorine atoms. XPS spectra were acquired using an SPECS (Berlin, Germany) X-ray photoelectron spectrometer. The samples were analyzed using a Mg anode operated at 225 W (E=1253.6 eV, 13 kV, 17.5 mA). The carbon (C 1s) line at 284.8 eV was used as reference in our determinations of the silver binding energies. A scanning interval of 0.1 eV was used for the final spectrum acquisition.

2.1.4. Gas permeation techniques

The constant-volume variable-pressure time-lag technique was used to experimentally obtain the transport and equilibrium parameters (i.e. diffusivity and solubility) of the gaseous species in the membrane matrix according to the solution-diffusion theory.

Figure 2.1 shows the experimental setup used to conduct the permeation experiments using the time-lag technique. This apparatus consists of two chambers separated by the membrane (47 mm in diameter). Before each run, the residual gas in both chambers and in the permeation cell is evacuated using a vacuum pump. At time zero the gas of interest is introduced into the upper chamber. The feed pressure is maintained constant at the upper chamber while the pressure increase in the lower chamber, which occurs due to the passage of gas through the membrane, is recorded. The pressure increase in the lower chamber starts only after a period of time known as the time-lag (ϴ). After the time-lag, the diffusion process continues in the quasi-steady state until the pressure in both chambers is equalized.

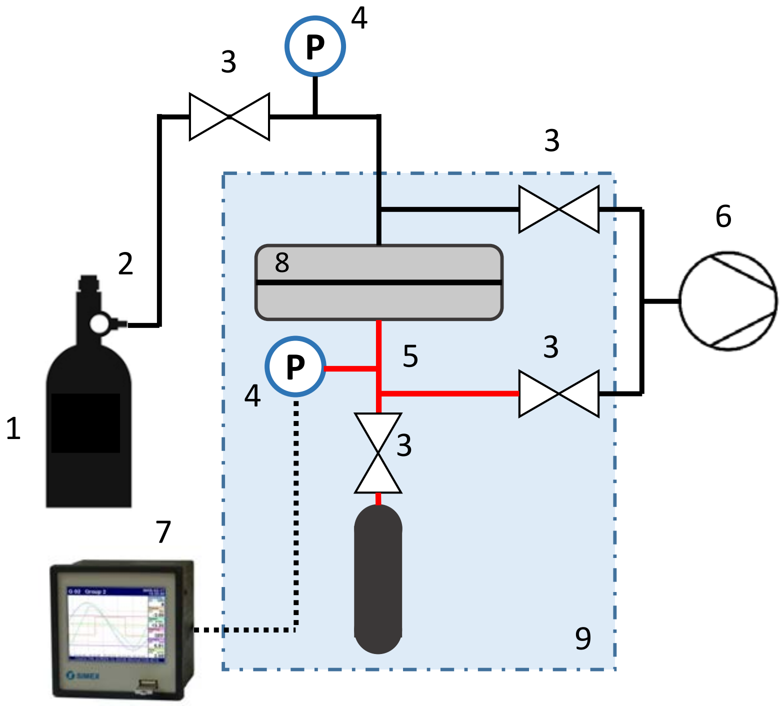

Figure. 2.1. Time-lag apparatus: 1) gas cylinder, 2) pressure controller, 3) gas valves, 4) pressure transducers, 5) permeation chamber, 6) vacuum pump, 7) data recording, 8) permeation cell, 9) temperature-controlled section.

The mathematical expression that describes the pressure increase in the lower chamber can be deduced by applying Fick’s second law in the limits of the membrane. By integrating Fick’s equation with the boundary conditions using Laplace transforms, operating and neglecting terms, the expression for the pressure in the permeate chamber versus time in the quasi-steady state flux is obtained:

$$P_L(t) = A\frac{R \cdot T \cdot S \cdot D \cdot P_0}{V \cdot L}\left(t - \frac{L^2}{6D}\right) \tag{1}$$

The above equation is a straight line, from which, the slope and the term that subtracts the time, known as “time- lag” (ϴ), can be extracted:

$$\Theta = {L^2}/{6D} \tag{2}$$

After re-arranging terms, diffusivity, solubility and permeability parameters can be obtained as:

$$D = {L^2}/{6\theta} \tag{3}$$

$$S = \frac{V \cdot L \cdot (slope)}{A \cdot D \cdot R \cdot T \cdot P_0} \tag{4}$$

$$P = D \cdot S \tag{5}$$

Where, L is the membrane thickness, ϴ is the “time-lag”, V is the permeate side volume, A is the permeation area, R is the gas constant, T is temperature and P_0 is the feed pressure.

On the other hand, the gas mixture permeation in facilitated transport membranes was studied using a continuous flow technique, Figure 2.2 In this technique, the membrane is placed in a permeation cell (90 mm in diameter) and the gas mixture, which is adjusted using mass flow controllers, is continuously fed into the upper chamber. Nitrogen gas is used in the lower chamber as sweeping gas. The pressure of both streams is controlled using two micrometric valves and two pressure transducers. The retentate and permeate streams are finally analyzed using gas chromatography and the experimental propylene flux is then calculated by a simple mass balance, as shown in Eq. 6. The analysis was performed in a gas chromatograph HP 6890 equipped with a thermal conductivity detector (TCD) and a column HP Al/S (30 m length, nominal diameter of 0.53 mm).

$$J_{C_3H_x} = \frac{1}{A_m}\frac{x_{C_3H_x}}{x_{N_2}}F_{N_2} \tag{6}$$

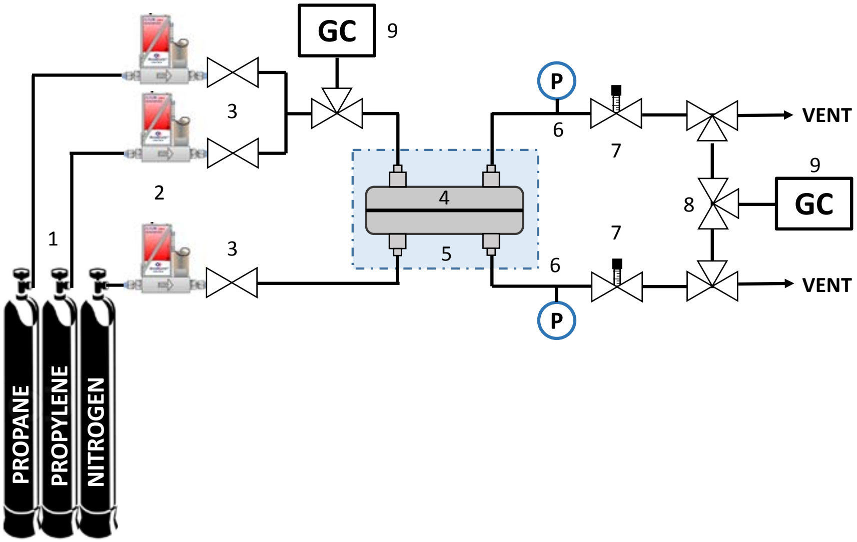

Figure. 2.2. Gas-mixture continuous-flow permeation setup: 1) gas cylinders, 2) mass flow controllers, 3) gas valves, 4) permeation cell, 5) temperature-controlled section, 6) pressure transducers, 7) needle valves, 8) three-way valves, 9) gas chromatograph.

For the permeation experiments under humid feed conditions a modification of the setup shown in Figure 2.2 was required. This modification is depicted in Figure 2.3. This setup allows generating any desired relative humidity in the feed stream by controlling the ratio of dry to humid feed.

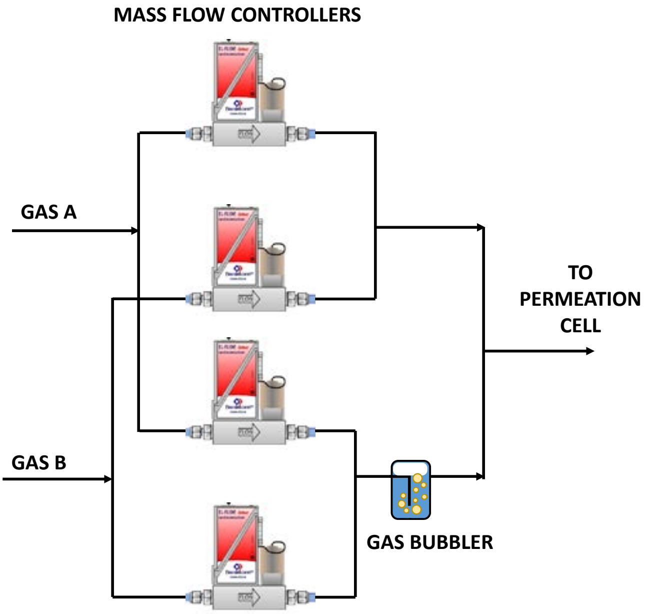
MASS FLOW CONTROLLERS
GAS A
GAS B
TO PERMEATION CELL
GAS BUBBLER

Figure. 2.3. Modification of the feed line setup to control the relative humidity of the feed stream.

Finally, permeation tests with real gas mixtures provided by the petrochemical industry were performed to assess if the membrane performance is affected by known contaminant trace components potentially present in industrial streams (i.e. acetylene, hydrogen sulfide and hydrogen [2]). The composition of these mixtures is shown in Table 2.1.

2.1.5. Experimental sequence

The experimental sequence for the time lag permeation tests is shown in Table 2.2. The feed pressure in the upper chamber was fixed at 3.5 bar while the permeate chamber was under vacuum.

Table 2.2. Time-lag technique experimental sequence.

Temperature (K)	*Membrane*	C_3H_6	C_3H_8
298	PVDF-HFP	•	•
	PVDF-HFP/BMImBF$_4$[a]	•	•
308	PVDF-HFP	•	•
	PVDF-HFP/BMImBF$_4$[a]	-	-
318	PVDF-HFP	•	•
	PVDF-HFP/BMImBF$_4$[a]	-	-

[a] Polymer/ionic liquid membrane composition was 80/20 wt.%

On the other hand, the experimental conditions for the gas-mixture continuous-flow permeation tests are shown in Table 2.3. The synthetic feed used in these experiments consisted of an equimolar propane/propylene gas mixture.

The silver loading indicated in Table 2.3 was calculated as the mass of silver salt added to 1 g of polymer or polymer/ionic liquid matrix. In this regard, silver loadings of 20, 40, 60 and 80 % were used during the experimental studies. However, these silver loadings produced different silver concentrations, expressed in mol/l, depending on the resulting membrane thickness of each specimen. For this reason, the specific silver concentration of each membrane will be indicated in the results section.

Table 2.3. Experimental conditions for the gas-mixture continuous-flow permeation tests.

Experimental condition	*Value*
T (K)	293/303/313
Feed composition	Synthetic/Industrial
Feed side pressure (bar)	1-4
Permeate side pressure (bar)	1
Silver load (wt.%)[a]	20/40/60/80
Polymer/ionic liquid mass ratio	(100/0) - (80/20)
Relative humidity (%RH)	0/25/50/100

[a] Calculated as the silver mass added over the polymer or polymer/ionic liquid mass.

2.2. Facilitated transport modeling

The gas transport mechanisms occurring inside the membrane are the result of the complex membrane structure. For this reason, the complexity of the composite membrane was approached by simplifying its nature, considering that the facilitated transport mechanism is shared between fixed site and mobile carrier, accounting for bounded and unbounded silver cations, respectively. A schematic representation of the transport mechanisms is depicted in Figure 2.4.

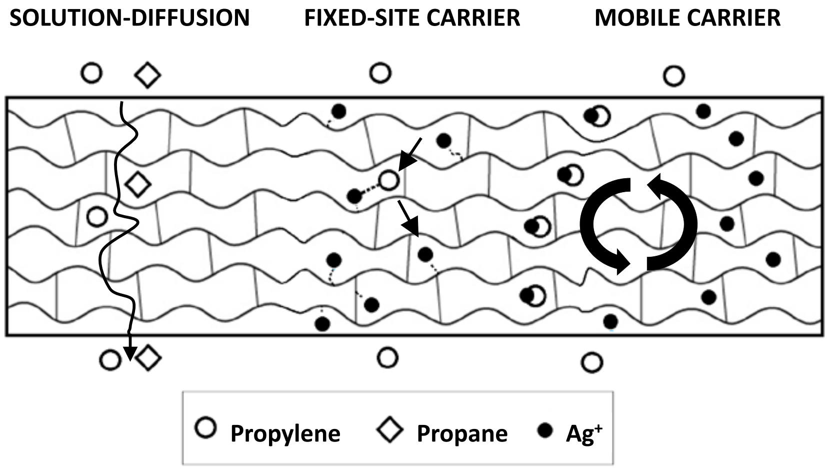

Figure. 2.4. Schematic representation of the gas transport mechanisms.

The total propylene flux through the membrane may be calculated as the sum of the contribution of each transport mechanism [3]:

$$J_{C_3H_6} = -D_{C_3H_6,m}\frac{dC_{C_3H_6}}{dx} - A\frac{dC_{C_3H_6}}{dx} - B\frac{dC_{C_3H_6}}{dx} \qquad (7)$$

The parameters A and B represent the “effective diffusivity” of the organometallic complex species in the mobile carrier and fixed-site carrier mechanisms respectively. Eq. 7 can be integrated along the membrane domain:

$$\begin{aligned} J_{C_3H_6} = D_{C_3H_6,m}\frac{C^0_{C_3H_6} - C^L_{C_3H_6}}{L} + A\frac{C^0_{C_3H_6} - C^L_{C_3H_6}}{L} \\ + B\frac{C^0_{C_3H_6} - C^L_{C_3H_6}}{L} \end{aligned} \qquad (8)$$

Where subscripts 0 and L refer to feed and permeate sides, respectively. If sorption equilibrium at the interphase is assumed, Eq. 8 can be reformulated as:

$$J_{C_3H_6} = D_{C_3H_6,m} \cdot S_{C_3H_6,m} \frac{p_{C_3H_6}^0 - p_{C_3H_6}^L}{L} + P_{comp} \frac{p_{C_3H_6}^0 - p_{C_3H_6}^L}{L} + K_H \frac{p_{C_3H_6}^0 - p_{C_3H_6}^L}{L} \tag{9}$$

Where P_{comp} is the permeability of the olefin based on the olefin-silver complex transport and K_{FC} acts as an effective permeability or “hopping parameter” for the olefin through the fixed carrier reactive pathway.

The permeability of the olefin-silver complex attributed to the mobile carrier mechanism P_{comp} is the product of its diffusivity in the ionic liquid times its chemical solubility; this latter parameter can be obtained from the complexation reaction between the silver cations and the propylene [4]:

$$Ag^+ + C_3H_6 \overset{K_{eq.}}{\Longleftrightarrow} Ag(C_3H_6)^+ \tag{10}$$

The equilibrium constant can be expressed as:

$$K_{eq} = \frac{[Ag(C_3H_6)^+]}{[Ag^+][C_3H_6]} \tag{11}$$

While the concentration of free cations is given by:

$$[Ag^+] = [Ag^T] - [Ag(C_3H_6)^+] \tag{12}$$

And solving for the complex species concentration:

$$[Ag(C_3H_6)^+] = \frac{K_{eq}[Ag^T][C_3H_6]}{1 + K_{eq}[C_3H_6]} \tag{13}$$

Introducing the relationship between the concentration of propylene physically absorbed and the partial pressure in the gas phase through a Henry type isotherm, the chemical solubility can be derived:

$$S_{C_3H_6,chem} = \frac{K_{eq} \cdot [Ag^T] \cdot H_{C_3H_6}}{1 + K_{eq} \cdot p_{C_3H_6} \cdot H_{C_3H_6}} \tag{14}$$

Finally, the olefin permeability through the mobile carrier mechanism can be expressed as:

$$P_{comp} = \frac{K_{eq.}[Ag^T] \cdot \ H_{C_3H_6}}{1 + K_{eq.} \cdot p_{C_3H_6} \cdot \ H_{C_3H_6}} \cdot D_{comp} \tag{15}$$

Where the equilibrium constant $K_{eq.}$, the physical solubility of the propylene in the ionic liquid $H_{C_3H_6}$, the olefin-paraffin complex diffusivity D_{comp}, and the influence of temperature on these parameters have been reported in previous works of the research group [4,5]:

$$H_{C_3H_6} \ = H_{C_3H_6,0} \ \cdot e^{\frac{-\Delta H_{sol}}{RT}} \tag{16}$$

$$ln\frac{K_{eq}}{K_{eq,ref}} \ = \frac{-\Delta H_r}{R} \ \cdot \left(\frac{1}{T} - \frac{1}{T_{ref}}\right) \tag{17}$$

$$D_{comp} \ = D_{comp,ref} \ \cdot e^{\frac{-Ea_D}{R}\left(\frac{1}{T} - \frac{1}{T_{ref}}\right)} \tag{18}$$

On the other hand, the transport flux due to the fixed site carrier mechanism is characterized by the “hopping parameter” K_{FC} , which is a function of the silver loading in the membrane and the temperature [6]. A mathematical expression can be derived for the dependence of K_H on temperature and silver concentration. The concentration of free cations ready to coordinate with propylene molecules to form the coordination complex can be derived from the chemical equilibrium. In this regard, the heterogeneous complexation reaction between propylene and silver cations bound to the polymer matrix is depicted by the following equation:

$$[Ag^{+}] + p_{C_3H_6} \overset{K_p}{\Leftrightarrow} [Ag(C_3H_6)^{+}] \tag{19}$$

The equilibrium constant can be expressed as:

$$K_p = \frac{[Ag(C_3H_6)^{+}]}{[Ag^{+}]p^{0}_{C_3H_6}} \tag{20}$$

Introducing Eq. 12 and solving for the free silver cations concentration:

$$[Ag^{+}] = \frac{[Ag^{T}]}{1 + K_p \cdot p^{0}_{C_3H_6}} \tag{21}$$

The proportionality between the value of K_{FC} and the variables is defined through the fitting parameter α:

$$K_{FC} = \alpha \left(\frac{[Ag^{T}]}{1 + K_p \cdot p^{0}_{C_3H_6}} \right) e^{\frac{Ea_{FC}}{R}\left(\frac{1}{293} - \frac{1}{T}\right)} \tag{22}$$

In Eq. 22 the influence of temperature in the hopping mechanism has been described through an Arrhenius-type expression, and the term in brackets refers to the concentration of free “uncomplexed” silver cations, as obtained from the heterogeneous chemical equilibrium, Eq. 19. The parameter α and the activation energy of the hopping parameter (Ea_{FC}) are the two fitting parameters of the model.

To summarize, the propylene flux is described as the sum of three contributions as follows:

$$J_{C_3H_6} = J_{C_3H_{6,SD}} + J_{C_3H_{6,MC}} + J_{C_3H_{6,FC}} \tag{23}$$

$$J_{C_3H_{6,SD}} = D_{C_3H_6,m} \cdot S_{C_3H_6,m} \frac{p^0_{C_3H_6} - p^L_{C_3H_6}}{L} \tag{24}$$

$$J_{C_3H_{6,MC}} = \frac{k_{eq} \cdot [Ag] \cdot H_{C_3H_6}}{1 + k_{eq} \cdot p^P_{C_3H_8} \cdot H_{C_3H_6}} D_{comp} \frac{p^0_{C_3H_6} - p^L_{C_3H_6}}{L} x_{IL} \tag{25}$$

$$J_{C_3H_{6,MC}} = K_{FC} \cdot \frac{p^0_{C_3H_6} - p^L_{C_3H_6}}{L} (1 - x_{IL}) \tag{26}$$

The contribution of the two different facilitated transport mechanisms was weighted based on the mass fraction of ionic liquid in the membrane composition x_{IL}. This approach assumes that the available silver cations are distributed according to the polymer/ionic liquid mass ratio.

The propane flux is caused by simple Fickian diffusion along the membrane, as described by the following equation:

$$J_{C_3H_{8,SD}} = D_{C_3H_8,m} \cdot S_{C_3H_8,m} \frac{p^0_{C_3H_8} - p^L_{C_3H_8}}{L} \tag{27}$$

The values of the organometallic complex diffusivity and its dependence on temperature were taken from an experimental study on supported ionic liquid membranes (SILMs). These membranes where synthesized introducing the BMImBF$_4$/AgBF$_4$ mixture in the pores of a hydrophilic PVDF support [5]. The value of the equilibrium constant for the complexation reaction, the propylene solubility in the ionic liquid media, and their enthalpies were extracted from absorption equilibria of propylene in ionic liquid/Ag$^+$ solutions [4].

2.3. Modeling and optimization of hybrid and multistage membrane processes

In this part of the PhD thesis, the potential economic savings generated by hybrid membrane-distillation and membrane multistage processes were assessed by comparing the economics of these processes with the distillation base case. In all the studied processes, the feed stream was the head product of a depropanizer column, as is the case for the benchmark distillation [7].

2.3.1. Distillation base case

To quantify the potential economic savings, the conventional distillation was established as base case. The feed stream consists of 360 kmol/h of a liquid propane/propylene equimolar mixture at 323 K and 20.27 bar. The product specifications are 0.995 propylene mole fraction in the distillate stream (i.e. polymer grade) and 0.95 propane mole fraction in the bottoms stream. Table 2.4 itemizes the base case details and economics, which were calculated using the *“Guthrie’s Modular Method for Costing and Sizing”* [8].

Table 2.4. Base case distillation details.

Parameter	*Value*
Feed temperature (K)	323
Feed pressure (bar)	20.27
Feed flowrate (kmol h^{-1})	360
Feed composition (C_3H_6 mol frac.)	0.5
Feed tray[a]	51
Distillation column number of stages	135
Reflux ratio	14.91
Reboiler duty (kW)	15128
Condenser duty (kW)	14169
Dist. temperature (K)	320.05
Dist. pressure (bar)	19.05
Dist. flowrate (kmol h^{-1})	171.43
Dist. composition (C_3H_6 mol frac.)	0.995
Bott. temperature (K)	331.57
Bott. pressure (bar)	20.41
Bott. flowrate (kmol h^{-1})	188.57
Bott. composition (C_3H_6 mol frac.)	0.05
Process CAPEX (MM$)	8.87
Process OPEX (MM$ y^{-1})	4.05
Process NPV COST (MM$)	39.67

[a] Column trays are numbered from bottom to top.

2.3.2. Multistage membrane processes modeling and optimization

The membrane processes assessment was focused on the optimization of the implicit trade-offs in two multistage facilitated transport processes, specifically, one conventional two-stage configuration and another two-stage configuration with a two-step second stage, commonly known as “two-and-one-half” stage process [9]. Figure 2.5 displays the studied flowsheets.

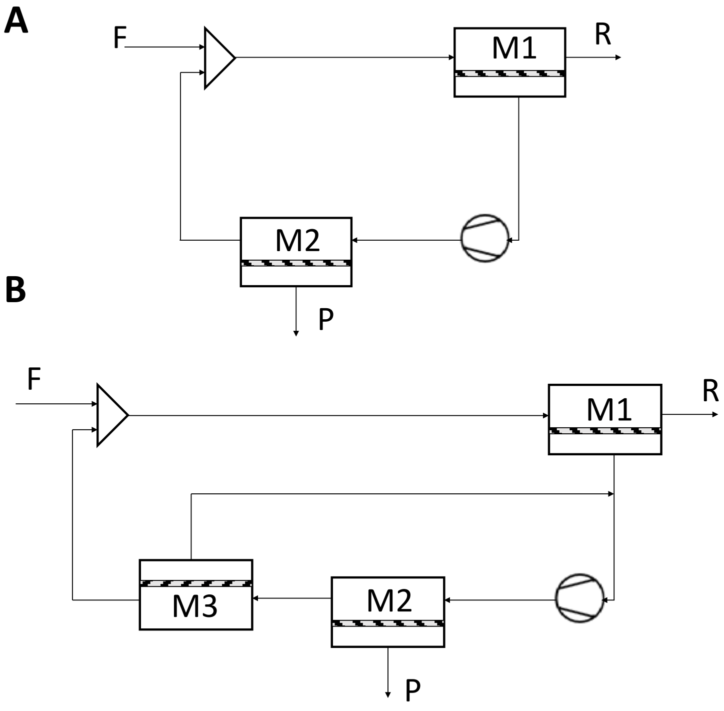

Figure. 2.5. Facilitated transport multistage membrane processes.

In this manner, the complex mixed-integer nonlinear formulations associated to superstructures could be avoided. Additionally, a simultaneous optimization of the process and the membrane material (i.e. carrier load) was possible thanks to the introduction of the previously developed facilitated transport model.

The membrane modules were modelled as hollow fiber modules, which is the most adequate configuration for gas separation, featuring high packing densities and energy efficiency [10–12]. Furthermore, the mass balances in the membrane modules were described as ordinary differential equations and were solved using orthogonal collocation on finite elements [13].

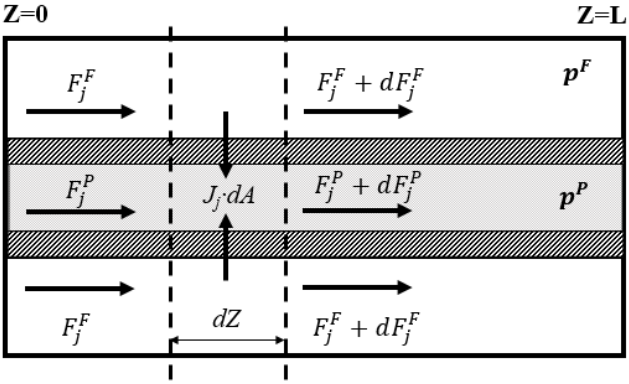

Figure. 2.6. Schematic diagram of the hollow fibers module.

The membrane model is depicted in Figure 2.6 and is based on the following assumptions:

- The feed and retentate streams flow through the shell and lumen sides of the fibers respectively.
- The module operates isothermally and in the steady state.
- The feed and product streams flow in co-current mode.
- Plug-flow is assumed at both sides of the membrane.
- The total feed and permeate pressures are operation constants.
- The only pressure drop in the membrane module is the transmembrane pressure.

The component molar flowrates were discretized according to the following mass balances:

$$dF_j^F(z) = -J_j(z) \cdot dA \tag{28}$$

$$dF_j^P(z) = J_j(z) \cdot dA \tag{29}$$

where F_j and J are the molar flowrate and the transmembrane flux of component j, respectively, and dA is the fiber outer wall area differential element. The dimensionless fiber axial length is defined as:

$$\bar{z} = \frac{z}{L} \qquad \bar{z} \in \ [0,1] \tag{30}$$

where L is the total fiber length. Rearranging terms, the mass balances (ODEs) and the boundary conditions can now be rewritten as:

$$\frac{dF_j^F(\bar{z})}{d\bar{z}} = -J_j(\bar{z}) \cdot A \tag{31}$$

$$\frac{dF_j^P(\bar{z})}{d\bar{z}} = J_j(\bar{z}) \cdot A \tag{32}$$

$$F_j^F|_{\bar{z}=0} = F_j^F(\bar{z} = 0) \tag{33}$$

$$F_j^P|_{\bar{z}=0} = 0 \tag{34}$$

The propylene transmembrane flux was described by implementing the specific model for facilitated transport previously developed. This avoided the use of a fixed permeability parameter and introduced the carrier concentration as a decision variable. In this way, the membrane material and the multistage process could be optimized at the same time.

The ordinary differential equations (Eq. 31-34) were solved as algebraic equations after discretization through implicit Runge-Kutta collocation methods using 100 finite elements and 3 internal collocation points.

The pressure, temperature and composition of the original feed, stream F in Figure 2.5, were fixed by common refinery specifications [7]. Table 2.5 displays the properties of the propylene/propane mixed stream, the target product purities and the process constants and constraints.

Table 2.5. Process feed specifications, parameters and constraints.

Parameter	*Value*
Feed temperature (K)	323
Feed pressure (bar)	18
Feed flowrate (kmol h^{-1})	360
Feed composition (C_3H_6 mole frac.)	0.50
Permeate pressure (bar)	1-18
Required C_3H_6 purity (x_i)	≥ 0.995
Required C_3H_8 purity (x_i)	≥ 0.950
C3H8 permeability (Barrer)[a]	20
Membrane thickness (μm)	20
Silver loading[b] (M)	0-6

[a] 1 Barrer = 10^{-10} cm^3 (STP) cm cm^{-2} s^{-1} $cmHg^{-1}$.

[b] Silver loading delimited according to the experimentally studied concentration range [7,10].

Finally, the objective function (NPVC) was calculated as a combination of OPEX and CAPEX, correcting the operating expenses according to the time value of money:

$$NPVC = CAPEX + OPEX \cdot (1 - (1 + r)^{-T})/r \qquad (35)$$

The compressor expenses were calculated according to the "*Guthrie's Modular Method for Costing and Sizing* " [8] and the membrane cost was calculated using the market prices for its constituents and the optimized composition.

The model constraints accounted for the same propane and propylene product purities established for the distillation base case.

Once the optimization model was solved, it returned:

- The optimal membrane area of each module.
- The optimal carrier concentration of each membrane.
- The optimal permeate pressure.
- The minimal NPVC to reach the separation specifications.

2.3.3. Hybrid membrane-distillation process modeling and optimization

In this work, the performance of state-of-the-art membrane materials to retrofit an existing distillation process was assessed. Taking advantage of the membranes effectiveness when used as concentrators [14], the proposed hybrid configuration uses a membrane stage to perform the bulk separation and the distillation column is left for the final product polishing. Figure 2.7 displays the proposed hybrid arrangement. Given that this hybrid process is intended to retrofit an existing distillation column, the operating costs (OPEX) of the hybrid process were evaluated and compared with the previously described base case distillation. For this reason, the same number of equilibrium stages of the benchmark distillation column was considered in the hybrid configuration.

The design of a membrane/distillation hybrid process involves solving an optimization problem, driven by the existing compromise between the membrane total cost and the column operating expenses.

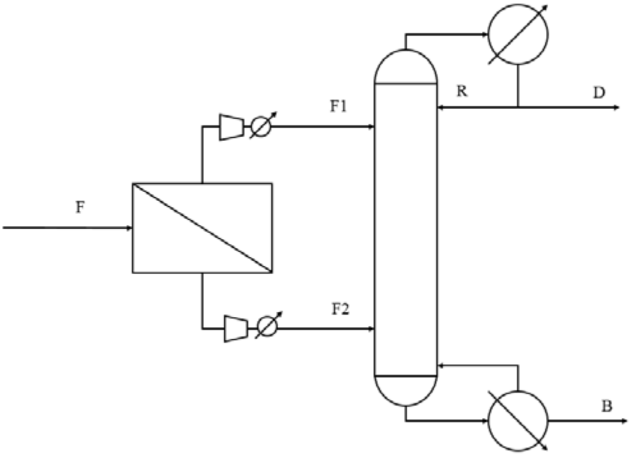

Figure. 2.7. Schematic diagram of the hybrid process.

In this case-study, the mathematical model for the membrane separator described before was implemented. Since the performance of diverse membrane materials was investigated, both propane and propylene transmembrane fluxes were calculated considering the permeability of each species as a material constant. For this reason, a selection of membrane materials to represent the current industrially attractive possibilities for a hybrid process was proposed, including the facilitated transport membranes developed in this PhD thesis. Table 2.6 summarizes the selected membranes features.

Table 2.6. Separation performance of the selected membranes.

Membrane	*C_3H_6 Permeance (GPU^a)*	*C_3H_6 Selectivity*	*Source*
CMS	42	23	[15]
ZIF-8	90	50	[16]
ZIF-8/ZIF-67/ZIF-8	111	210	[17]
PVDF-HFP/BMImBF$_4$/AgBF$_4$	40	150	[18]
6FDA-TeMPD	37^b	8.6	[19]
EC	7	7	[20]

^{a} 1 GPU=3.35x10^{-10} mol/m^2 Pa s
^{b} Calculated from reported permeability assuming 1 µm thickness

Finally, in a second part of this case-study, the permeability-selectivity trade-off exhibited by membrane materials was assessed, introducing an updated trade-off expression in the optimization model. In this way, a wider insight into state-of-the-art membrane performance can be provided.

The model for the distillation column was adapted from the work of Lang and Biegler [21]. A complete description can be found in the original source, here a brief description is presented. Figure 2.8 provides a schematic representation of the modeling strategy.

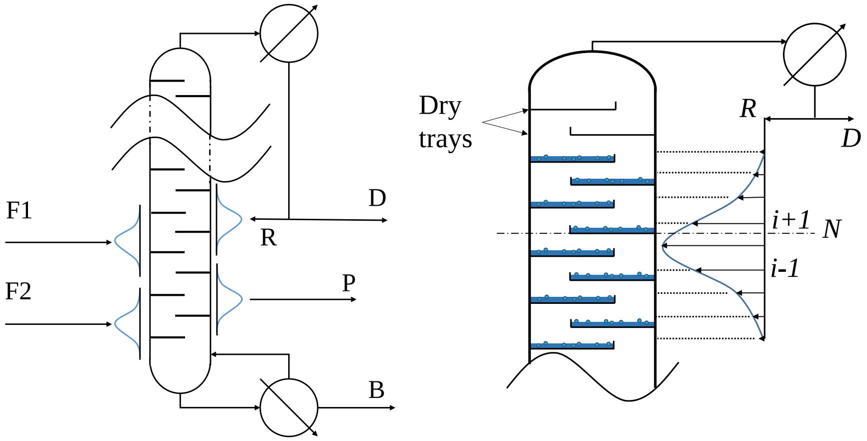

Figure. 2.8. Schematic diagram of the Distributed Stream-Tray Optimization Method (DSTO) and detail of reflux stream DDF.

In order to avoid discrete decision variables, this model uses differentiable distribution functions (DFF) for the feed, reflux and intermediate product streams (if present), in the form:

$$d_i = \frac{exp\left[-\left(\frac{i-N_c}{\sigma}\right)^2\right]}{\sum_k exp\left[-\left(\frac{k-N_c}{\sigma}\right)^2\right]} \quad i,k \in I \qquad (36)$$

which corresponds to the discretization of a Gaussian distribution with mean N_c and standard deviation σ. Thus, using DDFs, the feed and reflux streams can be distributed to all trays:

$$E_i = E \cdot e_i \qquad (37)$$

$$R_i = R \cdot r_i \qquad (38)$$

where E_i and R_i are the feed and reflux flowrates entering into the *i-th* tray, e_i and r_i are the corresponding differentiable distribution functions and E and R and are the total feed and reflux streams, respectively. Once the feed and reflux streams are defined through a DDF, the model uses the conventional MESH equations (material balances, equilibrium, summation and enthalpy balances) to formulate the distillation model. As described in [21] the model is also capable of calculating the number of trays by relaxing the equilibrium equations in the MESH equations so that the liquid phase disappears. This modification of the MESH equations allows dry trays to appear without pressure drop in the non-existing trays space above the reflux insertion point. The optimization model then chooses the column operation with the optimal number of dry trays, which translates to the optimum number of trays required.

The vapor-liquid equilibrium was introduced using the K-value charts for C_3 mixtures [22]. These charts are constructed upon experimental data, later displayed in nomograms. To allow its implementation in computer calculations, a corresponding states type approach has been reported in the bibliography [23]. This approach considers the equilibrium constant value as a function of pressure and temperature exclusively, neglecting the effects of composition. This assumption is valid for propane/propylene mixtures at the pressure and temperature range covered in this study.

The optimization objective was to minimize the total operating costs. Here it was included:

- Membrane depreciation.
- Permeate and retentate recompression.
- Reboiler and condenser duties.

The membrane depreciation was easily calculated as the membrane cost divided by the membrane lifetime, thus obtaining the annualized cost. The compressors, reboiler and condenser annualized operating expenses were calculated converting the resulting duties with the market price of the respective utilities.

Table 2.7 displays the properties of the propylene/propane feed stream, the target product purities and the process constants and constraints.

Table 2.7. Process feed specifications, parameters and constraints.

Parameter	*Value*
Feed temperature (K)	325
Feed pressure (bar)	18
Feed flowrate (kmol h^{-1})	360
Feed composition (C_3H_6 mol frac.)	0.5
Membrane feed side pressure (bar)	18
Membrane permeate side pressure (bar)	1
Distillation column number of stages	135
Distillate purity, $x^{D}_{C_3H_6,min}$	≥ 99.5
Bottoms purity, $x^{B}_{C_3H_8,min}$	≥ 95.0

Finally, the model constraints accounted for the same propane and propylene product purities established for the distillation base case.

Once the solver was run, it provided:

- The minimal operating expenses (and the partial contributions).
- The optimal membrane area.
- The optimal reflux ratio.

- The optimal feed tray locations.

2.3.4. Optimization software

The optimization models of both case-studies were implemented in the General Algebraic Modelling System (GAMS) and solved using the multistart heuristic algorithm OQNLP on a 3.40 GHz Intel® CoreTM i7-3770 processor. CONOPT has been used as local NLP solver for OQNLP with a time limit of 3000 seconds and a maximum of 3000 trial points and 3000 CONOPT calls. The GAMS code of both case-studies can be consulted in *Appendices A.3* and *A.4***.**

2.4. References

[1] M. Fallanza, Progress in the recovery of gaseous olefins. The combined role of membranes, facilitated transport and ionic liquids, Universidad de Cantabria, 2013.

[2] T.C. Merkel, R. Blanc, I. Ciobanu, B. Firat, A. Suwarlim, J. Zeid, Silver salt facilitated transport membranes for olefin/paraffin separations: Carrier instability and a novel regeneration method, J. Memb. Sci. 447 (2013) 177–189.

[3] R.D. Noble, Generalized microscopic mechanism of facilitated transport in fixed site carrier membranes, J. Memb. Sci. 75 (1992) 121–129.

[4] A. Ortiz, A. Ruiz, D. Gorri, I. Ortiz, Room temperature ionic liquid with silver salt as efficient reaction media for propylene/propane separation: Absorption equilibrium, Sep. Purif. Technol. 63 (2008) 311–318.

[5] M. Fallanza, A. Ortiz, D. Gorri, I. Ortiz, Experimental study of the separation of propane/propylene mixtures by supported ionic liquid membranes containing Ag+–RTILs as carrier, Sep. Purif. Technol. 97 (2012) 83–89.

[6] R. Zarca, A. Ortiz, D. Gorri, I. Ortiz, A practical approach to fixed-site-carrier facilitated transport modeling for the separation of propylene/propane mixtures through silver-containing polymeric membranes, Sep. Purif. Technol. 180 (2017) 82–89.

[7] W.L. Luyben, Dynamic simulation of flooded condensers, Chem. Eng. Res. Des. 118 (2017) 12–20.

[8] L.T. Biegler, I.E. Grossmann, A.W. Westerberg, Systematic Methods of Chemical Process Design, Prentice Hall PTR, New Jersey, 1997.

[9] R.W. Baker, Membrane Technology and Applications, 3rd Editio, Wiley, Chichester, 2012.

[10] D.C. Nymeijer, T. Visser, R. Assen, M. Wessling, Composite hollow fiber gas-liquid membrane contactors for olefin/paraffin separation, Sep. Purif. Technol. 37 (2004) 209–220.

[11] D.T. Coker, B.D. Freeman, G.K. Fleming, Modeling multicomponent gas separation using hollow-fiber membrane contactors, AIChE J. 44 (1998) 1289–1302.

[12] C.Y. Pan, Gas separation by high-flux, asymmetric hollow-fiber membrane, AIChE J. 32 (1986) 2020–2027.

[13] J.I. Marriott, E. Sørensen, I.D.L. Bogle, Detailed mathematical modeling of membrane modules, Comput. Chem. Eng. 25 (2001) 693–700.

[14] R. Spillman, Economics of gas separation membrane processes, in: R.D. Noble, S.A. Stern (Eds.), Membr. Sep. Technol. Princ. Appl., Elsevier Science, 1995.

[15] M. Xiaoli, Y.S. Lin, Ultrathin Carbon Molecular Sieve Membrane for Propylene/Propane Separation, AIChE J. 62 (2016) 491–499.

[16] Y. Pan, T. Li, G. Lestari, Z. Lai, Effective separation of propylene/propane binary mixtures by ZIF-8 membranes, J. Memb. Sci. 390–391 (2012) 93–98.

[17] H.T. Kwon, H.K. Jeong, A.S. Lee, H.S. An, J.S. Lee, Heteroepitaxially Grown Zeolitic Imidazolate Framework Membranes with Unprecedented Propylene/Propane Separation Performances, J. Am. Chem. Soc. 137 (2015) 12304–12311.

[18] R. Zarca, A. Ortiz, D. Gorri, I. Ortiz, Generalized predictive modeling for facilitated transport membranes accounting for fixed and mobile carriers, J. Memb. Sci. 542 (2017) 168–176.

[19] K. Okamoto, K. Noborio, J. Hao, K. Tanaka, H. Kita, Permeation and separation properties of polyimide membranes to 1, 3-butadiene and n-butane, J. Memb. Sci. 134 (1997) 171–179.

[20] A. Ito, S. -T Hwang, Permeation of propane and propylene through cellulosic polymer membranes, J. Appl. Polym. Sci. 38 (1989) 483–490.

[21] Y.D. Lang, L.T. Biegler, Distributed stream method for tray optimization, AIChE J. 48 (2002) 582–595.

[22] E.G. Scheibel, F.J. Jenny, Nomographs for Enthalpies of Pure Hydrocarbons and Their Mixtures, Ind. Eng. Chem. 37 (1945) 990–995.

[23] Dimitrios Tassios, Applied Chemical Engineering Thermodynamics, 1993rd ed., Springer, 1993.

Chapter 3

Results summary

Abstract

In this chapter, the main results obtained during the PhD thesis are summarized. In the first place, the experimental results regarding the membrane characterization though spectroscopic, thermogravimetric and microscopy techniques are discussed, paying special attention to the influence and relationships of the membrane structure with the resultant gas transport mechanisms. Then, gas permeation results obtained through time-lag and continuous-flow techniques are presented, exploring the influence of the most relevant operating conditions on the membrane performance and assessing the facilitated transport mathematical model fitting. Finally, the main results on process design and optimization of hybrid and multistage membrane processes are presented. This allowed evaluating the potential of the proposed membranes to intensify the propane/propylene separation process.

3.1. Membrane characterization

In this section, the results of the membrane characterization are presented. SEM and EDX techniques were used to study the membrane morphology and the silver distribution within the facilitated transport membrane, respectively. The thermogravimetric measurements allowed determining the potential water uptake, which is related to the feed humidity influence on the membrane performance. Finally, the spectroscopic techniques (FTIR, Raman and XPS) revealed the interactions between the membrane components, which explain the nature of the facilitated transport mechanisms occurring inside the membrane.

3.1.1. SEM-EDX

Figure 3.1 shows the cross-section and surface of PVDF-HFP, PVDF-HFP/BMImBF$_4$ and PVDF-HFP/BMImBF$_4$/AgBF$_4$ membranes.

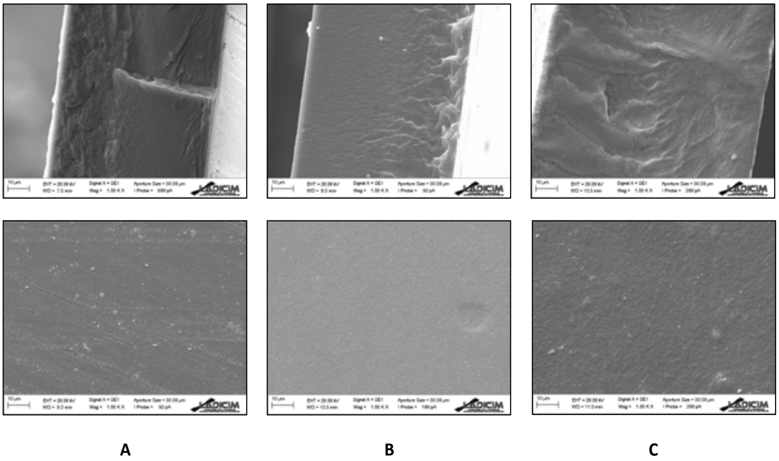

Figure. 3.1. Cross-section and surface morphology of: A) PVDF-HFP membrane B) PVDF-HFP/BMImBF$_4$ membrane, C) PVDF-HFP/BMImBF$_4$/AgBF$_4$ (5.23 mol/l).

The cross-section micrographs show a non-porous homogenous structure without cavities or voids in all three cases. There is no evidence of pure ionic liquid domains in the ionic liquid-containing membranes, Figure 3.1b and 3.1c, proving the complete mixture compatibility between the ionic liquid and the polymer. Furthermore, the addition of the silver salt, Figure 3.1c, does not modify the structure and maintains the original dense and homogeneous pattern.

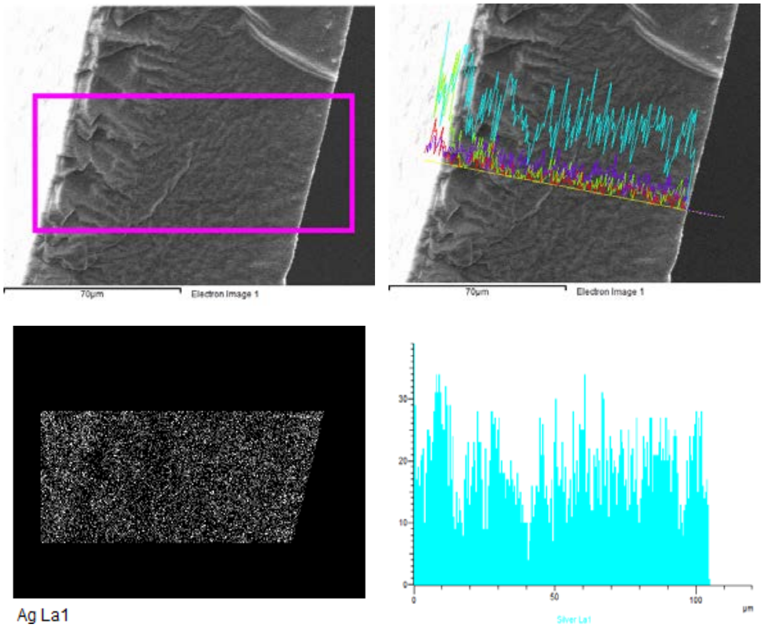

A

B

Figure. 3.2. Energy dispersive X-Ray spectroscopy distribution patterns of silver in the PVDF-HFP/BMImBF$_4$/AgBF$_4$ (5.23 mol/l) membrane: A) dispersion plot, B) scan-line.

The energy dispersive x-ray spectroscopy patterns in Figure 3.2 show a uniform distribution of the element silver along the cross-section of the membrane, with no evidence of silver particles or aggregation formation.

3.1.2. Thermogravimetric analysis (TGA)

The thermogravimetric curves of PVDF-HFP, PVDF-HFP/$AgBF_4$ and PVDF-HFP/$BMImBF_4$/$AgBF_4$ membranes are displayed in Figure 3.3.

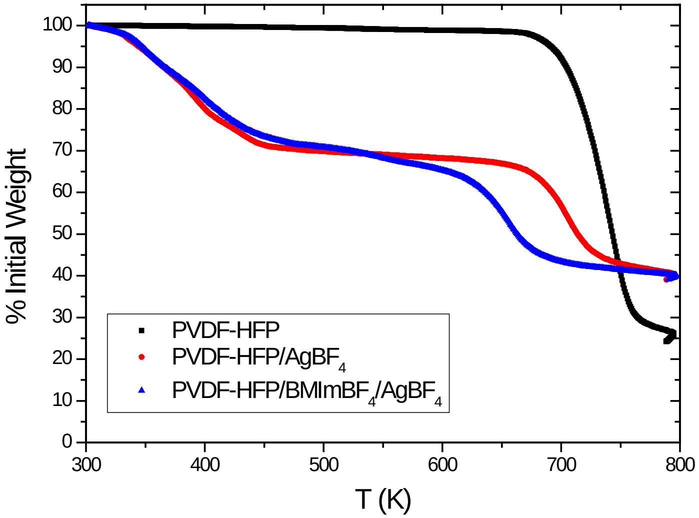

Figure. 3.3. TGA curves of the studied membranes.

The membrane samples were vacuum dried at 30 mbar and 298 K for 24 hours after casting to completely remove the remaining solvent. Prior to testing the samples were exposed to ambient moisture (~80% RH at room temperature) for 24 hours. In this manner, any water loss appearing at the beginning of the temperature ramp can be attributed to water evaporation. According to Figure 3.3, the pure polymer membrane exhibits no weight loss until it reaches its degradation temperature around 680 K, which reveals no water uptake. This is in good agreement with the hydrophobic nature of the fluoropolymer [1]. However, Figure 3.3 shows prominent mass losses of the silver-containing membranes in the 300-436

K temperature range. Thus, it can be concluded that the addition of the $AgBF_4$ salt to the membrane composition dramatically changes the nature of the facilitated transport membranes due to its high hygroscopicity, which results in water uptakes of around 25 wt.% when exposed to moist conditions. Moreover, the ionic liquid-containing membrane features a similar water uptake as the PVDF-HFP/$AgBF_4$ membrane, this is because $BMImBF_4$ is also a hygroscopic substance. Finally, the PVDF-HFP/$BMImBF_4$/$AgBF_4$ membrane starts degrading at 625 K, slightly below the pristine PVDF-HFP and PVDF-HFP/$AgBF_4$ membranes. This is caused by the influence of the ionic liquid on the polymer structure, which yields a multistep decomposition mechanism, as reported by Shalu et al. [2].

3.1.3. Fourier transform infrared spectroscopy (FTIR)

Figure 3.4 shows the polymer CF_2 symmetrical stretching band of PVDF-HFP, PVDF-HFP/$AgBF_4$ and PVDF-HFP/$BMImBF_4$/$AgBF_4$ membranes. The CF_2 peak of the pure polymer appears in the 1178 cm^{-1} band. After incorporation of the silver salt, the stretching band shifted to 1174 and 1172 cm^{-1} in the PVDF-HFP/$AgBF_4$ and PVDF-HFP/$BMImBF_4$/$AgBF_4$ respectively. This shift to lower wavelength indicates a weakening of the C-F bond caused by the interaction of silver cations with the fluorine atoms of the fluoropolymer, which is the basis of the fixed site carrier transport mechanism. This phenomenon has been previously observed by Chang and Kang [3] using FTIR on PVDF-HFP/HBF_4 polymer electrolytes.

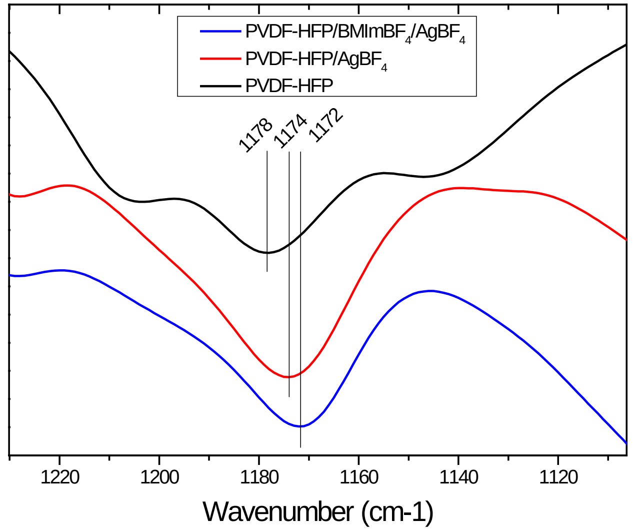

Figure. 3.4. FTIR spectra of the studied membranes.

3.1.4. RAMAN spectroscopy

Raman spectroscopy was used to analyze the regions of the BF_4^- stretching bands in the pure $AgBF_4$, and the silver-containing membranes. Figure 3.5 shows the BF_4^- stretching band region of PVDF-HFP/$AgBF_4$ and PVDF-HFP/$BMImBF_4$/$AgBF_4$ membranes. The symmetric stretching mode of BF_4^- has been previously reported at 774 cm^{-1} in the pure $AgBF_4$ [4]. However, the spectrum in Figure 3.5a shows a wavenumber shift to 767 cm^{-1} when the silver is added to the polymer. According to previous studies, this wavenumber corresponds to free ions [5,6], which means that this change in the Raman spectra is due to well-dissociated Ag^+ cations interacting with the PVDF-HFP backbone. Furthermore, this wavenumber shift from 774 to 767 cm^{-1} is still observable after addition of the ionic liquid $BMImBF_4$, Figure 3.5b. As the

BF_4^- stretching band also appears at 774 cm^{-1} in the pure ionic liquid [6], this shift suggests that the ionic liquid is also interacting with the Ag^+ cations and, to a certain extent, with the polymer backbone, as reported by Fallanza et al. [7].

3.1.5. X-ray photoelectron spectroscopy (XPS)

X-ray photoelectron spectroscopy was used to expand the knowledge on membrane structure and silver degradation. The Ag 3d regions of the XPS spectra can confirm the interactions between the silver cations and the polymer fluorine atoms. Figure 3.6 shows the XPS spectra of a PVDF-HFP/$BMImBF_4$/$AgBF_4$ composite membrane after a long term permeation experiment (110 days). Table 3.1 summarizes the two silver species observable after signal deconvolution. The Ag 3d5/2 band of pure $AgBF_4$ has been previously reported at 369.2 eV. However, in the composite membrane, the binding energy shifted to 368.47 eV. This reduction in the photoelectron binding energy is caused by the coordination between the silver atoms and the polymer backbone as demonstrated by Kim et al. [8], who found the same phenomenon for several $AgBF_4$/polymer blends. Additionally, a second silver species (Ag 3d5/2=368.26 Ag 3d3/2=374.25) is associated with the presence of metallic silver [9], presumably due to the silver reduction caused by the long term permeation test.

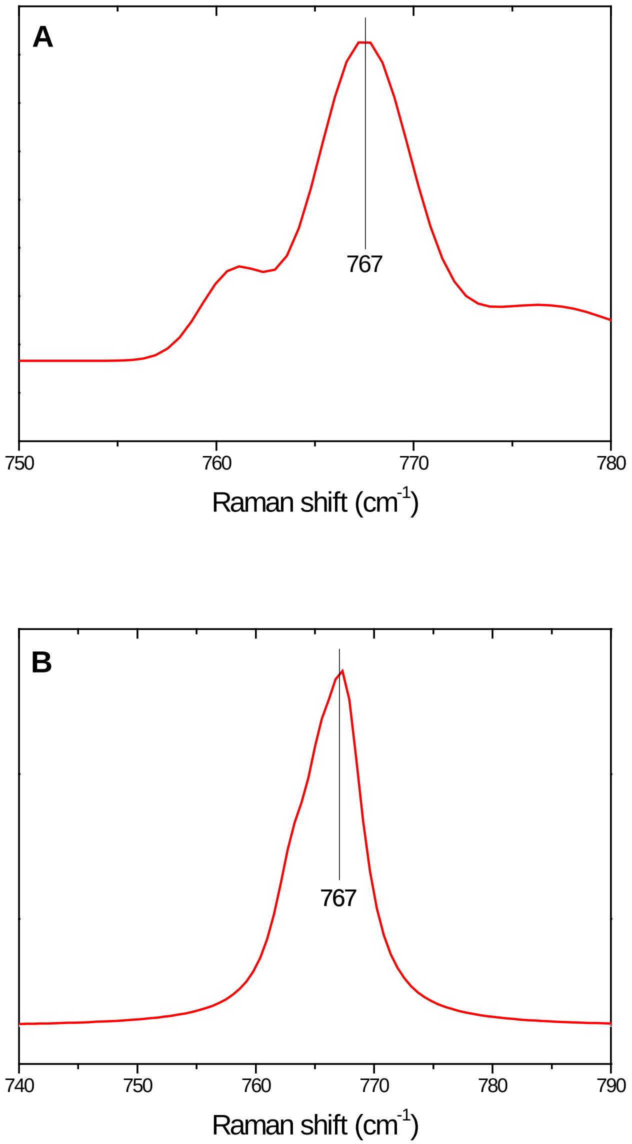

Figure. 3.5. Raman spectra of A) PVDF-HFP /$AgBF_4$ and B) PVDF-HFP/$BMImBF_4$/$AgBF_4$ membrane.

Table 3.1. XPS regions of PVDF-HFP/BMImBF$_4$/AgBF$_4$ membrane after permeation test.

	Region	*Position*
Species A	Ag 3d 5/2	368.47
	Ag 3d 3/2	374.54
Species B	Ag 3d 5/2	368.26
	Ag 3d 3/2	374.25

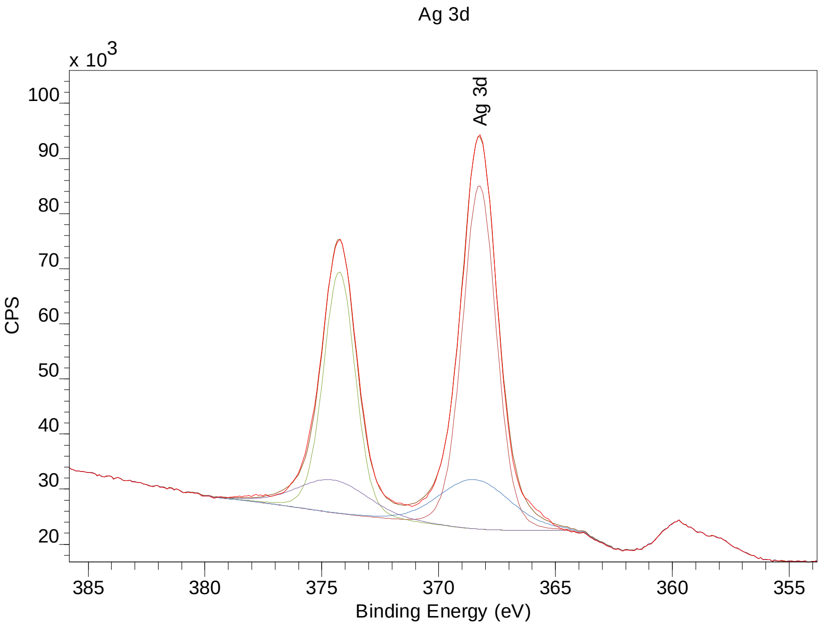

Figure. 3.6. XPS spectra of the PVDF-HFP/BMImBF$_4$/AgBF$_4$ membrane after permeation test.

3.2. Gas permeation and mathematical modeling

In this section, the results of the gas permeation experiments and the mathematical model fitting are discussed. First, the results of time-lag experiments with pure gases are presented. These experiments allowed to determine the gas transport properties of pristine PVDF-HFP and PVDF-HFP/BMImBF$_4$ membranes. Later, continuous-flow experiments with synthetic gas mixtures were performed to study the separation performance of the facilitated transport membranes, assessing the influence of the most important operating conditions (temperature, feed pressure and membrane composition). Additionally, the fitting of the developed mathematical model to the experimental data is reported in this section. Finally, the results of the long-term permeation and the permeation experiments with industrial gas mixtures are discussed.

3.2.1. Time-lag permeation

The experimental diffusivity, solubility and permeability values of propane and propylene in PVDF-HFP and PVDF-HFP/BMImBF$_4$ (80/20 wt.%) at different temperatures were obtained using the time-lag technique. Table 3.2 summarizes the experimental values of diffusivity, solubility and permeability of propane and propylene in PVDF-HFP membranes at different temperatures.

The results in Table 3.2 show a significant increase in permeability with increasing temperature. Given that the physical solubility slightly decreases, this effect of the temperature in the final permeability value is mainly caused by the influence of the diffusivity.

Table 3.2. Diffusivity, solubility and permeability of propylene and propane in PVDF-HFP at 298, 308 and 318 K.

	Temperature (K)	*Diffusivity ($x10^{13}$ m^2 s^{-1})*	*Solubility (mol bar^{-1} m^{-3})*	*Perm. (Barrer)*
C_3H_6	298	0.13	92.4	0.035
	308	0.4	63.1	0.075
	318	1.97	28.4	0.167
C_3H_8	298	0.04	77.8	0.01
	308	0.11	112	0.036
	318	0.16	118	0.058

[a] 1 Barrer = 10^{-10} cm^3 (STP) cm cm^{-2} s^{-1} $cmHg^{-1}$.

Table 3.3 shows the effect of adding the $BMImBF_4$ ionic liquid to the membrane composition. In the ionic liquid-containing membrane the gas diffusivity is markedly enhanced while the solubility decreases. The result is a remarkable permeability increase. This is caused by the ionic liquid entrapped within the dense polymeric matrix, which lowers the polymer chains rigidity and increases the free volume, facilitating the diffusion of the permeant species.

Table 3.3. Diffusivity, solubility and permeability of propylene and propane in PVDF-HFP and PVDF-HFP/$BMImBF_4$ at 298 K.

		Diffusivity ($x10^{13}$ m^2 s^{-1})	*Solubility (mol bar^{-1} m^{-3})*	*Perm. (Barrer)*
PVDF-HFP	C_3H_6	0.13	92.4	0.035
	C_3H_8	0.04	77.8	0.01
PVDF-HFP/$BMImBF_4$ (80/20)	C_3H_6	37.5	16.3	1.821
	C_3H_8	20.3	12.5	0.759

[a] 1 Barrer = 10^{-10} cm^3 (STP) cm cm^{-2} s^{-1} $cmHg^{-1}$.

b Silver loading delimited according to the experimentally studied concentration range .

However, these results confirm that the separation of propane/propylene mixtures by means of solution-diffusion mechanisms in PVDF-HFP membranes is ineffective due to the low permselectivity achieved.

The diffusivity and the physical solubility of propane and propylene in the polymer matrix are later used in the mathematical description of gas transport in the facilitated transport membranes, for this reason, the determination of these parameters is an important step for the mathematical modeling.

3.2.2. Gas-mixture permeation and model fitting

Figure 3.7 shows the propylene transmembrane flux in PVDF-HFP/$AgBF_4$ and PVDF-HFP/$BMImBF_4$/$AgBF_4$ with increasing feed partial pressure. As the partial pressure gradient offers the driving force for the separation process, it has a direct effect on the propylene flux. Nonetheless, the composite membrane performs high olefin fluxes even at the lower assessed partial pressures.

On the other hand, the effect of the temperature increase on the propylene flux is also observable in Figure 3.7. Higher temperatures favor the thermal rearrangements of the polymer chains, enhancing the fixed site carrier transport. Additionally, the diffusion of the gaseous species and the organometallic complex is increased with higher temperatures. As a result the propylene flux increases in both membranes. All these effects hinder the negative influence on the complexation equilibrium constant and the lower gas solubility caused at higher temperatures.

Finally, the addition of the ionic liquid, which gives rise to the mobile carrier transport mechanism, has a major effect on the propylene transport, as can be concluded by comparing the propylene transmembrane flux with and without $BMImBF_4$.

Regarding the separation performance, the high propylene fluxes combined with very low propane fluxes, typically below $1x10^{-5}$ mol m^{-2} s^{-1}, yield selectivity values of around 150.

The mathematical model prediction is noted with black lines in Figure 3.7, and suggests a good fitting of the calculated values. These results demonstrate the model capability to predict the propylene transmembrane flux in the studied range of the variables.

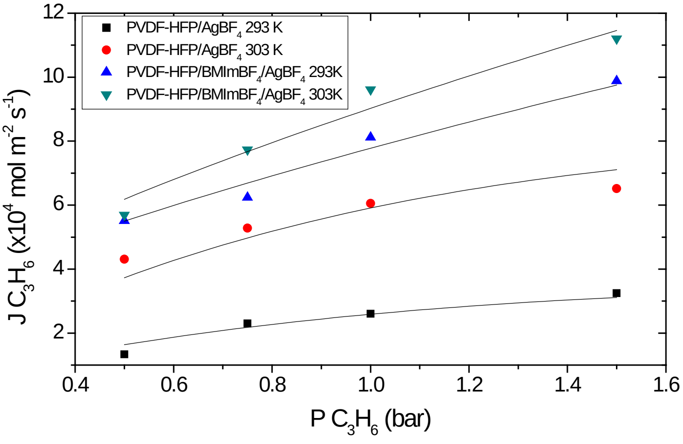

Figure. 3.7. Propylene experimental flux and model prediction in PVDF-HFP/$AgBF_4$ (5.53 mol/l) and PVDF-HFP/$BMImBF_4$/$AgBF_4$ (5.23 mol/l) with increasing partial pressure and 293-303K.

Regarding the propane flux, it can be easily predicted through the solution-diffusion theory using the experimentally obtained permeability.

In order to determine the separation behavior of the composite membranes over an extended period of time, a 110 days long-term permeation test on a PVDF-HFP/BMImBF$_4$/AgBF$_4$ membrane was performed. Furthermore, the effect of the feed gas humidity was assessed. Figure 3.8 shows the propylene and propane transmembrane flux during the experiment, which is divided into five sections (**I-V**) accounting for the relative humidity conditions.

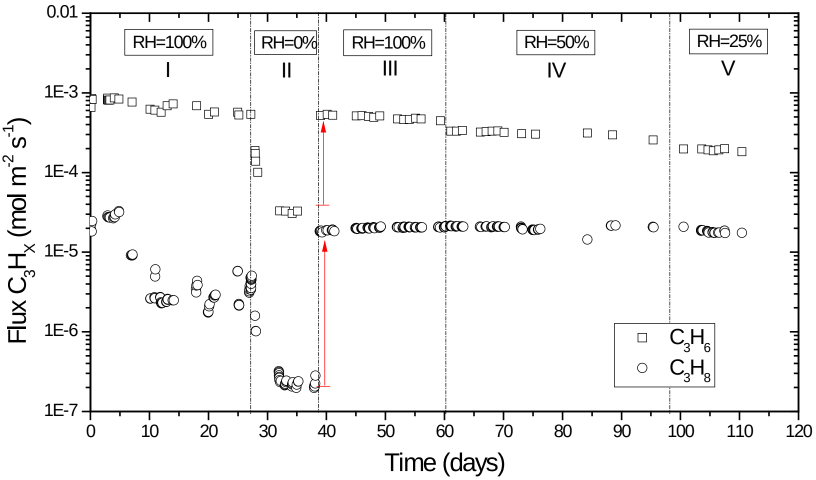

Figure. 3.8. Long term permeation experiment of a PVDF-HFP/BMImBF$_4$/AgBF$_4$ (4 mol/l) composite membrane at 298 K and 1.2 bar feed total pressure (C_3H_8/C_3H_6 50:50) under different relative humidity conditions.

A characteristic feature of these facilitated transport membranes under dry conditions is a sharp decrease of the permeation flux in the first operating hours ostensibly caused by the rapid loss of water and residual solvent by evaporation. To explore this, the humidity was kept at saturation at the beginning of the test (section **I**) and, subsequently, no flux decay was observed during the first 5 days, which confirms that the characteristic curve observed under dry gas conditions is due to solvent and water moisture evaporation.

After 27 days, during section **II**, the feed was changed to dry gases, which resulted in a major propane and propylene transmembrane flux decrease as water evaporation occurred within the membrane.

When the humidified gas mixture (100% RH) was fed again into the system (section **III**), the flux increase of both gaseous species was almost immediate, reaching the flux values attained prior to drying. This abrupt increase, noted with red arrows in Figure 3.8, reveals the exceptional capability of these membranes to absorb water from the environment. During sections **III**, **IV** and **V** a feed gas relative humidity of 100, 50 and 25% was used, respectively. These variations in the humidity conditions resulted in moderate changes in the propylene transmembrane flux while the propane flux remained almost constant at its highest level.

On the other side, it should be noted that, apart from the humidity influence, the propylene transmembrane flux undergoes a continuous slight decrease, evidenced by a constant slope in Figure 3.8. On the contrary, the propane flux does not suffer such decrease, which suggests that this phenomenon is caused by carrier deactivation. It was possible to quantify the deactivation rate by fitting the data for each section (**I-V**), to an exponential curve, which yielded the following expression:

$$J_{C_3H_6}(t) = J_{C_3H_6}(t_0) \cdot e^{-5.5x10^{-3} \cdot t} \qquad (39)$$

where $J_{C_3H_6}(t_0)$ is the initial propylene transmembrane flux at a given membrane composition, temperature, pressure and relative humidity conditions and the time *t* is introduced in days. This expression allows for membrane lifetime calculation if a minimum required performance is established.

Finally, combining a mathematical expression for the drying curve (Figure 3.8 section **II**) with the propylene flux at each relative humidity, it was possible to obtain a fitting curve for the propylene transmembrane flux as a function of the relative humidity (Eq. 40), Figure 3.9.

$$J_{C_3H_6}(RH) = 5.82x10^{-5} RH^{0.49} \tag{40}$$

Figure 3.9 evidences a sharp increase in the propylene flux with the relative humidity for RH<10% and a smooth increase after that value (dash line in Figure 3.9). A similar trend was reported by Catalano et al. [10] for oxygen and nitrogen in PFSI membranes.

Finally, Table 3.4 displays the permeability and selectivity values of the facilitated transport membrane for each relative humidity condition. The humidification of the feed gases produces major changes in the membrane performance, reducing the selectivity and increasing the permeability of both the olefin and the paraffin. This is a characteristic effect of water vapor-induced swelling [11,12]. The enlargement of the polymer free volume caused by the water uptake increases the diffusivity of the gaseous species and the propylene-silver complex, which leads to remarkable permeability values but at the expense of membrane selectivity.

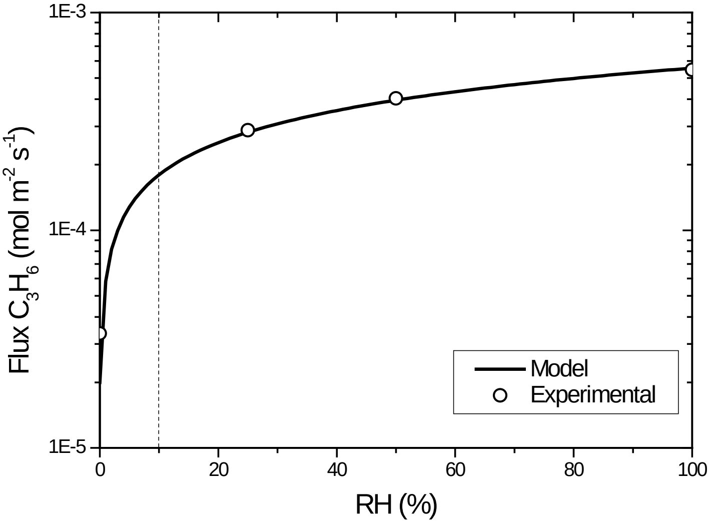

Figure. 3.9. Experimental data and mathematical regression for the dependency of the propylene transmembrane flux on the relative humidity.

Table 3.4. Average permeability and selectivity values of the PVDF-HFP/BMImBF$_4$/AgBF$_4$ membrane for each relative humidity during the long-term permeation test.

RH (%)	*P C_3H_8 (Barrer)*[a]	*P C_3H_6 (Barrer)*[a]	*α C_3H_6/C_3H_8 (-)*
0	1.2	172	144
25	97.3	1032	11
50	107.6	1666	16
100	106.5	2555	24

[a] 1 Barrer = 10^{-10} cm^3 (STP) cm cm^{-2} s^{-1} cmHg^{-1}.

3.2.3. Industrial gas mixture permeation

Figure 3.10 shows the facilitated transport membrane performance when the feed consists of a real propane/propylene mixture compared with a synthetic gas mixture. The industrial gas mixture is the product stream of a fluid catalytic cracking unit and its composition is displayed in Table 2.1. It mostly consists of a propane/propylene mixture (25:75) containing minor quantities of light paraffins and olefins.

Given that both feeds differ in composition, permeability, which is normalized by the partial pressure gradient, has been plotted instead of the transmembrane flux. Both permeation experiments have been performed under dry conditions to simulate refinery conditions, hence, both suffer the characteristic permeability decrease due to solvent and water evaporation in the first hours of operation. Since the propylene transmembrane flux is similar in both cases, Figure 3.10 evidences that the membrane performance is not affected by known contaminant trace components potentially present in industrial streams (i.e. acetylene, hydrogen sulfide and hydrogen [13]) during the experiment extent.

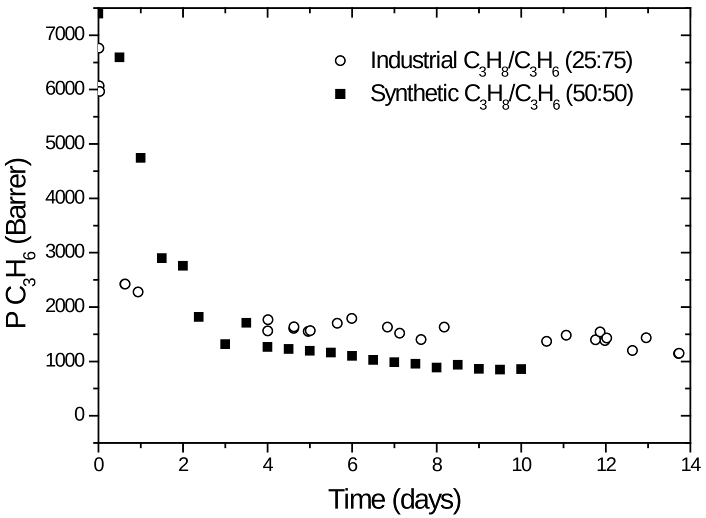

Figure. 3.10. Synthetic and industrial gas mixture permeation experiments on a PVDF-HFP/BMImBF$_4$/AgBF$_4$ membrane under dry conditions at 298 K and 1.2 bar total feed pressure.

3.3. Process design and optimization

In this section, the main results of process design and optimization are reported. The design and optimization methodology followed to obtain these results has been previously explained in *Chapter 2*. First, the hybrid membrane/distillation process is discussed, analyzing the OPEX savings potentially achieved when the membrane separator is used as a bulk concentrator and the existing distillation process is left for the final product refining. Then, the multistage membrane process approach is discussed. The use of the mathematical model to describe the propylene transmembrane flux allowed simultaneous optimization of the process and the membrane composition. These results complement the experimental study on membrane performance, aiming at the global objective of assessing the role of facilitated transport membranes in the intensification of propylene/propane separation processes.

3.3.1. Membrane/distillation hybrid process

The hybrid process optimization allowed calculating the operating expenses reduction achieved by retrofitting an existing distillation column with a membrane contactor. In the first place, several state-of-the-art membrane materials were studied for its implementation in the hollow fiber configuration, including the PVDF-HFP/$BMImBF_4$/$AgBF_4$ composite membranes developed by the research group. Next, the current membrane upper bound was introduced in the model to study the desirable permeability/selectivity combination of a hypothetically optimal membrane material. Additionally, the impact of the membrane cost on the economic evaluation was assessed.

The purity constraints introduced in all calculations considered a propylene purity of 99.5 mol.% and a propane purity of 95.0 mol.% in the head and tail streams of the distillation column, respectively.

Table 3.5 displays the resultant membrane area, reflux ratio and potential savings derived from the implementation of each selected membrane material in a hybrid configuration. The highly permeable and highly selective zeolitic imidazolate frameworks (ZIFs), carbon molecular sieves (CMS) and facilitated transport membranes (membranes **A-D**) can potentially reduce the operating expenses by around 30 to 55%. In addition, advanced polyimides, as 6FDA-TeMPD (**E**), which provide high permeance but moderate selectivity, are still capable of reducing the total operating costs “TOC” by 18%. Finally, the cellulosic membrane (**F**), due to its low permeance and selectivity, achieves a total operation costs reduction of around 10%.

Table 3.5. Membrane/distillation hybrid process optimization results.

ID	*Membrane*	*Area ($x10^3$ m^2)*	*Reflux*	*TOC Savings (%)*
-	None	-	14.9	0
A	ZIF8 / ZIF67/ZIF8	2.8	4.5	56.2
B	PVDF-HFP/$AgBF_4$/$BMImBF_4$	7.4	5.3	50.3
C	ZIF 8	2.9	7.4	38.3
D	6FDA-based polyimide CMS	5.8	8.7	29.2
E	6FDA-TeMPD	5.3	10.5	17.6
F	EC	23.2	11.2	9.9

The operating expenses reduction due to the implementation of a hollow fiber module in series is clearly related to the decrease in the required reflux ratio for a given product quality. Although the reboiler and condenser duties are very similar, the use of steam requires that more than 95% of the base case operating costs are generated by the reboiler. Figure 3.11 unfolds the total operating expenses for each case. As expected, the membrane module helps reducing the required reflux ratio, decreasing the steam supply to the reboiler and its associated cost. It is worth noting that, despite this reduction, the reboiler operating cost is still the largest contribution to the total operating costs, while the condenser and retentate compressor operating costs are almost negligible.

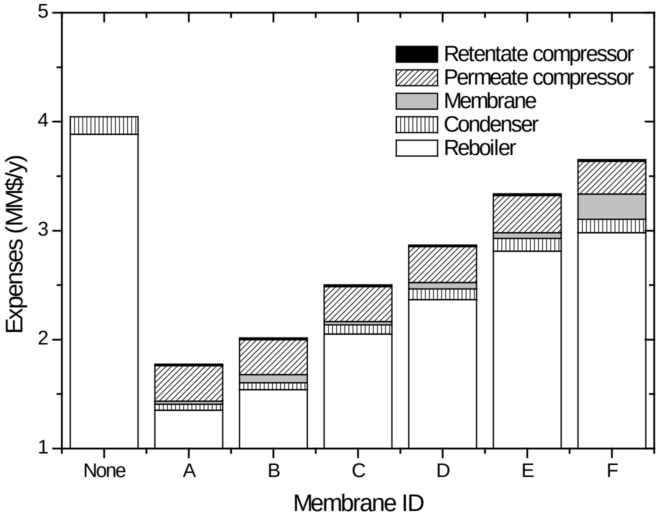

Figure. 3.11. Disaggregated operating costs for each case. A-F defined in Table 3.5.

Since the hybrid configuration may become uncompetitive compared to the conventional distillation depending on the membrane unitary cost, a sensitivity analysis of the optimum solutions was performed. Figure 3.12 displays the total operating cost variation for each membrane with increasing membrane prices up to 200$/m^2. In all cases, with the exception of the cellulosic membrane (**F**), the optimal configuration does not vary significantly, and the resultant TOC increase is proportional to the optimal membrane area. On the other hand, the cellulosic membrane hybrid configuration, due to the large area required, is not suitable for replacing the base case distillation when the membrane cost exceeds ~100$/m^2, and consequently, the membrane module has been removed during the optimization run.

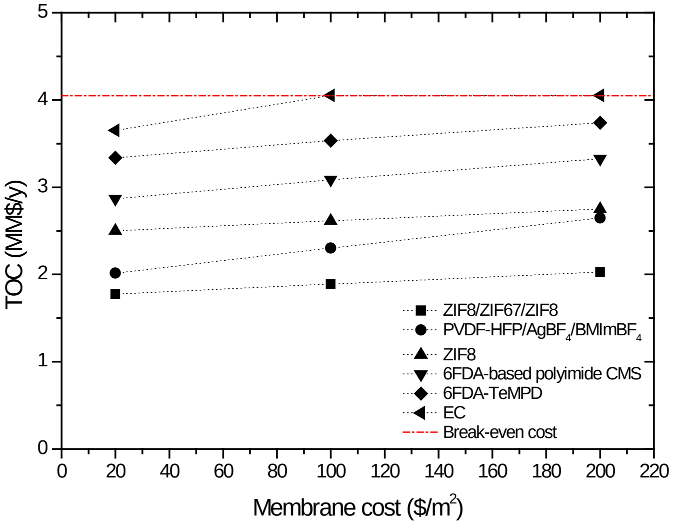

Figure. 3.12. Effect of the membrane cost on optimal TOC for the studied membranes.

This analysis reveals a remarkable range of suitability for medium to high performance membrane materials when implemented in a hybrid configuration, regarding the membrane production cost.

An interesting point when dealing with membranes is the trade-off existing between selectivity and gas permeability, which is limited by the upper-bound in the Robeson plot. By introducing the Robeson plot upper-bound expression in the optimization model we can explore the optimal permeability and selectivity values of a hypothetically optimal membrane material, given the membranes state-of-the-art [14,15]. Figure 3.13 represents an updated Robeson plot for propane/propylene mixtures.

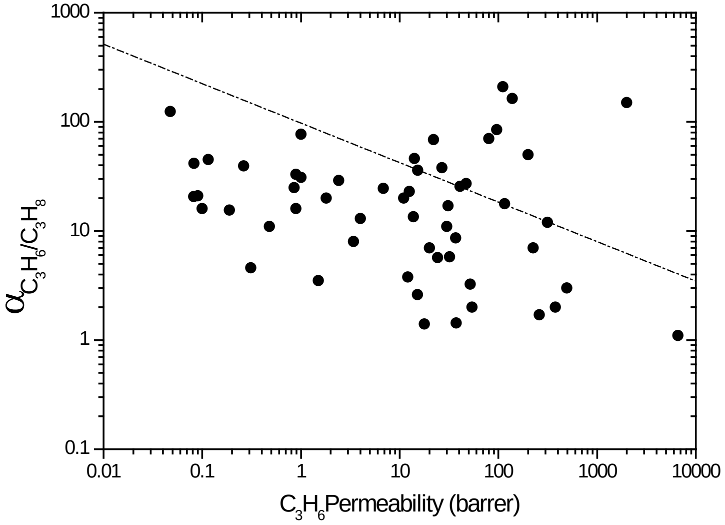

Figure. 3.13. Robeson plot for propane/propylene separation membranes displaying the upper-bound.

The corresponding mathematical expression is:

$$\alpha_{C_3H_6/C_3H_8} = 97.51 {P_{C_3H_6}}^{-0.362} \tag{41}$$

Once the upper-bound is introduced in the optimization problem, in addition to membrane area, reflux ratio and stream locations, the program also provides the optimal balance between permeability and selectivity. An active layer thickness of 1µm has been assumed, as this is a typical value in the hollow fiber manufacture.

Table 3.6. Upper-bound optimization results.

	Membrane cost ($/m^2)		
	20	100	200
Propylene permeability (Barrer[a])	16	74	134
Propylene selectivity	36	21	17
Membrane area (x10^3 m^2)	15	3.1	1.6
Reflux ratio	8	8.9	9.3
TOC (MM$/y)	2.77	3.02	3.13
Savings (%)	31.5	25.5	22.8

[a] 1 Barrer = 10^{-10} cm^3 (STP) cm cm^{-2} s^{-1} cmHg^{-1}.

It is worth noting the strong influence of the membrane cost on the optimal permeability/selectivity trade-off. As the membrane cost weight on the objective function increases, the membrane tends to increase the permeability at the expense of selectivity. In the most unfavorable case (i.e. 200$/m^2) the membrane is highly permeable and the selectivity falls to a value closer to the feed-to-permeate pressure ratio (18/1), which allows a prominent decrease in the required area while still maintaining an adequate permeate purity. These results are in good agreement with Huang et al. [16] findings on the pressure ratio-selectivity relationship: “High permeance membranes are always good, but the optimum membrane selectivity depends on the process and the operating conditions, particularly the pressure ratio”. Increasing the membrane selectivity far beyond the industrially suitable pressure ratio produces minor increments in the product purity at the expense of larger membrane areas, as the process enters in the pressure ratio-limited region.

3.3.2. Multistage membrane processes

This section presents and discusses the main results regarding the design and optimization of the proposed multistage membrane flowsheets. The feed stream to both flowsheets consisted of an equimolar propane/propylene mixture and the objective was to obtain propylene and propane purities of 99.5 mol.% and 95 mol.% respectively. The Net Present Value Cost (NPVC) of both multistage processes was compared with the NPVC of the reference distillation column. Additionally, a case-study considering a required propylene purity of 99.9 mol.% was studied to determine the influence of the purity constraints on the optimal solutions.

The optimized two stage flowsheet is displayed in Figure 3.14. The optimal design comprises two membrane stages showing considerable size differences. The first stage requires more than 14000 m^2 of membrane area to generate a propylene depleted retentate stream, thus achieving the desired propane purity. However, the second stage area is almost ten times smaller and is intended to produce a high purity propylene permeate regardless of the retentate purity.

Regarding the optimal carrier loading, its value is allowed to vary between the experimentally studied range from 0 to 6 M, where 0 M implies no facilitated transport and 6 M is the highest concentration assessed for PVDF-HFP/$BMImBF_4$/$AgBF_4$ membranes. Eventually, the optimization balances the cost-performance trade-off of the first stage at 2.51 M Ag^+, far below the upper limit. Since higher concentrations of carrier result in high membrane prices per unit area, this decreased optimal value helps to reduce the expenses caused by the large size of this stage. On the other hand, the second stage carrier loading hits the highest allowed level of 6 M Ag^+, which is consistent with the purity-oriented nature of this stage. Although the high carrier loading of the second stage raises the membrane specific cost to 324 $/m^2, the relative small size of this stage dampens the total membrane cost.

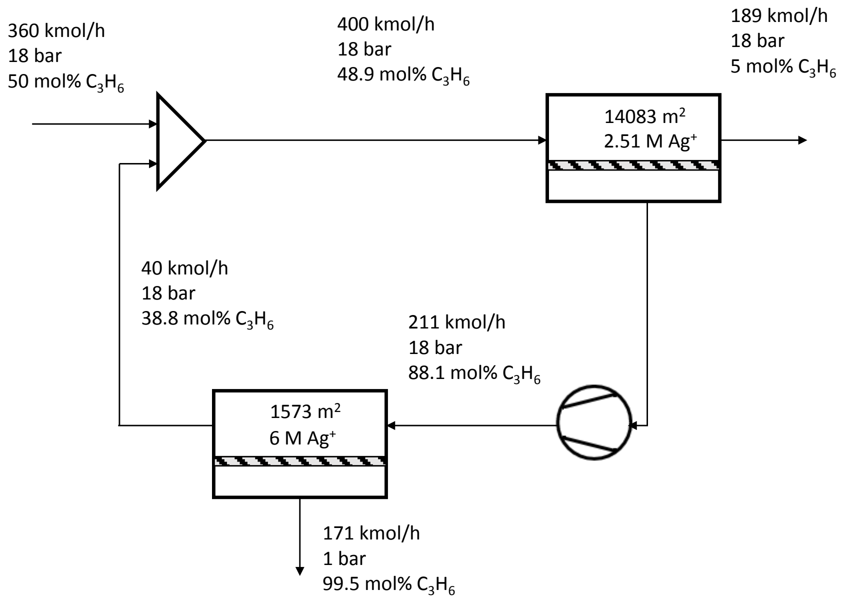
360 kmol/h
18 bar
50 mol% C_3H_6
400 kmol/h
18 bar
48.9 mol% C_3H_6
189 kmol/h
18 bar
5 mol% C_3H_6
14083 m^2
2.51 M Ag^+
40 kmol/h
18 bar
38.8 mol% C_3H_6
211 kmol/h
18 bar
88.1 mol% C_3H_6
1573 m^2
6 M Ag^+
171 kmol/h
1 bar
99.5 mol% C_3H_6

Figure. 3.14. Two stage process optimal design.

Finally, it should be noted that this multistage configuration generates a large reflux stream with high associated compression costs. Nonetheless, the optimal permeate pressure of both stages falls to 1 bar, promoting higher driving force in the modules at the expense of higher compression duty.

The “two-and-one-half stage” process optimization results are shown in Figure 3.15. The main feature of this process is the introduction of a third stage intended to recycle a propylene enriched stream back to the second stage feed, in this manner the outer loop recycle is reduced, minimizing the total membrane area requirements in the stage M1 and the subsequent compression duty.

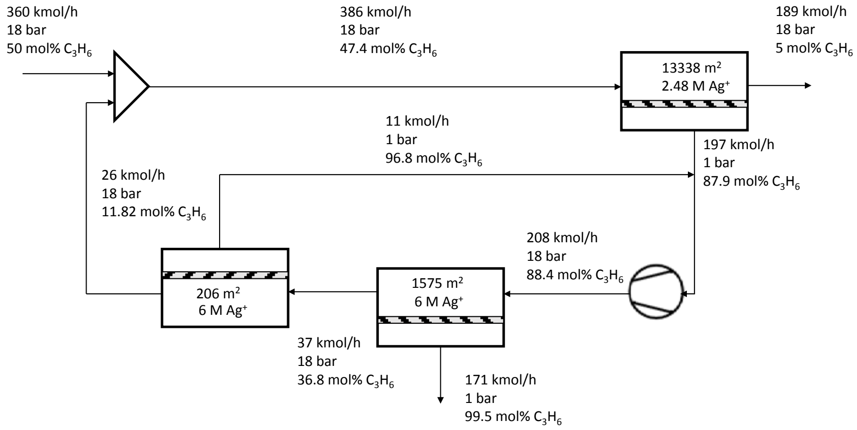
360 kmol/h
18 bar
50 mol% C_3H_6
386 kmol/h
18 bar
47.4 mol% C_3H_6
189 kmol/h
18 bar
5 mol% C_3H_6
13338 m^2
2.48 M Ag$^+$
11 kmol/h
1 bar
96.8 mol% C_3H_6
197 kmol/h
1 bar
87.9 mol% C_3H_6
26 kmol/h
18 bar
11.82 mol% C_3H_6
208 kmol/h
18 bar
88.4 mol% C_3H_6
1575 m^2
6 M Ag$^+$
206 m^2
6 M Ag$^+$
37 kmol/h
18 bar
36.8 mol% C_3H_6
171 kmol/h
1 bar
99.5 mol% C_3H_6

Figure. 3.15. Two-and-one-half stage process optimal design.

As in the two stage process, the first stage (M1) is significantly larger than the next stages (M2 and M3) and its optimal carrier concentration is below the upper bound, at 2.48 M Ag$^+$. Again, the M2 and M3 stages require the maximum carrier loading of 6 M Ag$^+$, which increases the membrane performance at the expense of higher membrane costs. However, although the introduction of a third stage helps to minimize the compression requirements by decreasing the recycle flowrate, this reduction is not significant enough and may not justify its implementation. This can be observed by the relative small size of stage M3, which is almost negligible compared with the other stages.

The NPVC of both membrane processes and the base case distillation are itemized in Table 3.7. The results reveal the prominent potential of facilitated transport membrane processes to replace the traditional distillation and to sharply decrease the investment expenses when implementing the two stage membrane process. On the other hand, the introduction of an additional separation step in the “two-and-one-half” stage flowsheet produces minor savings compared to the two stages process and, therefore, a less complex process may be preferred. It is worth noting that the main difference between the base case distillation and the membrane processes is not in the capital expenses but in the operating costs, which is consistent with the use of process steam in the distillation reboiler. Consequently, process intensification through membrane technology plays here a major role in energy saving.

Table 3.7. Multistage processes Net Present Value Cost compared to the distillation base case.

	Distillation	*Two Stages*	*"Two-and-one-half" Stages*
OPEX (MM$ y^{-1})	4.1	0.86	0.85
CAPEX (MM$)	8.9	5.0	4.9
NPVC (MM$)	39.7	11.56	11.4

Although propylene purities higher than 99.5% are not demanded by the polypropylene industry, it is instructive to consider a final comparison between the two-stage and two-and-half stage optimization models. For a propylene permeate specification of 99.9% we observe that the two stage process becomes infeasible and has no solution. In contrast, the two-and-half stage model is able to provide any permeate concentration, and consequently satisfies this specification. As shown in Table 3.8, the optimum for this process is achieved at a much higher cost, with more than double the NPVC.

Table 3.8. Multistage processes Net Present Value Cost for 99.9% propylene specification

	Propylene 99.5 %		*Propylene 99.9 %*	
	2 St.	*2.5 St.*	*2 St.*	*2.5 St.*
OPEX (MM$ y^{-1})	0.86	0.85	Not Feasible	2.05
CAPEX (MM$)	5.0	4.9		8.74
NPVC (MM$)	11.56	11.4		24.3

3.4. References

[1] X. Tian, X. Jiang, Poly(vinylidene fluoride-co-hexafluoropropene) (PVDF-HFP) membranes for ethyl acetate removal from water, J. Hazard. Mater. 153 (2008) 128–135.

[2] Shalu, S.K. Chaurasia, R.K. Singh, S. Chandra, Thermal stability, complexing behavior, and ionic transport of polymeric gel membranes based on polymer PVdF-HFP and ionic liquid, [BMIM][BF_4], J. Phys. Chem. B. 117 (2013) 897–906.

[3] J. Chang, S.W. Kang, CO_2 separation through poly(vinylidene fluoride-co-hexafluoropropylene) membrane by selective ion channel formed by tetrafluoroboric acid, Chem. Eng. J. 306 (2016) 1189–1192.

[4] E. Goreshnik, Z. Mazej, X-ray single crystal structure and vibrational spectra of AgBF4, Solid State Sci. 7 (2005) 1225–1229.

[5] Y.S. Park, S. Chun, Y.S. Kang, S.W. Kang, Durable poly(vinyl alcohol)/$AgBF_4$/$Al(NO_3)^3$ complex membrane with high permeance for propylene/propane separation, Sep. Purif. Technol. 174 (2017) 39–43.

[6] D. Ji, Y.S. Kang, S.W. Kang, Accelerated CO_2 transport on surface of AgO nanoparticles in ionic liquid $BMIMBF_4$, Sci. Rep. 5 (2015) 16362.

[7] M. Fallanza, A. Ortiz, D. Gorri, I. Ortiz, Polymer-ionic liquid composite membranes for propane/propylene separation by facilitated transport, J. Memb. Sci. 444 (2013) 164–172.

[8] J.H. Kim, S.W. Kang, Y.S. Kang, Threshold silver concentration for facilitated olefin transport in polymer/silver salt membranes, J. Polym. Res. 19 (2012) 9753.

[9] T.C. Kaspar, T. Droubay, S.A. Chambers, P.S. Bagus,

Spectroscopic Evidence for Ag(III) in Highly Oxidized Silver Films by X-ray Photoelectron Spectroscopy, J. Phys. Chem. C. 114 (2010) 21562–21571.

[10] J. Catalano, T. Myezwa, M.G. De Angelis, M.G. Baschetti, G.C. Sarti, The effect of relative humidity on the gas permeability and swelling in PFSI membranes, Int. J. Hydrogen Energy. 37 (2012) 6308–6316.

[11] W.S. Ho, D.C. Dalrymple, Facilitated transport of olefins in Ag+-containing polymer membranes, J. Memb. Sci. 91 (1994) 13–25.

[12] S. Hong, Effect of water on the facilitated transport of olefins through solid polymer electrolyte membranes, J. Memb. Sci. 181 (2001) 289–293.

[13] T.C. Merkel, R. Blanc, I. Ciobanu, B. Firat, A. Suwarlim, J. Zeid, Silver salt facilitated transport membranes for olefin/paraffin separations: Carrier instability and a novel regeneration method, J. Memb. Sci. 447 (2013) 177–189.

[14] J.A. Caballero, I.E. Grossmann, M. Keyvani, E.S. Lenz, N. Square, V. Pennsyl, Design of hybrid distillation - vapor membrane separation systems, Ind. Eng. Chem. Res. 48 (2009) 9151–9162.

[15] L.M. Robeson, The upper bound revisited, J. Memb. Sci. 320 (2008) 390–400.

[16] Y. Huang, T.C. Merkel, R.W. Baker, Pressure ratio and its impact on membrane gas separation processes, J. Memb. Sci. 463 (2014) 33–40.

Chapter 4

General conclusions and prospective view / Conclusiones generales y perspectivas

Abstract

This chapter highlights the most important findings achieved in the course of this thesis. The main conclusions extracted from both the experimental and the modeling work are presented, along with a brief discussion on the future outlook of the proposed technology. Even more important, some remarks on the remaining challenges that can condition the industrial applicability of the developed membranes are showcased for further research.

4.1. General conclusions

The main objective of this thesis is to assess the potential of novel PVDF-HFP/BMImBF$_4$/AgBF$_4$ composite membranes to replace current propane/propylene separation processes. In order to fulfill this objective, a thorough work on experimental characterization and modeling has been performed. The main conclusions drawn from the analysis of the results are now itemized:

a) PVDF-HFP/BMImBF$_4$/AgBF$_4$ facilitated transport composite membranes have been synthesized through the solvent casting method. The result is a dense homogeneous material with good mechanical properties.

b) The characterization techniques used to reveal the membrane structure confirm the formation of dense membranes and the existence of the chemical species and the interactions required to enable the facilitated transport mechanisms (i.e. fixed-site and mobile carriers). The evidences of such interactions comprise, on the one hand, the weakening of the C-F bound of the polymer CF$_2$ groups detected through FTIR and XPS, which is caused by the interaction between Ag$^+$ cations and the fluorine atoms of the PVDF-HFP, giving rise to a fixed-site carrier mechanism. And, on the other hand, the existence of free silver ions and uncomplexed ionic liquid within the polymer free volume, as revealed by Raman spectroscopy, which induces a mobile carrier transport mechanism.

c) The time-lag permeation technique of propane and propylene pure gases in PVDF-HFP and PVDF-HFP/BMImBF$_4$ membranes allowed calculating the diffusivity and solubility parameters of the permeant species in the polymer and polymer/ionic liquid matrices, which are valuable data for the rigorous development of a mathematical model. Additionally, these data confirm that the separation of propane/propylene mixtures only by means of the solution-diffusion mechanism in PVDF-HFP is unsuccessful. Finally, the addition of $BMImBF_4$ dramatically increases the gas diffusivity and slightly decreases the gas solubility. The result is a remarkable permeability enhancement caused by the plasticization effect of the ionic liquid upon addition in the polymer matrix.

d) Continuous-flow permeation experiments with gas mixtures determined the promising propylene/propane separation capabilities of the composite membranes under several operating condition, namely temperature, feed pressure, membrane composition and feed relative humidity. The results show propylene permeability values of roughly 200 Barrer and a propylene selectivity higher than 150 under dry conditions. On the other hand, it is worth highlighting the accused influence of the feed humidity on the membrane performance, yielding a propylene permeability higher than 2000 Barrer at 100%RH of the feed stream. However, this is achieved at the expense of the propylene selectivity, which is lowered to 20 at the above mentioned conditions. The TGA results confirm water uptakes of 25 wt.% of the silver-containing membranes, which explain this behavior under humid conditions.

e) A 110-days-long permeation experiment allowed quantifying the influence of silver degradation on the long-term membrane performance, which, albeit subtle, could affect the industrial applicability of the proposed membranes. This will depend on the membrane lifetime required for the economic sustainability of the separation process. XPS spectroscopy revealed that the degradation mechanism comprises the reduction of Ag^+ to Ag^0. Eventually, permeation experiments with real propane/propylene mixtures supplied by a petrochemical company revealed no additional degradation caused by the potential presence of minor contaminants.

f) The experimental data served to develop a semi-predictive mathematical model able to describe the transmembrane flux of the permeant species in the studied range of the operating variables. The model fitting to the experimental data confirms its usefulness for later process design and optimization.

g) The viability of the proposed membrane material for its industrial application has been studied through the design and optimization of membrane separation processes. A partial introduction of this technology in the form of a hybrid membrane/distillation process, as well as a full replacement of the distillation by multistage membrane processes have been assessed. The results reveal that the hybrid system could generate OPEX savings between 33 and 50% compared to the distillation base-case, depending on the final composite membranes price. On the other hand, a comparison of the Net Present Value Cost revealed that a two-stage process has a total NPVC of around 25% of the traditional distillation, while a two-and-one-half-stage process has no advantages unless the propylene purity required exceeds the current industry demands.

On the whole, these results confirm the remarkable potential of PVDF-HFP/BMImBF$_4$/AgBF$_4$ membranes implemented in alternative membrane-based separation processes to attain process intensification in the industrial propylene/propane separation. However, achieving full industrial applicability requires solving further challenges. First, the carrier degradation issues may shorten the membrane lifetime beyond a competitive standard. On the other hand, the membrane configuration plays a major role at the industrial scale, where high packing densities and ultrathin active layers are almost mandatory to ensure the economic sustainability of the whole process.

4.2. Recommendations for future research

Based on the general conclusions extracted from this thesis, and having identified the main obstacles encountered in the path to full industrial applicability, this section offers a brief guidance for future research works:

- Study possible strategies to solve the carrier degradation issues. This goal can be approached by developing degradation inhibitors that can be added as additives in the membrane composition. Other possibility comprises the development of regeneration methods that reverse the reduction process from Ag^0 to Ag$^+$.

- Synthesize industrially attractive membrane configurations, namely hollow fibers. This could be achieved either by coating of porous hollow fibers with the PVDF-HFP/BMImBF$_4$/AgBF$_4$ composite material, or by direct spinning of dual-layer fibers. In both approaches the objective should be the formation of a dense

selective layer as thin as possible, in the range of a few hundred nanometers.

4.3. Conclusiones generales

El principal objetivo de esta tesis es estudiar el potencial de las novedosas membranas compuestas de PVDF-HFP/BMImBF$_4$/AgBF$_4$ para reemplazar los actuales procesos de separación de mezclas propano/propileno. Para lograr este objetivo, se ha llevado a cabo un exhaustivo trabajo de caracterización experimental y modelado. Las principales conclusiones extraídas del análisis de los resultados se muestran a continuación:

a) Se han sintetizado membranas compuestas de transporte facilitado de PVDF-HFP/BMImBF$_4$/AgBF$_4$ mediante la técnica de solvent casting. El resultado es un material denso y homogéneo con buenas propiedades mecánicas.

b) Las técnicas de caracterización empleadas para determinar la estructura de la membrana confirman la estructura polimérica densa y la existencia de las interacciones y las especies químicas necesarias para dar lugar a los mecanismos de transporte tanto por carrier fijo como por carrier móvil. Las evidencias de dichas interacciones son, por un lado, el debilitamiento de los enlaces C-F de los grupos CF$_2$ del polímero, detectado por FTIR y XPS, y causado por la interacción entre los cationes Ag$^+$ y los átomos de flúor del PVDF-HFP, lo que da lugar al mecanismo de transporte por carrier fijo. Y, por otro lado, la existencia de iones plata libres y líquido iónico no complejado dentro del volumen libre del polímero, como revela la espectroscopia de Raman, lo cual induce un mecanismo de transporte por carrier móvil.

c) La técnica de permeación de propano y propileno mediante time-lag con gases puros en membranas de PVDF-HFP y PVDF-HFP/BMImBF$_4$ permitió calcular los parámetros de difusividad y solubilidad de las especies permeantes en el polímero y la mezcla polímero/líquido iónico, siendo estos unos valiosos datos para el desarrollo riguroso de un modelo matemático. Adicionalmente, estos datos confirman que la separación de mezclas propano/propileno únicamente mediante el mecanismo de disolución-difusión en PVDF-HFP resulta infructuosa. Finalmente, la adición de BMImBF$_4$ incrementa drásticamente la difusividad de los gases y reduce ligeramente su solubilidad. El resultado es un marcado aumento de la permeabilidad causado por el efecto de plastificación del líquido iónico en la matriz polimérica.

d) Los experimentos de permeación de flujo continuo con mezclas gaseosas determinaron las prometedoras capacidades de separación de las membranas compuestas bajo diferentes condiciones de operación, principalmente temperatura, presión de alimentación, composición de la membrana y humedad relativa de la corriente de alimentación. Los resultados muestran valores de permeabilidad de propileno de aproximadamente 200 Barrer y selectividades superiores a 150 bajo condiciones secas. Por otro lado, cabe resaltar la acusada influencia de la humedad de la corriente de alimentación en las prestaciones de la membrana, resultando en permeabilidades de propileno superiores a los 2000 Barrer con una humedad relativa del 100% en la corriente de alimentación. Sin embargo, esto se consigue a expensas de la selectividad hacia el propileno, que disminuye hasta un valor de 20 en las condiciones antes mencionadas. Los resultados de las termogravimetrías confirman retenciones de agua del 25% en peso en las membranas que contienen plata, lo que explica este comportamiento bajo condiciones húmedas.

e) Un experimento de permeación de larga duración llevado a cabo durante 110 días permitió cuantificar la influencia de la degradación de la plata en la capacidad de separación de las membranas a largo plazo. Dicha degradación, aunque sutil, podría afectar a la viabilidad industrial de las membranas propuestas. Esto dependerá fundamentalmente de la vida útil requerida para lograr la sostenibilidad económica del proceso de separación. La espectroscopia XPS reveló que el mecanismo de degradación comprende la reducción de Ag^+ a Ag^0. Finalmente, experimentos de permeación con mezclas reales suministradas por una compañía petroquímica no revelaron una mayor degradación causada por la potencial presencia de contaminantes menores.

f) Los datos experimentales obtenidos sirvieron para desarrollar un modelo matemático semipredictivo capaz de describir el flujo transmembranal de las especies permeantes en el rango estudiado de las variables de operación. El ajuste del modelo a los datos experimentales confirman la utilidad de dicho modelo para el posterior diseño y optimización de procesos.

g) La viabilidad del material de membrana propuesto para una aplicación industrial se ha estudiado a través del diseño y la optimización de procesos de separación mediante membranas. Para ello, se ha analizado una aplicación parcial de esta tecnología en forma de proceso híbrido membrana/destilación, así como una sustitución completa de la destilación mediante procesos de membrana multietapa. Los resultados revelan que el sistema híbrido puede generar unos ahorros en los costes de operación (OPEX) de entre el 33 y el 50% comparado con la destilación, dependiendo del precio final de la membrana compuesta. Por otro lado, una comparación del Valor Actual Neto de Costes (NPVC) reveló que un proceso de membrana de dos etapas tiene un NPVC del 25% del proceso de destilación, mientras que el proceso de dos etapas y media no presenta ventajas salvo que la pureza de propileno requerida exceda la pureza actualmente demandada por la industria.

En conjunto, estos resultados confirman el notable potencial de las membranas de PVDF-HFP/BMImBF$_4$/AgBF$_4$ implementadas en procesos de separación alternativos para alcanzar la intensificación de procesos en la separación industrial de mezclas propano/propileno. Sin embargo, alcanzar una completa viabilidad a escalada industrial requiere resolver retos adicionales. En primer lugar, los fenómenos de degradación del carrier pueden acortar la vida útil de la membrana más allá de un estándar competitivo. Por otro lado, la configuración de membrana juega un papel clave a escala industrial, en donde altas densidades de empaquetado y capas activas extremadamente delgadas son casi obligadas para asegurar la sostenibilidad económica del proceso.

4.4. Recomendaciones para investigación futura

Basándose en las conclusiones generales extraídas de esta tesis, y habiendo identificado los principales obstáculos en el camino hacia una completa viabilidad a escala industrial, esta sección ofrece una breve guía para futuros trabajos de investigación:

- Estudiar posibles estrategias para solucionar los problemas de degradación del carrier. Este objetivo se puede lograr desarrollando inhibidores de la degradación que pueden ser añadidos como aditivos en la composición de la membrana. Otra posibilidad comprende el desarrollo de métodos de regeneración que reviertan el proceso de degradación desde Ag^0 a Ag^+.

- Sintetizar configuraciones de membrana atractivas desde un punto de vista industrial, como son las fibras huecas. Esto se puede conseguir mediante “coating” de fibras huecas porosas con el material compuesto PVDF-HFP/$BMImBF_4$/$AgBF_4$, o directamente mediante “spinning” de fibras huecas de doble capa. En ambas estrategias el objetivo debe ser la formación de una capa densa selectiva tan delgada como sea posible, en el rango de unos pocos cientos de nanómetros.

Chapter 5

Scientific publications

5.1. JCR Scientific publications

R. Zarca, A. Ortiz, D. Gorri, I. Ortiz, A practical approach to fixed-site-carrier facilitated transport modeling for the separation of propylene/propane mixtures through silver-containing polymeric membranes, Sep. Purif. Technol. 180 (2017) 82–89. (JCR Impact Factor (2017): 3.927, Q1).

R. Zarca, A. Ortiz, D. Gorri, I. Ortiz, Generalized predictive modeling for facilitated transport membranes accounting for fixed and mobile carriers, J. Memb. Sci. 542 (2017) 168–176. (JCR Impact Factor (2017): 6.578, Q1).

R. Zarca, A. Ortiz, D. Gorri, L.T. Biegler, I. Ortiz, Optimized distillation coupled with state-of-the-art membranes for propylene purification, J. Memb. Sci. 556 (2018) 321–328. (JCR Impact Factor (2017): 6.578, Q1).

A copy of the above-mentioned articles is presented hereunder.

Separation and Purification Technology 180 (2017) 82–89

Contents lists available at ScienceDirect

Separation and Purification Technology

journal homepage: www.elsevier.com/locate/seppur

A practical approach to fixed-site-carrier facilitated transport modeling for the separation of propylene/propane mixtures through silver-containing polymeric membranes

Raúl Zarca, Alfredo Ortiz, Daniel Gorri, Inmaculada Ortiz *

Department of Chemical and Biomolecular Engineering, University of Cantabria, Av. Los Castros 46, 39005 Santander, Spain

ARTICLE INFO

Article history:
Received 9 January 2017
Received in revised form 24 February 2017
Accepted 25 February 2017
Available online 27 February 2017

Keywords:
Propylene
Propane
$AgBF_4$
PVDF-HFP
Membrane
Fixed-site carrier mathematical model

ABSTRACT

In this work, a new consistent mathematical model for the description of the olefin flux through Ag^+-containing polymeric dense membranes is proposed. A fixed site carrier "hopping" parameter acting as an effective permeability for this specific transport phenomenon is defined and calculated for the first time. This study reports a simple and versatile approach that can be incorporated into future models to simulate the more complex mobile/fixed hybrid mechanism acting in composite membranes.

Furthermore, in order to validate the model, the proof of concept has been carried out with PVDF-HFP/$AgBF_4$ facilitated transport membranes. The experimental analysis has been performed by the continuous flow permeation method through flat membranes containing increasing silver loads, from 17 to 38% w/w at olefin partial pressures ranging from 0.5 to 1.5 bar and temperatures of 293 and 303 K. These membranes showed a promising performance, reaching values of propylene permeability up to 1800 Barrer and very high propylene/propane selectivities. The reported model constitutes a very useful tool for process optimisation and scale-up.

© 2017 Elsevier B.V. All rights reserved.

1. Introduction

The global production of ethylene and propylene exceeds 200 million tones per year, being the purification stage responsible for 0.3% of the global energy use [1]. Current separation processes, mainly cryogenic distillation, consist on highly energy and capital intensive operations [2], which typically account for 45–55% of industrial processes energy consumption [1]. Some alternative processes to cryogenic distillation have been proposed over the last times, being the most studied: extractive distillation [3], physical adsorption on molecular sieves [4], and chemical adsorption [5]. Nonetheless, some problems as low olefin loads and complicated regeneration cycles have prevent these alternatives from replacing traditional distillation [6].

Recently, membrane technology has emerged as a possible solution that allows process intensification [7], which will lead to energy and capital savings in many gas separation processes, such as CO_2 capture [8], CO separation [9], natural gas purification [10] and hydrogen production [11]. In the short term, membranes can be used for bulk separation, using distillation for the final "refining" of the product. Such hybrid systems would reduce the energy requirements of olefin production by a factor of two or three [1]. A wide range of membrane compositions have been reported for olefin/paraffin separation, including liquid, polymeric and inorganic membranes [12–16]. However, these technologies face some major drawbacks. Liquid membranes show a serious lack of stability due to solvent evaporation [17]. Polymeric dense membranes suffer from poor performance in terms of selectivity and permeability due to the similar sizes of permeant species [18]. Lastly, inorganic membranes usually require complex and expensive preparation methods and show low mechanical resistance.

The development of new materials has promoted recent studies on their application to gas separation. In this regard, new studies assess the performance of nanocomposite membranes [19], mixed-matrix membranes containing metal organic frameworks (MOFs) [20–22], polymers with intrinsic microporosity (PIMs) [23] and membranes containing metallic nanoparticles [24], achieving high olefin/paraffin selectivities.

Among the membrane systems reported, those regarding the facilitated transport of olefins using a transition metal cation as carrier agent have shown great performance for olefin/paraffin separations [25–27]. The main advantage of carrier mediated facilitated transport membranes is their capability to achieve high values of selectivity and permeability at the same time, thus overcoming the existing tradeoff between these two variables

---

* Corresponding author.
E-mail address: ortizi@unican.es (I. Ortiz).

http://dx.doi.org/10.1016/j.seppur.2017.02.050
1383-5866/© 2017 Elsevier B.V. All rights reserved.

Nomenclature

A_m	membrane effective area [m^2]
C	concentration [$mol\ L^{-1}$]
D	diffusion coefficient [$m^2\ s^{-1}$]
Ea	activation energy [$kJ\ mol^{-1}$]
F	molar flowrate [$mol\ s^{-1}$]
J	molar flux [$mol\ m^{-2}\ s^{-1}$]
K_{eq}	equilibrium constant [$m^3\ mol^{-1}$]
K_H	fixed carrier effective permeability [$mol\ bar^{-1}\ m^{-1}\ s^{-1}$]
K_p	heterogeneous equilibrium constant [bar^{-1}]
L	membrane thickness [$m^3\ mol^{-1}\ s^{-1}$]
p	pressure [bar]
R	universal gas constant [8.314 $J\ mol^{-1}\ K^{-1}$]
S	gas solubility [$mol\ bar^{-1}\ m^{-3}$]
T	temperature [K]
x	mole fraction [–]

Greek letter	
α	fitting parameter
β	percolation threshold exponent [–]

Superscript/subscript	
0	feed side
C_3H_6	propylene
C_3H_8	propane
L	permeate side
N_2	nitrogen
m	membrane
ref	reference

[28,29]. Facilitated transport membranes for olefin/paraffin separation are prepared dissolving a silver salt within a polymeric matrix, forming a solid membrane, usually known as polymer electrolyte. On this matter, Bai et al. [30] synthesized ethyl-cellulose membranes modified with the incorporation of several metal-ions, achieving higher selectivity when testing silver cations instead of other transition metals. Kim et al. [31] tested EPR-coated polyester membranes with physically dispersed silver aggregates that dissolved in situ when in contact with the olefin, resulting in high selectivity towards the olefin; in addition, polymerized ionic liquids have been also assessed as a matrix for the incorporation of silver cations with promising results [32]. These membranes make use of the silver cations ability to selectively and reversibly coordinate with olefin molecules, following a π–bond complexation mechanism [33,34]. Additionally, our research group has developed composite membranes incorporating ionic liquids to the matrix polymer in order to improve the separation performance and stabilizing the silver cations in the membrane [28,35].

In this work, the use of dense polymeric facilitated transport membranes made of PVDF-HFP fluoropolymer and $AgBF_4$ silver salt is reported. When $AgBF_4$ dissolves into the polymer, it dissociates into Ag^+ and BF_4^- -ions. Then, Ag^+ ions tend to bond with those polymer atoms that can donate electrons to stabilize silver cations. Previous experimental studies have widely proven this distribution of cations, assessing their interactions with electron donor atoms of the polymer by means of FTIR spectra [36,37]. Once the membrane is in contact with the olefin, π-bonding complexation between the olefin and the cation takes place. Finally, due to the partial pressure gradient, the olefin follows a hopping movement from one fixed cation to the next, giving place to fixed carrier transport mechanism [38,39]. PVDF-HFP fluoropolymer was selected because of its well-known chemical, mechanical and thermal stability and its good miscibility with $AgBF_4$ silver salt; furthermore, besides the copolymerization with HFP decreases its crystallinity degree to around 0.3 [40], certain crystallinity in the polymer structure may reduce the paraffin sorption, while the olefin solubility remains high due to its complexation with the silver cations, increasing the selectivity of the membrane.

Previously, interesting works have been reported trying to describe this facilitated transport phenomenon in similar systems. In this regard, Smith and Quinn [41] studied the facilitated transport of carbon monoxide through cuprous chloride solutions; Ravanchi et al. [42] and Kasahara et al. [43] developed mathematical models for propane/propylene separation using supported liquid membranes and ion-gel membranes composed of gelled ionic liquids on PTFE supports, respectively.

The present work proposes a novel mathematical description for propylene flux through solid PVDF-HFP/Ag^+ facilitated transport membranes. Although previous reports of this research group have assessed the addition of ionic liquids as additives to promote carrier mobility [28], its use has been avoided in this study in order to limit the transport mechanisms to fixed site carrier and solution-diffusion. The mathematical approach at this stage involves the experimental determination of the activation energy (Ea), the equilibrium constant (Kp) and the influence of silver concentration (β), whereas the fitting parameter (α) has been estimated using Aspen Custom Modeler software. The model is able to describe the influence of the main operating variables on propylene flux, such as temperature, partial pressure and membrane composition. This model is the necessary tool for future process design, scale-up and optimization.

2. Experimental

2.1. Chemicals

Propylene and propane gases were purchased from Praxair with a purity of 99.5% for both gases. Poly(vinylidene fluoride-co-hexafluoropropylene) (PVDF-HFP) was supplied by Sigma Aldrich. Silver tetrafluoroborate ($AgBF_4$) with a minimum purity of 99% was purchased from Apollo Scientific Ltd. Tetrahydrofuran (THF) was used as solvent for membrane synthesis. All chemicals were used as received with no further purification.

2.2. Membrane synthesis

PVDF-HFP/$AgBF_4$ membranes were synthesized using the solvent casting method. The selected amount of PVDF-HFP is dissolved in 10 mL of THF by stirring in a sealed glass vial to prevent solvent evaporation. After 24 h of stirring at room temperature, the vial is heated at 50 °C during 5 min until the polymer is completely dissolved. Once the polymeric solution is prepared, it is mixed with the desired amount of silver salt and stirred for 10 min. Finally, the membrane precursor is poured in a Petri dish and located in a vacuum oven for 24 h at 25 °C and 300 mbar under dark conditions. The resulting thickness of the prepared dense films depends on the silver load, but in all cases, it is around 60 ± 10 μm. For calculation purposes, the real thickness of each membrane has been considered, being measured using a digital micrometer Mitutoyo Digimatic MDC-25SX (accuracy ± 0.001 mm).

2.3. Membrane morphology characterization

The cross-section and surface morphology of the membranes were observed using scanning electron microscopy (Carl Zeiss EVO MA 15). The samples were prepared by immersing and fracturing the membranes in liquid nitrogen followed by gold sputtering using a Balzers Union SCD040 sputter coating system. The line-scan spectrum of energy dispersive X-ray spectroscopy (EDX) was applied to the same samples of SEM to determine the silver distribution profile in the membrane cross-section.

2.4. Gas permeation experiments

The permeation experiments were conducted using the gas mixture continuous flow technique detailed elsewhere [28]; briefly, the membrane is placed in a permeation cell and the gas mixture is continuously fed into the upper chamber. Nitrogen gas is used in the lower chamber as sweeping gas. The retentate and permeate streams are finally analyzed using gas chromatography and the experimental propylene flux is calculated by a simple mass balance, as shown in Eq. (1).

$$J_{C_3H_6} = \frac{1}{A_m} \frac{x_{C_3H_6}}{x_{N_2}} F_{N_2} \tag{1}$$

where A_m is the effective membrane area, $x_{C_3H_6}$ and x_{N_2} are the propylene and nitrogen mole fractions, respectively, in the permeate chamber outlet stream and F_{N_2} is the nitrogen molar flow rate. Gas permeation experiments were carried out at the experimental conditions displayed in Table 1.

In order to assess the influence of silver concentration a set of three membranes with different silver loads were synthesized; membrane composition is shown in Table 2.

3. Mathematical modeling

The transport of propylene through the membrane is the result of two different transport mechanisms acting simultaneously, as illustrated in Fig. 1.

When a gas bulk is in contact with a non-porous material, gas molecules start to solubilize spontaneously in the polymer matrix. Adsorbed molecules then diffuse through the membrane, resulting in a net gas flux if a partial pressure gradient is applied. Furthermore, when a certain quantity of $AgBF_4$ is added to the membrane, it dissociates into its ions. Silver cations tend to form new bonds with those atoms present in the polymer matrix that can donate their electrons to stabilize Ag^+. These fixed silver cations promote the fixed carrier mechanism [44]. If the membrane is exposed to olefins, complexation takes place between the olefin molecules and the Ag^+ cations that are partially coordinated with the polymer matrix [45]. The olefin then follows a hopping mechanism until it reaches the other side of the membrane, where the olefin is released. The chemical reaction between the olefin and the silver cation is described as:

Table 1
Experimental conditions.

Experimental condition	Value
T (K)	293–313
Permeation area (cm^2)	53
N_2 flow ($mL\,min^{-1}$)	20
C_3H_6 flow ($mL\,min^{-1}$)	10
C_3H_8 flow ($mL\,min^{-1}$)	10
Feed side pressure (bar)	1–4
Permeate side pressure (bar)	1

Table 2
Membrane set.

Membrane	$AgBF_4$ load (% w/w)	Thickness (μm)	[Ag] ($mol\,L^{-1}$)
1	16.7	53	2.47
2	28.6	67	3.91
3	37.5	71	5.53

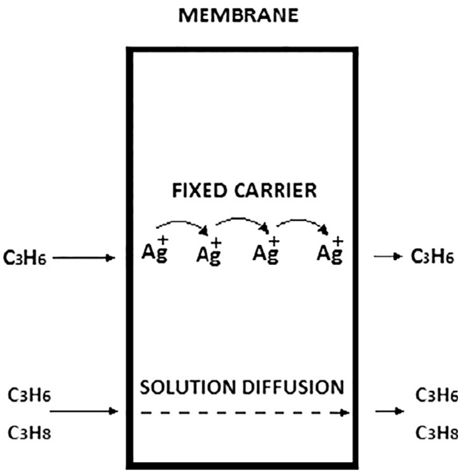

Fig. 1. Transport mechanisms acting within the membrane.

$$Ag^+ + C_3H_6 \overset{Keq}{\leftrightarrow} Ag^+(C_3H_6) \tag{2a}$$

In the heterogeneous form:

$$[Ag^+] + P_{C_3H_6} \overset{Kp}{\leftrightarrow} [Ag^+(C_3H_6)] \tag{2b}$$

The olefin flux given by the joint action of the two transport mechanisms can be expressed by Eq. (3) [46]:

$$J_{C_3H_6} = -D_{C_3H_6,m} \frac{dC_{C_3H_6}}{dx} - A \frac{dC_{C_3H_6}}{dx} \tag{3}$$

where the parameter A acts as an effective diffusivity in the fixed site carrier transport. Integrating Eq. (3) in the membrane domain results in Eq. (4):

$$J_{C_3H_6} = D_{C_3H_6,m} \frac{C^0_{C_3H_6} - C^L_{C_3H_6}}{L} + A \frac{C^0_{C_3H_6} - C^L_{C_3H_6}}{L} \tag{4}$$

Assuming a sorption equilibrium at the interface:

$$J_{C_3H_6} = D_{C_3H_6,m} \cdot S_{C_3H_6,m} \frac{p^0_{C_3H_6} - p^L_{C_3H_6}}{L} + K_H \frac{p^0_{C_3H_6} - p^L_{C_3H_6}}{L} \tag{5}$$

where K_H acts as an effective permeability or "hopping constant" for the olefin through the reactive pathway. The values of diffusivity (D) and solubility (S) of propylene in the PVDF-HFP matrix have been calculated in previous works [35]; however, in this case, the contribution of the solution diffusion mechanism can be neglected compared with the fixed carrier contribution. The transport capability of the fixed site carrier mechanism is a function of the membrane silver loading and the temperature [38]. A mathematical expression can be derived for the dependence of K_H with temperature and silver concentration, as shown in Eq. (6).

$$K_H = \alpha \left(\frac{[Ag^T]}{1 + K_P \cdot p^0_{C_3H_6}} \right)^{\beta} e^{\frac{Ea}{R}\left(\frac{1}{293} - \frac{1}{T}\right)} \tag{6}$$

The effect of temperature is given by an Arrhenius type expression, while the term in brackets is the concentration of uncomplexed silver cations, as obtained from the chemical equilibrium. The exponent β was introduced to correct the silver concentration influence on the propylene flux, given the percolation threshold observed in these membranes by several authors [47–49]. The parameter α is the fitting parameter of the model.

On the other hand, given that propane is only affected by fickian diffusion, its flux can be easily described by the solution-diffusion equation:

$$J_{C_3H_8} = D_{C_3H_8,m} \cdot S_{C_3H_8,m} \frac{p^0_{C_3H_8} - p^L_{C_3H_8}}{L} \qquad (7)$$

4. Results and discussion

4.1. Membrane morphology

Fig. 2 displays the SEM photographs of a PVDF-HFP membrane and PVDF-HFP/AgBF$_4$ membranes **1** and **3**. In all cases the PVDF-HFP forms a homogeneous dense polymeric matrix with no signs of porosity or differentiated layers. Furthermore, no particle clusters appear in the polymer electrolyte membranes, indicating that the added salt is completely dissolved.

The EDX spectra of the membrane with the highest silver loading displayed in Fig. 3 shows a uniform distribution of the element silver along the cross-section of the membrane, with no evidence of silver particles formation. This is in good agreement with the previously discussed works on the interactions between the Ag$^+$ cations and the polymer matrix [36,37].

4.2. Permeation results

In this section, the permeation results are discussed; the experimental propylene flux through the membranes **1**–**3** as a function of propylene partial pressure is depicted in Fig. 4 at 293 and 303 K, respectively.

As the difference of propylene partial pressure is the driving force in the permeation process, the olefin flux increases when

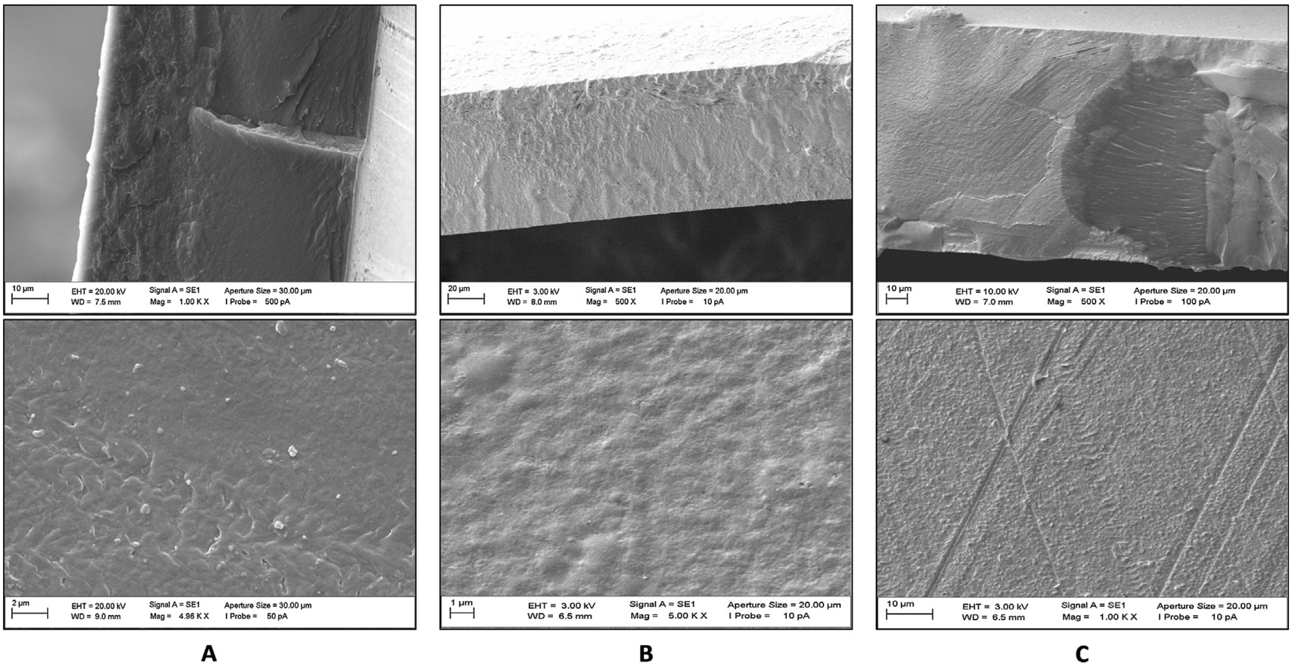

Fig. 2. Cross-section and surface morphology of: (A) Pure PVDF-HFP membrane, (B) membrane **1** [Ag] = 2.47 M, (C) membrane **3** [Ag] = 5.53 M.

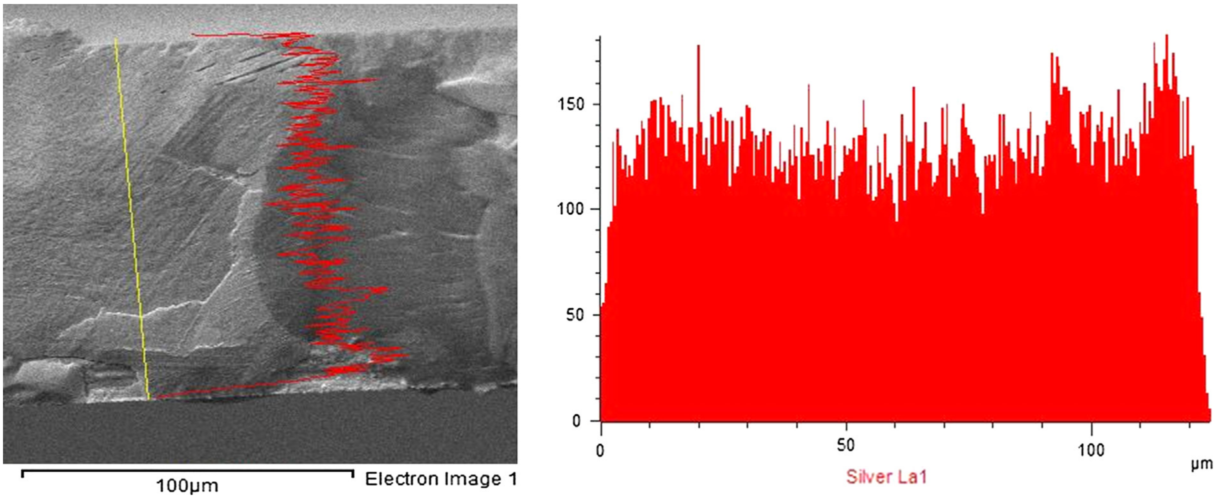

Fig. 3. SEM-EDX scan-line and silver distribution profile in the cross-section of membrane **3** [Ag] = 5.53 M.

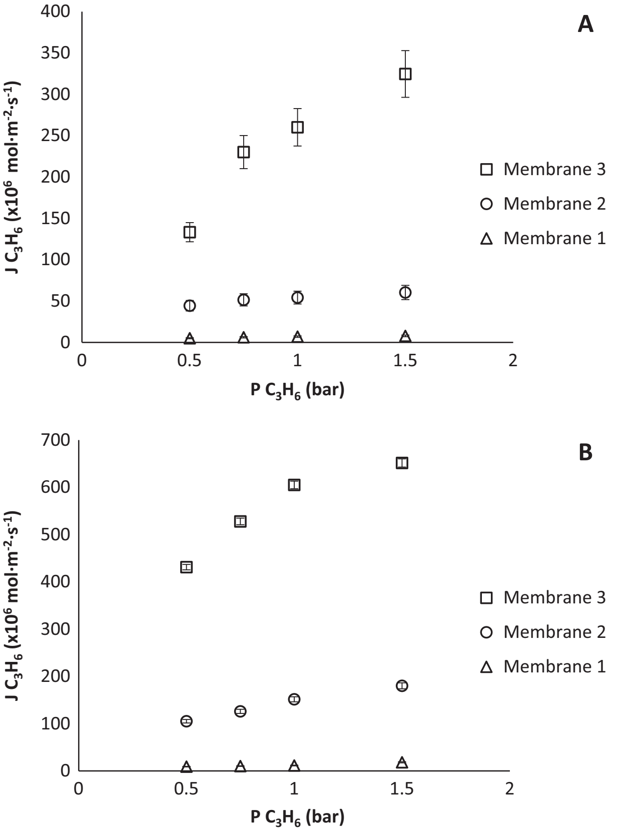

Fig. 4. Propylene flux at (a) 293 and (b) 303 K as a function of the feed partial pressure in membrane **1** [Ag] = 2.47 M, membrane **2** [Ag] = 3.91 M and membrane **3** [Ag] = 5.53 M.

its feed partial pressure rises. In contrast to the conventional solution-diffusion transport mechanism, that describes a linear increase of the permeate flux with increasing driving force, i.e. partial pressure difference, these membranes display the characteristic fixed-site-carrier facilitated transport profile described elsewhere [50]. At very low values of the driving force, most part of the transported molecules follow the complexing mechanism, resulting in a non-linear profile. On the other hand, for high driving forces, every silver cation is bound to propylene molecules and the carrier becomes saturated. In this state, any flux increase is mainly induced by the solution-diffusion mechanism, and thus, the linear trend is only achieved after surpassing a threshold value of the partial pressure gradient.

Comparing Fig. 4(a) and (b) it can be observed that the temperature has a strong influence on the permeation process, increasing the flux of propylene. This increase of the olefin flux is due to the enhancement in the gas diffusivity, as reported before [35]. The temperature also has a positive influence on the rate of complexation and decomplexation reactions, thus enhancing the olefin facilitated transport. In contrast to diffusivity, the solubility of both gases slightly decreases with temperature; nonetheless, the influence of this trend is completely overlapped by the diffusivity effect. However, as the paraffin diffusivity undergoes an increasing trend with temperature, it results in a selectivity decrease towards the olefin at higher temperatures.

Pristine PVDF-HFP copolymer is known for being a low permeable material. This property combined with transport facilitation towards propylene yields very high selectivity. In fact, the propane concentration in the permeate stream when testing membranes **1** and **2** was below the gas chromatograph detection limit (0.025 vol. %). The permeate stream of membrane **3** contained a minor quantity of propane at the higher feed pressures, as displayed in Fig. 5. The resulting selectivity ranges from 100 to 300. Given that previous studies involving pure gases report lower values of propane permeability in PVDF-HFP [35], a dragging effect caused by the high propylene fluxes is probably happening in membrane **3**, resulting in a propane permeability increase. Fig. 5 shows the difference between the experimental fluxes of propylene and propane.

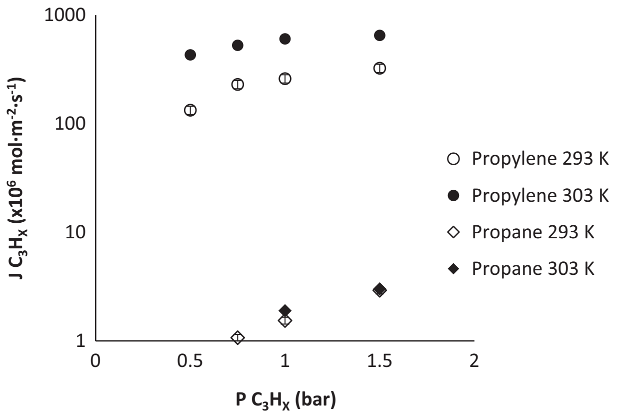

Fig. 5. Experimental fluxes of propylene and propane in membrane **3** at 293 and 303 K, at different partial pressure.

Thus, these experimental results demonstrate that it is possible to achieve high propylene flux and selectivity even at low partial pressures and moderate temperatures.

Comparing all three membranes in terms of silver loading and propylene flux, one can observe that the silver concentration has a major influence on the olefin permeability. When the silver content increases within the membrane, more silver cations are available to coordinate with olefin molecules. The result is a noticeable increase in propylene facilitated transport that follows an exponential trend, Fig. 6. A similar behaviour was reported by Yoon et al. [47] in PEOx and PVP with $AgBF_4$ and $AgCF_3SO_3$ silver salts, by Morisato et al. [48] in PA-12-PTMO/$AgBF_4$ membranes, and by Kim et al. [49] in different polymer/silver membranes, although it has not been previously reported in PVDF-HFP fluoropolymer. This trend evidences a percolation threshold; at low carrier concentrations, the facilitated transport is almost negligible, while increasing the concentration results in a major increase of the olefin flux. This phenomenon is related to the proximity between active sites; at low concentrations, the distance between two consecutive cations is too large to allow the facilitated transport; on the other hand, at higher concentrations the silver cations are close enough to transport the olefin. In these membranes, the percolation threshold seems to be surpassed at silver concentrations higher than 2.5 $mol{\cdot}L^{-1}$.

4.3. Mathematical model

One of the main targets of this work is to provide a simple yet effective model to predict the olefin flux in this polymer/silver system. This tool will be useful to design and optimize commercial attractive configurations as spiral wound or hollow fiber geometries. The model contains one fitting parameter and three calculated parameters.

In order to avoid interferences in parametric sensitivity, the experimental determination of the activation energy, the equilibrium constant and the exponent β has been carried out isolating

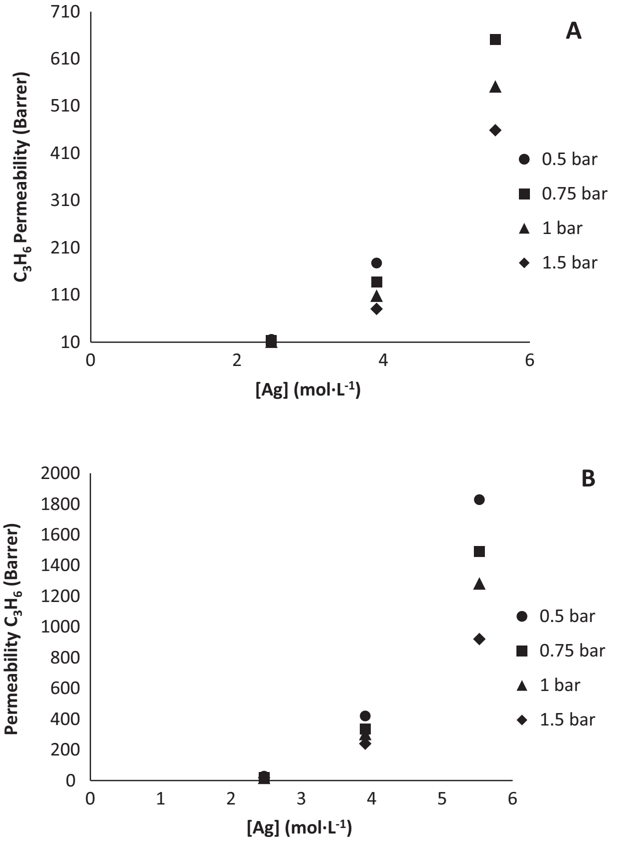

Fig. 6. Permeability of propylene with increasing silver concentration at (a) 293 and (b) 303 K.

the influence of temperature from the influence of silver concentration. The values of calculated parameters are shown in Table 3.

To calculate the activation energy of the permeation process, experimental data at constant pressure and constant silver concentration, modifying the temperature, were fitted to an Arrhenius type equation, Eq. (8):

$$\ln K_H = \ln \alpha' + \frac{Ea}{R}\left[\frac{1}{T_{ref}} - \frac{1}{T}\right] \tag{8}$$

Using the same methodology, the equilibrium constant K_P and the exponent β were determined by regression of permeability data at constant temperature, with silver concentration and olefin partial pressure, Eq. (9):

$$K_H = \alpha''\left(\frac{Ag}{1 + K_P \cdot p_i}\right)^{\beta} \tag{9}$$

Aspen Custom Modeler software was used to fit the experimental data to the model equations and estimate the fitting parameter α, which has a value of 3.24×10^{-11} for this particular case study.

Table 3
Calculated model parameters.

Parameter	Value
Activation energy, Ea (kJ mol^{-1})	61
Equilibrium constant, K_p (bar^{-1})	0.12
Beta exponent, β	4.235

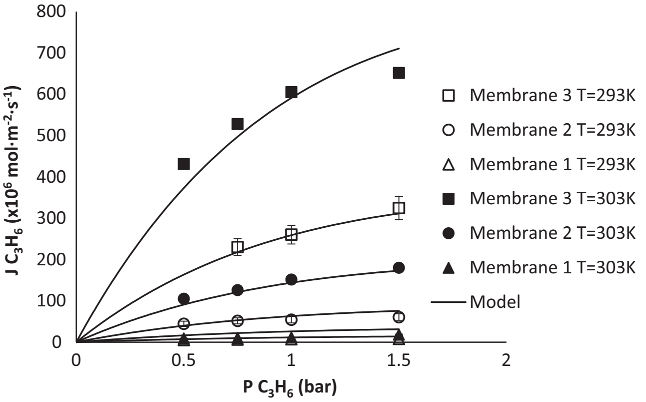

Fig. 7. Propylene experimental flux and model prediction for the membranes **1** to **3** at 293 and 303 K, and at different feed partial pressures.

Once the model parameters are determined, the model describes the permeation process of propylene through the facilitated transport membrane, providing that all operating variables are inside the studied range. Fig. 7 shows experimental and model flux values of propylene at several temperatures and olefin partial pressures with membranes **1** to **3**.

The estimated propylene fluxes are represented against the experimental propylene fluxes in the parity graph shown in Fig. 8. In the parity graph, a 15% error range is also displayed, proving that the majority of points fall within this range, and checking the adequacy of the proposed model to describe the experimental behavior of propane/propylene separation using PVDF-HFP/Ag^+ membranes.

4.4. Membranes comparison

Various polymer electrolytes comprising different polymer matrices and silver salts have been previously reported for propylene/propane separation. Table 4 displays the selectivity values achieved by other authors when similar propylene/propane gas mixtures were tested. It is remarkable the performance of the PDMS/$AgBF_4$ membranes reported by Kim et al. [51]; with the particularity that the silver cations are not bounded to the polymer chains, according to the authors; silver remains forming ionic aggregates that progressively dissolve upon its contact with the olefin. The use of PVDF-HFP as polymeric matrix reported in this work yields higher selectivity compared with other membranes that use the same silver salt, and shows great potential for the intensification of the olefin/paraffin separation process.

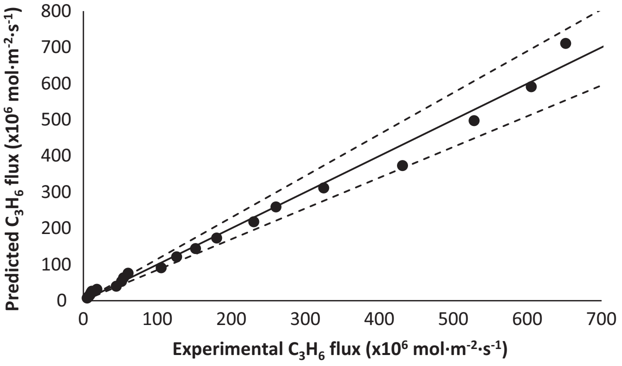

Fig. 8. Model parity graph with a 15% error range.

Table 4
Comparison with previous reported facilitated transport membranes.

Membrane	C_3H_6/C_3H_8 gas mixture	Feed pressure (bar)	Thickness (μm)	Permeance (GPU) [a]	Selectivity	Ref.
Poly(ethylene-co-propylene)/62 wt.% $AgBF_4$	50/50		1–2	7	55	[31]
PEBAX 1657/50 wt.% $AgBF_4$	50/50	4	25	4[b]	17.2	[27]
PEBAX 1657/50 wt.% $AgBF_4$	66/34	2	25	5[b]	20.2	[27]
PEOx/$AgBF_4$ [Ag]/[C = O] 1:1	50/50	2.76	1	35	58	[47]
PEOx/$AgCF_3SO_3$ [Ag]/[C = O] 1:1	50/50	2.76	1	32	19	[47]
PVP/$AgBF_4$ [Ag]/[C = O] 1:1	50/50	2.76	1	36	65	[47]
PVP/$AgCF_3SO_3$ [Ag]/[C = O] 1:1	50/50	2.76	1	28	18	[47]
PDMS/57 wt.% $AgBF_4$	50/50		2	13	150	[51]
PVDF-HFP/37.5 wt.% $AgBF_4$	50/50	2	71	25[b]	300	This work

[a] Permeance in GPU. 1 GPU = 1×10^{-6} cm^3 (STP)/cm^2 s cmHg.
[b] Calculated from reported permeability and thickness.

5. Conclusions

A mathematical expression for the "effective permeability" of propylene by the fixed carrier mechanism has been deduced and the fitting parameter has been estimated based on experimental data. The validity of the model has been checked by comparing simulated and experimental permeation data for propylene/propane gas mixtures in PVDF-HFP/Ag^+.

The resulting olefin fluxes follow the characteristic trend of facilitated transport processes when increasing the feed pressure, and indicate a promising performance in terms of propylene permeability. The silver loading dramatically increases the propylene flux in an exponential trend, which suggests the existence of a concentration threshold. The comparison between experimental and predicted values and the model parity graph suggest a reliable goodness of fit.

The mathematical approach reported in this work is susceptible to be applied in those membrane systems where the fixed carrier mechanism is present and allows to calculate its contribution to the total permeate flux in a fast and simple manner. Therefore, this model will be a valuable tool for future design and optimization of more complex propylene/propane separation systems (i.e. mobile-fixed carrier hybrid membranes) in more efficient process configurations.

Acknowledgement

Financial support from the Spanish Ministry of Science under the projects CTQ2015-66078-R and CTQ2016-75158-R (MINECO, Spain-FEDER 2014–2020) is gratefully acknowledged. Raúl Zarca also thanks the Universidad de Cantabria for a postgraduate fellowship.

References

[1] D.S. Sholl, R.P. Lively, Seven chemical separations to change the world, Nature 532 (2016) 435–437.
[2] J.L. Humphrey, A.F. Seibert, R.A. Koort, Separation Technologies: Advances and Priorities, U.S. Department of Energy Report No. DOE/ID/12920-1, 1991.
[3] R. Kumar, J.M. Prausnitz, C.J. King, Process design considerations for extractive distillation: separation of propylene-propane, in: D. Tassios (Ed.), Extractive and Azeotropic Distillation, American Chemical Society, Washington D.C., 1974, pp. 16–34.
[4] C.M. Shu, S. Kulvaranon, M.E. Findley, A.I. Liapis, Experimental and computational studies on propane-propylene separation by adsorption and variable-temperature stepwise desorption, Sep. Technol. 1 (1990) 18–28.
[5] R.T. Yang, Adsorbents: Fundamentals and Applications, John Wiley & Sons, Hoboken, NJ, 2003, pp. 191–230.
[6] R.B. Eldridge, Olefin/paraffin separation technology: a review, Ind. Eng. Chem. Res. 32 (1993) 2208–2212.
[7] J. Charpentier, In the frame of globalization and sustainability, process intensification, a path to the future of chemical and process engineering (molecules into money), Chem. Eng. J. 134 (2007) 84–92.
[8] T.C. Merkel, X. Wei, Z. He, L.S. White, J.G. Wijmans, R.W. Baker, Selective exhaust gas recycle with membranes for CO_2 capture from natural gas combined cycle power plants, Ind. Eng. Chem. Res. 52 (2013) 1150–1159.
[9] G. Zarca, W.J. Horne, I. Ortiz, A. Urtiaga, J.E. Bara, Synthesis and gas separation properties of poly(ionic liquid)-ionic liquid composite membranes containing a copper salt, J. Membr. Sci. 515 (2016) 109–114.
[10] M. Askari, T. Chung, Natural gas purification and olefin/paraffin separation using thermal cross-linkable co-polyimide/ZIF-8 mixed matrix membranes, J. Membr. Sci. 444 (2013) 173–183.
[11] R. Swaidan, B. Ghanem, I. Pinnau, Fine-tuned intrinsically ultramicroporous polymers redefine the permeability/selectivity upper bounds of membrane-based air and hydrogen separations, ACS Macro Lett. 4 (2015) 947–951.
[12] J. Caro, M. Noack, P. Kölsch, R. Schäfer, Zeolite membranes - state of their development and perspective, Microporous Mesoporous Mater. 38 (2000) 3–24.
[13] Y.S. Lin, I. Kumakiri, B.N. Nair, H. Alsyouri, Microporous inorganic membranes, Sep. Purif. Methods 31 (2002) 229–379.
[14] M. Fallanza, A. Ortiz, D. Gorri, I. Ortiz, Experimental study of the separation of propane/propylene mixtures by supported ionic liquid membranes containing Ag+–RTILs as carrier, Sep. Purif. Technol. 97 (2012) 83–89.
[15] S. Najari, S.S. Hosseini, M. Omidkhah, N.R. Tan, Phenomenological modeling and analysis of gas transport in polyimide membranes for propylene/propane separation, RSC Adv. 5 (2015) 47199–47215.
[16] K.-S. Liao, J.-Y. Lai, T.-S. Chung, Metal ion modified PIM-1 and its application for propylene/propane separation, J. Membr. Sci. 515 (2016) 36–44.
[17] M. Teramoto, H. Matsuyama, T. Yamashiro, Y. Katayama, Separation of ethylene from ethane by supported liquid membranes containing silver-nitrate as a carrier, J. Chem. Eng. Japan 19 (1986) 419–424.
[18] R. Faiz, K. Li, Polymeric membranes for light olefin/paraffin separation, Desalination 287 (2012) 82–97.
[19] H. Sun, B. Yuan, P. Li, T. Wang, Y. Xu, Preparation of nanoporous graphene and the application of its nanocomposite membrane in propylene/propane separation, Funct. Mater. Lett. 08 (2015) 1550019.
[20] U. Böhme, B. Barth, C. Paula, A. Kuhnt, W. Schwieger, A. Mundstock, J. Caro, M. Hartmann, Ethene/ethane and propene/propane separation via the olefin and paraffin selective metal-organic framework adsorbents CPO-27 and ZIF-8, Langmuir 29 (2013) 8592–8600.
[21] G. Chang, M. Huang, Y. Su, H. Xing, B. Su, Z. Zhang, Q. Yang, Y. Yang, et al., Immobilization of Ag(I) into a metal-organic framework with -SO_3H sites for highly selective olefin-paraffin separation at room temperature, Chem. Commun. 51 (2015) 2859–2862.
[22] H.T. Kwon, H. Jeong, Improving propylene/propane separation performance of Zeolitic-Imidazolate framework ZIF-8 Membranes, Chem. Eng. Sci. 124 (2015) 20–26.
[23] R.J. Swaidan, X. Ma, E. Litwiller, I. Pinnau, Enhanced propylene/propane separation by thermal annealing of an intrinsically microporous hydroxyl-functionalized polyimide membrane, J. Membr. Sci. 495 (2015) 235–241.
[24] C.G.F. Rezende, C.P. Borges, A.C. Habert, Sorption of propylene and propane in polyurethane membranes containing silver nanoparticles, J. Appl. Polym. Sci. 133 (2016).
[25] J.H. Kim, B.R. Min, J. Won, S.H. Joo, H.S. Kim, Y.S. Kang, Role of polymer matrix in polymer/silver complexes for structure, interactions, and facilitated olefin transport, Macromolecules 36 (2003) 6183–6188.
[26] J.H. Kim, B.R. Min, J. Won, Y.S. Kang, Revelation of facilitated olefin transport through silver-polymer complex membranes using anion complexation, Macromolecules 36 (2003) 4577–4581.
[27] R. Surya Murali, K. Yamuna Rani, T. Sankarshana, A.F. Ismail, S. Sridhar, Separation of binary mixtures of propylene and propane by facilitated transport through silver incorporated poly(ether-block-amide) membranes, Oil Gas Sci. Technol. 70 (2015) 381–390.
[28] M. Fallanza, A. Ortiz, D. Gorri, I. Ortiz, Polymer-ionic liquid composite membranes for propane/propylene separation by facilitated transport, J. Membr. Sci. 444 (2013) 164–172.
[29] L. Liu, X. Feng, A. Chakma, Unusual behavior of poly(ethylene oxide)/$AgBF_4$ polymer electrolyte membranes for olefin–paraffin separation, Sep. Purif. Technol. 38 (2004) 255–263.
[30] S. Bai, S. Sridhar, A.A. Khan, Recovery of propylene from refinery off-gas using metal incorporated ethylcellulose membranes, J. Membr. Sci. 174 (2000) 67–79.

[31] J.H. Kim, B.R. Min, Y.W. Kim, S.W. Kang, J. Won, Y.S. Kang, Novel composite membranes comprising silver salts physically dispersed in poly(ethylene-co-propylene) for the separation of propylene/propane, Macromol. Res. 15 (2007) 343–347.

[32] L.C. Tomé, D. Mecerreyes, C.S.R. Freire, L.P.N. Rebelo, I.M. Marrucho, Polymeric ionic liquid membranes containing IL-Ag^+ for ethylene/ethane separation via olefin-facilitated transport, J. Mater. Chem. A 2 (2014) 5631–5639.

[33] J.S. Dewar, A review of the pi-complex theory, Bull. Soc. Chim. Fr. 18 (1951) C71–C79.

[34] L.M. Galán Sánchez, G.W. Meindersma, A.B. Haan, Potential of silver-based room-temperature ionic liquids for ethylene/ethane separation, Ind. Eng. Chem. Res. 48 (2009) 10650–10656.

[35] R. Zarca, A. Ortiz, D. Gorri, I. Ortiz, Facilitated transport of propylene through composite polymer-ionic liquid membranes. Mass transfer analysis, Chem. Prod. Process Model. 11 (2016) 77–81, http://dx.doi.org/10.1515/cppm-2015-0072.

[36] J. Chang, S.W. Kang, CO_2 separation through poly(vinylidene fluoride-co-hexafluoropropylene) membrane by selective ion channel formed by tetrafluoroboric acid, Chem. Eng. J. 306 (2016) 1189–1192.

[37] S. Sunderrajan, B.D. Freeman, C.K. Hall, I. Pinnau, Propane and propylene sorption in solid polymer electrolytes based on poly(ethylene oxide) and silver salts, J. Membr. Sci. 182 (2001) 1–12.

[38] E.L. Cussler, R. Aris, A. Bhown, On the limits of facilitated diffusion, J. Membr. Sci. 43 (1989) 149–164.

[39] R.D. Noble, Analysis of facilitated transport with fixed site carrier membranes, J. Membr. Sci. 50 (1990) 207–214.

[40] S. Abbrent, J. Plestil, D. Hlavata, J. Lindgren, J. Tegenfeldt, Å. Wendsjö, Crystallinity and morphology of PVdF-HFP-based gel electrolytes, Polymer 42 (2001) 1407–1416.

[41] D.R. Smith, J.A. Quinn, The facilitated transport of carbon monoxide through cuprous chloride solutions, AIChE J. 26 (1980) 112–120.

[42] M.T. Ravanchi, T. Kaghazchi, A. Kargari, Facilitated transport separation of propylene-propane: experimental and modeling study, Chem. Eng. Process. 49 (2010) 235–244.

[43] S. Kasahara, E. Kamio, R. Minami, H. Matsuyama, A facilitated transport ion-gel membrane for propylene/propane separation using silver ion as a carrier, J. Membr. Sci. 431 (2013) 121–130.

[44] R. Faiz, K. Li, Olefin/paraffin separation using membrane based facilitated transport/chemical absorption techniques, Chem. Eng. Sci. 73 (2012) 261–284.

[45] A. Ortiz, L.M. Galán Sanchez, D. Gorri, A.B. De Haan, I. Ortiz, Reactive ionic liquid media for the separation of propylene/propane gaseous mixtures, Ind. Eng. Chem. Res. 49 (2010) 7227–7233.

[46] R.D. Noble, Generalized microscopic mechanism of facilitated transport in fixed site carrier membranes, J. Membr. Sci. 75 (1992) 121–129.

[47] Y. Yoon, J. Won, Y.S. Kang, Polymer electrolyte membranes containing silver ion for facilitated olefin transport, Macromolecules 33 (2000) 3185–3186.

[48] A. Morisato, Z. He, I. Pinnau, T.C. Merkel, Transport properties of PA12-PTMO/$AgBF_4$ solid polymer electrolyte membranes for olefin/paraffin separation, Desalination 145 (2002) 347–351.

[49] J.H. Kim, S.W. Kang, Y.S. Kang, Threshold silver concentration for facilitated olefin transport in polymer/silver salt membranes, J. Polym. Res. 19 (2012) 9753.

[50] R.D. Noble, C.A. Koval, Review of facilitated transport membranes, in: Y. Yampol'skii, I. Pinnau, B. Freeman (Eds.), Materials Science of Membranes for Gas and Vapor Separation, John Wiley & Sons, Hoboken, NJ, 2006, pp. 411–435.

[51] J.H. Kim, J. Won, Y.S. Kang, Olefin-induced dissolution of silver salts physically dispersed in inert polymers and their application to olefin/paraffin separation, J. Membr. Sci. 241 (2004) 403–407.

Journal of Membrane Science 542 (2017) 168–176

Contents lists available at ScienceDirect

Journal of Membrane Science

journal homepage: www.elsevier.com/locate/memsci

Generalized predictive modeling for facilitated transport membranes accounting for fixed and mobile carriers

Raúl Zarca, Alfredo Ortiz, Daniel Gorri, Inmaculada Ortiz*

Department of Chemical and Biomolecular Engineering, University of Cantabria, Av. Los Castros 46, 39005 Santander, Spain

ARTICLE INFO

Keywords:
Propylene-propane separation
Facilitated transport
Silver
Membrane
Mathematical model

ABSTRACT

The present work expands previous modeling knowledge on facilitated transport membranes for olefin/paraffin separation. A new robust and practical mathematical model for the description of light olefin flux in composite polymer/ionic liquid/Ag^+ membranes is reported. The model takes into account three different transport mechanisms, i.e., solution-diffusion, fixed-site carrier and mobile carrier transport mechanisms. Fixed-site carrier contribution that appears thanks to the bounding of silver cations with the polymer chains is described through a “hopping parameter”. Furthermore, given that the addition of an ionic liquid to the membrane composition promotes carrier mobility, the inclusion of a dedicated expression is necessary for a realistic description of mobile-carrier transport phenomena. The contribution of each mechanism in weighted based on the membrane composition.

In order to check the model suitability, simulated values have been matched to experimental data obtained by continuous flow propane/propylene permeation experiments through PVDF-HFP/$BMImBF_4$/$AgBF_4$ composite membranes, working with 50:50 gas mixtures at different temperature and pressure. The resultant model offers good predictions for olefin flux and provides a very useful tool for process optimization and scaling-up. To our knowledge, this is the first time that mobile and fixed site carrier mechanisms performance are simultaneously modeled considering the influence of temperature, pressure and carrier loading.

1. Introduction

The separation of light olefin/paraffin mixtures has been recently defined as one of the key chemical separations that can bring great global benefits once improved. Replacing traditional distillation by new processes that do not require a phase change could lower the energy intensity of the process by a factor of ten [1]. In this sense, membrane technology offers a modular and cost-effective solution able to reduce the energy demand of the separation process by means of process intensification [2].

Several approaches have been reported to synthesize effective olefin/paraffin separation membranes. The simplest way is to exploit the intrinsic separation properties of polymers in a dense membrane configuration. Dense polymeric membranes made of glassy, rubbery and cellulosic polymers perform high selectivities at the expense of low permeabilities [3–6]. More recently, new materials have been tested for their application in alkane/alkene separation, including polymers with intrinsic microscopy [7,8], metal-organic frameworks [9,10], carbon molecular sieves [11,12] and graphene [13], displaying a wide distribution of results.

However, the intrinsic separation properties of polymers are vastly improved when a metallic cation with the ability to reversibly and selectively react with the olefin is dissolved in the polymer matrix, resulting in the facilitated transport mechanism [14]. In this context, silver cations are known for their capability to form stable complexes with the olefin via π-bonding mechanism [15,16].

Gas separation based on facilitated transport has been approached working in liquid phase, mainly in the form of supported liquid membranes [17–20], but their poor mechanical stability and the solvent losses by evaporation are major drawbacks for real industrial application, especially when subjected to pressure gradients [21]. In order to overcome this handicap, the use of ionic liquids as liquid phase has been recently assessed [22]. Besides their negligible vapor pressure, ionic liquids are non-flammable excellent solvents whose chemical and physical properties can be tailored by a judicious selection of cation, anion, and substituents [23,24].

The unique properties of ionic liquids can be used to improve membrane performance in polymer electrolyte membranes. On the one hand, the presence of an ionic liquid within the free volume of the polymer promotes mobility among the silver cations which, after

---

* Corresponding author.
E-mail address: ortizi@unican.es (I. Ortiz).

http://dx.doi.org/10.1016/j.memsci.2017.08.010
Received 21 June 2017; Received in revised form 27 July 2017; Accepted 4 August 2017
Available online 09 August 2017
0376-7388/ © 2017 Elsevier B.V. All rights reserved.

Nomenclature

A	mobile carrier effective olefin diffusivity [$m^2\,s^{-1}$]
A_m	membrane effective area [m^2]
B	fixed-site carrier effective olefin diffusivity [$m^2\,s^{-1}$]
C	concentration [$mol\,L^{-1}$]
D	diffusion coefficient [$m^2\,s^{-1}$]
Ea	activation energy [$kJ\,mol^{-1}$]
F	molar flowrate [$mol\,s^{-1}$]
H	Henry's solubility constant [$mol\,bar^{-1}\,m^{-3}$]
ΔH_{sol}	Henry's constant enthalpy [$kJ\,mol^{-1}$]
J	molar flux [$mol\,m^{-2}\,s^{-1}$]
K_{eq}	equilibrium constant [$m^3\,mol^{-1}$]
K_H	fixed carrier effective permeability [$mol\,bar^{-1}\,m^{-1}\,s^{-1}$]
K_p	heterogeneous equilibrium constant [bar^{-1}]
L	membrane thickness [m]
P	permeability [$mol\,bar^{-1}\,m^{-1}\,s^{-1}$]
p	pressure [bar]
R	universal gas constant [$8.314\,J\,mol^{-1}\,K^{-1}$]
ΔH_r	complexation reaction enthalpy [$kJ\,mol^{-1}$]
S	gas solubility [$mol\,bar^{-1}\,m^{-3}$]
T	temperature [K]
X	mole fraction [-]
x	membrane thickness dimension [m]

Greek letter

α	fitting parameter

Superscript / subscript

0	feed side
C_3H_6	propylene
C_3H_8	propane
comp	organometallic complex
D	organometallic complex diffusion
eq	chemical equilibrium
FC	fixed-site carrier
IL	ionic liquid
L	permeate side
N_2	nitrogen
m	membrane
MC	mobile carrier
r	reaction
ref	reference
SD	solution-diffusion

binding to the olefin, will diffuse through a mobile-carrier transport mechanism [25]; in this way, the characteristic fixed-carrier “percolation threshold” is avoided and facilitated transport occurs even at low silver concentrations [26]. On the other hand, the lack of volatility of ionic liquids mitigates the stability issues produced by solvent evaporation during the first operating hours. In addition, it is remarkable that silver ions are more stable when surrounded by ionic liquid molecules [16,27,28].

Composite facilitated transport membranes prepared by introducing a room temperature ionic liquid inside the polymer electrolyte free volume, have shown great performance for olefin/paraffin separation, easily surpassing the trade-off between permeability and selectivity for polymeric membranes [29]. Several approaches have been assessed, including the use of polymerized ionic liquids as polymeric matrix [30]. The internal structure of a composite membrane consists of a polymeric matrix with the ionic liquid molecules entrapped within the free volume. The silver cations are distributed; some are bonded to the polymer electronegative atoms while others are solvated by the ionic liquid. In the first case, the olefin “hops” from a cation site to a different cation site in a sequence of complexation-decomplexation steps, achieving a net flux thanks to the activity gradient [31,32]. In the second case, the whole Ag^+-olefin complex diffuses through the ionic liquid domains existing within the polymer free volume [22].

The use of membranes to carry out this separation has been modeled for various materials and configurations. Regarding polymeric membranes, Najari et al. [33] studied and compared several models, including the frame of reference/bulk flow and Maxwell-Stefan models for polyimide membranes, while Sridhar and Khan [34] and Castoldi et al. [35] developed mathematical models focusing on industrial membrane configurations.

Regarding facilitated transport membranes, their promising performance has promoted several works on mathematical modeling to explain the transport phenomena in solid-state membranes; being the most recognized the dual sorption model [36,37], the limited mobility of chained carriers model [38,39] and the concentration fluctuation model [40,41]. In addition, mobile carrier facilitated transport in the liquid phase has been previously modeled for several separation systems as nitric oxide in ferrous chloride solutions [42] and enriched-air production [43]. However, all of them find their application in membranes that perform according to one facilitated transport mechanism, making them unsuitable for composite membranes that perform according to hybrid mobile/fixed carrier transport.

In this work, the main goal is to develop a general and broadly applicable mathematical model able to describe the olefin flux through polymer-IL composite membranes as a function of the membrane composition and operating conditions. The model expresses the total flux as a sum of the contributions caused by the three mentioned mechanisms. A new expression to define the fixed-site carrier effective permeability through a “hopping parameter” is used along with the mathematical expressions for mobile carrier and solution-diffusion mechanisms. The model contains two fitting parameters that have been estimated using modeling software, fitting the mathematical model to experimental data.

The experimental values have been obtained by continuous flow propane/propylene gas-mixture permeation experiments on composite membranes made of PVDF-HFP, the ionic liquid 1-butyl-3-methylimidazolium tetrafluoroborate ($BMImBF_4$) and $AgBF_4$ silver salt. The separation capability of this membrane composition had been previously checked by this research group [29] but the polymer/ionic liquid ratio has been optimized for the experimental section of this work. The imidazolium-based $BMImBF_4$ ionic liquid was selected based on previous screening works that revealed a proper propylene solubility and good miscibility with the PVDF-HFP fluoropolymer [44]. The use of a silver salt with the same anion as the ionic liquid intends to reduce the number of chemical species in the composite membranes, hence reducing its complexity. Finally, the PVDF-HFP fluoropolymer presents moderate crystallinity [45], which is related to the low physical solubility of the gaseous species. Therefore, as the olefin sorption is vastly enhanced by the chemical complexation, the use of a low permeable polymer in conjunction with facilitated transport results in very high selectivities and permeabilities. In addition, PVDF-HFP presents remarkable mechanical, thermal and chemical stability.

As opposed to previous models reported in the literature, this model is able to simulate the three transport mechanisms simultaneously acting in the membrane, weighting at the same time their relative contribution. Therefore, the reported model provides a useful predictive tool to be applied in such systems where fixed-site carrier and mobile carrier transport mechanisms coexist, thus simplifying the optimization and scaling-up of composite membranes-based separation units.

2. Experimental

2.1. Chemicals

Propylene and propane gases were purchased from Praxair with a purity of 99.5% for both gases. Poly(vinylidene fluoride-co-hexafluoropropylene) (PVDF-HFP) was supplied by Sigma Aldrich. The ionic liquid $BMImBF_4$ with a minimum purity of 99% and a halide content of less than 500 ppm was provided by Iolitec. Silver tetrafluoroborate ($AgBF_4$) with a minimum purity of 99% was purchased from Apollo Scientific Ltd. Tetrahydrofuran (THF) was supplied by Panreac and was used as solvent for membrane synthesis. All chemicals were used as received with no further purification.

2.2. Membrane synthesis

The composite membranes for the experimental tests were prepared by the solvent casting method. The desired amount of PVDF-HFP was dissolved in THF using a 10 mL sealed glass vial to avoid solvent losses by evaporation. The content was stirred during 24 h at room temperature. To achieve complete dissolution of the polymer, the mixture was subjected to a heating step at 50 °C during 5 min. After that, the selected amounts of ionic liquid and silver salt were added to the solution and the whole mixture was stirred at room temperature during 15 min. The membrane precursor was poured in a glass dish and then introduced in a vacuum oven overnight at 800 mbar and 25 °C. Finally, a more severe evaporation step at full vacuum (~1 mbar) during 1 h was performed for further solvent removal. Light exposure was avoided during the whole synthesis process to prevent silver reduction. The resulting thickness of the prepared dense films was around 100 µm. For calculation purposes, the real thickness of each membrane was measured using a digital micrometer Mitutoyo Digimatic MDC-25SX (accuracy ± 0.001 mm).

2.3. Gas permeation experiments

The gas permeation experiments were conducted using the gas-mixture continuous-flow technique. A complete description of the permeation method has been included in previous works [29]. Essentially, the membrane was placed in a steel permeation cell and the desired olefin/paraffin mixture was passed through the upper chamber. Nitrogen was used as sweeping gas through the permeate side. The cell was located in a temperature-controlled oven. The feed and permeate streams were analyzed using a gas HP 6890 chromatograph equipped with a thermal conductivity detector (TCD). A simple mass balance allows calculating the experimental flow of each gaseous species through the membrane:

$$J_{C_3H_X} = \frac{1}{A_m}\frac{x_{C_3H_X}}{x_{N_2}}F_{N_2} \tag{1}$$

Where A_m is the effective membrane area, $x_{C_3H_X}$ and x_{N_2} are the gaseous species mole fractions, respectively, in the permeate chamber outlet stream and F_{N_2} is the nitrogen molar flow rate. The permeation experiments were conducted at the experimental conditions shown in Table 1, where the studied variables are the temperature, ranging from 293 to 303 K, the feed pressure, ranging from 1 to 3 bar and the membrane silver loading from 1.3 to 5.2 mol L^{-1}.

2.4. Membrane morphology characterization

Scanning electron microscopy (Carl Zeiss EVO MA 15) was employed to observe the cross-section and surface morphology of the synthesized membranes. The samples were prepared by liquid nitrogen fracturing to avoid altering the sectional morphology, followed by gold sputtering in a Balzers Union SCD040 sputter coating system. The line-scan spectrum of energy dispersive X-ray spectroscopy (EDX) was applied to the same samples of SEM to assess the silver dispersion profile in the membrane cross-section.

3. Mathematical modeling

The gas transport mechanisms occurring inside the membrane are the result of the complex membrane structure. In the reported model, we approach the complexity of the composite membrane structure by simplifying its nature, considering that the transport mechanism is shared between fixed site and mobile carrier, accounting for bounded and unbounded silver cations, respectively. On the one hand, fixed-site carrier mechanism appears when the silver cations bind to polymer atoms that can donate electrons and stabilize (i.e. fluorine atoms present in PVDF-HFP backbone). Experimental studies in the literature report the capability of fluorine atoms in C-F groups to form co-ordination bonds with cations as Ag^+ [46,47]. In this regard, PVDF-HFP has been previously reported for the preparation of polymer electrolytes by blending with HBF_4, resulting in the proton coordination with the polymer fluorine atoms [48]. The $AgBF_4$ solubility in a polymer matrix by means of coordination with the electron-donor atoms of the polymer chains has been also reported [49]. On the other hand, the presence of ionic liquid molecules within the free volume of the polymer facilitates the existence of unbound silver cations with higher freedom to diffuse. When the olefin complexes with one of these silver cations, the whole organometallic complex diffuses through the membrane. This transport mechanism is known as "mobile carrier". A schematic representation of the transport mechanisms is depicted in Fig. 1.

The total propylene flux through the membrane may be calculated as the sum of the contribution of each transport mechanism [32]:

$$J_{C_3H_6} = -D_{C_3H_6,m}\frac{dC_{C_3H_6}}{dx} - A\frac{dC_{C_3H_6}}{dx} - B\frac{dC_{C_3H_6}}{dx} \tag{2}$$

The parameters A and B represent the "effective diffusivity" of the organometallic complex specie in the mobile carrier and fixed-site carrier mechanisms respectively. Eq. (2) can be integrated along the membrane domain:

$$J_{C_3H_6} = D_{C_3H_6,m}\frac{C^0_{C_3H_6} - C^L_{C_3H_6}}{L} + A\frac{C^0_{C_3H_6} - C^L_{C_3H_6}}{L} + B\frac{C^0_{C_3H_6} - C^L_{C_3H_6}}{L} \tag{3}$$

Where subscripts 0 and L refer to feed and permeate sides, respectively. If sorption equilibrium at the interphase is assumed, Eq. (3) can be reformulated as:

$$J_{C_3H_6} = D_{C_3H_6,m}\cdot S_{C_3H_6,m}\frac{p^0_{C_3H_6} - p^L_{C_3H_6}}{L} + P_{comp}\frac{p^0_{C_3H_6} - p^L_{C_3H_6}}{L} + K_H\frac{p^0_{C_3H_6} - p^L_{C_3H_6}}{L} \tag{4}$$

Where P_{comp} is the permeability of the olefin based on the olefin-silver complex transport and K_H acts as an effective permeability or "hopping

Table 1
Experimental conditions.

Experimental condition	Value
T (K)	293–303
Permeation area (cm^2)	53
N_2 flow (mL min^{-1})	20
C_3H_6 flow (mL min^{-1})	15
C_3H_8 flow (mL min^{-1})	15
C_3H_8/C_3H_6 feed gas ratio	50:50
Feed side pressure (bar)	1–3
Permeate side pressure (bar)	1
Silver concentration (mol L^{-1})	1.3–5.2
Polymer/ionic liquid mass ratio	80:20

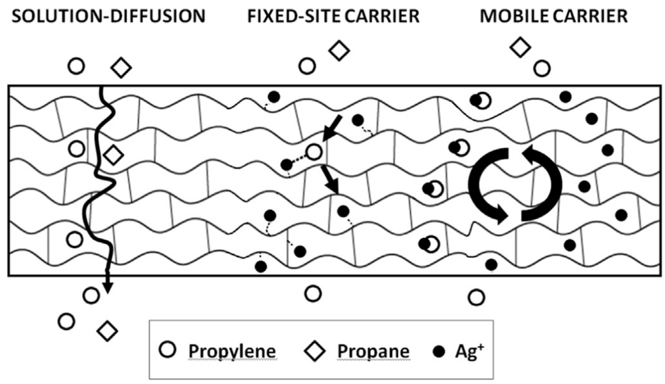

Fig. 1. Schematic representation of the gas transport mechanisms.

parameter” for the olefin via fixed site carrier mechanism. The diffusivity and solubility values of propylene in the PVDF-HFP/BMImBF$_4$ matrix have been reported previously [50]; however, in many cases, the contribution of the solution-diffusion mechanism can be neglected compared with that caused by facilitated transport.

The permeability of the olefin-silver complex attributed to the mobile carrier mechanism is the product of its diffusivity in the ionic liquid times its chemical solubility; this latter parameter can be obtained from the complexation reaction between the silver cations and the propylene as follows [27]:

$$Ag^+ + C_3H_6 \overset{Keq}{\longleftrightarrow} Ag^+(C_3H_6) \tag{5}$$

The equilibrium constant can be expressed as:

$$k_{eq} = \frac{[Ag^+(C_3H_6)]}{[Ag^+]\cdot[C_3H_6]} \tag{6}$$

While the concentration of free cations is given by:

$$[Ag^+] = [Ag^T] - [Ag^+(C_3H_6)] \tag{7}$$

Solving for the complex specie concentration:

$$[Ag^+(C_3H_6)] = \frac{k_{eq}[Ag^T]\cdot[C_3H_6]}{1 + k_{eq}[C_3H_6]} \tag{8}$$

Furthermore, after the relationship between the concentration of propylene physically absorbed and the partial pressure in the gas phase through a Henry type isotherm the resulting equation is:

$$[Ag^+(C_3H_6)] = \frac{k_{eq}[Ag^T]\cdot p_{C_3H_6}H_{C_3H_6}}{1 + k_{eq}p_{C_3H_6}H_{C_3H_6}} \tag{9}$$

So that the ratio between the organometallic complex concentration and the propylene partial pressure in the gas phase, i.e. a chemical solubility coefficient, can be obtained as:

$$S_{C_3H_6,chem} = \frac{k_{eq}[Ag^T]\cdot H_{C_3H_6}}{1 + k_{eq}p_{C_3H_6}H_{C_3H_6}} \tag{10}$$

Finally, the olefin permeability through the mobile carrier mechanism can be expressed as:

$$P_{comp} = \frac{k_{eq}[Ag^T]\cdot H_{C_3H_6}}{1 + k_{eq}p_{C_3H_6}H_{C_3H_6}}\cdot D_{comp} \tag{11}$$

Where the equilibrium constant k_{eq}, the physical solubility of the propylene in the ionic liquid $H_{C_3H_6}$, the olefin-paraffin complex diffusivity D_{comp}, and the influence of temperature on these parameters have been reported in previous works [22,27]:

$$\mathrm{H}_{C_3H_6} = \mathrm{H}_{C_3H_6,0}\, e^{\frac{-\Delta H_{sol}}{RT}} \tag{12}$$

$$\ln\frac{k_{eq}}{k_{eq,ref}} = -\frac{\Delta H_r}{R}\left(\frac{1}{T} - \frac{1}{T_{ref}}\right) \tag{13}$$

$$\mathrm{D_{comp}} = D_{comp,ref}\, e^{-\frac{Ea_D}{R}\left(\frac{1}{T} - \frac{1}{T_{ref}}\right)} \tag{14}$$

In addition, it should be taken into account that the transport flux due to the fixed site carrier mechanism, characterized by the “hopping parameter” $\mathrm{K_{FC}}$, is a function of the silver loading in the membrane and the temperature [51]. A mathematical expression can be derived for the dependence of $\mathrm{K_{FC}}$ on temperature and silver concentration. The concentration of free cations ready to coordinate with propylene molecules to form the coordination complex can be derived from the chemical equilibrium. In this regard, the heterogeneous complexation reaction between propylene and silver cations bound to the polymer matrix is depicted by the following equation:

$$[Ag^+] + P_{C_3H_6} \overset{k_p}{\leftrightarrow} [Ag^+(C_3H_6)] \tag{15}$$

Again, the equilibrium constant can be expressed as:

$$k_p = \frac{[Ag^+(C_3H_6)]}{[Ag^+]\cdot p^0_{C_3H_6}} \tag{16}$$

Introducing Eq. (7) and solving for the free silver cations concentration:

$$[Ag^+] = \frac{[Ag^T]}{1 + k_p p^0_{C_3H_6}} \tag{17}$$

The proportionality between the value of $\mathrm{K_{FC}}$ and the variables is defined through the fitting parameter α:

$$\mathrm{K_{FC}} = \alpha\left(\frac{[Ag^T]}{1 + k_P\cdot p^0_{C_3H_6}}\right) e^{\frac{Ea_{FC}}{R}\left(\frac{1}{293} - \frac{1}{T}\right)} \tag{18}$$

In Eq. (18) the influence of temperature in the hopping mechanism has been described through an Arrhenius-type expression, and the term in brackets refers to the concentration of free “uncomplexed” silver cations, as obtained from the heterogeneous chemical equilibrium, Eq. (16). The value of the heterogeneous equilibrium constant has been taken from previous works based on the fixed-site carrier mechanism [51]. The parameter α and the activation energy of the hopping parameter (Ea_{FC}) are the two fitting parameters of the model.

To summarize, the propylene flux is described as the sum of three contributions as follows:

$$J_{C_3H_6} = J_{C_3H_6,SD} + J_{C_3H_6,MC} + J_{C_3H_6,FC} \tag{19a}$$

$$J_{C_3H_6,SD} = D_{C_3H_6,m}\cdot S_{C_3H_6,m}\frac{p^0_{C_3H_6} - p^L_{C_3H_6}}{L} \tag{19b}$$

$$J_{C_3H_6,MC} = \frac{k_{eq}[Ag]H_{C_3H_6}}{1 + k_{eq}p_{C_3H_6}H_{C_3H_6}}\cdot D_{comp}\frac{p^0_{C_3H_6} - p^L_{C_3H_6}}{L}x_{IL} \tag{19c}$$

$$J_{C_3H_6,FC} = K_{FC}\frac{p^0_{C_3H_6} - p^L_{C_3H_6}}{L}(1 - x_{IL}) \tag{19d}$$

The contribution of the two different mechanisms of facilitated transport mechanism has been weighted based on the mass fraction of ionic liquid in the membrane composition x_{IL}. This approach assumes that the available silver cations are distributed according to the polymer/ionic liquid mass ratio and homogeneously dispersed as observed in EDX analysis.

The propane flux is caused by simple Fickian diffusion along the membrane, as described by the following equation:

$$J_{C_3H_8} = D_{C_3H_8,m}\cdot S_{C_3H_8,m}\frac{p^0_{C_3H_8} - p^L_{C_3H_8}}{L} \tag{20}$$

With the exception of the fitting parameters, α and Ea_{FC}, the values of model parameters have been extracted from previous works. In the case of mobile carrier, the values of the organometallic complex diffusivity and its dependence on temperature were taken from an experimental study on supported ionic liquid membranes (SILMs). These membranes where synthesized introducing the $BMImBF_4/AgBF_4$ mixture in the pores of a hydrophilic PVDF support [22]. The value of the equilibrium constant for the complexation reaction, the propylene solubility in the ionic liquid, and their enthalpies were extracted from absorption equilibria of propylene in ionic liquid/Ag^+ solutions [27]. The value of the heterogeneous equilibrium constant was calculated in a previous study on fixed site carrier mechanism [51].

It is worth noticing that the values of the estimated parameters are dependent on the chemical nature of the involved species (permeant gas, polymer, carrier and ionic liquid) and the interactions between them. As a result, the procedure to implement this model in similar hybrid systems implies the use of case-specific model parameters and the estimation of a new pair of values for both α and Ea_{FC}.

4. Results and discussion

4.1. Membrane morphology

Fig. 2 shows the cross-section and surface of a PVDF-HFP membrane, a PVDF-HFP/$BMImBF_4$ membrane and a composite PVDF-HFP/$BMImBF_4/AgBF_4$. The cross-section micrographs show a non-porous homogenous structure without cavities or voids in all three cases. There is no evidence of pure ionic liquid domains in membranes **B** and **C**, proving the complete mixture between the ionic liquid and the polymer. Furthermore, the addition of the silver salt in membrane **C** does not modify the structure but maintains the original dense and homogeneous pattern.

Further knowledge on membrane structure can be extracted from the EDX analysis. EDX makes use of x-ray spectrum emitted by the solid sample bombarded with a focused beam of electrons to obtain a localized chemical analysis. When the sample is hit by the electron beam, electrons are ejected from the atoms of the sample's surface. The resulting electron vacancies are filled by electrons from a higher energy state, and an x-ray is emitted to balance the energy difference between the two electrons' states. The x-ray energy is characteristic of the element from which it was emitted.

In this work, EDX was used in conjunction with SEM to obtain scanlines and plot-mapping patterns of elemental silver on cross-sectional images of the composite membrane. The energy dispersive x-ray spectroscopy patterns shown in Fig. 3 confirm that no ionic aggregates or silver particles are formed inside the membrane, which is in good agreement with the previous discussion on silver salt dissolution. Thus, the silver is homogeneously dispersed along the membrane thickness with no layers of preferential accumulation.

4.2. Permeation results

Table 2 displays the experimental performance of the composite membranes assessed in this work. The experimental effective permeability has been calculated normalizing the experimental flux with the membrane thickness and the partial pressure gradient, as shown in Eq. (21).

$$P_{C_3H_X} = J_{C_3H_X}\frac{L}{\Delta p_{C_3H_X}} \tag{21}$$

Facilitated transport phenomena yielded remarkably high values of propylene permeability. On the other hand, the composite material causes very low propane permeability, as it is only due to Fickian diffusion. As a result, the membrane provides remarkably high separation selectivity values. The results show that the propane permeability suffers a slight increase as the silver loading rises. Although the behavior of the paraffin is unusual, similar behavior has been observed in some previous studies, such as those reported by Kim et al. [52] and Surya Murali et al. [53].

Fig. 4 depicts the influence of the feed partial pressure on the experimental olefin flux. As the partial pressure gradient offers the driving force of the separation process, it has a direct effect on the propylene flux. Nonetheless, the composite membrane performs high olefin fluxes even at the lower assessed partial pressures, forecasting its suitability for the separation of other olefin/paraffin mixtures with minor presence

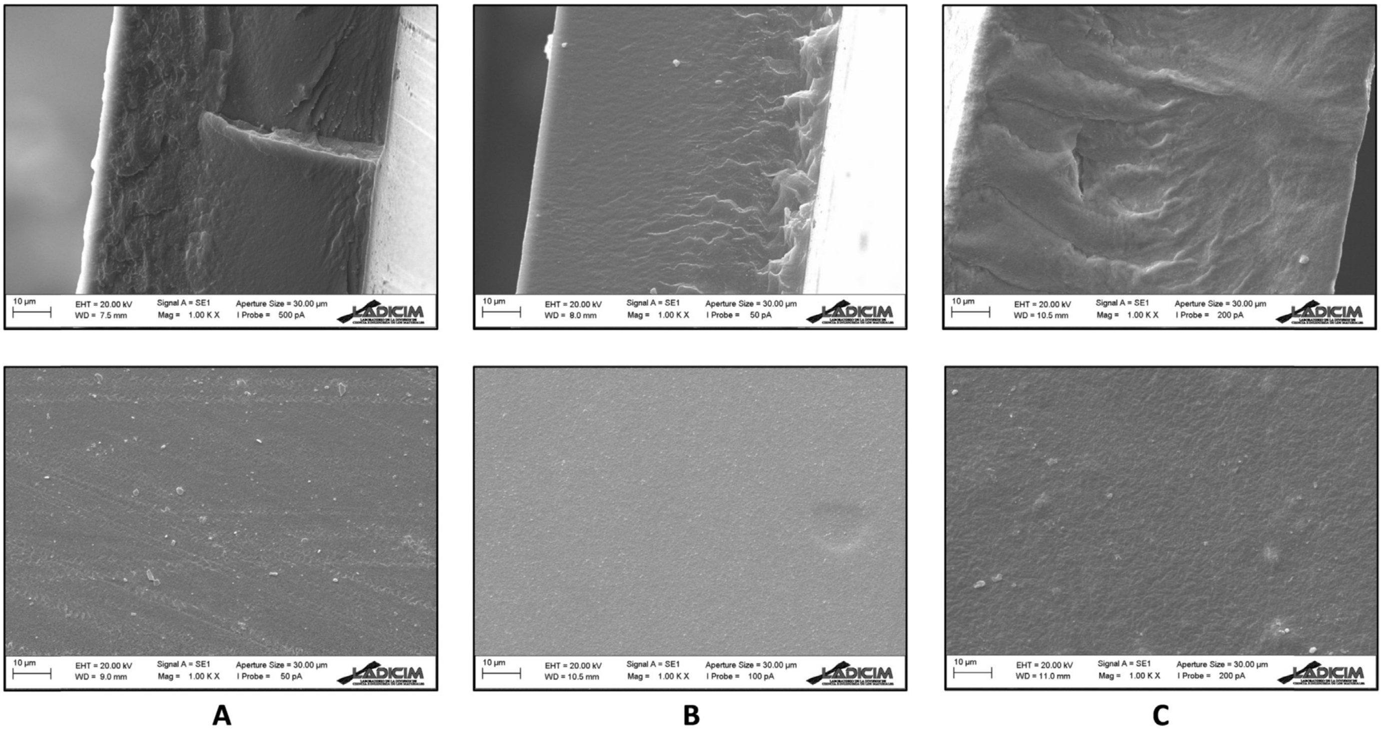

Fig. 2. Cross-section and surface morphology of: A) PVDF-HFP membrane B) PVDF-HFP/$BMImBF_4$ membrane, C) PVDF-HFP/$BMImBF_4/AgBF_4$ 5.2 mol/L.

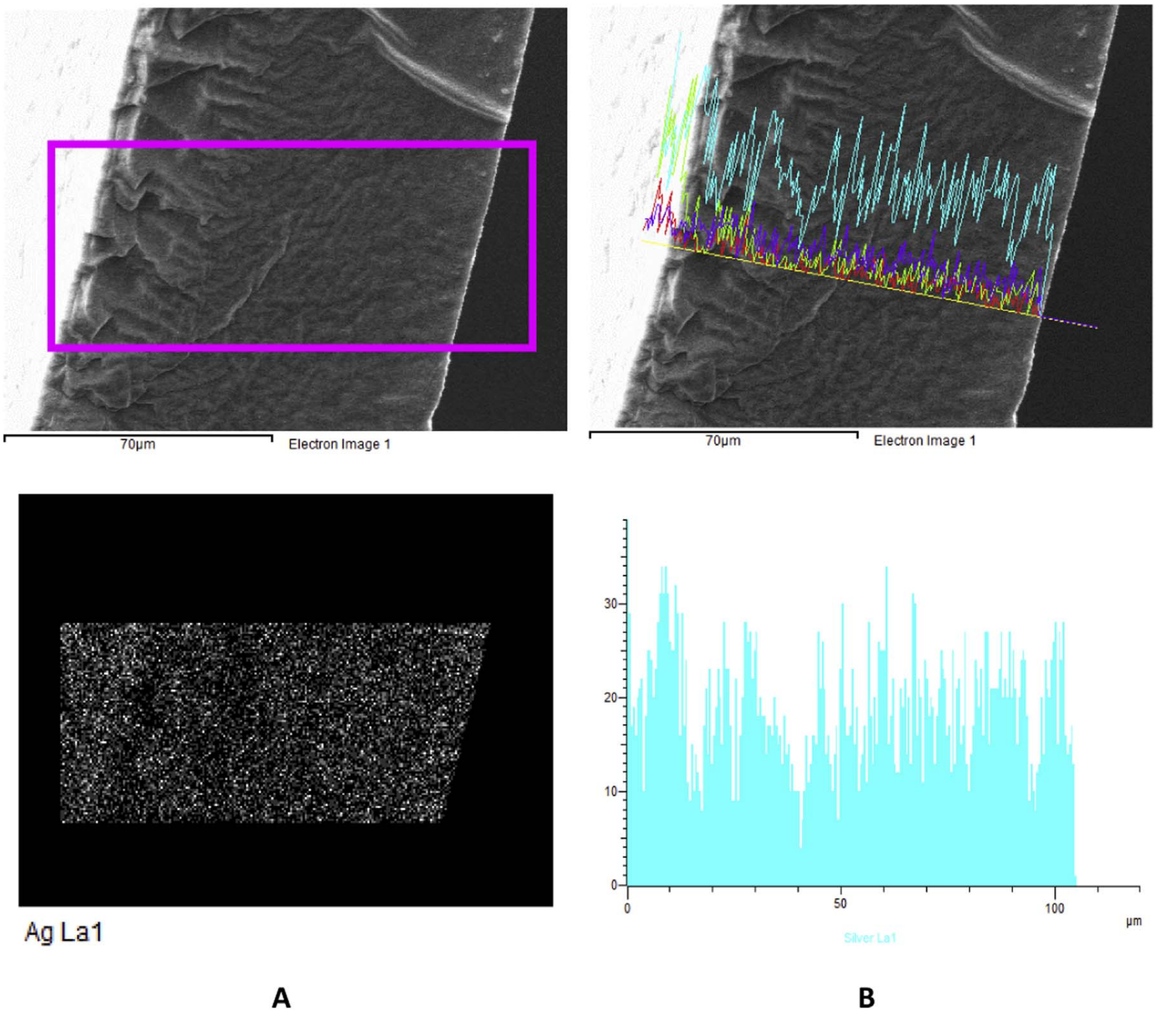

Fig. 3. Energy dispersive X-Ray spectroscopy patterns of silver in the PVDF-HFP/BMImBF$_4$/AgBF$_4$ 5.2 mol/L membrane: A) dispersion plot, B) scan-line.

Table 2
Experimental permeability and propylene/propane selectivity at 293 K and 0.5 bar feed partial pressure of each gas.

[Ag] (M)	P C_3H_8 (Barrer)	P C_3H_6 (Barrer)	$\alpha_{i/j}$
1.31	6.1	890	146
2.62	10.8	1374	127
3.92	14.4	2342	163
5.23	24.7	3291	133

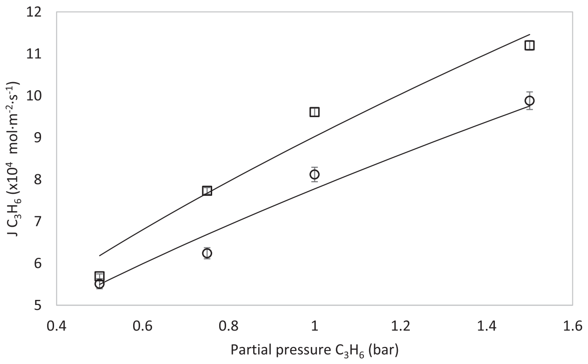

Fig. 4. Experimental and predicted propylene flux in the PVDF-HFP/BMImBF$_4$/AgBF$_4$ 5.2 mol/L membrane at 293 (○) and 303 K (□) with increasing partial pressure.

of the olefin. On the other hand, the effect of the temperature increase on the propylene flux is also depicted in Fig. 4. The resulting higher flux at 303 K is mainly caused by the positive effect of temperature on the organometallic complex diffusivity. Although the solubility of the gaseous species decreases at higher temperatures and the complexation equilibrium constant is negatively affected by the temperature, these effects are hindered by the diffusivity influence on the permeation process [50].

The non-linear trend observed in Fig. 4 is an indication that a selective reaction is taking place within the membrane, which is consistent with the facilitated transport mechanism. It is a well known behavior in facilitated transport membranes that the partial pressure markedly influences the permeability of the gas that interacts with the carrier [47]. Taking into account that the permeability has been defined as a phenomenological parameter by means of Eq. (21), the values calculated from the experimental fluxes are shown in Fig. 5. A typical behavior of facilitated transport membranes can be seen, characterized by a decreasing permeability value with the olefin partial pressure as the carrier becomes saturated.

The effect of silver concentration on the propylene flux is shown in Fig. 6. A linear increase of the experimental flux is clearly observed with increasing silver concentration. As opposed to polymer electrolyte membranes, ionic-liquid-containing composite membranes do not perform the characteristic “percolation threshold” [26,51,54,55]. This effect is caused when the silver concentration is low enough to prevent hoping of the olefin molecules from site-to-site in systems where fixed site carrier is the only facilitated transport mechanism. In composite

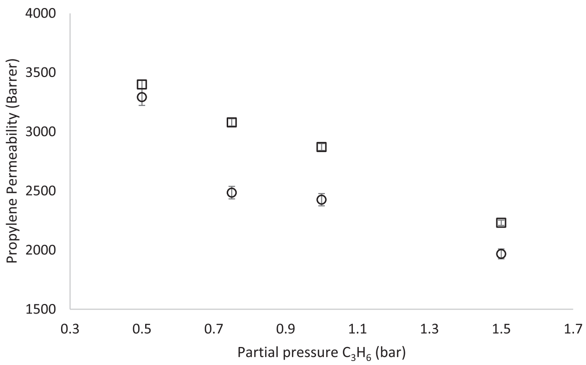

Fig. 5. Propylene permeability at 293 (○) and 303 K (□) with increasing feed partial pressure in the PVDF-HFP/BMImBF$_4$/AgBF$_4$ 5.2 mol/L membrane.

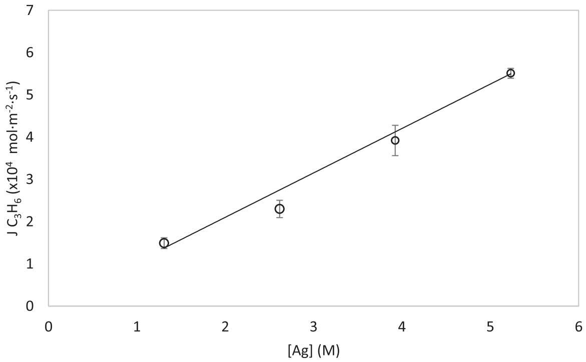

Fig. 6. Experimental and predicted propylene flux in the PVDF-HFP/BMImBF$_4$/AgBF$_4$ membrane at 293 K and a propylene feed partial pressure of 0.5 bar with increasing silver loading.

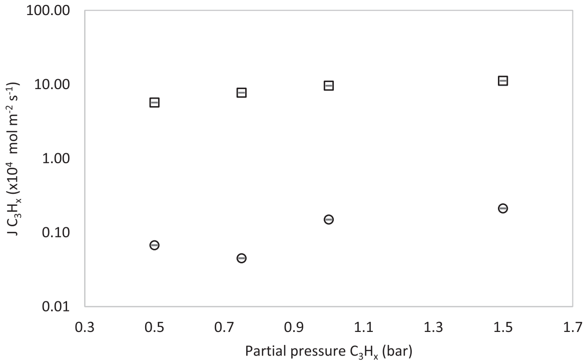

Fig. 7. Propylene (□) and propane (○) experimental flux at 303 K in the PVDF-HFP/BMImBF$_4$/AgBF$_4$ 5.2 mol/L membrane with increasing feed partial pressure.

Table 3
Values of model parameters from previous works.

Parameter	Value	Reference
$D_{comp,ref}$ ($\times 10^{11}$ m^2 s^{-1})	3.22[a]	[22]
Ea_D (kJ mol^{-1})	7.13	[22]
k_p (bar^{-1})	0.12	[51]
$H_{C_3H_6,0}$ ($\times 10^3$ mol ar^{-1} m^{-3})	4.28	[27]
ΔH_{sol} (kJ mol^{-1})	−24.1	[27]
$k_{eq,ref}$ (m^3 mol)	0.337[b]	[27]
ΔH_r (kJ mol^{-1})	−11.0	[27]

[a] The reference temperature is 293 K.
[b] The reference temperature is 278 K.

Table 4
Estimated model parameters.

Parameter	Value
Fixed-site carrier activation energy, Ea (kJ mol^{-1})	14.8
Fitting parameter, α ($\times 10^{11}$ m^2 bar^{-1} s^{-1})	1.35

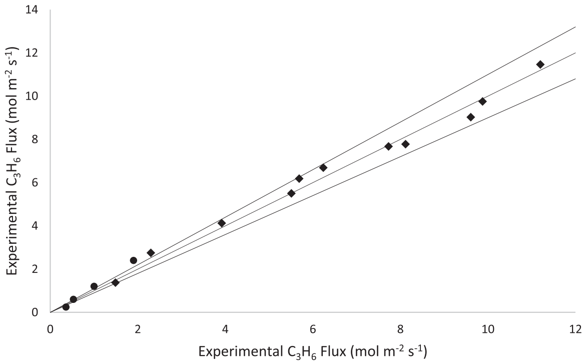

Fig. 8. Model parity graph displaying a 10% error range: composite membranes (◆) SILMs (•).

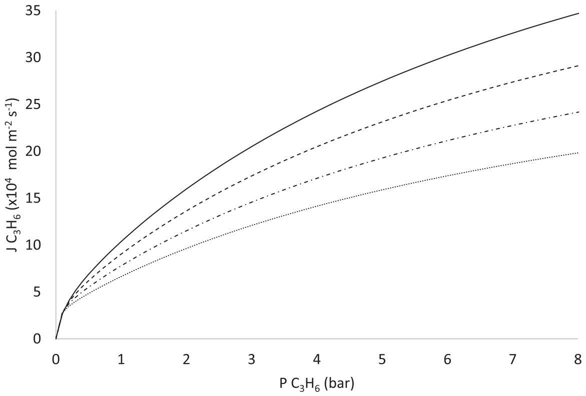

Fig. 9. Propylene flux prediction in PVDF-HFP/BMImBF$_4$/AgBF$_4$ 5.23 M at 283 K (dot line); 293 K (dot-dash line); 303 K (dash line) and 313 K (solid line) over an extended propylene partial pressure range.

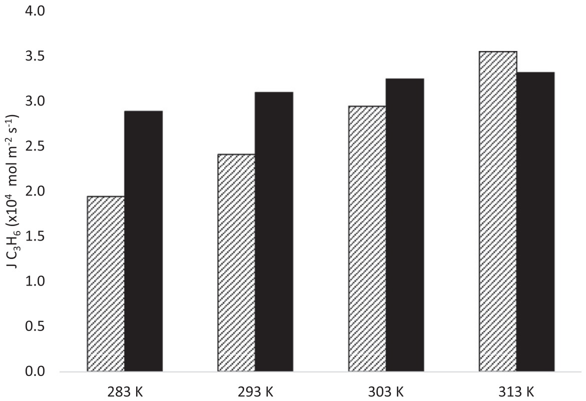

Fig. 10. Predicted contribution of each facilitated transport mechanism to the total flux with increasing temperature at 0.5 bar propylene partial pressure in PVDF-HFP/BMImBF$_4$/AgBF$_4$ 5.23 M: fixed-site carrier (in stripes) and mobile carrier (in black).

membranes, the presence of the ionic liquid ensures transport facilitation via mobile carrier even at low silver concentrations.

Fig. 7 depicts the comparison between propylene and propane fluxes in a logarithmic scale. The noticeable difference between the flux values is due to two simultaneous phenomena, that is: in addition to the facilitated transport of propylene, the PVDF-HFP crystallinity reduces the paraffin physical solubility, yielding very low flux via conventional solution-diffusion [45]. As a result, permeability selectivities higher than 150 are achieved, which satisfy the requirements for most of the industrial applications.

4.3. Model results

The model parameters taken from previous experimental studies are shown in Table 3. The proposed model has two estimated parameters: the fitting parameter α, and the fixed site carrier activation energy Ea_{FC}. Model regression to experimental data for each specific case study is needed in order to determine the values of these parameters. Aspen Custom Modeler software was employed in this work for estimation tasks. The resulting values of the fitting parameters for this particular case study are displayed in Table 4.

Once the fitting parameters are obtained, the model is able to describe the system performance providing that the input data are within the studied range. Figs. 4 and 6 compare the model predicted values to experimental data and prove the model accuracy to simulate the transmembrane flux for changing temperature, feed pressure and silver loading. The model values have been plotted against the experimental data to build the model parity graph, displaying a 10% error range, Fig. 8. Besides, this generalized model is also capable of simulating the performance of SILMs when the fixed-site carrier contribution is neglected; in order to confirm this possibility, the parity graph includes the experimental and model results of supported ionic liquid membranes (SILMs) reported in previous works [22]. It can be seen that the majority of the points fall within the acceptable error interval, suggesting an accurate fitting between the experimentally obtained values and the model calculations.

With aim at the model application, it is also possible to extrapolate the model calculations out of the range of the studied variables, while taking into account the possible deviations associated with the extrapolation method. In this manner, the present model is a useful predictive tool to calculate the transmembrane flux in composite membranes performing a hybrid mobile/fixed carrier gas transport mechanisms. Fig. 9 shows the predicted propylene flux in a wide range of propylene feed partial pressures and four temperatures for the highest silver loading assessed in this work. The values at pressures outside the 0.5–1.5 bar interval and at 283 and 313 K are model extrapolations. Process design and decision-making using composite membranes could be improved implementing the proposed mathematical expressions to predict the material performance.

Finally, with the model, it is possible to calculate the contribution of the individual facilitated transport mechanisms to the total flux, as shown in Fig. 10. The contribution of the solution-diffusion mechanism has been neglected because it represents less than 1% of the total flux in all cases. Note that the values at 283 K and 313 K have been extrapolated. The results show that, although the flux always shows an increasing trend with temperature, this variable has a greater effect on the fixed-site carrier mechanism compared to the mobile carrier. This behavior is explained through the negative effect of temperature on the solubility term in the mobile carrier contribution.

5. Conclusions

A novel mathematical model able to describe the facilitated transport of propylene in composite membranes is reported. The model takes into account the different transport mechanisms featured in polymer/ionic-liquid/carrier systems, namely, solution-diffusion, fixed-site carrier and mobile carrier transport, describing the total gas flux as the sum of the contributions by each mechanism.

In order to check the suitability of the model simulated results where compared to experimental data obtained working with PVDF-HFP/$BMImBF_4$/$AgBF_4$ membranes in continuous-flow gas-mixture permeation tests, varying the temperature, silver loading and feed pressure. It has been checked that the addition of $BMImBF_4$ ionic liquid, which makes the membranes differ from solid state polymer electrolyte membranes, avoids the characteristic “percolation threshold” phenomena and allows transport facilitation even at low carrier concentration.

The model needs two fitting parameters $\alpha = 1.35 \times 10^{-11}\ \mathrm{m^2\ bar^{-1}\ s^{-1}}$ and $Ea = 14.8\ \mathrm{kJ\ mol^{-1}}$ that are case-sensitive depending on the chemical nature of the species (olefin, polymer, silver salt, ionic liquid) and their interactions. The reported model becomes a useful tool to predict the transmembrane flux via facilitated transport in those systems featuring fixed-site carrier and mobile carrier mechanisms simultaneously. In this regard, it will allow further design and optimization of more efficient membrane configurations.

Acknowledgement

Financial support from projects CTQ2015-66078-R and CTQ2016-75158-R (MINECO, Spain-FEDER 2014–2020) is gratefully acknowledged. Raúl Zarca also thanks the Universidad de Cantabria for a postgraduate fellowship.

References

[1] D.S. Sholl, R.P. Lively, Seven chemical separations to change the world, Nature 532 (2016) 6–8.
[2] J.C. Charpentier, In the frame of globalization and sustainability, process intensification, a path to the future of chemical and process engineering (molecules into money), Chem. Eng. J. 134 (2007) 84–92.
[3] O.M. Ilinitch, G.L. Semin, M.V. Chertova, K.I. Zamaraev, Novel polymeric membranes for separation of hydrocarbons, J. Memb. Sci. 66 (1992) 1–8.
[4] K. Okamoto, A. Taguchi, J. Hao, K. Tanaka, H. Kita, Permeation and separation properties of polyimide membranes to olefins and paraffins, J. Memb. Sci. 121 (1996) 197–207.
[5] A. Ito, S.-T. Hwang, Permeation of propane and propylene thrugh cellulosic polymer membranes, J. Appl. Polym. Sci. 38 (1989) 483–490.
[6] R. Faiz, K. Li, Polymeric membranes for light olefin/paraffin separation, Desalination 287 (2012) 82–97.
[7] R.J. Swaidan, X. Ma, E. Litwiller, I. Pinnau, Enhanced propylene/propane separation by thermal annealing of an intrinsically microporous hydroxyl-functionalized polyimide membrane, J. Memb. Sci. 495 (2015) 235–241.
[8] K.S. Liao, J.Y. Lai, T.S. Chung, Metal ion modified PIM-1 and its application for propylene/propane separation, J. Memb. Sci. 515 (2016) 36–44.
[9] V.F.D. Martins, A.M. Ribeiro, A. Ferreira, U.H. Lee, Y.K. Hwang, J.S. Chang, J.M. Loureiro, A.E. Rodrigues, Ethane/ethylene separation on a copper benzene-1,3,5-tricarboxylate MOF, Sep. Purif. Technol. 149 (2015) 445–456.
[10] M. Hartmann, U. Böhme, M. Hovestadt, C. Paula, Adsorptive Separation of Olefin/Paraffin Mixtures with ZIF-4, Langmuir 31 (2015) 12382–12389.
[11] O. Salinas, X. Ma, Y. Wang, Y. Han, I. Pinnau, Carbon molecular sieve membrane from a microporous spirobisindane-based polyimide precursor with enhanced ethylene/ethane mixed-gas selectivity, RSC Adv. 7 (2017) 3265–3272.
[12] R.J. Swaidan, X. Ma, I. Pinnau, Spirobisindane-based polyimide as efficient precursor of thermally-rearranged and carbon molecular sieve membranes for enhanced propylene/propane separation, J. Memb. Sci. 520 (2016) 983–989.
[13] H.-X. Sun, B.-B. Yuan, P. Li, T. Wang, Y.-Y. Xu, Preparation of nanoporous graphene and the application of its nanocomposite membrane in propylene/propane separation, Funct. Mater. Lett. 8 (2015) 1550019.
[14] I. Pinnau, L.G. Toy, Solid polymer electrolyte composite membranes for olefin/paraffin separation, J. Memb. Sci. 184 (2001) 39–48.
[15] D.J. Safarik, R.B. Eldridge, Olefin/Paraffin Separations by Reactive Absorption: a Review, Ind. Eng. Chem. Res. 37 (1998) 2571–2581.
[16] A. Ortiz, L.M. Galán, D. Gorri, A.B. De Haan, I. Ortiz, Kinetics of reactive absorption of propylene in RTIL-Ag^+ media, Sep. Purif. Technol. 73 (2010) 106–113.
[17] M. Teramoto, H. Matsuyama, T. Yamashiro, Y. Katayama, Separation of ethylene from ethane by supported liquid membranes containing silver-nitrate as a carrier, J. Chem. Eng. Jpn. 19 (1986) 419–424.
[18] S. Duan, A. Ito, A. Ohkawa, Separation of propylene/propane mixture by a supported liquid membrane containing triethylene glycol and a silver salt, J. Memb. Sci. 215 (2003) 53–60.
[19] G. Zarca, I. Ortiz, A. Urtiaga, Copper(I)-containing supported ionic liquid membranes for carbon monoxide/nitrogen separation, J. Memb. Sci. 438 (2013) 38–45.
[20] M.T. Ravanchi, T. Kaghazchi, A. Kargari, Supported liquid membrane separation of propylene-propane mixtures using a metal ion carrier, Desalination 250 (2010) 130–135.
[21] D. Gorri, M. Fallanza, A. Ortiz, I. Ortiz, Supported liquid membranes for pervaporation processes, Ref. Modul. Chem. Mol. Sci. Chem. Eng. (2017).
[22] M. Fallanza, A. Ortiz, D. Gorri, I. Ortiz, Experimental study of the separation of propane/propylene mixtures by supported ionic liquid membranes containing

Ag^+–RTILs as carrier, Sep. Purif. Technol. 97 (2012) 83–89.

[23] T. Welton, Room-temperature ionic liquids. solvents for synthesis and catalysis, Chem. Rev. 99 (1999) 2071–2083.

[24] J.P. Hallett, T. Welton, Room-temperature ionic liquids: solvents for synthesis and catalysis. 2, Chem. Rev. 111 (2011) 3508–3576.

[25] R. Faiz, K. Li, Olefin/paraffin separation using membrane based facilitated transport/chemical absorption techniques, Chem. Eng. Sci. 73 (2012) 261–284.

[26] J.H. Kim, S.W. Kang, Y.S. Kang, Threshold silver concentration for facilitated olefin transport in polymer/silver salt membranes, J. Polym. Res. 19 (2012).

[27] A. Ortiz, A. Ruiz, D. Gorri, I. Ortiz, Room temperature ionic liquid with silver salt as efficient reaction media for propylene/propane separation: absorption equilibrium, Sep. Purif. Technol. 63 (2008) 311–318.

[28] A. Ortiz, L. Galán, D. Gorri, B. De Haan, I. Ortiz, Reactive ionic liquid media for the separation of propylene / propane gaseous mixtures, Ind. Eng. Chem. Res. 49 (2010) 7227–7233.

[29] M. Fallanza, A. Ortiz, D. Gorri, I. Ortiz, Polymer-ionic liquid composite membranes for propane/propylene separation by facilitated transport, J. Memb. Sci. 444 (2013) 164–172.

[30] L.C. Tomé, D. Mecerreyes, C.S.R. Freire, L.P.N. Rebelo, I.M. Marrucho, Polymeric ionic liquid membranes containing IL–Ag^+ for ethylene/ethane separation via olefin-facilitated transport, J. Mater. Chem. A 2 (2014) 5631.

[31] R.D. Noble, Facilitated transport with fixed-site carrier membranes, J. Chem. Soc., Faraday Trans. 87 (1991) 2089–2092.

[32] R.D. Noble, Generalized microscopic mechanism of facilitated transport in fixed site carrier membranes, J. Memb. Sci. 75 (1992) 121–129.

[33] S. Najari, S.S. Hosseini, M. Omidkhah, N.R. Tan, Phenomenological modeling and analysis of gas transport in polyimide membranes for propylene/propane separation, RSC Adv. 5 (2015) 47199–47215.

[34] S. Sridhar, A.A. Khan, Simulation studies for the separation of propylene and propane by ethylcellulose membrane, J. Memb. Sci. 1 (159) (1999) 209–219.

[35] M.T. Castoldi, Modeling of the Separation of Propene / Propane Mixtures by Permeation through Membranes in a Polymerization System, 2007, pp. 1259–1269.

[36] M. Ohyanagi, H. Nishide, K. Suenaga, E. Tsuchida, Effect of polymer matrix and metal species on facilitated oxygen transport in metalloporphyrin (Oxygen Carrier) fixed membranes, Macromolecules 21 (1988) 1590–1594.

[37] T. Suzuki, Y. Soejima, H. Nishide, E. Tsuchida, Effect of an oxygen-binding reaction at the cobalt porphyrin site fixed in a polymer membrane on facilitated oxygen transport, Bull. Chem. Soc. Jpn. 68 (1995) 1036–1041.

[38] D.R. Smith, J.A. Quinn, The facilitated transport of carbon monoxide through cuprous chloride solutions, AIChE J. 26 (1980) 112–120.

[39] R.D. Noble, Analysis of facilitated carrier membranes transport with fixed site, J. Memb. Sci 50 (1990) 207–214.

[40] Y.S. Kang, J.M. Hong, J. Jang, U.Y. Kim, Analysis of facilitated transport in solid membranes with fixed site carriers: 1. Single RC circuit model, J. Memb. Sci. 109 (1996) 149–157.

[41] J.M. Hong, Y.S. Kang, J. Jang, U.Y. Kim, Analysis of facilitated transport in polymeric membrane with fixed site carrier: 2. Series RC circuit model, J. Memb. Sci. 109 (1996) 159–163.

[42] W.J. Ward, Analytical and experimental studies of facilitated transport, AIChE J. 16 (1970) 405–410.

[43] B.M. Johnson, R.W. Baker, S.L. Matson, K.L. Smith, I.C. Roman, M.E. Tuttle, H.K. Lonsdale, Liquid membranes for the production of oxygen-enriched air. II. Facilitated-transport membranes, J. Memb. Sci. 31 (1987) 31–67.

[44] M. Fallanza, M. González-Miquel, E. Ruiz, A. Ortiz, D. Gorri, J. Palomar, I. Ortiz, Screening of RTILs for propane/propylene separation using COSMO-RS methodology, Chem. Eng. J. 220 (2013) 284–293.

[45] S. Abbrent, J. Plestil, D. Hlavata, J. Lindgren, J. Tegenfeldt, Å. Wendsjö, Crystallinity and morphology of PVdF–HFP-based gel electrolytes, Polymer 42 (2001) 1407–1416.

[46] H. Plenio, R. Diodone, Coordination chemistry with CF Units as B Donors: Ag^+ complexes of partially fluorinated crown ethers with direct metal-fluorine interactions, Chem. Ber. 129 (1996) 1211–1217.

[47] P.K. Sazonov, L.K. Minacheva, A.V. Churakov, V.S. Sergienko, G. a Artamkina, Y.F. Oprunenko, I.P. Beletskaya, Lariat ethers with fluoroaryl side-arms: a study of CFmetal cation interaction in the complexes of N-(o-fluoroaryl)azacrown ethers, Dalton Trans. (2009) 843–850.

[48] J. Chang, S.W. Kang, CO_2 separation through poly(vinylidene fluoride-co-hexafluoropropylene) membrane by selective ion channel formed by tetrafluoroboric acid, Chem. Eng. J. 306 (2016) 1189–1192.

[49] S. Sunderrajan, B.D. Freeman, C.K. Hall, I. Pinnau, Propane and propylene sorption in solid polymer electrolytes based on poly(ethylene oxide) and silver salts, J. Memb. Sci. 182 (2001) 1–12.

[50] R. Zarca, A. Ortiz, D. Gorri, I. Ortiz, Facilitated transport of propylene through composite polymer-ionic liquid membranes. mass transfer analysis, Chem. Prod. Process Model. 11 (2016) 77–81.

[51] R. Zarca, A. Ortiz, D. Gorri, I. Ortiz, A practical approach to fixed-site-carrier facilitated transport modeling for the separation of propylene/propane mixtures through silver-containing polymeric membranes, Sep. Purif. Technol. 180 (2017) 82–89.

[52] J.H. Kim, B.R. Min, J. Won, Y.S. Kang, Complexation mechanism of olefin with silver ions dissolved in a polymer matrix and its effect on facilitated olefin transport, Chem. - A Eur. J. 8 (2002) 650–654.

[53] R. Surya Murali, K. Yamuna Rani, T. Sankarshana, A.F. Ismail, S. Sridhar, Separation of binary mixtures of propylene and propane by facilitated transport through silver incorporated Poly(Ether-Block-Amide) membranes, Oil Gas. Sci. Technol. – Rev. d'IFP Energ. Nouv. 70 (2015) 381–390.

[54] Y. Yoon, J. Won, Y.S. Kang, Polymer electrolyte membranes containing silver ion for facilitated olefin transport, Macromolecules 33 (2000) 3185–3186.

[55] A. Morisato, Z. He, I. Pinnau, T.C. Merkel, Transport properties of PA12-PTMO/$AgBF_4$ solid polymer electrolyte membranes for olefin/paraffin separation, Desalination 145 (2002) 347–351.

Journal of Membrane Science 556 (2018) 321–328

Contents lists available at ScienceDirect

Journal of Membrane Science

journal homepage: www.elsevier.com/locate/memsci

Optimized distillation coupled with state-of-the-art membranes for propylene purification

Raúl Zarca[a], Alfredo Ortiz[a], Daniel Gorri[a], Lorenz T. Biegler[b], Inmaculada Ortiz[a,*]

[a] Department of Chemical and Biomolecular Engineering, University of Cantabria, Av. Los Castros 46, 39005 Santander, Spain
[b] Department of Chemical Engineering, Carnegie-Mellon University, 5000 Forbes Avenue, Pittsburgh, PA 15213-3890, United States

ARTICLE INFO

Keywords:
Optimization
Propylene
Propane
Hybrid distillation
Membrane
Mathematical model
Process intensification

ABSTRACT

The growing production of polyolefins, mainly polyethylene and polypropylene, currently demands increasing outputs of polymer-grade light olefins. The most commonly adopted process for the separation of olefin/paraffin mixtures is performed by energy intensive high pressure or cryogenic distillation, which is considered the most expensive operation in the petrochemical industry. The use of membrane technology offers a compact and modular solution for capital and energy savings, thanks to process intensification. In this work, we move one step forward in the design of hybrid propane/propylene separation systems, using computer aided modeling tools to identify economically optimal combinations of distillation and state-of-the-art membranes. A model is proposed to optimize a hybrid configuration, whereby the membrane performs the bulk separation and the distillation column is intended for the final product polishing, accounting for membrane investment cost and process operating expenses. The decision variables are the membrane area and the column reflux ratio, and the model is able to calculate the optimal feed trays. The upper-bound properties of selected membranes, which define their performance and reliability criteria, have been studied, benchmarking the economic evaluation against conventional distillation in order to assess the expedience of a hybrid system implementation.

1. Introduction

The use of ethylene and propylene as main building blocks for a wide number of essential chemicals turns them into the most important feedstocks of the petrochemical industry. The separation of these light olefins from their homologous paraffin entails a costly high pressure or cryogenic distillation with a prominent contribution to the worldwide energy consumption [1]. Although major efforts have been carried out to develop alternative separation processes, mainly enhanced distillations [2] and physical/chemical adsorptions [3,4], none of them have succeeded in replacing traditional distillation.

Process intensification by means of membrane technology is one of the most promising strategies to overcome this handicap, performing the separation at mild temperature and pressure conditions using modular and compact equipment [5]. A characteristic feature of membrane materials is the existing trade-off between the amount of gas that passes though the film (i.e. permeability) and the selectivity towards the desired gaseous species. In addition, this effect can be a decisive factor for further industrial application.

Dense polymeric membranes, based exclusively on solution-diffusion transport, offer poor performance in terms of selectivity, and their potential industrial application may be found in the recovery of unreacted olefin after polymerization, where selectivity values of 3–5 may be adequate [6,7]. The search for better separation capabilities has led to the development of new materials that excel in olefin/paraffin separation applications. Carbon molecular sieves prepared through pyrolysis of polymer precursors display a complex morphology combining ultramicropores and micropores, which are responsible for the molecular sieving and the solubility, respectively. These show propane/propylene selectivity values up to 50 and permeability values around 20 barrer [8–10]. Zeolitic imidazolate framework (ZIF) membranes present a structure built upon metals with tetrahedral coordination geometries interlinked with imidazolate ligands, which separates the mixture based on the differences in diffusivity through the pore system. These ceramic membranes perform selectivity values as high as 70 with a permeability ranging between 100 and 400 barrer [11–13]. Finally, facilitated transport membranes make use of silver cations as carrier, selectively transporting the olefin through the membrane and, reaching a selectivity higher than 100 with permeability values typically surpassing 1000 barrer [14–16]. Additionally, the use of ionic liquids and silver nanoparticles to enhance the performance and carrier stability has been reported to produce favorable effects [17,18]. These

---

[*] Corresponding author.
E-mail address: ortizi@unican.es (I. Ortiz).

https://doi.org/10.1016/j.memsci.2018.04.016
Received 8 February 2018; Received in revised form 5 April 2018; Accepted 10 April 2018
Available online 12 April 2018
0376-7388/ © 2018 Elsevier B.V. All rights reserved.

Nomenclature

A	membrane permeation area [m^2]
C_p	heat capacity at constant pressure [$J\,mol^{-1}\,K^{-1}$]
C_v	heat capacity at constant volume [$J\,mol^{-1}\,K^{-1}$]
d	differentiable distribution function
E	feed stream
e	feed stream DDF
ΔH_{vap}	enthalpy of vaporization [$J\,mol^{-1}$]
h	set of model algebraic equations
J	molar flux [$mol\,m^{-2}\,s^{-1}$]
L	hollow fiber length [m]
L'	lower limit of the decision variables
L''	upper limit of the decision variables
N	compression stages
N_c	DDF mean
P	permeability [barrer]
p	pressure [bar]
Q	heat duty [W]
R	reflux stream
r	reflux stream DDF
T	temperature [K]
t	set of model constraints
v	vector of model decision variables
W	compression duty [W]
x	liquid mole fraction [-]
y	vapor mole fraction [-]
z	hollow fiber axial dimension [m]

Greek letter

α	selectivity [-]
δ	active layer thickness [m]
γ	permeate-to-feed pressure ratio [-]
η	compressors efficiency [-]
λ	C_p/C_v ratio [-]
μ	molar flowrate [$mol\,h^{-1}$]
Θ	grouped parameter [-]
σ	standard deviation [-]

Superscript / subscript

B	bottoms stream
C_3H_6	propylene
C_3H_8	propane
D	distillate stream
F	feed side
I	column tray
j	component
k	column tray
P	permeate side

permeation results outperform the propylene/propane upper bound of dense polymers [19,20]. However, it has been demonstrated by Park et al. that, "designing materials with selectivity values much greater than the pressure ratio yields little or no improvement in product purity" [21].

Besides material separation performance, another critical aspect is the membrane configuration. Among the possible configurations, hollow fiber membranes are widely recognized for their adequacy in industrial gas separations, offering high packing density and energy efficiency [22]. In this regard, carbon molecular sieves, ZIF's and facilitated transport membranes can be processed to produce hollow fibers [8,23].

Whilst the complete replacement of the conventional distillation would require materials that exceed the current upper-bound, state-of-the-art membranes could be effectively implemented in a hybrid process [1,24,25]. A hybrid process is defined as a process array combining different unit operations, which are interlinked and optimized to accomplish a predefined task [26]. It is worth noting that the hybrid membrane/distillation concept comprises a limited number of arrangements [27,28]. All these alternatives have been previously reported in the literature by Moganti et al. [29], and Pressley and Ng [24].

The design of a membrane/distillation hybrid process involves solving an optimization problem, driven by the existing compromise between the membrane total cost and the column operating expenses. Although it is conceivable to expand the optimization problem to all possible configurations using a complex superstructure, the limited number of different arrangements allows optimizing each configuration independently in a more efficient manner [30]. Following this strategy, Caballero et al. [30] developed a model to optimize the ethane/ethylene separation using the parallel arrangement (i.e. feeding the membrane with an intermediate column product and then feeding back the column with the permeate and retentate streams); likewise, Kookos [31] optimized the same configuration for propane/propylene mixtures.

Recently, Wessling et al. [32] proposed the use of upper-bound membrane properties coupled with process modeling to find the optimal combination of permeability and selectivity for gas separation. In this work, we extend this concept to hybrid systems by developing an optimization model of a membrane/distillation hybrid process for propylene/propane separation. A model of the membrane module is proposed considering a co-current hollow fiber configuration. The distillation column is modeled formulating the MESH equations (material balance, equilibrium, summation and enthalpy balance), and for tray optimization we avoid the use of binary variables, and the subsequent MINLP problem, by using the Distributed Stream-Tray Optimization Method (DSTO) developed by Lang and Biegler [33].

This optimization is intended as a proof of concept of the state-of-the-art membrane materials, introducing the selectivity and permeability reported values and comparing the total operating costs resulting from the implementation of a hybrid process with those of the base case distillation.

2. Optimization methodology

2.1. Problem statement

In this work, the problem can be formulated as: given the head product of an industrial depropanizer, assess the potential capability of state-of-the-art membrane materials to reduce the economic impact of the gas separation by optimizing a hybrid hollow fiber/distillation separation system. As the hybrid system is highly suitable for retrofitting existing distillation columns, the conventional distillation will be taken as reference for the number of equilibrium stages.

2.2. Hollow fiber membrane model

In the proposed process configuration the membrane module receives the depropanizer head product. Although this stream is typically condensed and fed into the next distillation column [34], we will assume that the condenser would be partially by-passed if a hybrid process were to be implemented. In this way, a vapor stream is available to be directly introduced into the hollow fibers module.

The mathematical description of the membrane unit considers the following assumptions:

- The module operates isothermally and in the steady state.
- The feed stream is introduced in the shell side of the fibers, with the permeate circulating in the lumen side.
- The feed and permeate streams flow in a co-current configuration.
- Plug-flow in both sides is assumed.
- The total pressure in the feed and permeate sides are kept constant as operating conditions.
- There is no pressure drop due to fluid dynamics, the only pressure gradient is the transmembrane pressure.
- The gas permeability is a material constant.

Fig. 1 shows a schematic diagram of the hollow fibers module. The mass balances for component j in the feed and permeate sides are as follows:

$$dF_j^F(z) = -J_j(z)\cdot dA \tag{1}$$

$$dF_j^P(z) = J_j(z)\cdot dA \tag{2}$$

where F_j is the molar flowrate of component j, and dA is the fiber wall area differential element. Given that the reported permeability can be considered as a normalized flux, we revert this conversion to calculate the permeation flux through the active layer, as outlined by the solution-diffusion theory [35]:

$$J_j(z) = \frac{P_j}{\delta}\cdot\left[p_j^F(z) - p_j^P(z)\right] \tag{3}$$

where P_j is the permeability of component j, δ is the thickness of the active layer and p_j^F and p_j^P are feed and permeate partial pressures of component j, respectively. This should be interpreted as an approximation to homogenize the calculation method when evaluating membrane materials that perform a variety of transport mechanisms. The following dimensionless variables are defined:

$$\bar{z} = \frac{z}{L} \qquad \bar{z} \in [0,1] \tag{4}$$

$$\gamma = \frac{p^P}{p^F} \qquad \gamma \in [0,1] \tag{5}$$

$$\overline{F_j}(z) = \frac{F_j(z)}{F_T^F(z=0)} \qquad \overline{F_j} \in [0,1] \tag{6}$$

$$x_j(z) = \frac{F_j^F(z)}{\sum F_j^F(z)} \qquad x_j \in [0,1] \tag{7}$$

$$y_j(z) = \frac{F_j^P(z)}{\sum F_j^P(z)} \qquad y_j \in [0,1] \tag{8}$$

which stand for feed and permeate mole fraction, dimensionless axial length, permeate-to-feed pressure ratio and dimensionless molar flowrate, respectively; L is the fiber length. In addition, a grouped parameter is defined:

$$\Theta_j = \frac{A\cdot P_j\cdot p^F}{\delta\cdot F_{T,z=0}^F} \tag{9}$$

where A is the total membrane area. Rearranging terms, the mass balances can be rewritten as:

$$\frac{d\overline{F_j^F}}{d\bar{z}} = -\Theta_j\cdot(x_j - \gamma\, y_j) \tag{10}$$

$$\frac{d\overline{F_j^P}}{d\bar{z}} = \Theta_j\cdot(x_j - \gamma\, y_j) \tag{11}$$

$$\overline{F_j^F}|_{\bar{z}=0} = 1 \tag{12}$$

$$\overline{F_j^P}|_{\bar{z}=0} = 0 \tag{13}$$

These ordinary differential equations (ODEs) (Eqs. (10–13)) are discretized using implicit Runge-Kutta collocation methods and solved as algebraic equations.

2.3. Distillation model

For the distillation column, the model is taken from the work of Lang and Biegler [33]. A complete description of the mathematical development can be found in the original manuscript, here we provide a brief overview. In order to avoid discrete decision variables, the model uses differentiable distribution functions (DFF) for the feed streams, reflux stream and intermediate product streams (if present), in the form:

$$d_i = \frac{\exp\left[-\left(\frac{i-N_c}{\sigma}\right)^2\right]}{\sum_k \exp\left[-\left(\frac{k-N_c}{\sigma}\right)^2\right]} \qquad i, k \in I \tag{14}$$

which corresponds to the discretization of a Gaussian distribution with mean N_c and standard deviation σ. Thus, using DDFs, the feed and reflux streams can be distributed to all trays:

$$E_i = E\cdot e_i \tag{15}$$

$$R_i = R\cdot r_i \tag{16}$$

where E_i and R_i are the feed and reflux flowrates entering into the i-th tray, e_i and r_i are the corresponding differentiable distribution functions and E and. are the total feed and reflux streams, respectively. Once the feed and reflux streams are defined through a DDF, the model uses the conventional MESH equations (material balances, equilibrium, summation and enthalpy balances) to formulate the distillation model. As described in [33] the model is also capable of calculating the number of trays by relaxing the equilibrium equations in the MESH equations so that the liquid phase disappears. This modification of the MESH equations allows dry trays to appear without pressure drop in the non-existing trays above the reflux insertion point. The optimization model then chooses the column operation with the optimal number of dry trays, which translates to the optimum number of trays required. Fig. 2 depicts an overview of the modeling strategy.

The vapor-liquid equilibrium has been introduced using the K-value charts for C_3 mixtures [36]. These charts are constructed upon experimental data, later displayed in nomograms. To allow its implementation in computer calculations, a corresponding states type approach has been reported in the bibliography [37]. This approach considers the equilibrium constant value as a function of pressure and temperature exclusively, neglecting the effects of composition. This assumption is valid for propane/propylene mixtures at the pressure and temperature range covered in this study.

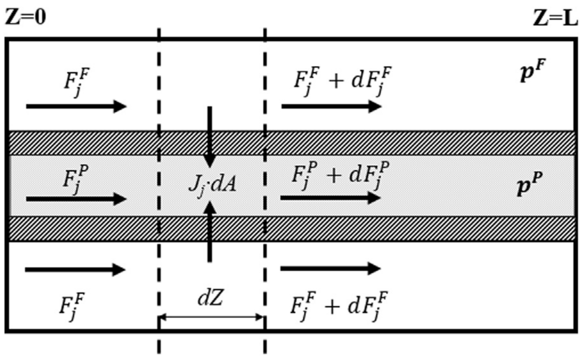

Fig. 1. Schematic diagram of the hollow fibers module.

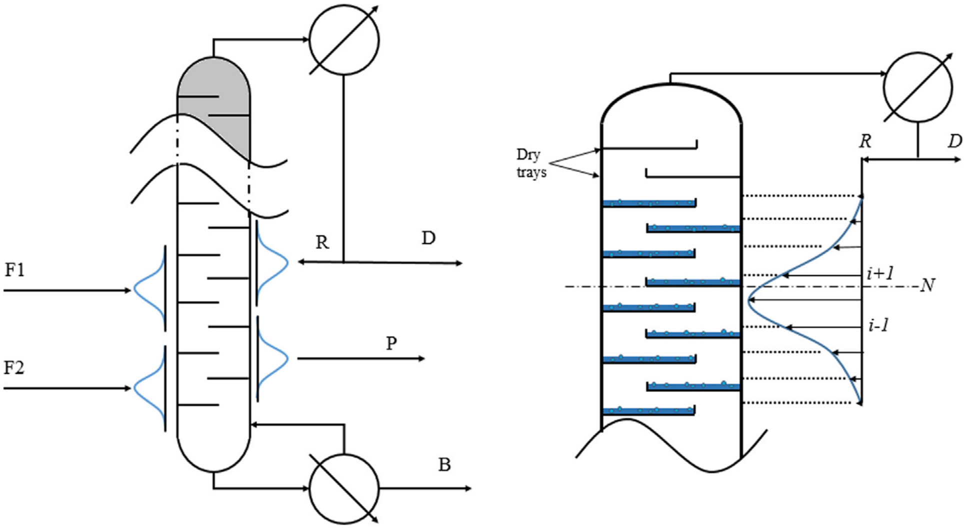

Fig. 2. Schematic diagram of the Distributed Stream-Tray Optimization Method (DSTO) and detail of reflux stream DDF.

2.4. Distillation benchmark

To quantify the potential economic savings, we establish the conventional distillation as base case. The feed stream consist of 360 kmol/h of a liquid propane/propylene equimolar mixture at 323 K and 20.27 bar. The product specifications are 0.995 propylene mole fraction in the distillate stream (i.e. polymer grade) and 0.95 propane mole fraction in the bottoms stream. The column has 135 equilibrium stages including the reboiler and condenser with a total reflux ratio of 14.9. The base case distillation reflux ratio has been calculated using the same vapor-liquid equilibrium method discussed before. In this way we remove any bias caused by the use of different thermodynamic methods when comparing results. More detailed information about the base case can be found in Table 1.

2.5. State-of-the-art membrane materials

We propose a selection of membrane materials to represent the current industrially attractive possibilities for a hybrid process. In the field of carbon molecular sieves, Ma et al. [38] recently reported a high performance membrane prepared via pyrolysis of defect-free polymers on a γ-alumina support. In this way, they managed to synthesize CMS membranes with an active layer of 0.3 µm, yielding propylene permeances around 42 GPU with a selectivity of 23.

Table 1
Distillation parameters.

Parameter	Value
Feed temperature (K)	323
Feed pressure (bar)	20.27
Feed flowrate (kmol h^{-1})	360
Feed composition (C_3H_6 mol frac.)	0.50
Feed tray[a]	51
Distillation column number of stages	135
Reflux ratio	14.91
Reboiler duty (kW)	15,128
Condenser duty (kW)	14,169
Dist. temperature (K)	320.05
Dist. pressure (bar)	19.05
Dist. flowrate (kmol h^{-1})	171.43
Dist. composition (C_3H_6 mol frac.)	0.995
Bott. temperature (K)	331.57
Bott. pressure (bar)	20.41
Bott. flowrate (kmol h^{-1})	188.57
Bott. composition (C_3H_6 mol frac.)	0.05

[a] Column trays are numbered from bottom to top.

Regarding ZIF membranes, Pan et al. [39] reported a ZIF-8 membrane performing propylene permeances up to 90 GPU and selectivity values around 50. These membranes were synthesized by hydrothermal seeded growth on α-alumina supports, and resulted in an effective layer thickness of 2.2 µm. Using a heteroepitaxial growth method, Kwon et al. [40] created a selective membrane displaying successive zeolitic selective layers on α-alumina supports. They achieved a ZIF-8/ZIF-67/ZIF-8 structure performing a propylene permeance of 110 GPU and selectivity values around 210.

Recently, our research group has reported facilitated transport membranes showing a propylene permeance up to 40 GPU with a selectivity of 150 [15]. This membrane was synthesized incorporating silver cations in a PVDF-HFP/$BMImBF_4$ polymer/ionic liquid matrix. The selective coordination of propylene with the silver cations is responsible for the high olefin solubility, while the dense nature of the fluoropolymer limits the paraffin transport.

Furthermore, two well studied membranes, a polyimide [41] and an cellulosic membrane [42] have been introduced in this study as exponents of previous generations of materials for comparison purposes. Table 2 summarizes the selected membranes features.

Finally, the permeability-selectivity trade-off exhibited by membrane materials has been assessed, introducing an updated trade-off expression in the optimization model. In this way, a wider insight into state-of-the-art membrane performance can be provided.

2.6. Hybrid process optimization

The hybrid process flowsheet is displayed in Fig. 3. Briefly, the propane/propylene gaseous mixture coming from the previous

Table 2
Separation performance of the selected membranes.

Membrane	C_3H_6 permeance (GPU[a])	C_3H_6 selectivity	Source
CMS	42	23	[38]
ZIF-8	90	50	[39]
ZIF-8/ZIF-67/ZIF-8	111	210	[40]
PVDF-HFP/$BMImBF_4$/$AgBF_4$	40	150	[15]
6FDA-TeMPD	37[b]	8.6	[41]
EC	7	7.0	[42]

[a] 1 GPU = 3.35×10^{-10} mol/m^2 Pa s.

[b] Calculated from reported permeability assuming 1 µm thickness.

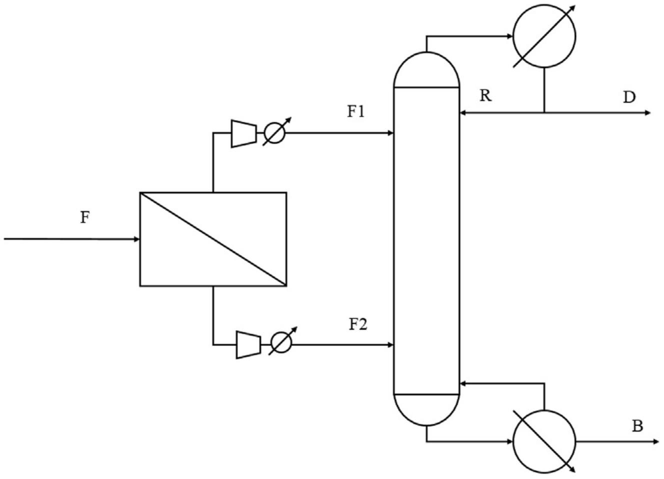

Fig. 3. Schematic diagram of the hybrid process.

Table 3
Hybrid process parameters.

Parameter	Value
Feed temperature (K)	325
Feed pressure (bar)	18
Feed flowrate (kmol h^{-1})	360
Feed composition (C_3H_6 mol frac.)	0.50
Membrane feed side pressure (bar)	18
Membrane permeate side pressure (bar)	1
Distillation column number of stages	135
Distillate purity, $x^D_{C_3H_6,min}$ (mol%)	≥ 99.5
Bottoms purity, $x^B_{C_3H_8,min}$ (mol%)	≥ 95.0

depropanizer unit is fed into the hollow fiber module. Then, the resultant retentate and permeate streams are recompressed and introduced in the distillation column to perform the final refining step. In order to assess the membrane performance when retrofitting the existing process, and as far as only operating costs are evaluated, the same number of equilibrium stages of the benchmark distillation column is considered in the hybrid configuration. In addition, the base case distillate and bottoms purities are taken as the hybrid process constraints. Heat integration strategies are not considered in the present work, as they may depend upon the configuration of each specific production plant. The process parameters are summarized in Table 3.

In this work, the optimization objective aims to minimize the total operating costs. Here we include:

- Membrane depreciation.
- Permeate and retentate recompression.
- Reboiler and condenser duties.

The membrane depreciation can be easily calculated as the membrane cost divided by the membrane lifetime, thus obtaining the annualized cost. The compressors duty can be calculated as follows:

$$W = \frac{\mu N}{\eta}\left(\frac{\lambda}{\lambda - 1}\right) R T_{feed}\left[\left(\frac{p_N}{p_{feed}}\right)^{\frac{\lambda-1}{\lambda N}} - 1\right] \tag{17}$$

where μ is the molar flowrate, N is the number of compression stages, η is the compressor efficiency, λ is the C_p/C_v ratio of the compressed gas, and p_N is the outlet pressure. The reboiler and condenser duties are calculated using the following expression:

$$Q = \mu \sum_j x_j \Delta H_{vap,j} \tag{18}$$

Table 4
Process parameters for the economic estimation.

Parameter	Value
Membrane unitary cost ($ m^{-2})	20
Membrane lifetime (year)	2
Post-compression pressure (bar)	20.27
Post-compression temperature (K)	323
Permeate compressor number of stages	3
Retentate compressor number of stages	1
Compression efficiency	0.72
$\gamma = C_p/C_v$	1.15
Energy cost ($ kW h^{-1})	7.70E-02
Steam@150 psi cost ($ mol^{-1})	3.23E-04
Cooling water cost ($ mol^{-1})	5.70E-07
Plant service factor	0.904

where x_j and $\Delta H_{vap,j}$ are the mole fraction and enthalpy of vaporization of component j in the stream, respectively.

The compression and heat exchange duties are further converted to annualized expenses using the respective utilities price. Table 4 shows the parameters regarding the economic calculations.

To conclude, the objective function can be formulated in the standard form as:

$$\begin{aligned} &Minimize\ \ TOC(v)\\ &s.\,t.\\ &\quad h(v) = 0\\ &\quad t(v) \geq 0\\ &\quad L' \leq v \leq L'' \end{aligned} \tag{19}$$

where TOC is the total annualized operating cost, v is the vector of model decision variables, h (v) is the set of model algebraic equations, t (v) is the set of model constraints (Eqs. (20–21)) and L' and L'' are the lower and upper limits of the decision variables, respectively.

$$x^D_{C_3H_6} \geq x^D_{C_3H_6,min} \tag{20}$$

$$x^B_{C_3H_8} \geq x^B_{C_3H_8,min} \tag{21}$$

The model has been implemented in the General Algebraic Modeling System (GAMS) and solved using the multistart heuristic algorithm OQNLP on a 3.40 GHz Intel® Core™ i7–3770 processor. The GAMS code is available as electronic supplementary information. CONOPT has been used as local NLP solver for OQNLP with a time limit of 3000 s and a maximum of 3000 trial points and 3000 CONOPT calls. The number of single equations and single variables, which depend on the case study, are displayed in Table 5.

Once the solver is run, it provides:

- The minimal operating expenses (and the partial contributions).
- The optimal membrane area.
- The optimal reflux ratio.
- The optimal feed tray locations.

3. Results and discussion

In this section, we first present the results obtained for the hybrid configuration with the selected membrane materials. Next, the current

Table 5
Models statistics.

	BCD[a]	HP[b]	HP-OMP[c]
Number of single equations	4061	4669	4671
Number of single variables	4335	4945	4948

[a] Base Case Distillation.
[b] Hybrid Process.
[c] Hybrid Process- Optimal Membrane Properties.

Table 6
Optimization results.

ID	Membrane	C_3H_6 permeance (GPU)	Selectivity	Area ($\times 10^3$ m^2)	Reflux	TOC (MM$/y)	Savings (%)
–	None	–	–	–	14.9	4.05	0.0
A	ZIF8 / ZIF67/ZIF8	111	209	2.8	4.5	1.78	56.2
B	PVDF-HFP/$AgBF_4$/$BMImBF_4$	40	150	7.4	5.3	2.02	50.3
C	ZIF 8	91	50	2.9	7.4	2.50	38.3
D	6FDA-based polyimide CMS	42	23	5.8	8.7	2.87	29.2
E	6FDA-TeMPD	37	8.9	5.3	10.5	3.34	17.6
F	EC	6	7.0	23.2	11.2	3.65	9.9

membrane upper bound is introduced in the model to study the desirable permeability/selectivity combination of a hypothetically optimal membrane material. Additionally, the impact of the membrane cost on the economic evaluation is assessed.

3.1. *State-of-the-art membranes optimization results*

Table 6 displays the resultant membrane area, reflux ratio and potential savings derived from the implementation of each membrane in a hybrid configuration. The highly permeable and highly selective ZIFs, CMS and facilitated transport membranes (A-D) can potentially reduce the operating expenses by around 30–55%. In addition, advanced polyimides, as 6FDA-TeMPD (E), which provide high permeance but moderate selectivity, are still capable of reducing the total operating costs by 18%. Finally, the cellulosic membrane (F), due to its low permeance and selectivity, achieves a TOC reduction of around 10%.

The TOC reduction due to the implementation of a hollow fiber module in series is clearly related to the decrease in the required reflux ratio for a given product quality. Although the reboiler and condenser duties are very similar, the use of steam requires that more than 95% of the base case operating costs are generated by the reboiler. Fig. 4 unfolds the total operating expenses for each case. As expected, the membrane module helps reduce the required reflux ratio, decreasing the steam supply to the reboiler and its associated cost. It is worth noting that, despite this reduction, the reboiler operating cost is still the largest contribution to the total operating costs, while the condenser and retentate compressor operating costs are almost negligible.

Focusing on the intermediate streams (F1 and F2 in Fig. 3), it is noticeable how the optimal solution comprises, in all cases, approximately the same flowrates, and the total savings are eventually determined by the purity achieved in these streams as can be seen in Table 7. In this regard, the optimal membrane area for case **B** is higher than that of case **D**. Though both have the same propylene permeance, the first is far more selective. Here, the extra cost is offset by the purity reached in the permeate stream. Comparing membranes with similar selectivity (**E** and **F**), we observe the strong dependence of the optimal required area on the membrane permeance.

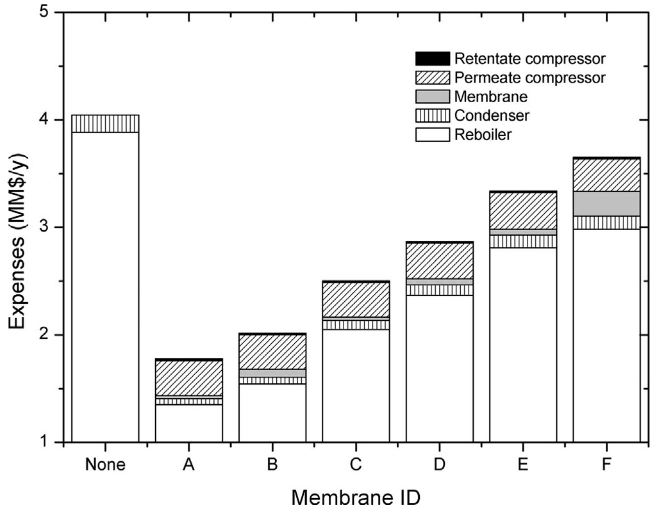

Fig. 4. Disaggregated operating costs for each case. A-F defined in Table 6.

Since the hybrid configuration may become uncompetitive compared to the conventional distillation depending on the membrane unitary cost, it is advisable to perform a sensitivity analysis of the optimum solutions. Fig. 5 displays the TOC variation for each membrane with increasing membrane prices up to 200 \$/m^2. In all cases, with the exception of the cellulosic membrane, the optimal configuration does not vary significantly, and the resultant TOC increase is proportional to the optimal membrane area. On the other hand, the cellulosic membrane hybrid configuration, due to the large area required, is not suitable for replacing the base case distillation when the membrane cost exceeds ~100 \$/m^2, and consequently, the membrane module has been removed during the optimization run.

This analysis reveals a remarkable range of suitability for medium to high performance membrane materials when implemented in a hybrid configuration, regarding the membrane production cost.

3.2. *Upper-bound role in the hybrid configuration*

An interesting point when dealing with membranes is the trade-off existing between selectivity and gas permeability, which is limited by the upper-bound in the Robeson plot. By introducing the Robeson plot upper-bound expression in the optimization model we can explore the optimal permeability and selectivity values of a hypothetically optimal membrane material, given the membranes state-of-the art [30,31]. Fig. 6 represents an updated Robeson plot for propane/propylene mixtures.

The corresponding mathematical expression is:

$$\alpha_{C_3H_6/C_3H_8} = 97.51 P_{C_3H_6}^{-0.362} \tag{22}$$

This updated upper-bound is slightly displaced towards the high-performance region compared to the previous version reported by Burns and Koros [19], as a result of the continuous research in membrane materials over the recent years. In this section we will evaluate the membrane productivity in terms of permeability instead of permeance, due to the nature of the Robeson plot, which is intended to compare materials and not specific membrane morphologies.

Once the upper-bound is introduced in the optimization problem, in addition to membrane area, reflux ratio and stream locations, the program also provides the optimal balance between permeability and selectivity. An active layer thickness of 1 µm has been assumed, as this is a typical value in the hollow fiber manufacture. The same hybrid process parameters considered in the previous discussion have been used for this section (see Table 3). The results obtained in this section are summarized in Table 8.

The optimal solution involves, in this case, very similar intermediate flowrates to those discussed in the previous section (see Table 7), and the potential reflux reduction is again determined by the purity of theses streams (F1 and F2 in Fig. 3). It is worth noting the strong influence of the membrane cost on the optimal permeability/selectivity trade-off. As the membrane cost weight on the objective function

Table 7
Intermediate streams results.

ID	Membrane	F1 flowrate (kmol/h)	F2 flowrate (kmol/h)	F1C_3H_6 purity (kmol/h)	F2C_3H_6 purity (kmol/h)	F1 feed tray[a]	F2 feed tray[a]	Savings (%)
A	ZIF8 / ZIF67/ZIF8	159	201	0.985	0.115	108	19	56.2
B	PVDF-HFP/AgBF$_4$/ BMImBF$_4$	157	203	0.981	0.127	102	19	50.3
C	ZIF 8	158	202	0.950	0.149	83	18	38.3
D	6FDA-based polyimide CMS	161	199	0.906	0.170	75	19	29.2
E	6FDA-TeMPD	167	193	0.815	0.227	70	24	17.6
F	EC	147	213	0.806	0.289	74	30	9.9

[a] Column trays are numbered from bottom to top.

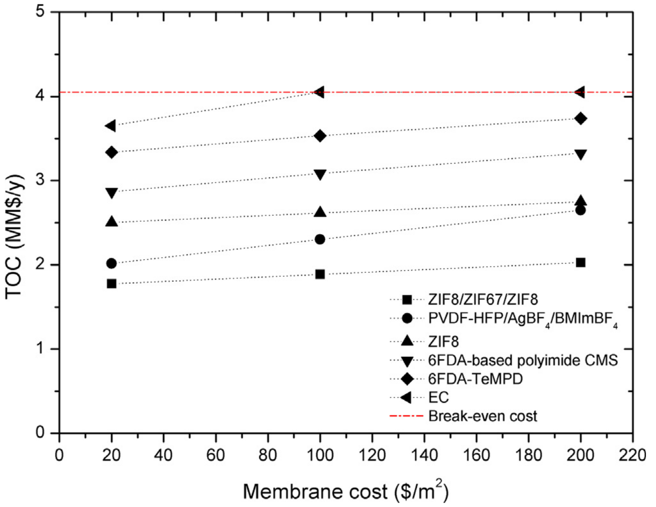

Fig. 5. Effect of the membrane cost on optimal TOC for the studied membranes.

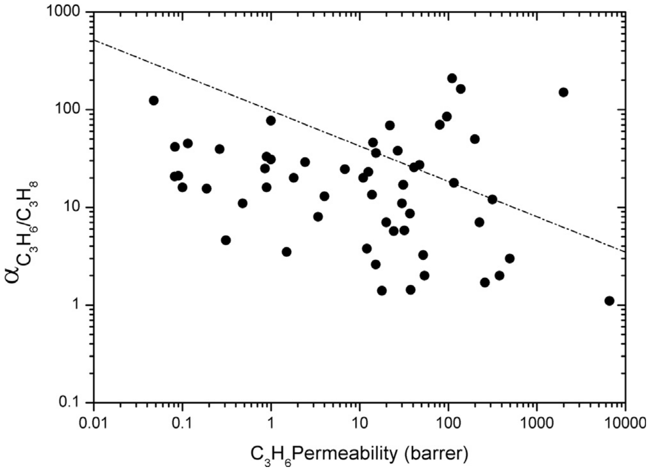

Fig. 6. Robeson plot for propane/propylene separation membranes displaying the upper-bound.

Table 8
Upper-bound optimization results.

	Membrane cost ($/m^2)		
	20	100	200
Propylene permeability (barrer[a])	16	74	134
Propylene selectivity	36	21	17
Membrane area ($\times 10^3$ m^2)	15.0	3.1	1.6
F1 flowrate (kmol/h)	155	158	157
F2 flowrate (kmol/h)	205	202	203
F1C_3H_6 purity	0.937	0.901	0.885
F2C_3H_6 purity	0.171	0.187	0.203
F1 feed tray[b]	82	76	76
F2 feed tray[b]	21	21	23
Reflux ratio	8.0	8.9	9.3
TOC (MM$/y)	2.77	3.02	3.13
Savings (%)	31.5	25.5	22.8

[a] 1 barrer = 3.348×10^{-16} mol m/m^2 Pa s.

[b] Column trays are numbered from bottom to top.

increases, the membrane tends to increase the permeability at the expense of selectivity. In the most unfavorable case (i.e. 200 $/m^2) the membrane is highly permeable and the selectivity falls to a value closer to the pressure ratio, which allows a prominent decrease in the required area while still maintaining an adequate permeate purity. These results are in good agreement with Huang et al. [43] findings on the pressure ratio-selectivity relation: "High permeance membranes are always good, but the optimum membrane selectivity depends on the process and the operating conditions, particularly the pressure ratio". Increasing the membrane selectivity far beyond the industrially suitable pressure ratio produces minor increments in the product purity at the expense of larger membrane areas, as the process enters in the pressure ratio-limited region.

Comparing with the real membranes selected for this study, the carbon molecular sieve (membrane D) would be the option of choice, given the conservative upper-bound considered in Eq. (22), which is below the performance of membranes A, B and C. This gives an idea of the state-of-the-art membrane materials performance for process intensification when implemented in a hybrid configuration.

4. Conclusions

Membrane technology offers remarkable opportunities to intensify the olefin/paraffin separation process when implemented in hybrid systems along with the conventional distillation. In this work, the optimization of a membrane/distillation hybrid process with state-of-the-art membranes yielded total operating cost savings of 10–50% compared with the distillation benchmark.

The evaluation of the Robeson plot upper-bound reveals the importance of the operating conditions when it comes to select the most suitable membrane. Especially, the pressure ratio may limit the advantages of highly selective membranes. In this regard, membrane researchers should consider the particularities of each specific application in order to tailor the membrane properties accordingly.

Acknowledgements

Financial support from the Spanish Ministry of Science under the projects CTQ2015–66078-R and CTQ2016–75158-R (MINECO, Spain-FEDER 2014–2020) is gratefully acknowledged. Raúl Zarca also thanks the Universidad de Cantabria for a postgraduate fellowship.

Appendix A. Supplementary material

Supplementary data associated with this article can be found in the online version at http://dx.doi.org/10.1016/j.memsci.2018.04.016.

References

[1] D.S. Sholl, R.P. Lively, Seven chemical separations to change the world, Nature 532 (2016) 435–437.

[2] Kumar, R., Prausnitz, J.M., King, C.J., 1972. Process design considerations for extractive distillation: separation of propylene-propane. In: Dimitrios P. Tassios (ed.), Extractive and Azeotropic Distillation. pp. 16–34.

[3] C.M. Shu, S. Kulvaranon, M.E. Findley, A.I. Liapis, Experimental and computational studies on propane-propylene separation by adsorption and variable-temperature stepwise desorption, Sep. Technol. 1 (1990) 18–28.

[4] J. Padin, S.U. Rege, R.T. Yang, L.S. Cheng, Molecular sieve sorbents for kinetic separation of propane/propylene, Chem. Eng. Sci. 55 (2000) 4525–4535.

[5] J.C. Charpentier, In the frame of globalization and sustainability, process intensification, a path to the future of chemical and process engineering (molecules into money), Chem. Eng. J. 134 (2007) 84–92.

[6] R.W. Baker, Future directions of membrane gas separation technology, Ind. Eng. Chem. Res. 41 (2002) 1393–1411.

[7] R. Faiz, K. Li, Polymeric membranes for light olefin/paraffin separation, Desalination 287 (2012) 82–97.

[8] L. Xu, et al., Olefins-selective asymmetric carbon molecular sieve hollow fiber membranes for hybrid membrane-distillation processes for olefin/paraffin separations, J. Membr. Sci. 423–424 (2012) 314–323.

[9] M. Askari, T.-S. Chung, Natural gas purification and olefin/paraffin separation using thermal cross-linkable co-polyimide/ZIF-8 mixed matrix membranes, J. Membr. Sci. 444 (2013) 173–183.

[10] J. Liu, et al., A new carbon molecular sieve for propylene/propane separations, Carbon 85 (2015) 201–211.

[11] K. Li, et al., Zeolitic imidazolate frameworks for kinetic separation of propane and propene, J. Am. Chem. Soc. 131 (2009) 10368–10369.

[12] B. Demir, M.G. Ahunbay, Propane/propylene separation in ion-exchanged zeolite-like metal organic frameworks, Microporous Mesoporous Mater. 198 (2014) 185–193.

[13] H.T. Kwon, H.K. Jeong, Improving propylene/propane separation performance of Zeolitic-imidazolate framework ZIF-8 membranes, Chem. Eng. Sci. 124 (2015) 20–26.

[14] M. Fallanza, A. Ortiz, D. Gorri, I. Ortiz, Polymer-ionic liquid composite membranes for propane/propylene separation by facilitated transport, J. Membr. Sci. 444 (2013) 164–172.

[15] R. Zarca, A. Ortiz, D. Gorri, I. Ortiz, Generalized predictive modeling for facilitated transport membranes accounting for fixed and mobile carriers, J. Membr. Sci. 542 (2017) 168–176.

[16] M.T. Ravanchi, T. Kaghazchi, A. Kargari, Supported liquid membrane separation of propylene-propane mixtures using a metal ion carrier, Desalination 250 (2010) 130–135.

[17] S.W. Kang, et al., Effect of the polarity of silver nanoparticles induced by ionic liquids on facilitated transport for the separation of propylene/propane mixtures, J. Membr. Sci. 322 (2008) 281–285.

[18] S. Jeong, S.W. Kang, Effect of Ag_2O nanoparticles on long-term stable polymer/AgBF4/Al(NO3)3complex membranes for olefin/paraffin separation, Chem. Eng. J. 327 (2017) 500–504.

[19] R.L. Burns, W.J. Koros, Defining the challenges for C3H6/C3H8 separation using polymeric membranes, J. Membr. Sci. 211 (2003) 299–309.

[20] L.M. Robeson, The upper bound revisited, J. Membr. Sci. 320 (2008) 390–400.

[21] H.B. Park, J. Kamcev, L.M. Robeson, M. Elimelech, B.D. Freeman, Maximizing the right stuff: the trade-off between membrane permeability and selectivity, Science 356 (2017) 1138–1148.

[22] D.C. Nymeijer, T. Visser, R. Assen, M. Wessling, Composite hollow fiber gas-liquid membrane contactors for olefin/paraffin separation, Sep. Purif. Technol. 37 (2004) 209–220.

[23] A.J. Brown, et al., Interfacial microfluidic processing of metal-organic framework hollow fiber membranes, Science 345 (2014) 72–75.

[24] T.G. Pressly, K.M. Ng, A break-even analysis of distillation-membrane hybrids, AIChE J. 44 (1998) 93–105.

[25] A. Norkobilov, D. Gorri, I. Ortiz, Comparative study of conventional, reactive-distillation and pervaporation integrated hybrid process for ethyl tert-butyl ether production, Chem. Eng. Process. Process Intensif. 122 (2017) 434–446.

[26] F. Lipnizki, R.W. Field, P.-K. Ten, Pervaporation-based hybrid process: a review of process design, applications and economics, J. Membr. Sci. 153 (1999) 183–210.

[27] W. Stephan, R.D. Noble, C.A. Koval, Design methodology for a membrane/distillation column hybrid process, J. Membr. Sci. 99 (1995) 259–272.

[28] T. Pettersen, A. Argo, R.D. Noble, C.A. Koval, Design of combined membrane and distillation processes, Sep. Technol. 6 (1996) 175–187.

[29] S. Moganti, R.D. Noble, C.A. Koval, Analysis of a membrane/distillation column hydrid process, J. Membr. Sci. 93 (1994) 31–44.

[30] J.A. Caballero, et al., Design of hybrid distillation - vapor membrane separation systems, Ind. Eng. Chem. Res. 48 (2009) 9151–9162.

[31] I.K. Kookos, Optimal design of membrane/distillation column hybrid processes, Ind. Eng. Chem. Res. 42 (2003) 1731–1738.

[32] B. Ohs, J. Lohaus, M. Wessling, Optimization of membrane based nitrogen removal from natural gas, J. Membr. Sci. 498 (2016) 291–301.

[33] Y.D. Lang, L.T. Biegler, Distributed stream method for tray optimization, AIChE J. 48 (2002) 582–595.

[34] W.L. Luyben, Dynamic simulation of flooded condensers, Chem. Eng. Res. Des. 118 (2017) 12–20.

[35] J.G. Wijmans, R.W. Baker, The solution-diffusion model: a review, J. Membr. Sci. 107 (1995) 1–21.

[36] E.G. Scheibel, F.J. Jenny, Nomographs for enthalpies of pure hydrocarbons and their mixtures, Ind. Eng. Chem. 37 (1945) 990–995.

[37] Dimitrios Tassios, Applied Chemical Engineering Thermodynamics, Springer, Berlin, 1993.

[38] X. Ma, Y.S. Lin, X. Wei, J. Kniep, Ultrathin carbon molecular sieve membrane for propylene/propane separation, AIChE J. 62 (2016) 491–499.

[39] Y. Pan, T. Li, G. Lestari, Z. Lai, Effective separation of propylene/propane binary mixtures by ZIF-8membranes, J. Membr. Sci. 390–391 (2012) 93–98.

[40] H.T. Kwon, H.K. Jeong, A.S. Lee, H.S. An, J.S. Lee, Heteroepitaxially grown zeolitic imidazolate framework membranes with unprecedented propylene/propane separation performances, J. Am. Chem. Soc. 137 (2015) 12304–12311.

[41] K. Okamoto, K. Noborio, J. Hao, K. Tanaka, H. Kita, Permeation and separation properties of polyimide membranes to 1,3-butadiene and n-butane, J. Membr. Sci. 134 (1997) 171–179.

[42] A. Ito, S.-T. Hwang, Permeation of propane and propylene through cellulosic polymer membranes, J. Appl. Polym. Sci. 38 (1989) 483–490.

[43] Y. Huang, T.C. Merkel, R.W. Baker, Pressure ratio and its impact on membrane gas separation processes, J. Membr. Sci. 463 (2014) 33–40.

Appendices

A.1 List of additional scientific publications

Scientific articles published in non-JCR indexed journals

R. Zarca, A. Ortiz, D. Gorri, I. Ortiz, Facilitated transport of propylene through composite polymer-ionic liquid membranes. Mass transfer analysis, Chem. Prod. Process. Model. 11 (2016) 77–81. (CiteScore 2017: 0.96).

Scientific articles submitted to JCR indexed journals

R. Zarca, A. Ortiz, D. Gorri, L.T. Biegler, I. Ortiz, Optimization of multistage olefin/paraffin separation membrane processes through rigorous modeling, AIChE J. *Under review*.

R. Zarca, A.C.C. Campos, A. Ortiz, D. Gorri, I. Ortiz, Comprehensive study on PVDF-HFP/BMImBF$_4$/AgBF$_4$ membranes for propylene purification, J. Memb. Sci. *Under review*.

DE GRUYTER Chem. Prod. Process Model. 2016; aop

Raúl Zarca, Alfredo Ortiz*, Daniel Gorri and Inmaculada Ortiz

Facilitated Transport of Propylene Through Composite Polymer-Ionic Liquid Membranes. Mass Transfer Analysis

DOI 10.1515/cppm-2015-0072
Received December 22, 2015; accepted December 22, 2015

Abstract: Separation of light gaseous olefins from paraffin's of the refinery process off-gasses has been traditionally performed by cryogenic distillation, which is a highly capital and energy intensive operation. This handicap creates an incentive for the investigation of alternative olefin/paraffin separation technologies. In this regard, membrane technology supposes a potential solution for process intensification. Previous works of our research group reported the use of facilitated transport composite membranes integrating the use of PVDF-HFP polymer, $BMImBF_4$ ionic liquid and $AgBF_4$ silver salt. In this type of membranes, the silver cations react selectively and reversibly with the olefin, allowing the separation via mobile and fixed carrier mechanisms. Ionic liquids were selected as membrane additives because in addition to their negligible vapor pressure that avoids solvent losses by evaporation, they provide stability to the metallic cation dissolved inside, and modify the structure improving the facilitated transport. This technology offers a commercial attractive separation alternative thanks to their modular form of operation, high values of selectivity and permeability and low operational costs. In the present work, propane/propylene permeation experiments involving the use ionic liquids and different membrane compositions were performed. Moreover, basing on the transport and equilibrium parameters previously obtained, a mathematical model description of the system will be proposed fitting the remaining parameters and allowing the design and optimization of the propane/propylene separation process at industrial levels.

Keywords: facilitated transport, propylene, ionic liquids, silver, membrane composite

1 Introduction

Light olefins such as ethylene and propylene are important petrochemical building blocks which are further processed to yield a wide range of final products such as cosmetics, textile products, paints, tools or plastics for instance. Light olefins are usually obtained, as a mixture with paraffins, by steam cracking processes, fluidized catalytic cracking or alkane dehydrogenation.

The separation of these streams is a key issue because it is one of the most difficult and also the most costly separation process in the petrochemical industry. Traditional separation processes like low-temperature distillation, require voluminous equipment operating at high pressures or low temperatures and very large reflux ratios due to the very small difference in the relative volatilities between olefins and their corresponding paraffins [1]. In recognition of these costs alternative energy-saving separation processes are required.

In this sense, membrane technology presents a great potential for energy and capital saving and therefore the use of membranes has been the focal point of research of many authors. Criteria for selecting the most suitable membrane for a given application are complex; nonetheless, durability, mechanical and thermal stability at the operating conditions, productivity and separation efficiency and costs are important stipulations that must be considered [2]. Among these requirements selectivity and permeation rate are clearly the most basic, while the relative importance of the rest of them varies with the application. Therefore a wide variety of different membrane alternatives can be considered [3]. The use of polymeric, inorganic and supported liquid membranes for olefin/ paraffin separation has been studied rather extensively, however these membranes may suffer severe plasticization effect, low stability, poor mechanical resistance and expensive and complex preparation methods and therefore their performance has not met the requirements for commercial applications [4, 5].

Recently our research group proposed the use of novel polymer-ionic liquid-Ag^+ composite as facilitated transport membranes to carry out the separation of

---

***Corresponding author: Alfredo Ortiz,** Department of Chemical & Biomolecular Engineering, University of Cantabria, Av. Los Castros s/n., 39005 Santander, Spain, E-mail: alfredo.ortizsainz@unican.es
Raúl Zarca, Daniel Gorri, Inmaculada Ortiz, Department of Chemical & Biomolecular Engineering, University of Cantabria, Av. Los Castros s/n., 39005 Santander, Spain

Brought to you by | New York University Bobst Library Technical Services
Authenticated
Download Date | 2/5/16 10:43 AM

propane/propylene mixtures [6]. The separation performance is mostly associated to the ability of the olefins to react selective and reversibly with silver cations Ag^+, by π-complexation mechanism. Consequently silver ions act as carriers for the transport of olefins, thus facilitating their selective permeation across the membrane [7, 8]. Ionic liquids (IL) were selected as membrane additives because in addition to their negligible vapor pressure that avoids solvent losses by evaporation, they offer more affinity for the olefinic compounds compared to saturated hydrocarbons and at the same time they provide stability to the metallic cation dissolved inside acting as a medium for facilitated transport with mobile carrier [9, 10]. Based on previous results the ionic liquid used in this work has been 1-butyl 3-methylimidazolium tetrafluoroborate ($BMImBF_4$) since it provided the best results in terms of separation selectivity and propylene solubility [11–13]. On the other hand, the polymer used in this work is poly(vinylidene fluoride-co-hexafluoropropylene) (PVDF-HFP) due to its well-known thermal, chemical and mechanical properties. Furthermore it is partially miscible with $BMImBF_4$ and compatible with hydrocarbons which avoid plasticization effects. Once the membrane is fabricated the ionic liquid remains integrated within the polymer matrix, thereby increasing the stability of the membrane even at high transmembrane pressures. As the composite membrane is composed by a polymeric matrix and a liquid phase entrapped inside the polymeric matrix, the silver salt added to the membrane is distributed between these two phases. Therefore both facilitated transport mechanisms (fixed carrier and mobile carrier) take place, leading to high permeabilities combined with high separation selectivities. Figure 1 shows and schematic diagram of the transport mechanisms of propane and propylene across polymer/ionic liquid composite membrane. The PVDF-HFP/$BMImBF_4$–Ag^+ facilitated transport membranes reported in a previous work provided very promising results when tested with 50/50 %v/v C_3H_8/C_3H_6 mixtures obtaining C_3H_6 permeabilities up to 6,630 barrer and C_3H_8/C_3H_6 selectivities over 700 combined with good long term stability [6].

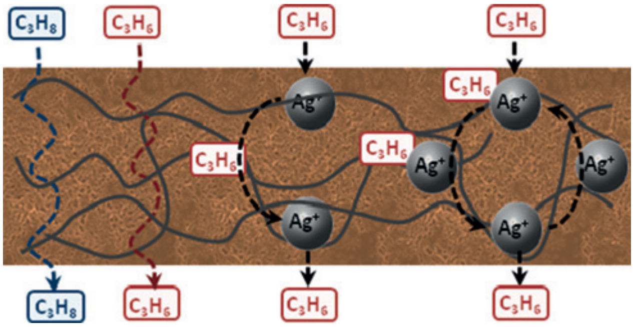

Figure 1: Proposed facilitated transport composite membrane structure.

In this work permeation experiments using constant volume time-lag method were performed in order to obtain diffusivity and solubility parameters of propylene and propane in PVDF-HFP polymer matrix and ionic liquid/polymer composite membranes. These results combined with facilitated transport experimental data obtained from our previous works [6, 11] will allow the development of a mathematical model able to describe the behavior of the facilitated transport mechanisms of propylene through the composite membrane and estimate the unknown facilitated transport parameters.

2 Experimental section

2.1 Membrane preparation

The PVDF-HFP/$BMImBF_4$ composite membranes were prepared by the solvent casting technique. First of all the polymer is dissolved in 10 mL of THF at 40 °C for 8 h in a closed vial to avoid the evaporation of the solvent. Once the polymer has been dissolved, it is mixed with the ionic liquid and stirred for 5 min. Finally the membrane precursor mixture is placed in a Petri dish and the solvent is evaporated at 25 °C and 300 mbar under dark conditions for 24 h. The thickness of the membranes prepared in this work depends on the membrane composition, but in all cases the prepared membranes presented a range thickness between 40–100 μm. Permeabilities have been calculated taking into account the real thickness of each membrane which was measured using a digital micrometer Mitutoyo Digmatic Series 369 (accuracy ± 0.001 mm).

2.2 Time-lag experiments

Figure 2 shows the experimental setup used for conducting permeation experiments using the time-lag technique at constant-volume and variable pressure. This apparatus consists of two chambers separate by the membrane (47 mm diameter). At time zero the gas of interest is introduced into the upper chamber. The feed pressure is maintained constant at the upper chamber while the pressure increase in the lower chamber, which occurs due to the passage of gas through the membrane, is recorded. The appreciable increase in pressure in the

Brought to you by | New York University Bobst Library Technical Services
Authenticated
Download Date | 2/5/16 10:43 AM

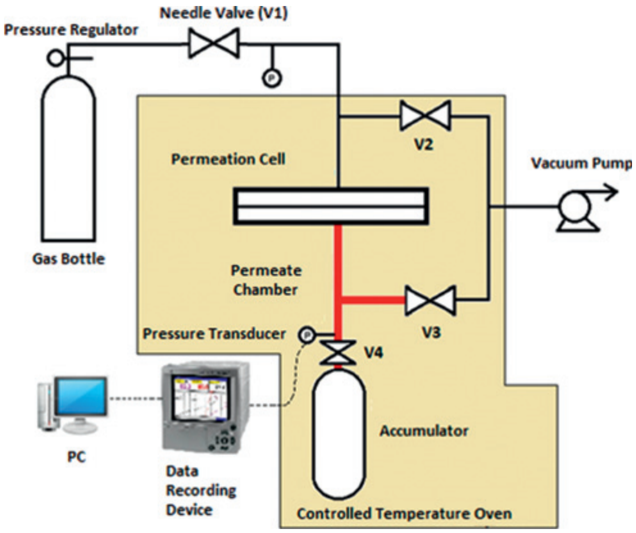

Figure 2: Time-lag apparatus scheme.

lower chamber occurs only after a period of time known as time-lag (Θ). After the time-lag a diffusion process begins in quasi-steady state until the pressure in both chambers is equalized. The mathematical expression that describes the increased pressure in the lower chamber can be obtained by applying Fick's second law in the limits of the membrane. By integrating Fick's equation with the boundary conditions by Laplace transforms, operating and neglecting terms, we reach the expression for the pressure in the permeate chamber versus time for the quasi-steady flux:

$$P_L(t) = A\frac{R \cdot T \cdot S \cdot D \cdot P_0}{V \cdot L}\left(t - \frac{L^2}{6D}\right) \tag{1}$$

The above equation is a straight line, from which one can extract the term that subtracts the time, known as "time-lag" (Θ) and the slope:

$$\theta = \frac{L^2}{6D} \tag{2}$$

After re-arranging terms, diffusivity, solubility and permeability parameters can be obtained as:

$$D = \frac{L^2}{6\theta} \tag{3}$$

$$S = \frac{V \cdot L \cdot (Slope)}{A \cdot D \cdot R \cdot T \cdot P_0} \tag{4}$$

$$P = D \cdot S \tag{5}$$

Where, L is the membrane thickness, Θ is the "*time-lag*", V is the permeate side volume, A is the permeation area, R is the gas constant, T is temperature and P_0 is the feed pressure.

3 Results and discussion

The results of permeation experiments are discussed. Permeability of propylene, propane and carbon dioxide, as a reference gas, at different temperatures in PVDF-HFP and PVDF-HFP-BMImB$_4$ (80/20 %wt.) membranes are experimentally obtained.

Figure 3 shows the propylene permeation time lag experiment at 289 K in a PVDF-HFP membrane. The characteristic initial stage corresponds to the time-lag (Θ) and the straight line corresponds to the quasi-steady state permeation stage. We can observe the long duration required for the experiment to reach quasi-steady state permeation flux and the slight increase in pressure in the permeate chamber, which gives an idea of the low permeability values expected in this polymer. In all cases the supply pressure described here is 3.5 bar. The permeate chamber has a volume of 16.6 cm^3.

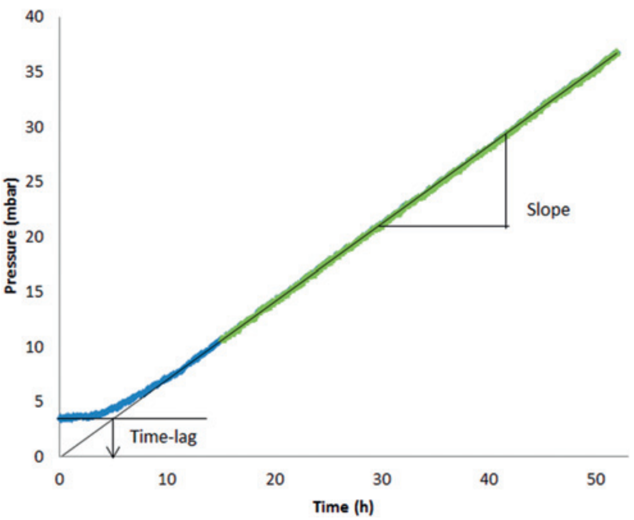

Figure 3: Permeate side pressure increase for propylene in PVDF-HFP membrane at 298 K.

Table 1 summarizes the experimental values of diffusivity, solubility and permeability of CO$_2$, propane and propylene in PVDF-HFP membranes at different temperatures.

Permeability of CO$_2$ in the dense polymer membrane is an order of magnitude higher than that of propylene and propane. This effect is due to a significant increase in diffusivity because the smaller size of the CO$_2$ molecule.

Furthermore, permeability values for propylene and propane are very similar. So it is confirmed that this type of dense membranes, in which the mass transfer takes place only by the solution-diffusion mechanism, cannot be used to carry out the separation of propane/propylene

Brought to you by | New York University Bobst Library Technical Services
Authenticated
Download Date | 2/5/16 10:43 AM

Table 1: Diffusivity, solubility and permeability of CO_2, propane and propylene PVDF-HFP 298, 308 and 318 K.

	Temperature (K)	D ($\times 10^9$ cm^2/s)	S ($\times 10^5$ mol/bar/cm^3)	P (barrer)
CO_2	298	2.16	6.12	0.373
	308	4.44	5.79	0.811
	318	11.6	4.12	1.430
Propylene	298	0.13	9.24	0.035
	308	0.4	6.31	0.075
	318	1.97	2.84	0.167
Propane	298	0.04	7.78	0.010
	308	0.11	11.2	0.036
	318	0.16	11.8	0.058

Table 2: Diffusivity of CO_2, propane and propylene in PVDF-HFP at 298 K and Lennard-Jones diameter [14].

	D ($\times 10^9$ cm^2/s)	Lennard-Jones diameter (Å)
CO_2	2.16	3.94
Propylene	0.13	4.68
Propane	0.04	5.12

mixtures. For the three pure gases is observed that the diffusion coefficients are inversely proportional to their kinetic diameters, as shown in Table 2.

Results in Table 1 show a significant increase in permeability when temperature increases. The temperature significantly increases diffusivity whereas the solubility decreases slightly. Activation energies for the three gases using Arrhenius equation were calculated in order to know the influence of temperature on the permeation process. Activation energies are shown in Table 3, from which it can be observed that the permeation of propane is more sensitive to temperature than propylene and being the lowest for the CO_2.

Table 3: Activation energies of CO_2, propylene and propane in PVDF-HFP.

Gas	E_a (kJ/mol)
CO_2	53
Propylene	61
Propane	69

In order to study the influence of the addition of an ionic liquid to the polymer matrix permeation experiments in an 80 % PVDF-HFP and 20 % of $BMImBF_4$ composite membrane were conducted. The addition of the ionic liquid ($BMImBF_4$) increases the diffusivity between two and three orders of magnitude and thus the permeability is enhanced between one and two orders given that the solubility slightly decreases, as can be observed in Table 4.

Table 4: Diffusivity, solubility and permeability of propylene and propane in HFP-PVDF and PVDF-HFP/$BMImBF_4$ at 298 K.

	Gas	D ($\times 10^9$ cm^2/s)	S ($\times 10^5$ mol/bar/cm^3)	P (barrer)
PVDF-HFP	Propylene	0.13	9.24	0.035
	Propane	0.04	7.78	0.010
PVDF-HFP/ $BMImBF_4$ (80/20)	Propylene	37.5	1.63	1.821
	Propane	20.3	1.25	0.759

This increase in diffusivity is a result of the presence of the ionic liquid that is entrapped in the polymer matrix, lowering the rigidity of the polymer chains and increasing the free volume, which facilitates the diffusion of the permeant species.

4 Conclusions

Experimental diffusivity, solubility and permeability values of propane and propylene in PVDF-HFP and PVDF-HFP-$BMImBF_4$ (80/20 wt %) membranes at different temperatures have been successfully obtained using the time-lag technique. These parameters along with other previously obtained and C_3H_6/C_3H_8 separation experimental data will allow the development of a mathematical model able to describe the behavior of the facilitated transport mechanisms of propylene through the composite membrane considering all three mechanisms and design, sizing and optimization of industrial units.

Funding: This research was supported by the Spanish Ministry under the projects CTQ2012-31639 (MINECO, SPAIN-FEDER 2007–2013) and (CTM2013-44081-R).

References

1. RBN Energy [Internet]. On-purpose propylene via propane dehydrogenation. RBN Energy LLC. [Houston] [Cited 2015 December 21]. Available at: https://rbnenergy.com

Brought to you by | New York University Bobst Library Technical Services
Authenticated
Download Date | 2/5/16 10:43 AM

2. Eldridge RB. Olefin/paraffin separation technology: a review. Ind Eng Chem Res 1993;32:2208–12.
3. Baker RW. Research needs in the membrane separation industry: looking back, looking forward. J Memb Sci 2010;362:134–6.
4. Faiz R, Li K. Olefin/paraffin separation using membrane based facilitated transport/chemical absorption techniques. Chem Eng Sci 2012;73:261–84.
5. Das M, Koros WJ. Performance of 6FDA-6FpDA polyimide for propylene/propane separations. J Memb Sci 2010;365:399–408.
6. Fallanza M, Ortiz A, Gorri D, Ortiz I. Polymer-ionic liquid composite membranes for propane/propylene separation by facilitated transport. J Memb Sci 2013;444:164–72.
7. Noble RD. Generalized microscopic mechanism of facilitated transport in fixed site carrier membranes. J Memb Sci 1992;75:121–9.
8. Merkel TC, Blanc R, Ciobanu I, Firat B, Suwarlim A, Zeid J. Silver salt facilitated transport membranes for olefin/paraffin separations: carrier instability and a novel regeneration method. J Memb Sci 2013;447:177–89.
9. Ortiz A, Ruiz A, Gorri D, Ortiz I. Room temperature ionic liquid with silver salt as efficient reaction media for propylene/propane separation: absorption equilibrium. Sep Purif Technol 2008;63:311–18.
10. Ortiz A, Galán Sanchez LM, Gorri D, De Haan AB, Ortiz I. Reactive ionic liquid media for the separation of propylene/propane gaseous mixtures. Ind Eng Chem Res 2010;49:7227–33.
11. Fallanza M, Ortiz A, Gorri D, Ortiz I. Experimental study of the separation of propane/propylene mixtures by supported ionic liquid membranes containing Ag^+-RTILs as carrier. Sep Purif Technol 2012;97:83–9.
12. Ortiz A, Galán LM, Gorri D, De Haan AB, Ortiz I. Kinetics of reactive absorption of propylene in RTIL-Ag^+ media. Sep Purif Technol 2010;73:106–13.
13. Ortiz A, Gorri D, Irabien T, Ortiz I. Separation of propylene/propane mixtures using Ag^+-RTIL solutions. Evaluation and comparison of the performance of gas-liquid contactors. J Memb Sci 2010;360:130–41.
14. Yampolskii Y, Pinnau I, Freeman B. Material science of membranes for gas and vapor separation. John Wiley: Chippenham, 2006.

Brought to you by | New York University Bobst Library Technical Services
Authenticated
Download Date | 2/5/16 10:43 AM

Optimization of multistage olefin/paraffin membrane separation processes through rigorous modeling

Journal:	*AIChE Journal*
Manuscript ID	AIChE-18-20813
Wiley - Manuscript type:	Research Article
Date Submitted by the Author:	09-Aug-2018
Complete List of Authors:	Zarca, Raúl; Universidad de Cantabria, Departamento de Ingenierías Química y Biomolecular Ortiz, Alfredo; Universidad de Cantabria , Departamento de Ingenierías Química y Biomolecular Gorri, Daniel; Universidad de Cantabria, Departamento de Ingenierías Química y Biomolecular Biegler, Lorenz; Carnegie Mellon University, Ortiz, Inmaculada; Universidad de Cantabria, Departamento de Quimica ETSII y T
Keywords:	Optimization, propylene, multistage process, membrane, mathematical model

SCHOLARONE™
Manuscripts

Optimization of multistage olefin/paraffin membrane separation processes through rigorous modeling

Authors: Raúl Zarca[1], Alfredo Ortiz[1], Daniel Gorri[1], Lorenz T. Biegler[2], Inmaculada Ortiz[1]*.

[1]Department of Chemical and Biomolecular Engineering. University of Cantabria, Av. Los Castros 46, 39005 Santander, Spain

[2]Department of Chemical Engineering, Carnegie-Mellon University, 5000 Forbes Avenue, Pittsburgh, Pennsylvania 15213-3890, United States

*corresponding author: ortizi@unican.es

Submitted to AIChE Journal

August 2018

Abstract

In this work, we explore the capabilities of an NLP optimization model to determine the viability of facilitated transport membrane processes intended to replace traditional distillation currently employed for propane/propylene separation. An NLP optimization model for multistage membrane processes has been formulated, introducing the mathematical description of the facilitated transport mechanisms in the PVDF-HFP/BMImBF$_4$/AgBF$_4$ membranes previously developed by our research group. For the first time, a simultaneous optimization of the process and the membrane material (i.e. carrier concentration) has been performed, thanks to the implementation of the governing equations for the fixed site and mobile carrier mechanisms. Once the model is solved in GAMS it returns the optimal membrane area, carrier loading and permeate pressure of each stage based on Net Present Value Cost (NPVC) minimization. Different process flowsheets were evaluated and the results show prominent reductions on NPVC for facilitated transport multistage processes when compared to distillation.

Keywords

Optimization, propylene, propane, multistage process, membrane, mathematical model, process intensification.

1. Introduction

Propane/propylene gaseous mixtures resulting from fluid catalytic cracking and steam cracking are commonly separated using high pressure or cryogenic distillation, which is associated to major energy and capital consumptions.[1] Through the last years, process intensification by means of membrane technology has emerged as a promising alternative to large, expensive and energy-intensive distillation units.[2]

Many membrane materials have been reported for olefin/paraffin separation, including polymers,[3,4] and more complex materials, such as carbon molecular sieves,[5-7] zeolitic imidazolate frameworks (ZIFs)[8-11] or facilitated transport membranes.[12,13] Among these, facilitated transport membranes can easily surpass the permeability-selectivity trade-off of polymeric membranes thanks to the reversible reaction between the olefin and a carrier cation, typically silver, which is added to the membrane composition.[14] Facilitated transport membranes have been synthesized following different approaches, from supported liquid membranes (SLM)[15,16] to supported ionic liquid membranes (SILM)[17] that replace organic solvents with non-volatile room temperature ionic liquids (RTILs)[18] in order to avoid solvent losses through evaporation.[19] Recently, composite facilitated transport membranes prepared by solvent casting of a polyvinylidene fluoride - hexafluoropropylene (PVDF-HFP) polymeric solution containing the ionic liquid and the silver salt have been reported.[20] In these dense membranes, which feature a combination of fixed site and mobile carrier transport mechanisms,[21] selectivities up to 150 and propylene permeabilities higher than 1000 Barrer have been achieved that avoid the issues of supported liquid membranes.

Since a single-stage membrane process that produces polymer grade propylene and fuel grade propane simultaneously is not feasible due to the purity-recovery trade-off inherent in membrane operation, the implementation of membrane technology to intensify the olefin/paraffin separation process can be carried out according to two different approaches. The first one involves the use of membrane modules along with new or existing distillation columns to create a hybrid process that reduces the required reflux ratio and its associated expenses.[22-27] The second approach achieves complete replacement of the distillation column with membrane technology by designing and optimizing appropriate multistage/multistep membrane processes.[28,29]

In particular, several trade-offs should be balanced when designing a multistage membrane process based on facilitated transport membranes. Firstly, the total membrane area of each stage determines the flowrates and purities of the product streams in that stage. Thus, higher stage areas generate larger permeate flowrates at the expense of permeate purity. In addition, the transmembrane flux of the transported species in these membranes is strongly dependent on the carrier loading, as derived from the experimental analysis and the mathematical models.[17,21] However, high carrier concentrations imply high membrane cost per unit area, which could affect the process economics. Finally, higher transmembrane pressures increase the available driving force for the permeation but at the expense of higher recompression requirements.

Moreover, the whole process flowsheet can be optimized in order to obtain the optimal process configuration in terms of number of stages, mixers, splitters and compressors. This type of optimization involves the design of superstructures that are solved using binary variables, which result in complex mixed integer nonlinear programming problems “MINLP”.[30] However, MINLP problems are difficult to solve because they combine challenges of nonlinear and mixed integer programming, and require dedicated methods for its resolution.[31] Instead, while it is often possible to study all potential multistage configurations in one single superstructure, most studies dealing with superstructure optimization for gas separation conclude with a two-stage optimal configuration.[32-35]

Therefore, in this work we focus on the optimization of the implicit trade-offs in two multistage facilitated transport processes, specifically, one conventional two-stage configuration and one two-stage configuration with a two-step second stage, commonly known as "two-and-one-half" stage process.[28] In this manner, the complex mixed-integer nonlinear formulations associated to superstructures can be replaced with a nonlinear programming problem. The membrane modules have been modelled as hollow fiber modules, which is the most adequate configuration for gas separation, featuring high packing densities and energy efficiency.[34,36-38] Furthermore, the mass balances in the membrane modules have been described as ordinary differential equations and have been solved using orthogonal collocation on finite elements.[39] Consequently, black box modeling approaches can be avoided, thus allowing the study of the transmembrane flux profiles along the fibers. These profiles will show how the optimization works in balancing the recovery-purity trade-off by varying the membrane total area of each stage. Additionally, a simultaneous optimization of the process and the membrane material (i.e. carrier load) has been possible thanks to the introduction of the equations that govern the facilitated transport mechanisms.[21] To the best of our knowledge, this is the first time that this joint optimization is performed without solving an upper-bound type equation for the selectivity-permeability trade-off, whose solution does not necessarily represent a real membrane material.[40] Finally, the objective function accounts for the process economics, which assesses the potential of facilitated transport multistage processes to replace current distillation.

2. Theoretical Background

2.1. Single-Stage and Multistage Membrane Processes

In membrane process design the basic unit is the membrane stage, which can be defined as an operating unit, comprising one or more membrane modules, which performs a specific task different from any other membrane stages existing in the same process. A single-stage process, shown in Figure 1, is the simplest membrane process that can be designed, although some major limitations in membrane operations affect these processes. In particular, membrane material selectivity and the industrially reachable pressure ratio prevent satisfying high product purity and recovery simultaneously, and process engineers may have to sacrifice one of these specifications. Therefore, single-stage processes are often used for bulk concentration prior to further purification processes.[41]

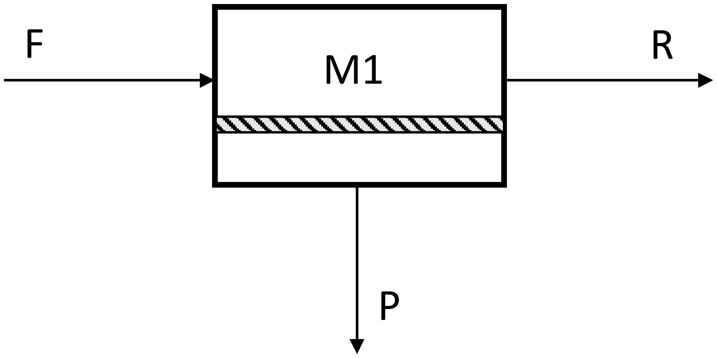

Figure 1. Single-stage membrane process.

To overcome the limitations of single-stage membrane processes more stages could be interconnected, generating different multistage configurations. Staging a membrane process involves solving the trade-off between capital expenses (additional compressors and membrane modules) and product recovery. Although there are many multistage configurations, the two-stage and the so-called two-and-one-half stage processes,[42] are preferred over three stage or higher multistage processes.[28] In the two-stage process, shown in Figure 2, the recompressed permeate of the first stage is fed into a second stage for a further purification step. The retentate of the second stage is then recycled and mixed with the original feed.

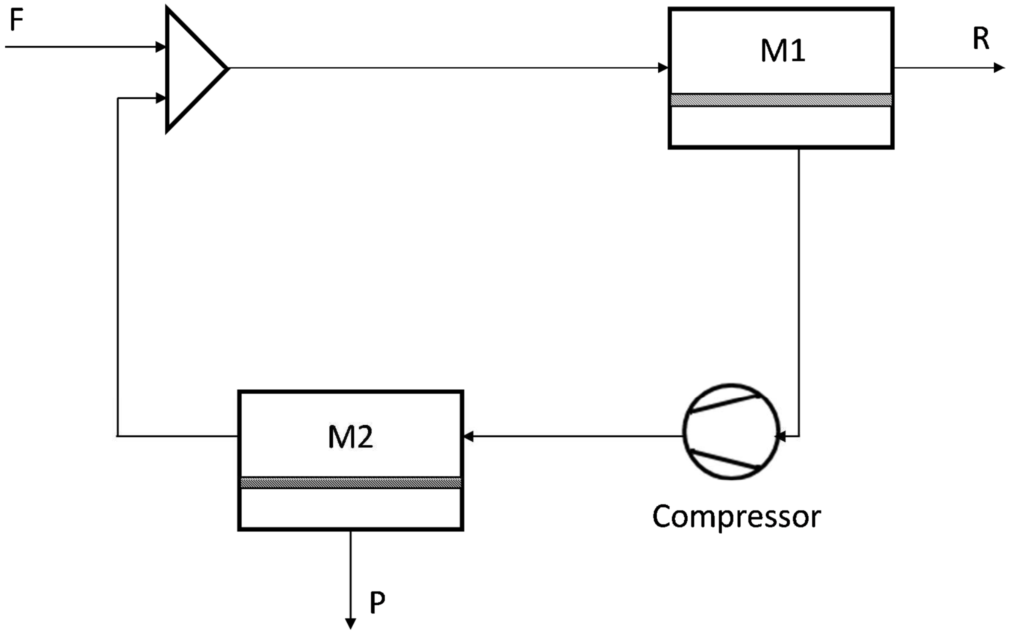

Figure 2. Two-step membrane process.

In comparison, the two-and-one-half process shown in Figure 3 uses a two-step separation for the second stage and the permeate of the second step is recycled to the first step feed. This configuration can achieve any desired concentration of the more permeable gas by controlling the relative size of the second stage modules. Moreover, to balance the tradeoffs and calculate the feed and permeate pressures and the membrane area of each stage, process optimization is required.

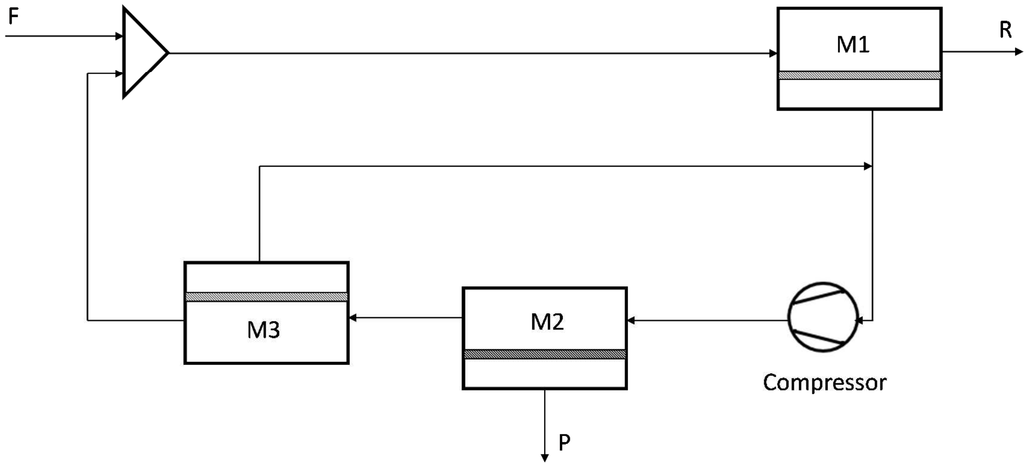

Figure 3. Two-and-one-half membrane process.

2.2. Discretized membrane model

Previous studies on membrane process optimization usually make use of simplified membrane models. These shortcut models are typically implemented within superstructures that are solved as mixed-integer optimization problems.[32] For processes where a more detailed description of the membrane separator is needed as in the case of hollow fibers modules, a perfect cross-flow model is usually employed. This model assumes plug-flow in the high pressure side of the fiber, usually the lumen side, and perfect mixed flow in the permeate side, i.e. shell side.[23] However, assuming that the feed flows through the lumen side may seem unrealistic in gas separation hollow fibers, whereby the active layer is often formed in the outer fiber surface. In addition, most membrane models assume fixed permeability/selectivity values for a given membrane material. In contrast, the rigorous facilitated transport model used in this work requires calculating the partial pressure profiles along the module. To address these issues, a fully discretized optimization model has been developed in this work.

The membrane model is depicted in Figure 4 and is based on the following assumptions:

- The feed and retentate streams flow through the shell and lumen sides of the fibers respectively.
- The module operates isothermally and in steady state.
- The feed and product streams flow in co-current mode.
- Plug-flow is assumed at both sides of the membrane.
- The total feed and permeate pressures are operation constants.
- The only pressure drop in the membrane module is the transmembrane pressure.

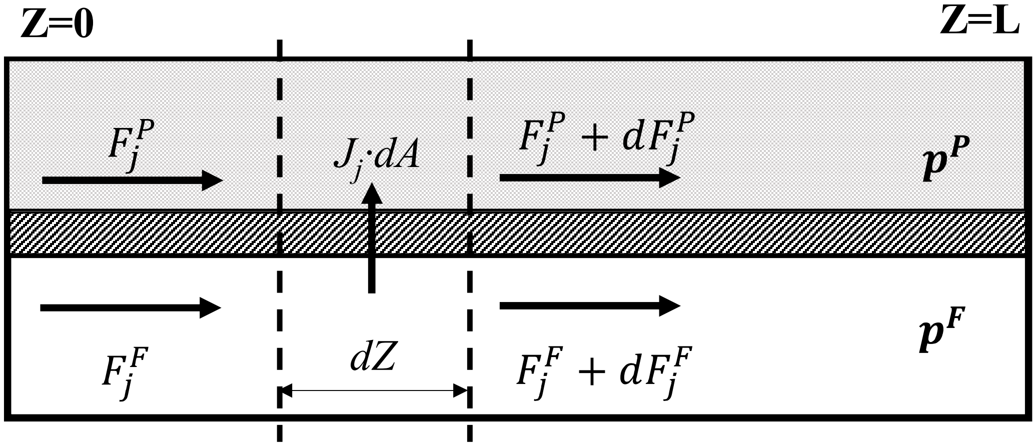

Figure 4. Schematic diagram of the hollow fibers model.

The component molar flowrates are discretized according to the following mass balances:

$$dF_j^F(z) = -J_j(z) \cdot dA \tag{1}$$

$$dF_j^P(z) = J_j(z) \cdot dA \tag{2}$$

where F_j and J_j are the molar flowrate and the transmembrane flux of component j, respectively, and dA is the fiber outer wall area differential element. The dimensionless fiber axial length is defined as:

$$\bar{z} = \frac{z}{L} \qquad \bar{z} \in [0,1] \tag{3}$$

where L is the total fiber length. Rearranging terms, the mass balances (ODEs) and the boundary conditions can now be rewritten as:

$$\frac{dF_j^F(\bar{z})}{d\bar{z}} = -J_j(\bar{z}) \cdot A \tag{4}$$

$$\frac{dF_j^P(\bar{z})}{d\bar{z}} = J_j(\bar{z}) \cdot A \tag{5}$$

$$F_j^F|_{\bar{z}=0} = F_j^F(\bar{z} = 0) \tag{6}$$

$$F_j^P|_{\bar{z}=1} = F_j^P(\bar{z} = 1) \tag{7}$$

One of the main features of this work is that the membrane material optimization (i.e. carrier concentration) and the multistage process optimization are performed simultaneously. For this purpose, the rigorous facilitated transport model previously developed by this research group has been implemented in the optimization,[21] particularly for PVDF-HFP/BMImBF$_4$/AgBF$_4$ membranes containing silver as carrier. In this model, which was specifically developed for facilitated transport membranes that combine fixed and mobile carrier mechanisms, the permeability of the paraffin can be considered constant. Thus its transmembrane flux is described through the solution-diffusion model:[43]

$$J_{C_3H_8}(\bar{z}) = \frac{P_{C_3H_8}}{\delta}\left[p^F_{C_3H_8}(\bar{z}) - p^P_{C_3H_8}(\bar{z})\right] \tag{8}$$

where $P_{C_3H_8}$ is the paraffin permeability, δ is the active layer thickness and $p^F_{C_3H_8}$ and $p^P_{C_3H_8}$ are the feed and permeate partial pressure of the paraffin.

Conversely, the olefin flux, i.e. the preferentially transported species, is affected by the complexation reaction with the silver cations:

$$[Ag^+] + C_3H_6 \overset{k_{eq}}{\Leftrightarrow} Ag^+(C_3H_6) \tag{9}$$

The flux can be calculated as the sum of the contributions of three transport mechanisms: solution-diffusion, fixed-site carrier and mobile carrier:

$$J_{C_3H_6}(\bar{z}) = J_{C_3H_{6,SD}}(\bar{z}) + J_{C_3H_{6,MC}}(\bar{z}) + J_{C_3H_{6,FC}}(\bar{z}) \tag{10}$$

$$J_{C_3H_{6,SD}}(\bar{z}) = D_{C_3H_6,m} \cdot S_{C_3H_6,m}\frac{p^F_{C_3H_6}(\bar{z}) - p^P_{C_3H_6}(\bar{z})}{} \tag{11}$$

$$J_{C_3H_{6,MC}}(\bar{z}) = \frac{k_{eq}\cdot[Ag]\cdot H_{C_3H_6}}{1+k_{eq}\cdot p^P_{C_3H_8}(\bar{z})\cdot H_{C_3H_6}} D_{comp}\,\frac{p^F_{C_3H_6}(\bar{z}) - p^P_{C_3H_6}(\bar{z})}{\delta}\, x_{IL} \tag{12}$$

$$J_{C_3H_{6,MC}}(\bar{z}) = K_{FC}(\bar{z}) \cdot \frac{p^F_{C_3H_6}(\bar{z}) - p^P_{C_3H_6}(\bar{z})}{}(1 - x_{IL}) \tag{13}$$

$$K_{FC}(\bar{z}) = \alpha\left(\frac{[Ag^T]}{1+k_p p^P_{C_3H_6}(\bar{z})}\right) \tag{14}$$

where k_{eq} is the complexation constant, $H_{C_3H_6}$ is the propylene solubility in the composite membrane, x_{IL} is the ionic liquid mass fraction in the membrane composition, α is a fitting parameter for the fixed-site carrier mechanism and $[Ag^T]$ is the silver concentration in the membrane. The temperature dependencies have been omitted as isothermal operation has been assumed. The contribution of the Fickian diffusion to the olefin transmembrane flux (Eq.11) is negligible compared to the contribution of the facilitated transport mechanisms (Eq. 12-13) and, in consequence, it has not been included in the optimization. A detailed description of the model can be found in the original source.[21] Table 1 shows the values of the model parameters.

Table 1. Facilitated transport model parameters at 323 K.

Parameter	Value	Reference
D_{comp} ($x10^{11}$ m^2 s^{-1})	4.30	[17]
x_{IL} (-)	0.20	[21]
$H_{C_3H_6}$ (mol bar^{-1} m^{-3})	31.97	[18]
k_{eq} (m^3 mol^{-1})	0.17	[18]
α ($x10^{11}$ m^2 mol^{-1} s^{-1})	2.37	[21]

As commented before, the use of this specific model for facilitated transport avoids using a fixed permeability parameter and introduces carrier concentration as a decision variable. In this way, the membrane material and the multistage process can be optimized at the same time.

Finally, the ordinary differential equations (Eqs 4-7) are solved as algebraic equations after discretization through implicit Runge-Kutta collocation methods using 100 finite elements and 3 internal collocation points.

2.3. Optimization details

The aim of this work is to optimize two multistage membrane processes: a) a two-stage and b) a two-and-one-half stage, intended to produce polymer grade propylene, and enriched propane, from a C_3 refinery stream minimizing the Net Present Value Costs (NPVC) of both configurations. The pressure, temperature and composition of the original feed, stream *F* in Figures 1-3, are fixed by common refinery specifications.[44] Table 2 displays the properties of the propylene/propane mixed stream, the target product purities and the process constants and constraints.

Table 2. Process feed specifications, parameters and constraints.

Parameter	**Value**
Feed temperature (K)	323
Feed pressure (bar)	18
Feed flowrate (kmol h^{-1})	360
Feed composition (C_3H_6 mole frac.)	0.50
Permeate pressure (bar)	1-18
Required C_3H_6 purity (x_i)	≥ 0.995
Required C_3H_8 purity (x_i)	≥ 0.950
C_3H_8 permeability (Barrer) [a]	20
Membrane thickness (μm)	20
Silver loading[b] (M)	0-6

[a] 1 Barrer = 10^{-10} cm^3 (STP) cm cm^{-2} s^{-1} $cmHg^{-1}$.

[b] Silver loading delimited according to the experimentally studied concentration range.[20,21]

The decision variables of the model are:

- The membrane area of each module.
- The carrier concentration of each membrane.
- The permeate pressure.

The mathematical standard form of the optimization problem can be described as:

$$\begin{aligned} & Minimize\ NPVC(v) \\ & s.t. \\ & \quad h(v) = 0 \\ & \quad t(v) \geq 0 \\ & U' \leq v \leq U'' \end{aligned} \tag{15}$$

where v is the vector of decision variables, $h(v)$ represents the set of model algebraic equations, $t(v)$ is the set of constraints (Eqs. 16-17) and U' and U'' are the lower and upper limits of the decision variables, respectively.

$$x_{C_3H_6} \geq x_{C_3H_6,min} \tag{16}$$

$$x_{C_3H_8} \geq x_{C_3H_8,min} \tag{17}$$

Finally, the objective function (NPVC) has been calculated as a combination of OPEX and CAPEX, correcting the operating expenses according to the time value of money:

$$NPVC = CAPEX + OPEX \cdot (1 - (1 + r)^{-T})/r \tag{18}$$

The parameters and constants used are shown in Table 3. A detailed description of the economic calculations can be found in a previous work.[45] Briefly, the compressor expenses have been calculated according to the *Guthrie's Modular Method for Costing and Sizing* [46] and the membrane cost is calculated using the market prices for its constituents and the optimized composition:

$$MCA = \delta \cdot (PL \cdot PP + ILL \cdot ILP + [Ag]^{+} \cdot M_{Ag} \cdot AGP) \tag{19}$$

where MCA is the membrane cost per unit area, δ is the membrane thickness and M_{Ag} is the molar mass of $AgBF_4$. The membrane replacement cost has been introduced through a membrane replacement factor MR.

Table 3. Economic evaluation parameters.

Parameter	**Symbol**	**Value**
Membrane		
Membrane replacement factor (%)	*MR*	1
Polymer load (g m^{-3})	*PL*	1.11x10^{6}
Ionic liquid load (g m^{-3})	*ILL*	2.76x10^{5}
Polymer cost (\$ g^{-1})	*PP*	0.7
Ionic liquid cost (\$ g^{-1})	*ILP*	0.8
Silver salt cost (\$ g^{-1})	*AGP*	13.0
Compressor		
Compressor stages	N_{st}	3
Cost function exponent	*a*	0.77
Electricity price (\$ kWh^{-1})	*EP*	0.15
Isentropic efficiency	η_c	0.70
Material and pressure factor	*MPF*	1
Compression ratio	Cr_{max}	2.62
Module factor	*MF*	3.11
Ratio of heat capacities	Υ	1.15
Reference cost (\$)	C_0	23000
Reference size (kW)	S_0	74.57
Update factor	*UF*	4.71
Project		
Annual operation (h y^{-1})	*OF*	8000
Investment rate (%)	*r*	10
Period (y)	T_{inv}	15

The optimization model renders a NLP problem solved in GAMS using as solver the multi-start heuristic algorithm OQNLP on a 3.40 GHz Intel® Core™ i7–3770 processor. The model statistics are detailed in Table 4. The model is solved in less than 0.1 seconds when CONOPT is used as local solver for OQNLP.

Table 4. Models statistics

	Two-stages	Two-and-one-half stages
Number of single equations	4314	8122
Number of single variables	4321	8130

3. Results and Discussion

This section presents and discusses the main results regarding the design and optimization of the proposed flowsheets. The feed stream to both flowsheets consists of an equimolar propane/propylene mixture and the objective is to obtain propylene and propane purities of 99.5 mol% and 95 mol% respectively. The Net Present Value Cost (NPVC) of both multistage processes will be compared with the NPVC of the reference distillation column.

3.1. Multistage membrane process optimization results

The optimized two stage flowsheet is displayed in Figure 5. The optimal design comprises two membrane stages showing considerable size differences. The first stage requires more than 14000 m^2 of membrane area to generate a propylene depleted retentate stream, thus achieving the desired propane purity. However, the second stage area is almost ten times smaller and is intended to produce a high purity propylene permeate regardless of the retentate purity.

Regarding the optimal carrier loading, its value is allowed to vary between the experimentally studied range from 0 to 6 M, where 0 M implies no facilitated transport and 6 M is the highest concentration assessed for PVDF-HFP/BMImBF$_4$/AgBF$_4$ membranes. Eventually, the optimization balances the cost-performance trade-off of the first stage at 2.51 M Ag^+, far below the upper limit. Since higher concentrations of carrier result in high membrane prices per unit area, this decreased optimal value helps to reduce the expenses caused by the large size of this stage. On the other hand, the second stage carrier loading hits the highest allowed level of 6 M Ag^+, which is consistent with the purity-oriented nature of this stage. Although the high carrier loading of the second stage raises the membrane specific cost to 324 \$/m^2, the relative small size of this stage dampens the total membrane cost.

Finally, it should be noted that this multistage configuration generates a large reflux stream with high associated compression costs. Nonetheless, the optimal permeate pressure of both stages falls to 1 bar, promoting higher driving force in the modules at the expense of higher compression duty.

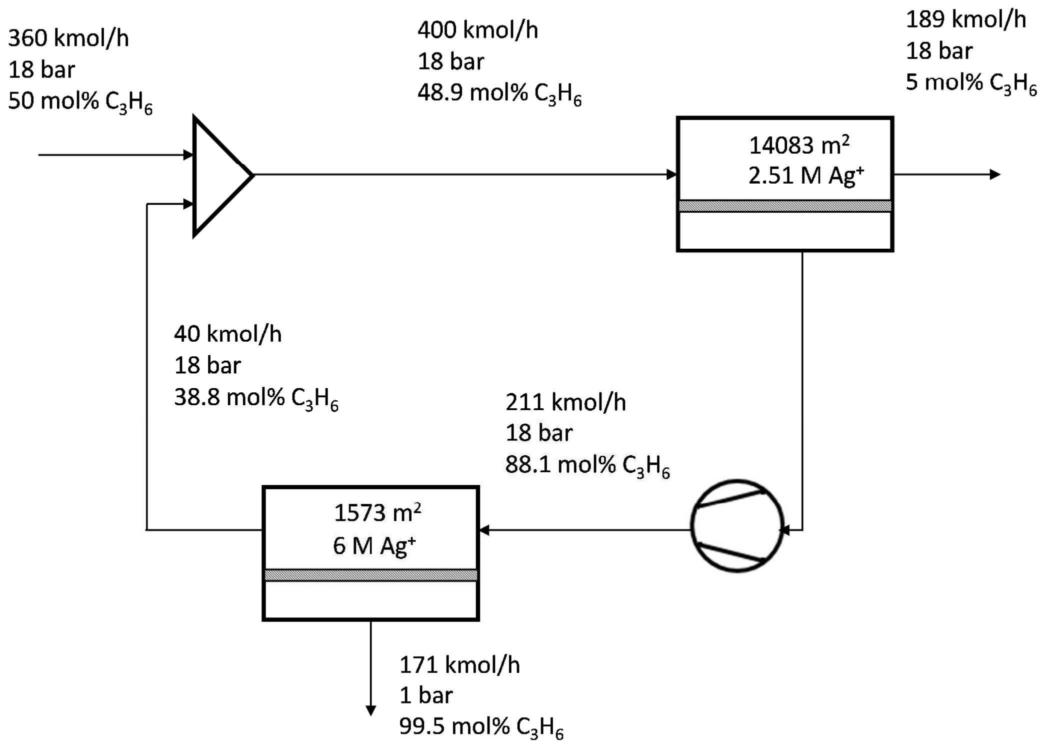
360 kmol/h
18 bar
50 mol% C_3H_6
400 kmol/h
18 bar
48.9 mol% C_3H_6
189 kmol/h
18 bar
5 mol% C_3H_6
14083 m^2
2.51 M Ag$^+$
40 kmol/h
18 bar
38.8 mol% C_3H_6
211 kmol/h
18 bar
88.1 mol% C_3H_6
1573 m^2
6 M Ag$^+$
171 kmol/h
1 bar
99.5 mol% C_3H_6

Figure 5. Two stage process optimal design.

In order to gain better insight on the optimal stage design, the transmembrane flux profiles along the fiber modules have been calculated. Figure 6 displays the propylene and propane transmembrane flux along the dimensionless axial length in each membrane stage. As it can be observed in Figure 6A the propylene transmembrane flux of stage M1 starts at a high level (~6x10^{-3} mol m^{-2} s^{-1}) thanks to the facilitated transport mechanisms and the significant driving force achieved in the hollow fibers. The resulting high permeation flux in combination with the large membrane area depletes the propylene concentration of the retentate stream and, eventually, its driving force falls until the transmembrane flux of propane (~6×10^{-4} mol m^{-2} s^{-1}) exceeds that of the propylene. In contrast, Figure 6B shows the same profiles in stage M2, but in this case the propylene transmembrane flux remains almost constant due to the reduced membrane area required, which produces a polymer grade propylene stream as permeate but maintains a notable propylene concentration in the retentate.

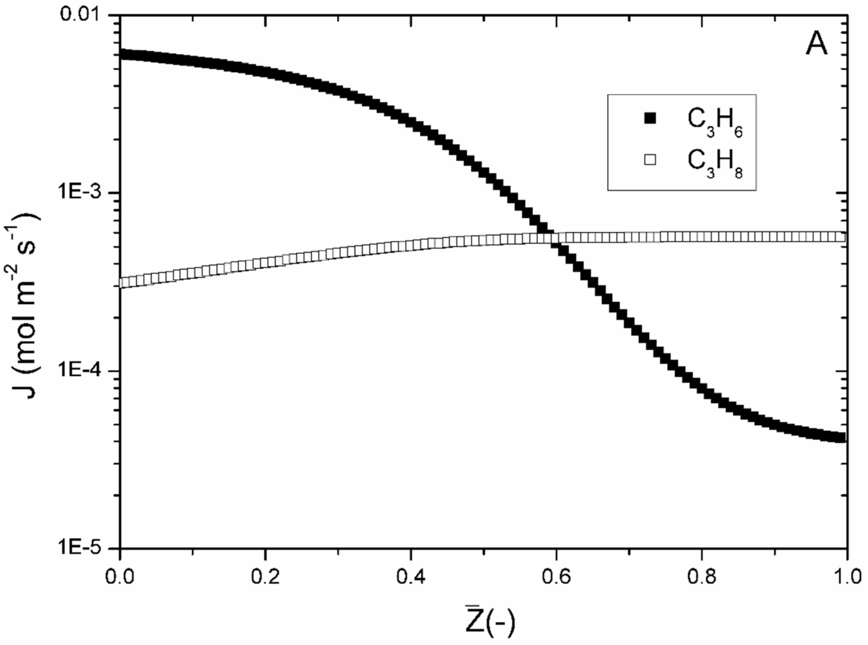

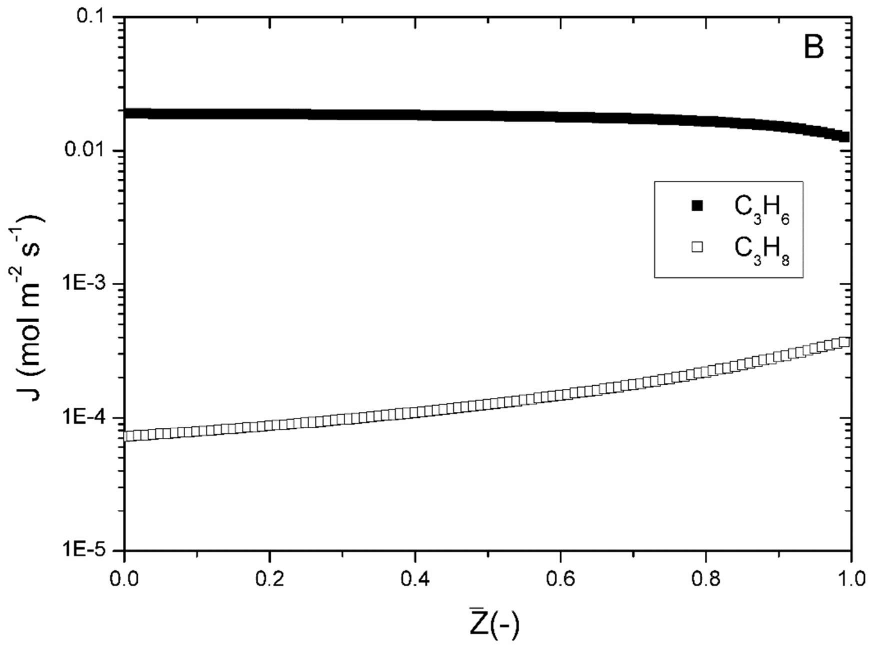

Figure 6. Propylene and propane transmembrane flux in stages M1 (A) and M2 (B) of the two stage process.

This is a good example of how optimization can solve the intrinsic tradeoff between productivity and purity, and displaces it towards high permeate volume production or high product purity depending on the specific task of each stage within the multistage process.

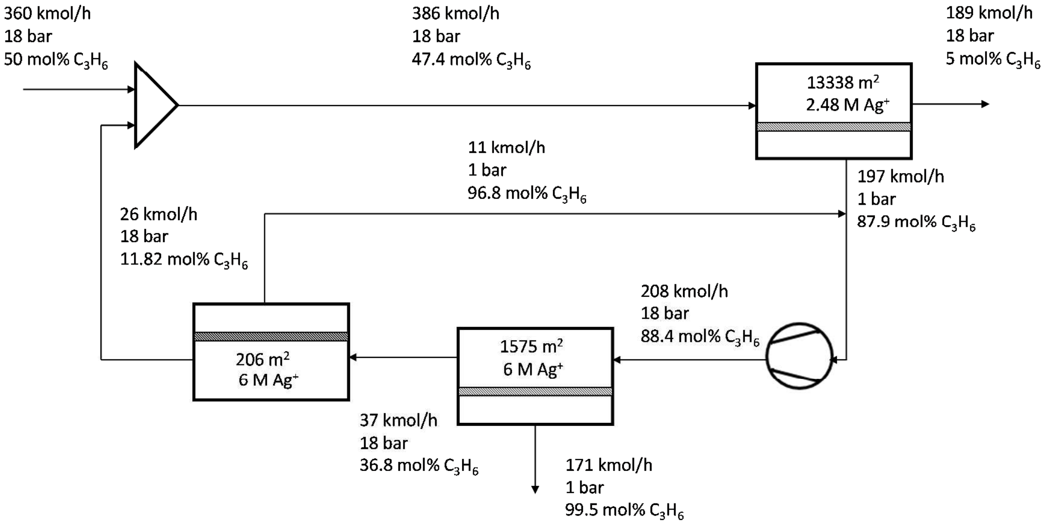
360 kmol/h
18 bar
50 mol% C3H6
386 kmol/h
18 bar
47.4 mol% C3H6
189 kmol/h
18 bar
5 mol% C3H6
13338 m²
2.48 M Ag+
11 kmol/h
1 bar
96.8 mol% C3H6
197 kmol/h
1 bar
87.9 mol% C3H6
26 kmol/h
18 bar
11.82 mol% C3H6
208 kmol/h
18 bar
88.4 mol% C3H6
206 m²
6 M Ag+
1575 m²
6 M Ag+
37 kmol/h
18 bar
36.8 mol% C3H6
171 kmol/h
1 bar
99.5 mol% C3H6

Figure 7. Two-and-one-half stage process optimal design.

The "two-and-one-half stage" process optimization results are shown in Figure 7. The main feature of this process is the introduction of a third stage intended to recycle a propylene enriched stream back to the second stage feed, in this manner the outer loop recycle is reduced, minimizing the total membrane area requirements in the stage M1 and the subsequent compression duty. As in the two stage process, the first stage (M1) is significantly larger than the next stages (M2 and M3) and its optimal carrier concentration is below the upper bound, at 2.48 M Ag^+. Again, the M2 and M3 stages require the maximum carrier loading of 6 M Ag^+, which increases the membrane performance at the expense of higher membrane costs. However, although the introduction of a third stage helps to minimize the compression requirements by decreasing the recycle flowrate, this reduction is not significant enough and may not justify its implementation. This can be observed by the relatively small size of stage M3, which is almost negligible compared with the other stages. The optimization results of both processes are detailed in Table 5.

Table 5. Optimization results of the multistage processes

	Two Stages	Two-and-one-half Stages
Compressor power (kW)	697	688
M1 total area (m^2)	14083	13338
M2 total area (m^2)	1574	1575
M3 total area (m^2)	*n/a*	206
M1 carrier loading (M)	2.51	2.48
M2 carrier loading (M)	6	6
M3 carrier loading (M)	*n/a*	6
M1 membrane cost ($\$ m^{-2}$)	147	145
M2 membrane cost ($\$ m^{-2}$)	324	324
M3 membrane cost ($\$ m^{-2}$)	*n/a*	324
M1 permeate pressure (bar)	1	1
M2 permeate pressure (bar)	1	1
M3 permeate pressure (bar)	*n/a*	1

A brief analysis of the transmembrane flux profiles in the "two-and-one-half" stage process reveals similar design criteria as in the first studied case. Figure 8A-C displays the propylene and propane transmembrane flux along the dimensionless axial length of the fibers module.

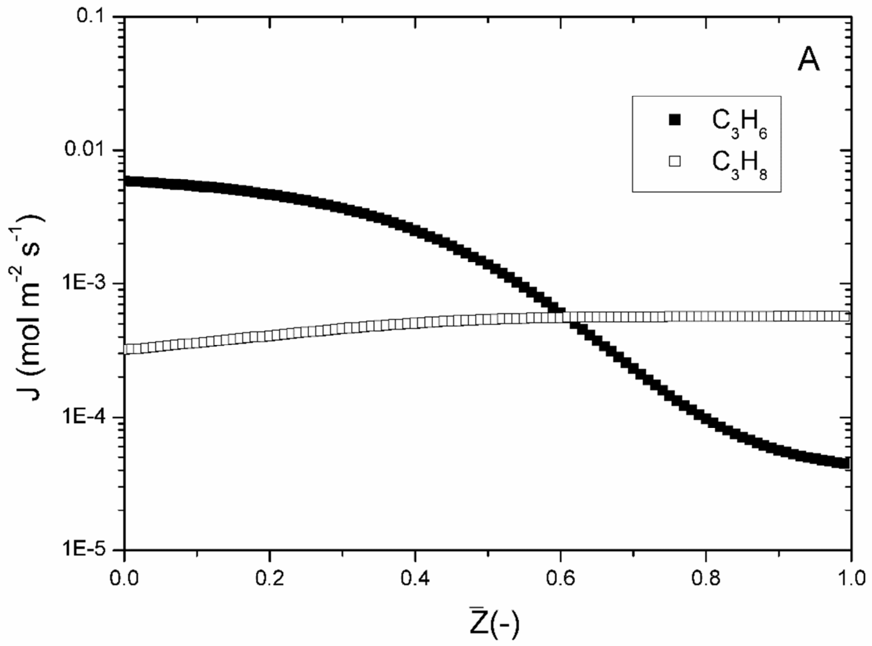

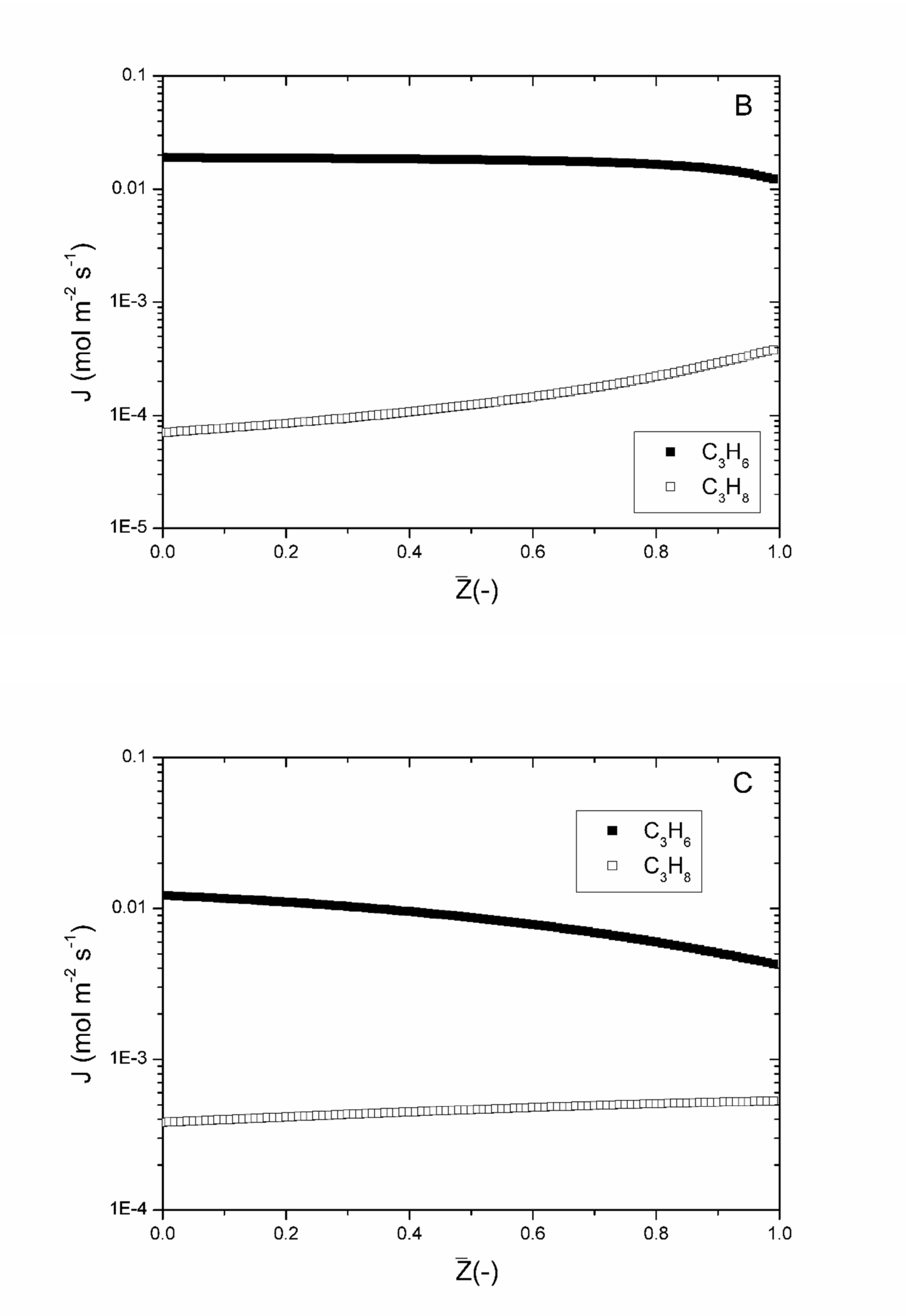

Figure 8. Propylene and propane transmembrane flux in stages M1 (A), M2 (B) and M3 (C) of the "two-and-one-half" stage process.

As commented before, the large membrane area required in the first stage is intended to achieve the desired propane purity in one single pass, as a result, most of the propylene permeates and its driving force is reduced until its transmembrane flux falls below the propane level, see Figure 8A. Notice that this is not detrimental when the product stream is the retentate, as is the case for stage M1. However, the subsequent stages, Figures 8B-C, are intended to produce a propylene-enriched permeate and consequently, the propylene transmembrane flux remains high along the fiber modules, thanks to the relatively small areas involved in these stages.

3.2. NPVC comparison

The NPVC of both membrane processes and the base case distillation are itemized in Table 6. The results reveal the prominent potential of facilitated transport membrane processes to replace the traditional distillation and to sharply decrease the investment expenses when implementing the two stage membrane process. On the other hand, the introduction of an additional separation step in the “two-and-one-half” stage flowsheet produces minor savings compared to the two stages process and, therefore, a less complex process may be preferred. It is worth noting that the main difference between the base case distillation and the membrane processes is not in the capital expenses but in the operating costs, which is consistent with the use of process steam in the distillation reboiler. As expected, process intensification through membrane technology plays here a major role in energy saving.

Table 6. Multistage processes Net Present Value Cost compared to the distillation base case.

	Distillation	Two Stages	"Two-and-one-half" Stages
OPEX (MM\$ y^{-1})	4.1[a]	0.86	0.85
CAPEX (MM\$)	8.9[a]	5.0	4.9
NPVC (MM\$)	39.7[a]	11.56	11.40

[a] Calculated according to the “Guthrie’s Modular Method for Costing and Sizing” [46] based on the design parameters presented elsewhere.[24]

3.3. Comparison for an Extreme Purity Specification

Although propylene purities higher than 99.5% are not demanded by the polypropylene industry, it is instructive to consider a final comparison between the two-stage and two-and-half stage optimization models. For a propylene permeate specification of 99.9% we observe that the two stage process becomes infeasible and has not solution. In contrast, the two-and-half stage model is able to obtain any permeate concentration, and consequently satisfies this specification. As shown in Table 7, the optimum for this process is achieved at a much higher cost, with more than double the NPVC.

Table 7. Multistage processes Net Present Value Cost for 99.9% propylene specification

	Propylene 99.5 %		Propylene 99.9 %	
	Two stages	"Two-and-one-half" stages	Two stages	"Two-and-one-half" stages
OPEX (MM$ y^{-1})	0.86	0.85	Not feasible	2.05
CAPEX (MM$)	5.0	4.9		8.74
NPVC (MM$)	11.56	11.4		24.3

4. Conclusions

The complete replacement of propane/propylene distillation processes by membrane technology strongly relies on adequate membrane processes and materials design. In this work, the simultaneous optimization of multistage processes and facilitated transport membrane composition reveals potential Net Present Value Cost reductions of around 70% compared to the base case distillation. Additionally, the optimization results showed minor differences between the two studied multistage processes. Thus, the simpler two-stage layout may be more adequate in a real scenario. Finally, full discretization of the model reveals how the recovery-purity trade-off and the position of each stage within the multistage flowsheet affect the transmembrane flux profiles along the modules. In this sense, this work outlines the importance of previous mathematical modeling of transport phenomena as valuable foundations for further computer aided process engineering.

Acknowledgements

Financial support from the Spanish Ministry of Science under the projects CTQ2015-66078-R and CTQ2016-75158-R (MINECO, Spain-FEDER 2014–2020) is gratefully acknowledged. Raúl Zarca also thanks the Universidad de Cantabria for the postgraduate fellowship.

Nomenclature

A membrane effective area [m^2]

D diffusion coefficient [m^2 s^{-1}]

F molar flowrate [mol s^{-1}]

H Henry’s solubility constant [mol bar^{-1} m^{-3}]

h set of model algebraic equations

J molar transmembrane flux [mol m^{-2} s^{-1}]

K_{eq} equilibrium constant [m^3 mol^{-1}]

K_{FC} fixed carrier effective permeability [mol bar^{-1} m^{-1} s^{-1}]

K_p heterogeneous equilibrium constant [bar^{-1}]

L fiber length [m]

P permeability [mol bar^{-1} m^{-1} s^{-1}]

p pressure [bar]

R universal gas constant [8.314 J mol^{-1} K^{-1}]

r investment rate [%]

S gas solubility in the membrane [mol bar^{-1} m^{-3}]

T investment period [y]

t set of model constraints

U’ lower limit of the decision variables

U” upper limit of the decision variables

x molar fraction [-]

x_{IL} ionic liquid mass fraction [-]

z hollow fiber axial dimension [m]

Greek letter

α fitting parameter

δ active layer thickness [m]

Superscript / subscript

0 feed side

C_3H_6 propylene

C_3H_8 propane

comp organometallic complex

FC fixed-site carrier

IL ionic liquid

L permeate side

m membrane

MC mobile carrier

r reaction

SD solution-diffusion

References

1. Sholl DS, Lively RP. Seven chemical separations to change the world. *Nature*. 2016;532(7600):435-437.

2. Charpentier JC. In the frame of globalization and sustainability, process intensification, a path to the future of chemical and process engineering (molecules into money). *Chem Eng J*. 2007;134(1-3):84-92.

3. Faiz R, Li K. Polymeric membranes for light olefin/paraffin separation. *Desalination*. 2012;287:82-97.

4. Staudt-Bickel C, Koros WJ. Olefin/paraffin gas separations with 6FDA-based polyimide membranes. *J Membr Sci*. 2000;170(2):205-214.

5. Xu L, Rungta M, Brayden MK, et al. Olefins-selective asymmetric carbon molecular sieve hollow fiber membranes for hybrid membrane-distillation processes for olefin/paraffin separations. *J Membr Sci*. 2012;423-424:314-323.

6. Liu J, Liu Y, Kayrak Talay D, Calverley E, Brayden M, Martinez M. A new carbon molecular sieve for propylene/propane separations. *Carbon*. 2015;85:201-211.

7. Xiaoli M, Lin YS, Wei X, Kniep J. Ultrathin Carbon Molecular Sieve Membrane for Propylene/Propane Separation. *AIChE J*. 2016;62(2):491-499.

8. Kwon HT, Jeong HK, Lee AS, An HS, Lee JS. Heteroepitaxially Grown Zeolitic Imidazolate Framework Membranes with Unprecedented Propylene/Propane Separation Performances. *J Am Chem Soc*. 2015;137(38):12304-12311.

9. Liu D, Ma X, Xi H, Lin YS. Gas transport properties and propylene/propane separation characteristics of ZIF-8 membranes. *J Membr Sci*. 2014;451:85-93.

10. An H, Park S, Kwon HT, Jeong HK, Lee JS. A new superior competitor for exceptional propylene/propane separations: ZIF-67 containing mixed matrix membranes. *J Membr Sci*. 2017;526:367-376.

11. Da Silva FA, Rodrigues AE. Propylene/propane separation by vacuum swing adsorption using 13X zeolite. *AIChE J*. 2001;47(2):341-357.

12. Faiz R, Li K. Olefin/paraffin separation using membrane based facilitated transport/chemical absorption techniques. *Chem Eng Sci*. 2012;73:261-284.

13. Yoon Y, Won J, Kang YS. Polymer electrolyte membranes containing silver ion for facilitated olefin transport. *Macromolecules*. 2000;33(9):3185-3186.

14. Nymeijer K, Visser T, Brilman W, Wessling M. Analysis of the Complexation Reaction between Ag+ and Ethylene. *Ind Eng Chem Res*. 2004;43(11):2627-2635.

15. Duan S, Ito A, Ohkawa A. Separation of propylene/propane mixture by a supported liquid membrane containing triethylene glycol and a silver salt. *J Membr Sci*. 2003;215(1-2):53-60.

16. Ravanchi MT, Kaghazchi T, Kargari A. Supported liquid membrane separation of propylene-propane mixtures using a metal ion carrier. *Desalination*. 2010;250(1):130-135.

17. Fallanza M, Ortiz A, Gorri D, Ortiz I. Experimental study of the separation of propane/propylene mixtures by supported ionic liquid membranes containing Ag+–RTILs as carrier. *Sep Purif Technol*. 2012;97:83-89.

18. Ortiz A, Ruiz A, Gorri D, Ortiz I. Room temperature ionic liquid with silver salt as efficient reaction media for propylene/propane separation: Absorption equilibrium. *Sep Purif Technol*. 2008;63(2):311-318.

19. Teramoto M, Matsuyama H, Yamashiro T, Katayama Y. Separation of Ethylene From Ethane By Supported Liquid Membranes Containing Silver-Nitrate As a Carrier. *J Chem Eng Japan*. 1986;19:419-424.

20. Fallanza M, Ortiz A, Gorri D, Ortiz I. Polymer-ionic liquid composite membranes for propane/propylene separation by facilitated transport. *J Membr Sci*. 2013;444:164-172.

21. Zarca R, Ortiz A, Gorri D, Ortiz I. Generalized predictive modeling for facilitated transport membranes accounting for fixed and mobile carriers. *J Membr Sci*. 2017;542(August):168-176.

22. Kookos IK. Optimal design of membrane/distillation column hybrid processes. *Ind Eng Chem Res*. 2003;42(8):1731-1738.

23. Caballero JA, Grossmann IE, Keyvani M, Lenz ES, Square N, Pennsyl V. Design of hybrid distillation - vapor membrane separation systems. *Ind Eng Chem Res*. 2009;48:9151-9162.

24. Zarca R, Ortiz A, Gorri D, Biegler LT, Ortiz I. Optimized Distillation Coupled With State-of-the-Art Membranes for Propylene Purification. *J Membr Sci*. 2018;556:321-328.

25. Tula AK, Befort B, Garg N, Camarda K V., Gani R. Sustainable process design & analysis of hybrid separations. *Comput Chem Eng*. 2017;105:96-104.

26. Eliceche AM, Daviou MC, Hoch PM, Ortiz I. Optimisation of azeotropic distillation columns combined with pervaporation membranes. *Comput Chem Eng*. 2002;26(4-5):563-573.

27. Pressly TG, Ng KM. A Break-Even Analysis of Distillation-Membrane Hybrids. *AIChE J*. 1998;44(1):93-105.

28. Baker RW. Membrane Technology and Applications. 3rd ed. Chichester: Wiley; 2012.

29. Ahmad F, Lau KK, Shariff AM, Murshid G. Process simulation and optimal design of membrane separation system for CO2 capture from natural gas. *Comput Chem Eng*. 2012;36(1):119-128.

30. Qi R, Henson MA. Membrane system design for multicomponent gas mixtures via mixed-integer nonlinear programming. *Comput Chem Eng*. 2000;24(12):2719-2737.

31. Zhou K, Chen X, Shao Z, Wan W, Biegler LT. Heterogeneous parallel method for mixed integer nonlinear programming. *Comput Chem Eng*. 2014;66:290-0300.

32. Ohs B, Lohaus J, Wessling M. Optimization of membrane based nitrogen removal from natural gas. *J Membr Sci*. 2016;498:291-301.

33. Kunde C, Kienle A. Global optimization of multistage binary separation networks. *Chem Eng Process*. 2018;131: 164-177.

34. Nymeijer DC, Visser T, Assen R, Wessling M. Composite hollow fiber gas-liquid membrane contactors for olefin/paraffin separation. *Sep Purif Technol*. 2004;37(3):209-220.

35. Aliaga-Vicente A, Caballero JA, Fernandez-Torres MJ. Synthesis and optimization of membrane cascade for gas separation via mixed-integer nonlinear programming. *AIChE J*. 2017;63(6):1989-2006.

36. Coker DT, Freeman BD, Fleming GK. Modeling multicomponent gas separation using hollow-fiber membrane contactors. *AIChE J*. 1998;44(6):1289-1302.

37. Gilassi S, Taghavi SM, Rodrigue D, Kaliaguine S. Simulation of gas separation using partial element stage cut modeling of hollow fiber membrane modules. *AIChE J*. 2017;64(5): 1766-1777.

38. Pan CY. Gas separation by high-flux, asymmetric hollow-fiber membrane. *AIChE J*. 1986;32(12):2020-2027.

39. Marriott JI, Sørensen E, Bogle IDL. Detailed mathematical modeling of membrane modules. *Comput Chem Eng*. 2001;25:693–700.

40. Burns RL, Koros WJ. Defining the challenges for C3H6/C3H8 separation using polymeric membranes. *J Membr Sci*. 2003;211(2):299-309.

41. Spillman R. Economics of gas separation membrane processes. In: Noble RD, Stern SA, eds. Membrane Separations Technology. Principles and Applications. Amsterdam: Elsevier Science; 1995.

42. Baker RW, Wijmans JG. Two-stage Membrane Process and Apparatus. US Patents 5,256,295 and 5,256,296, 1993.

43. Wijmans JG, Baker RW. The solution-diffusion model: a review. *J Membr Sci*. 1995;107(1-2):1-21.

44. Luyben WL. Dynamic simulation of flooded condensers. *Chem Eng Res Des*. 2017;118:12-20.

45. Zarca G, Urtiaga A, Biegler LT, Ortiz I. An optimization model for assessment of membrane-based post-combustion gas upcycling into hydrogen or syngas. *J Memb Sci*. 2018;563:83-92.

46. Biegler LT, Grossmann IE, Westerberg AW. Systematic methods of chemical process design. Upper Saddle River, NJ: Prentice Hall PTR; 1997.

Comprehensive study on PVDF-HFP/BMImBF$_4$/AgBF$_4$ membranes for propylene purification

Authors: Raúl Zarca[1], Antoniel Carlos C. Campos[2], Alfredo Ortiz[1], Daniel Gorri[1], Inmaculada Ortiz[1]*.

[1]Department of Chemical and Biomolecular Engineering. University of Cantabria, Av. Los Castros 46, 39005 Santander, Spain

[2]Institute of Chemistry, Rio de Janeiro State University (UERJ), Campus Maracanã, P H L C, São Francisco Xavier St., 524, Rio de Janeiro, RJ, Brazil, 20550-900.

*corresponding author: ortizi@unican.es

Journal of Membrane Science

July 2018

Abstract

In this work, a comprehensive analysis of PVDF-HFP/BMImBF$_4$/AgBF$_4$ facilitated transport membranes for olefin/paraffin separation is presented. Previous works of our research group have reported high flux and propylene selectivity under dry conditions and using synthetic gas mixtures, highlighting the promising potential of these membranes for industrial applications. This work advances in the understanding of the phenomena involved in membrane performance and moves one step forward in the knowledge of the industrial viability of this membrane system. First, the internal interactions between the silver cations and the polymer backbone, the silver salt dissociation and the silver degradation have been studied using FTIR, Raman and XPS spectroscopic techniques. Secondly, the experimental membrane performance during 110 days and working at changing relative humidity conditions in the feed gas has been assessed. Thermogravimetric techniques helped determining the water uptake capability of the facilitated transport membrane. Thirdly, real gas mixtures from a fluid catalytic cracking unit were provided by the industry and used in permeation experiments to check the membrane behavior under industrial-like conditions. The results provide experimental evidence for the previously theorized facilitated transport mechanisms and reveal a major influence of feed gas humidity on membrane performance. On the other hand, the industrial gas mixture produces no deviation from synthetic feed conditions due to trace contaminants. Finally, the carrier deactivation in long-term permeation has been quantified through a mathematical expression.

Keywords

Propylene, membrane, facilitated transport, humidity, real gas mixture, silver degradation.

1. Introduction

The separation of propane/propylene mixtures is one of the most costly processes in the petrochemical industry, caused by the similar physicochemical properties of both species, which requires the use of energy intensive cryogenic or high pressure distillation [1]. Among the most promising alternatives to traditional distillation, membrane technology offers a compact, modular and simple operation, allowing for process intensification [2]. In the last years, facilitated transport membranes have demonstrated exceptional separation performance in terms of permeability and selectivity [3]. These membranes make use of transition metal cations, typically silver, that can selectively and reversibly react with the olefin according to the Dewar-Chatt-Duncanson model [4,5]. This principle has been implemented in different configurations in recent times. The most basic approach consists in filling the pores of a polymeric support with a liquid solution of the carrier salt. However, this supported liquid membranes (SLM) lack from stability due to solvent evaporation and dragging [6–9]. Although the use of novel ionic liquids has overcome the solvent evaporation problems, the expelling out of solvent from the pores due to the transmembrane pressure is still a major drawback [10–13]. Proper mechanical stability and separation performance can be achieved combining the properties of dense membranes with facilitated transport through the synthesis of polymer/salt systems. In these systems, the silver salt is dissolved along with the polymer and the membrane is then fabricated through solvent casting [14], which results in a dense facilitated transport membrane usually described as a polymer electrolyte [15–17]. The internal structure and olefin/paraffin separation performance of these systems have been studied rather extensively in oxygen-containing polar polymers such as poly(2-oxazoline) POZ, poly(vinyl alcohol) (PVA) and poly(vinyl pyrrolidone) (PVP) [18–20]. Additionally, several studies have assessed the potential of these electrolytes for energy applications using fluoropolymers and lithium salt blends [21,22]. However, deeper knowledge on fluoropolymer-silver salt interactions is required in order to fully understand its gas separation potential.

In this regard, recent works of our research group have demonstrated the promising performance of fluoropolymer/silver salt membranes containing imidazolium based ionic liquids [23–25]. The presence of the ionic liquid, a non-volatile additive, serves two purposes: it helps stabilizing the silver cations, partially mitigating the carrier deactivation issues [5,26,27], and it acts as a fluid medium that enables mobile carrier transport. In these works, 1-butyl-3-methylimidazolium tetrafluoroborate ($BMImBF_4$) ionic liquid is used for its affinity to olefinic compounds and for having the same anion as the silver salt, which reduces the system complexity [28]. Poly(vinylidene fluoride-co-hexafluoropropylene) PVDF-HFP is selected for its high thermal, chemical and mechanical stability. In addition, it contains fluorine atoms that are likely to form weak interactions with the Ag^+ cations according to the Pearson's Hard-Soft–Acid-Base (HSAB) theory [29], which gives rise to fixed site carrier transport. $AgBF_4$ is used as carrier precursor because the lattice energy of BF_4^- anion is low enough to allow the olefin-silver complexation [30]. However, the internal interactions caused by the complexity of this membrane system and its responses to changes in the feed humidity conditions are still unclear. Furthermore, few studies assess the performance of silver-containing membranes in the long-term, and what is more important, there is a lack of information regarding permeation of real gas mixtures provided by the industry, which is especially critical given the instability issues caused by silver reduction.

In this work, the internal structure of the PVDF-HFP/$BMImBF_4$/$AgBF_4$ membrane is assessed implementing various spectroscopic techniques. Moreover, the long-term membrane stability is studied performing a 110 days-long permeation experiment, and the influence of the feed relative humidity on the membrane performance is explored and quantified by modifying the feed humidification conditions. Finally, the behavior of these membranes under real conditions is studied permeating a FCC refinery gas mixture provided by the industry.

2. Experimental

2.1 Chemicals

Propylene and propane were supplied by Praxair with a purity of 99.5%. Poly(vinylidene fluoride-co-hexafluoropropylene) (PVDF-HFP) was purchased from Sigma Aldrich. 1-Butyl-3-methylimidazolium tetrafluoroborate ($BMImBF_{4)}$ with a minimum purity of 99% and halide content of less than 500 ppm was supplied by Iolitec. Silver tetrafluoroborate ($AgBF_4$) with a minimum purity of 99% was supplied by Apollo Scientific Ltd. Tetrahydrofuran (THF) purchased from Panreac was used as solvent for membrane synthesis. The industrial propane/propylene gas mixture was kindly provided by Petronor S.A. All chemicals were used as received without further purification.

2.2 Membrane synthesis

The facilitated transport membranes studied in this work have been synthesized using the solvent casting method described in previous works [24,25]. The resulting membrane thickness is roughly 100 μm. The real thickness of each specific membrane has been measured with a Mitutoyo Digimatic MDC-25SX (accuracy ± 0.001 mm) digital micrometer and used for calculation purposes. The membrane composition of the studied membranes consist of 0.8g of PVDF-HFP, 0.2g of $BMImBF_4$ and 0.6g of $AgBF_4$. In the polymer/salt membranes the ionic liquid addition has been omitted.

2.3 Gas permeation experiments

A continuous-flow permeation technique has been used for the permeation experiments. A detailed description of this technique and the experimental apparatus can be found in previous works [23]. Briefly, mass flow controllers are used to generate a feed mixture that is further introduced in the upper chamber of a permeation cell where the membrane is located. Nitrogen is used as sweeping gas in the lower chamber and the permeate and retentate streams are then analyzed using gas chromatography to determine the transmembrane flux of each species. However, for humidified feed testing the experimental apparatus has been modified with the set-up depicted in Figure 1, which allows generating any desired relative humidity in the feed stream by controlling the ratio of dry to humidified feed.

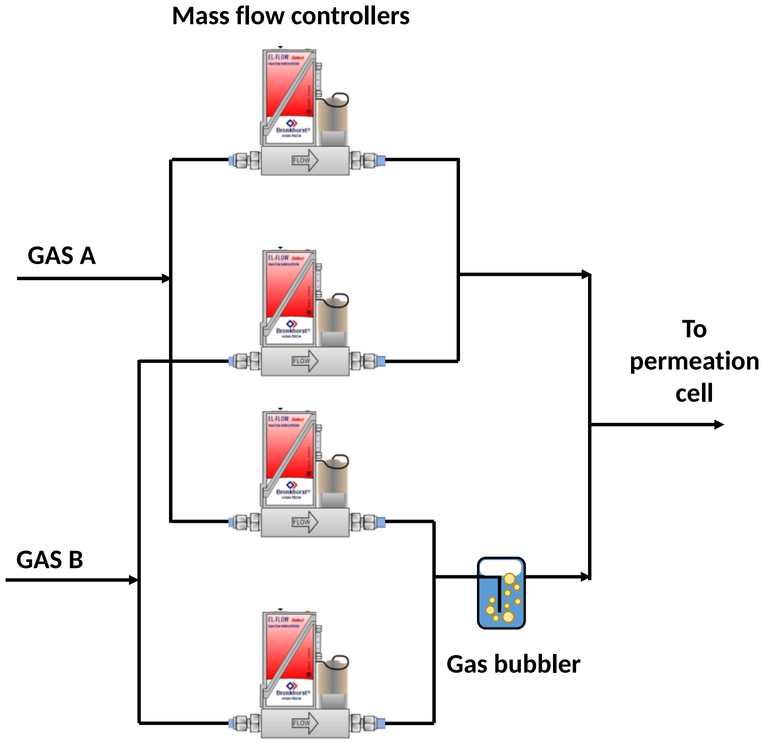
Mass flow controllers
GAS A
GAS B
To permeation cell
Gas bubbler

Figure 1. Set-up for relative humidity control.

The permeation experiments where conducted at the experimental conditions shown in Table 1.

Table 1. Experimental conditions

Experimental condition	Value

T (K)	298
Permeation area (cm^2)	53
N_2 flow (mL min^{-1})	20-40
C_3H_6 flow (mL min^{-1})	20
C_3H_8 flow (mL min^{-1})	20
C_3H_8 /C_3H_6 feed gas ratio	50:50
Feed side pressure (bar)	1.2
Permeate side pressure (bar)	1

2.4 Membrane characterization techniques

Different characterization techniques were implemented to assess the internal structure, water uptake capability and carrier degradation of the facilitated transport membranes. TGA analysis were performed using a TG-DTA 60H Shimadzu thermobalance and Fourier transform infrared (FTIR) spectra were recorded using a Perkin Elmer Spectrum Two spectrometer. Additionally, Raman spectroscopy was carried out using a Horiba T64000 triple spectrometer equipped with a confocal microscope and a Jobin Yvon Symphony CCD detector cooled with liquid nitrogen. A 488 nm beam from a Kr-Ar ion laser was focused through a 100x objective, using 2 mW laser power in all measurements. The spectral curves were fitted using Lorentzian functions. Finally, XPS spectra were acquired using an SPECS (Berlin, Germany) X-ray photoelectron spectrometer. The samples were analyzed using an Mg anode operated at 225 W (E=1253.6 eV, 13 kV, 17.5 mA). The carbon (C 1s) line at 284.8 eV was used as the reference in our determinations of the binding energies of the silver. A scanning interval of 0.1 eV was used for the final spectrum acquisition.

3. Results

3.1 Thermogravimetric analysis

The thermal analysis has been performed to assess the potential water uptake of the studied membranes. Figure 2 displays the thermogravimetric curves of PVDF-HFP, PVDF-HFP/$AgBF_4$ and PVDF-HFP/$BMImBF_4$/$AgBF_4$ membranes.

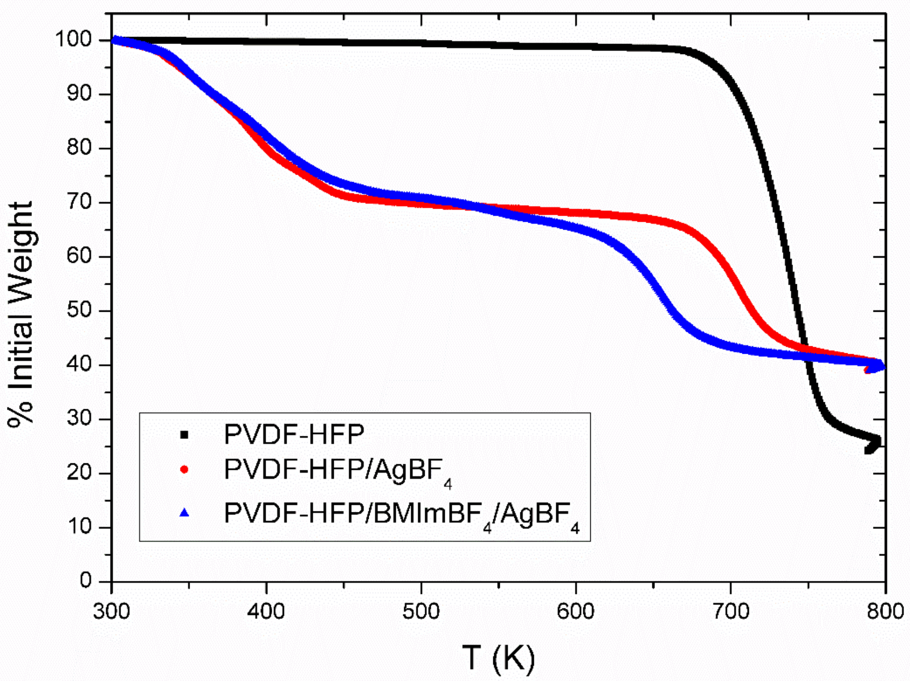

Figure 2. TGA curves of the studied membranes.

The membrane samples were vacuum dried at 30 mbar and 298 K for 24 hours after casting to completely remove the remaining solvent. Prior to testing the samples were exposed to ambient moisture (~80% RH at room temperature) for 24 hours. In this manner, any water loss appearing at the beginning of the temperature ramp can be attributed to water evaporation. According to Figure 2, the pure polymer membrane exhibits no weight loss until it reaches its degradation temperature around 680 K, which reveals no water uptake. This is in good agreement with the hydrophobic nature of the fluoropolymer [31]. However, Figure 2 shows prominent mass losses of the silver-containing membranes in the 300-436 K temperature range. Thus, it can be concluded that the addition of the $AgBF_4$ salt to the membrane composition dramatically changes the nature of the facilitated transport membranes due to its high hygroscopicity, which results in water uptakes of around 25 wt% when exposed to moist conditions.

3.2 Fourier transform infrared spectroscopy (FTIR)

The interaction between the Ag^+ cations and the fluorine atoms of the polymer chains can be studied through infrared spectroscopy analyzing the polymer CF_2 symmetrical stretching mode and comparing that of the pure polymer with the silver-containing membranes, see Figure 3.

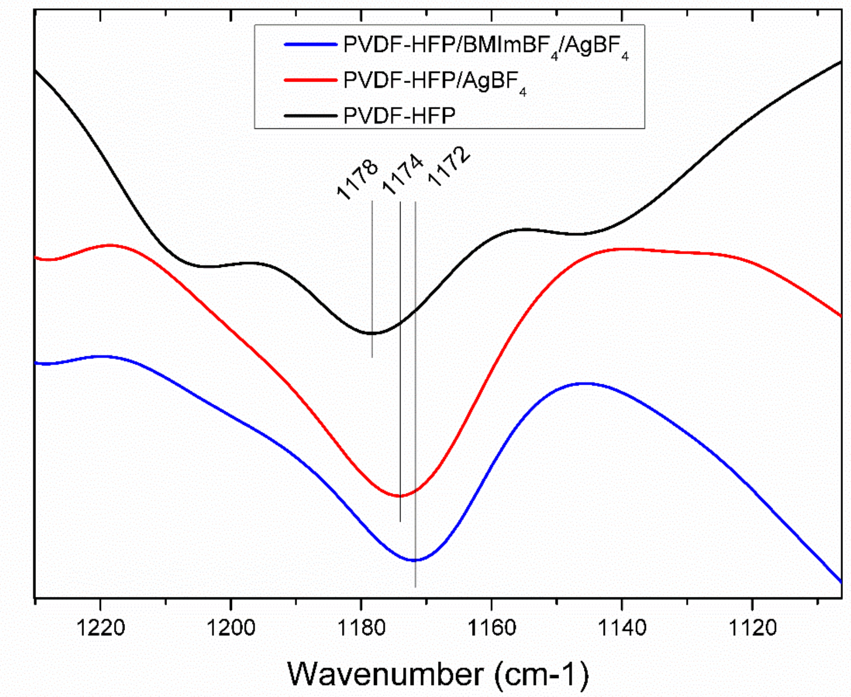

Figure 3. FTIR spectra of the studied membranes.

The CF_2 peak of the pure polymer appears in the 1178 cm^{-1} band. After incorporation of the silver salt, the stretching band shifted to 1174 and 1172 cm^{-1} in the PVDF-HFP/$AgBF_4$

and PVDF-HFP/BMImBF$_4$/AgBF$_4$ respectively. This shift to lower wavelength indicates a weakening of the C-F bond caused by the interaction of silver cations with the fluorine atoms of the fluoropolymer, which is the basis of the fixed site carrier transport mechanism. This phenomenon has been previously studied by Chang and Kang (2016) using FTIR on PVDF-HFP/HBF$_4$ polymer electrolytes [32].

3.3 RAMAN spectroscopy

Better insight on the AgBF$_4$ dissociation behavior can be achieved using Raman spectroscopy to analyze the regions of the BF$_4^-$ stretching bands in the pure AgBF$_4$, and the silver-containing membranes. Figure 4 shows the BF$_4^-$ stretching band region of PVDF-HFP/AgBF$_4$ and PVDF-HFP/BMImBF$_4$/AgBF$_4$ membranes. The symmetric stretching mode of BF$_4^-$ has been previously reported at 774 cm^{-1} in the pure AgBF$_4$ [33]. However, the spectrum in Figure 4a shows a wavenumber shift to 767 cm^{-1} when the silver is added to the polymer. According to previous studies, this wavenumber corresponds to free ions [20,34], which means that this change in the Raman spectra is due to well-dissociated Ag$^+$ cations interacting with the PVDF-HFP backbone. Furthermore, this wavenumber shift from 774 to 767 cm^{-1} is still observable after addition of the ionic liquid BMImBF$_4$, Figure 4b. As the BF$_4^-$ stretching band also appears at 774 cm^{-1} in the pure ionic liquid [34], this shift suggests that the ionic liquid is also interacting with the Ag$^+$ cations and, to a certain extent, with the polymer backbone, as reported by Fallanza et al. [23].

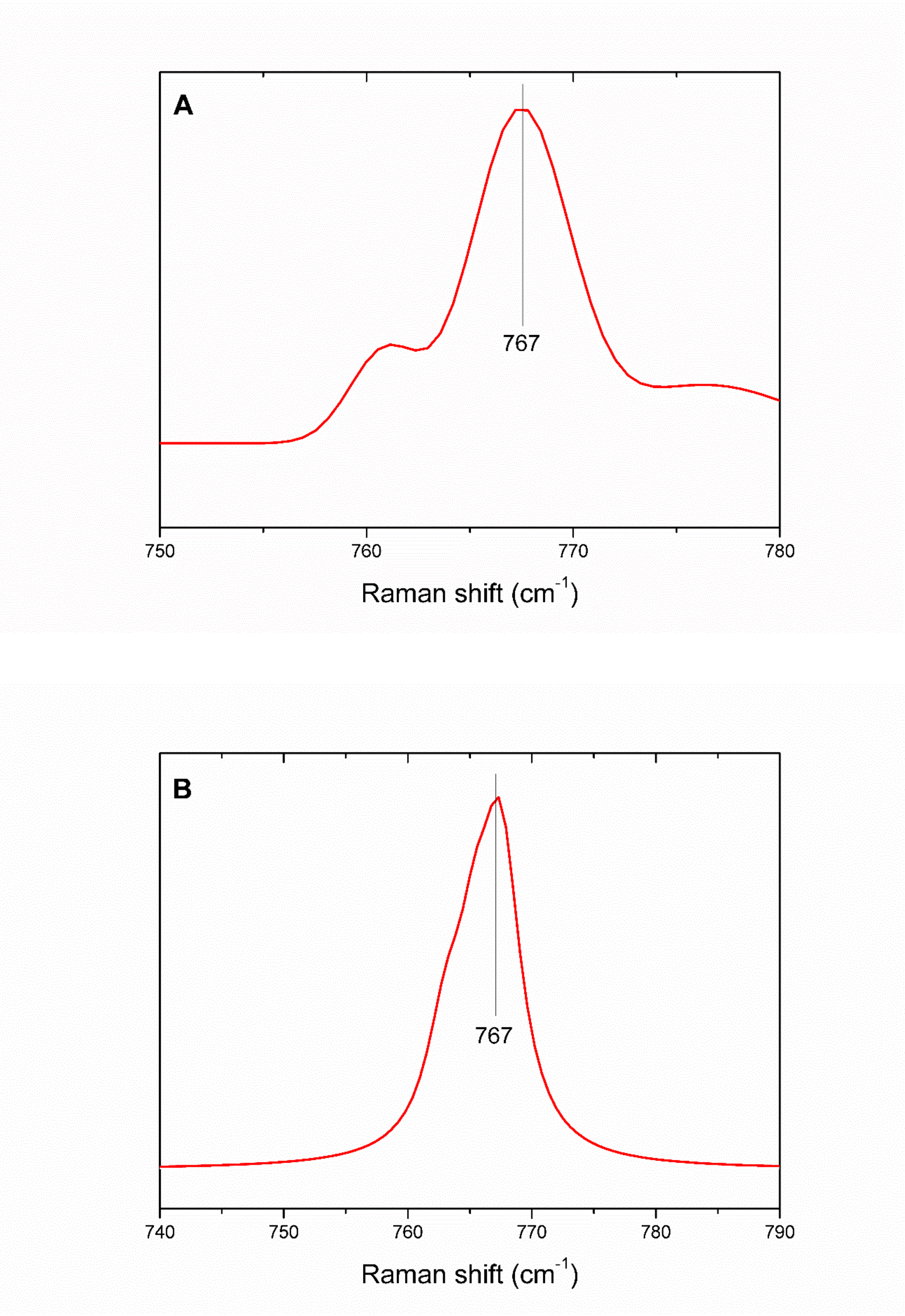

Figure 4. Raman spectra of A) PVDF-HFP /AgBF$_4$ and B) PVDF-HFP/BMImBF$_4$/AgBF$_4$ membrane.

3.4 X-ray photoelectron spectroscopy (XPS)

X-ray photoelectron spectroscopy has been used to expand the knowledge on membrane structure and degradation. The Ag 3d regions of the XPS spectra can confirm the interactions between the silver cations and the polymer fluorine atoms. Figure 5 shows the XPS spectra of a PVDF-HFP/BMImBF$_4$/AgBF$_4$ composite membrane after a long term permeation experiment (110 days). Table 2 summarizes the two silver species observable after signal deconvolution. The Ag 3d5/2 band of pure AgBF$_4$ has been previously reported at 369.2 eV. However, in the composite membrane, the binding energy has shifted to 368.47 eV. This reduction in the photoelectron binding energy is caused by the coordination between the silver atoms and the polymer backbone as demonstrated by Kim et al (2012), who found the same phenomenon for several AgBF$_4$/polymer blends [35]. Additionally, a second silver species (Ag 3d5/2=368.26 Ag 3d3/2=374.25) is associated with the presence of metallic silver [36], presumably due to the silver reduction caused by the long term permeation test.

Table 2. XPS regions of PVDF-HFP/BMImBF$_4$/AgBF$_4$ membrane after permeation test.

	Region	Position
Species A	Ag 3d 5/2	368.47
	Ag 3d 3/2	374.54
Species B	Ag 3d 5/2	368.26
	Ag 3d 3/2	374.25

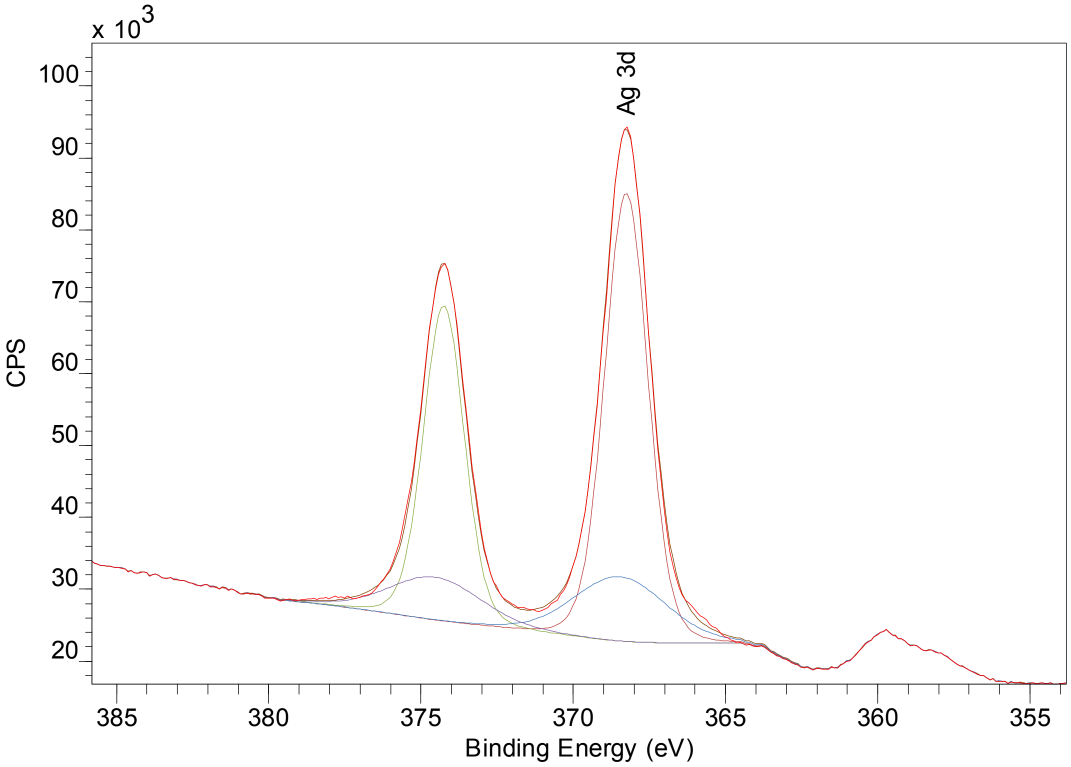

Figure 5. XPS spectra of the PVDF-HFP/BMImBF$_4$/AgBF$_4$ membrane after permeation test.

3.5 Long-term permeation under humid conditions

Figure 6 shows a 110 days long-term permeation test on a PVDF-HFP/BMImBF$_4$/AgBF$_4$ facilitated transport composite membrane. The feed gas consisted of an equimolar propane/propylene mixture at 1.2 bar total pressure. The main goal of this experiment is to determine the separation behavior of a composite membrane over an extended period of time, assessing both the feed gas relative humidity effect and the possible loss of performance due to carrier deactivation. Figure 6 is divided into five sections (**I-V**) accounting for the relative humidity conditions and following the sequence of the experimental runs. A characteristic feature of this facilitated transport membranes under dry conditions is a sharp decrease of the permeation flux in the first operating hours ostensibly caused by the rapid loss of water and residual solvent by evaporation, Figure 7 (section **II**). At the beginning of the test (section **I**) the humidity was kept at saturation and no flux decay was observed during the first 5 days, which confirms that the characteristic curve observed under dry gas conditions is due to solvent and water moisture evaporation. From day 5 to day 27 some instability in membrane performance occurred due to controlled changes in the temperature and pressure conditions within the experiments. In Figure 6 this is more evident for the propane flux due to the semi-logarithmic scale.

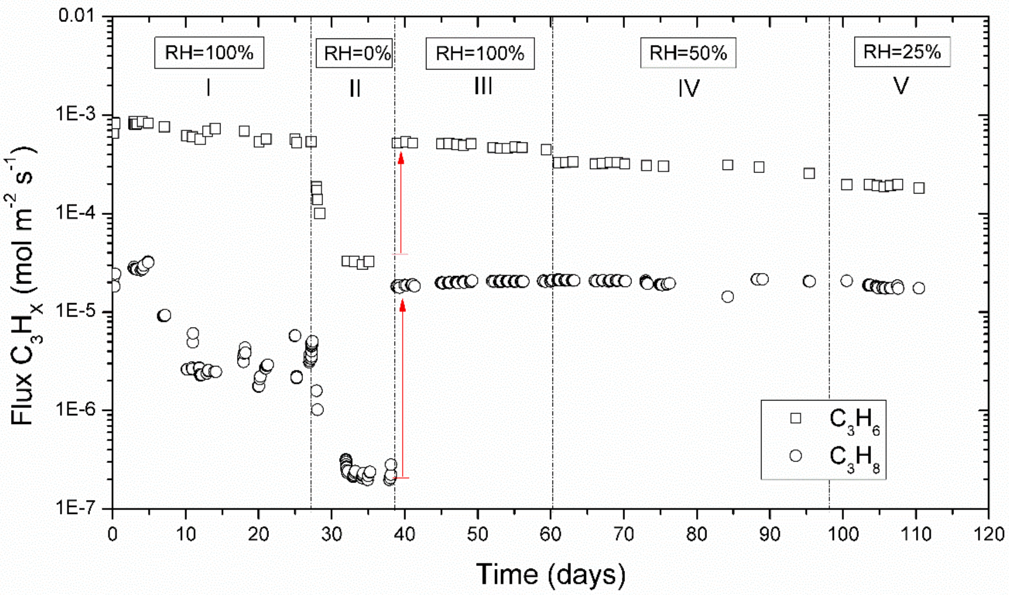

Figure 6. Long term permeation experiment of PVDF-HFP/BMImBF$_4$/AgBF$_4$ composite membrane at 298 K and 1.2 bar feed pressure (C_3H_8/C_3H_6 50:50) under different relative humidity conditions.

After 27 days, during section **II**, the feed was changed to dry gases, which resulted in a major propane and propylene transmembrane flux decrease as water evaporation occurred within the membrane. A detailed depiction of the drying curve is shown in Figure 7.

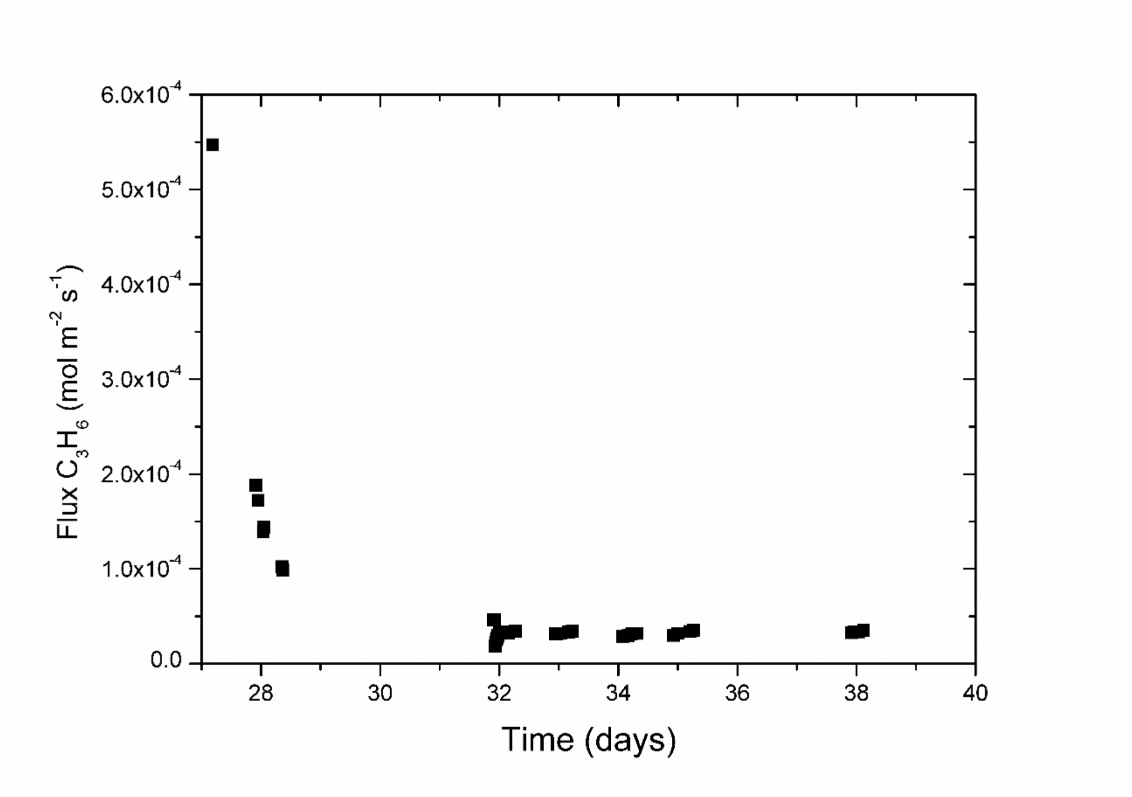

*Figure 7. Propylene transmembrane flux decrease in section **II**.*

When the humidified gas mixture was fed again into the system (section **III**), the flux increase of both gaseous species was almost immediate, reaching the flux values attained prior to drying. This abrupt increase, noted with red arrows in Figure 6, reveals the exceptional capability of these membranes to absorb water from the environment. During sections **III**, **IV** and **V** a feed gas relative humidity of 100, 50 and 25% was used, respectively. These variations in the humidity conditions resulted in moderate changes in the propylene transmembrane flux while the propane flux remained almost constant at its highest level.

However, it should be noted that, apart from the humidity influence, the propylene transmembrane flux undergoes a continuous slight decrease, evidenced by a constant slope in Figure 6. On the contrary, the propane flux does not suffer such decrease, which suggests that this phenomenon is caused by carrier deactivation. Furthermore, it was possible to quantify the deactivation rate by fitting the data for each section (**I-V**), to an exponential curve, which yielded the following expression:

$$J_{C_3H_6}(t) = J_{C_3H_6}(t_0) \cdot e^{-5.5x10^{-3} \cdot t} \qquad (1)$$

where $J_{C_3H_6}(t_0)$ is the initial propylene transmembrane flux at a given temperature, pressure and relative humidity conditions and the time *t* is introduced in days. This expression allows for membrane lifetime calculation if a minimum required performance is established.

This carrier deactivation prevents from fitting a mathematical expression for the propylene flux dependency on relative humidity because each experimental section has been obtained at different times and, consequently, the propylene flux is not only affected by the relative humidity but also by the elapsed time from the start of the experiment. However, using Equation 1, it was possible to project the propylene flux values to a common initial point. Finally, combining a mathematical expression for the drying curve (Figure 7) with the propylene flux at each relative humidity, it was possible to obtain a fitting curve for the propylene transmembrane flux as a function of the relative humidity (Eq. 2), Figure 8.

$$J_{C_3H_6}(RH) = 5.82x10^{-5} RH^{0.49} \qquad (2)$$

Figure 8 evidences a sharp increase in the propylene flux with the relative humidity for RH<10% and a smooth increase after that value (dash line in Figure 8); this finding supports the fact that even with a low relative humidity in the gaseous feed stream it is possible to almost saturate the membrane with water. A similar trend has been reported by Catalano et al. (2012) for oxygen and nitrogen in PFSI membranes [37].

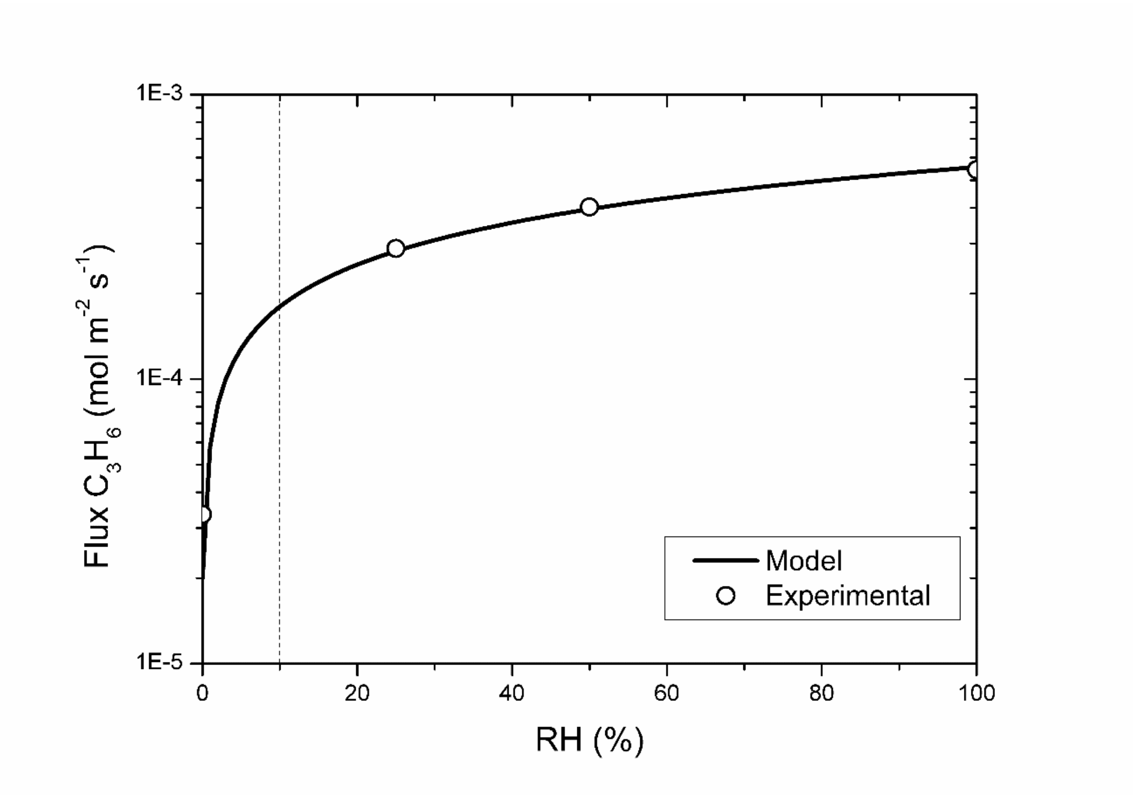

Figure 8. Experimental data and mathematical regression for the dependency of the propylene transmembrane flux on the relative humidity.

Finally, Table 3 displays the permeability and selectivity values of the facilitated transport membrane for each relative humidity condition. The humidification of the feed gases produces major changes in the membrane performance, reducing the selectivity and increasing the permeability of both the olefin and the paraffin. This is a characteristic effect of water vapor-induced swelling [38,39]. The enlargement of the polymer free volume caused by the water uptake increases the diffusivity of the gaseous species and the propylene-silver complex, which leads to notable permeability values but at the expense of membrane selectivity.

Table 3. Average permeability and selectivity values of the PVDF-HFP/BMImBF$_4$/AgBF$_4$ membrane for each relative humidity during the long-term permeation test.

RH (%)	P C_3H_8 (Barrer)[a]	P C_3H_6 (Barrer)[a]	α C_3H_6/C_3H_8 (-)
0	1.2	172	144
25	97.3	1032	11
50	107.6	1666	16
100	106.5	2555	24

[a] 1 Barrer = 10^{-10} cm^3 (STP) cm cm^{-2} s^{-1} $cmHg^{-1}$.

Although membrane swelling is usually responsible for lowering the polymeric membranes selectivity below the industrially required values, in this case, the selectivity remains high enough to consider humid operation as a useful tool to tailor the permeability-selectivity trade-off. Thus, wet gas could be implemented as a controlling agent when productivity is preferred over product purity. In this way, multistage membrane processes performing a refining separation after a bulk concentration could modulate the purity-productivity trade-off in each stage by controlling the feed gas relative humidity [40].

3.6 Industrial gas mixture permeation test

Figure 9 shows the facilitated transport membrane performance when the feed consists of a real propane/propylene mixture compared with a synthetic gas mixture. The industrial gas mixture is the product stream of a fluid catalytic cracking unit and its composition is displayed in Table 4. It mostly consists of a propane/propylene mixture (25:75) containing minor quantities of light paraffins and olefins.

Table 4. Industrial gas mixture composition.

Component	Concentration (mol%)
Methane	0.0034
Ethane	0.1503
Ethylene	0.0099

Propane	24.8837
Propylene	74.7208
Isobutane	0.1872
N-butane	0.0016
Trans-butene	0.0214
Iso-butene	0.0218
Hydrogen sulfide	< 0.2 ppm
Acetylene	< 0.2 ppm
Hydrogen	< 0.2 ppm

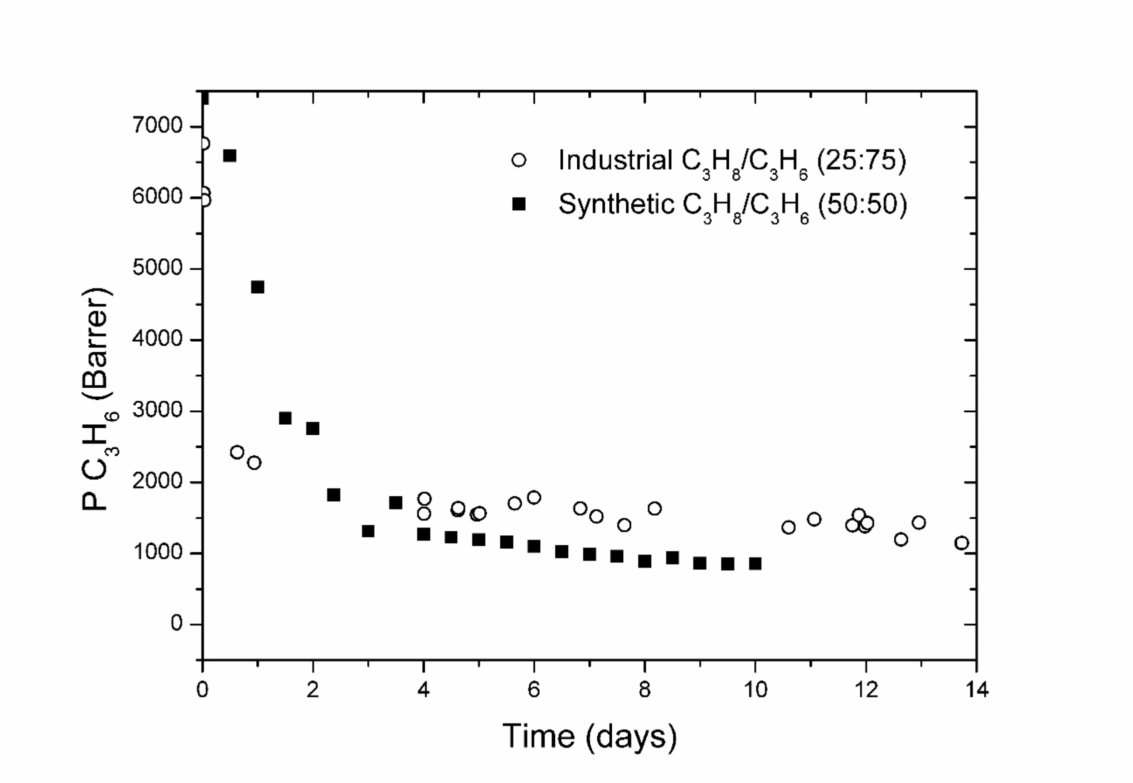

Figure 9. Synthetic and industrial gas mixture permeation experiments on a PVDF-HFP/BMImBF$_4$/AgBF$_4$ membrane under dry conditions at 298 K and 1.2 bar total feed pressure.

Given that both feeds differ in composition, permeability, which is normalized by the partial pressure gradient, has been plotted instead of the transmembrane flux. Both permeation experiments have been performed under dry conditions to simulate refinery conditions, hence, both suffer the characteristic permeability decrease due to solvent and water evaporation in the first hours of operation. Since the propylene transmembrane flux is similar in both cases, Figure 9 evidences that the membrane performance is not affected by known contaminant trace components potentially present in industrial streams (i.e. acetylene, hydrogen sulfide and hydrogen [41]) during the experiment extent.

These results confirm that the prominent separation performance of the studied membranes is not restricted to laboratory conditions with synthetic gas mixtures and demonstrate the suitability of these composite facilitated transport membranes to treat real feed streams.

4. Conclusions

The spectroscopic characterization of PVDF-HFP/BMImBF$_4$/AgBF$_4$ membranes used in the separation of propane/propylene mixtures confirm the existence of weak interactions between the Ag$^+$ cations and the fluorine atoms of the polymeric backbone, which along with the addition of ionic liquids result in a hybrid fixed site/mobile carrier transport mechanism yielding high olefin permeability and selectivity. The long-term permeation experiment carried out under changing feed gas humidity conditions revealed a slight permeability decrease due to silver degradation, which is mainly associated to silver reduction, supported by XPS spectra of the used membrane; this loss of membrane activity was observed to be independent of the experimental conditions. Although this degradation is slow enough to allow moderate membrane lifetimes, remediation methods can be further studied to achieve even larger operating periods. On the other hand, the humidification of the feed gas can severely alter the membrane performance, increasing the permeability of the permeant species and decreasing the membrane selectivity due to water vapor-induced swelling. In this regard, thermogravimetric analysis revealed up to 25 wt% membrane water uptake. Since the membrane showed moderate selectivity even at saturation, wet gas could be implemented as a controlling agent when productivity is preferred over product purity. Finally, permeation under real gas conditions revealed no additional degradation caused by minor contaminants that could potentially affect silver stability.

Acknowledgements

Financial support from the Spanish Ministry of Science under the projects CTQ 2015-66078-R and CTQ2016 -75158-R (MINECO, Spain- FEDER 2014–2020) is gratefully acknowledged. Raúl Zarca also thanks the Universidad de Cantabria for the postgraduate fellowship.

References

[1] D.S. Sholl, R.P. Lively, Seven chemical separations to change the world, Nature. 532 (2016) 435–437.

[2] J.C. Charpentier, In the frame of globalization and sustainability, process intensification, a path to the future of chemical and process engineering (molecules into money), Chem. Eng. J. 134 (2007) 84–92.

[3] R. Faiz, K. Li, Olefin/paraffin separation using membrane based facilitated transport/chemical absorption techniques, Chem. Eng. Sci. 73 (2012) 261–284.

[4] D.J. Safarik, R.B. Eldridge, Olefin/Paraffin Separations by Reactive Absorption: A Review, Ind. Eng. Chem. Res. 37 (1998) 2571–2581.

[5] A. Ortiz, L.M. Galán, D. Gorri, A.B. De Haan, I. Ortiz, Kinetics of reactive absorption of propylene in RTIL-Ag+ media, Sep. Purif. Technol. 73 (2010) 106–113.

[6] M.T. Ravanchi, T. Kaghazchi, A. Kargari, Supported liquid membrane separation of propylene-propane mixtures using a metal ion carrier, Desalination. 250 (2010) 130–135.

[7] S. Azizi, T. Kaghazchi, A. Kargari, Propylene/propane separation using N-methyl pyrrolidone/AgNO3 supported liquid membrane, J. Taiwan Inst. Chem. Eng. 57 (2015) 1–8.

[8] M. Teramoto, H. Matsuyama, T. Yamashiro, Y. Katayama, Separation of Ethylene From Ethane By Supported Liquid Membranes Containing Silver-Nitrate As a Carrier, J. Chem. Eng. Japan. 19 (1986) 419–424.

[9] S. Duan, A. Ito, A. Ohkawa, Separation of propylene/propane mixture by a

supported liquid membrane containing triethylene glycol and a silver salt, J. Memb. Sci. 215 (2003) 53–60.

[10] M. Fallanza, A. Ortiz, D. Gorri, I. Ortiz, Experimental study of the separation of propane/propylene mixtures by supported ionic liquid membranes containing Ag+–RTILs as carrier, Sep. Purif. Technol. 97 (2012) 83–89.

[11] G. Zarca, I. Ortiz, A. Urtiaga, Copper(I)-containing supported ionic liquid membranes for carbon monoxide/nitrogen separation, J. Memb. Sci. 438 (2013) 38–45.

[12] R. Fortunato, C.A.M. Afonso, M.A.M. Reis, J.G. Crespo, Supported liquid membranes using ionic liquids: Study of stability and transport mechanisms, J. Memb. Sci. 242 (2004) 197–209.

[13] P. Scovazzo, Testing and evaluation of room temperature ionic liquid (RTIL) membranes for gas dehumidification, J. Memb. Sci. 355 (2010) 7–17.

[14] R. Zarca, A. Ortiz, D. Gorri, I. Ortiz, Facilitated Transport of Propylene Through Composite Polymer-Ionic Liquid Membranes. Mass Transfer Analysis, Chem. Prod. Process Model. 11 (2016) 77–81.

[15] Y. Yoon, J. Won, Y.S. Kang, Polymer electrolyte membranes containing silver ion for facilitated olefin transport, Macromolecules. 33 (2000) 3185–3186.

[16] H. Kataoka, Y. Saito, M. Tabuchi, Y. Wada, T. Sakai, Ionic conduction mechanism of PEO-type polymer electrolytes investigated by the carrier diffusion phenomenon using PGSE-NMR, Macromolecules. 35 (2002) 6239–6244.

[17] L. Liu, X. Feng, A. Chakma, Unusual behavior of poly(ethylene oxide)/AgBF4 polymer electrolyte membranes for olefin-paraffin separation, Sep. Purif. Technol.

38 (2004) 255–263.

[18] S.U. Hong, J.H. Jin, J. Won, Y.S. Kang, Polymer-salt complexes containing silver ions and their application to facilitated olefin transport membranes, Adv. Mater. 12 (2000) 968–971.

[19] J.H. Kim, B.R. Min, K.B. Lee, J. Won, Y.S. Kang, Coordination structure of various ligands in crosslinked PVA to silver ions for facilitated olefin transport, Chem. Commun. 2 (2002) 2732–2733.

[20] Y.S. Park, S. Chun, Y.S. Kang, S.W. Kang, Durable poly(vinyl alcohol)/AgBF4/Al(NO3)3 complex membrane with high permeance for propylene/propane separation, Sep. Purif. Technol. 174 (2017) 39–43.

[21] T. Liu, Z. Chang, Y. Yin, K. Chen, Y. Zhang, X. Zhang, The PVDF-HFP gel polymer electrolyte for Li-O2 battery, Solid State Ionics. 318 (2018) 88–94.

[22] S. Abbrent, J. Plestil, D. Hlavata, J. Lindgren, J. Tegenfeldt, Å. Wendsjö, Crystallinity and morphology of PVdF–HFP-based gel electrolytes, Polymer (Guildf). 42 (2001) 1407–1416.

[23] M. Fallanza, A. Ortiz, D. Gorri, I. Ortiz, Polymer-ionic liquid composite membranes for propane/propylene separation by facilitated transport, J. Memb. Sci. 444 (2013) 164–172.

[24] R. Zarca, A. Ortiz, D. Gorri, I. Ortiz, Generalized predictive modeling for facilitated transport membranes accounting for fixed and mobile carriers, J. Memb. Sci. 542 (2017) 168–176.

[25] R. Zarca, A. Ortiz, D. Gorri, I. Ortiz, A practical approach to fixed-site-carrier facilitated transport modeling for the separation of propylene/propane mixtures

through silver-containing polymeric membranes, Sep. Purif. Technol. 180 (2017) 82–89.

[26] A. Ortiz, L. Galán, D. Gorri, B. De Haan, I. Ortiz, Reactive Ionic Liquid Media for the Separation of Propylene / Propane Gaseous Mixtures, Ind. Eng. Chem. Res. 49 (2010) 7227–7233.

[27] A. Ortiz, A. Ruiz, D. Gorri, I. Ortiz, Room temperature ionic liquid with silver salt as efficient reaction media for propylene/propane separation: Absorption equilibrium, Sep. Purif. Technol. 63 (2008) 311–318.

[28] M. Fallanza, M. González-Miquel, E. Ruiz, A. Ortiz, D. Gorri, J. Palomar, I. Ortiz, Screening of RTILs for propane/propylene separation using COSMO-RS methodology, Chem. Eng. J. 220 (2013) 284–293.

[29] R.G. Pearson, Hard and Soft Acids and Bases, J. Am. Chem. Soc. 85 (1963) 3533–3539.

[30] C.K. Kim, J. Won, H.S. Kim, Y.S. Kang, H.G. Li, C.K. Kim, Density functional theory studies on the dissociation energies of metallic salts: Relationship between lattice and dissociation energies, J. Comput. Chem. 22 (2001) 827–834.

[31] X. Tian, X. Jiang, Poly(vinylidene fluoride-co-hexafluoropropene) (PVDF-HFP) membranes for ethyl acetate removal from water, J. Hazard. Mater. 153 (2008) 128–135.

[32] J. Chang, S.W. Kang, CO2 separation through poly(vinylidene fluoride-co-hexafluoropropylene) membrane by selective ion channel formed by tetrafluoroboric acid, Chem. Eng. J. 306 (2016) 1189–1192.

[33] E. Goreshnik, Z. Mazej, X-ray single crystal structure and vibrational spectra of

AgBF4, Solid State Sci. 7 (2005) 1225–1229.

[34] D. Ji, Y.S. Kang, S.W. Kang, Accelerated CO2 transport on surface of AgO nanoparticles in ionic liquid BMIMBF4, Sci. Rep. 5 (2015) 16362.

[35] J.H. Kim, S.W. Kang, Y.S. Kang, Threshold silver concentration for facilitated olefin transport in polymer/silver salt membranes, J. Polym. Res. 19 (2012) 9753.

[36] T.C. Kaspar, T. Droubay, S.A. Chambers, P.S. Bagus, Spectroscopic Evidence for Ag(III) in Highly Oxidized Silver Films by X-ray Photoelectron Spectroscopy, J. Phys. Chem. C. 114 (2010) 21562–21571.

[37] J. Catalano, T. Myezwa, M.G. De Angelis, M.G. Baschetti, G.C. Sarti, The effect of relative humidity on the gas permeability and swelling in PFSI membranes, Int. J. Hydrogen Energy. 37 (2012) 6308–6316.

[38] W.S. Ho, D.C. Dalrymple, Facilitated transport of olefins in Ag+-containing polymer membranes, J. Memb. Sci. 91 (1994) 13–25.

[39] S. Hong, Effect of water on the facilitated transport of olefins through solid polymer electrolyte membranes, J. Memb. Sci. 181 (2001) 289–293.

[40] R. Zarca, A. Ortiz, D. Gorri, L.T. Biegler, I. Ortiz, Optimized Distillation Coupled With State-of-the-Art Membranes for Propylene Purification, J. Memb. Sci. 556 (2018) 321–328.

[41] T.C. Merkel, R. Blanc, I. Ciobanu, B. Firat, A. Suwarlim, J. Zeid, Silver salt facilitated transport membranes for olefin/paraffin separations: Carrier instability and a novel regeneration method, J. Memb. Sci. 447 (2013) 177–189.

A.2 Contributions to scientific meetings

1- Highlighting the benefits of using state-of-the-art membranes in the propylene production through process optimization. R. Zarca, A. Ortiz, D. Gorri, L.T. Biegler, I. Ortiz. Euromembrane Conference 2018. Valencia (Spain). July 2018. *Poster.*

2- Performance of new composite facilitated transport membranes for olefin/paraffin separation. R. Zarca, A. Ortiz, D. Gorri, I. Ortiz. 10th World Congress on Chemical Engineering (WCCE10). Barcelona (Spain). October 2017. *Oral presentation.*

3- Ethane/ethylene separation through facilitated transport ionic liquid composite membranes. R. Zarca, A. Ortiz, D. Gorri, I. Ortiz. 5th Iberoamerican Meeting on Ionic Liquids (IMIL 2017). Sao Paulo (Brasil). April 2017. *Oral presentation.*

4- High performance facilitated transport composite membranes for real industrial olefin/paraffin separation. R. Zarca, M. Fallanza, A. Ortiz, D. Gorri, I. Ortiz. International Congress on Membranes and Membrane Processes (ICOM 2017). San Francisco (USA). July-August 2017. *Oral presentation.*

5- Propane/propylene separation through facilitated transport composite membranes. R. Zarca, A. Ortiz, D. Gorri, I. Ortiz. European Membrane Society Summer School 2016. Bertinoro (Italy). June-July 2016. *Poster.*

6- Assessment of mass transfer parameters in olefin facilitated transport through polymer-ionic liquid composite membranes. D. Gorri, R. Zarca, A. Ortiz, I. Ortiz. International Conference on Properties and Phase Equilibria for Product and Process Design (PPEPPD 2016). Oporto (Portugal). May 2016. *Poster.*

7- Propane/propylene separation through facilitated transport composite membranes. A. Ortiz, R. Zarca, D. Gorri, I. Ortiz. X Ibero-American Conference on Membrane Science and Technology (CITEM 2016). Ciudad de México (México). May 2016. *Poster.*

8- Facilitated transport of propylene through composite polymer-ionic liquid membranes. Mass transfer analysis. A. Ortiz, R. Zarca, D. Gorri, I. Ortiz. 12th International Conference on Membrane Science and

Technology (MST 2015). Teheran (Iran). November 2015. *Oral presentation.*

9- Mass transfer analysis in the facilitated transport of propylene through composite polymer-ionic liquid membranes. R. Zarca, A. Ortiz, D. Gorri, I. Ortiz. Euromembrane Conference 2015. Aachen (Germany). September 2015. *Oral presentation.*

10- Facilitated transport composite membranes base on polymer-ionic liquids-Ag^+ for propane/propylene separation. R. Zarca, A. Ortiz, D. Gorri, I. Ortiz. Iberoamerican Meeting on Ionic Liquids 2015 (IMIL 2015) Madrid (Spain). July 2015. *Poster*.

11- Polymer-ionic liquids-Ag^+ composite membranes for propane/propylene separation. R. Zarca, A. Ortiz, D. Gorri, I. Ortiz. European Membrane Society Summer School 2015. Liberec (Czech Republic). June 2015. *Poster.*

12- Polymer/ionic liquid composite membranes for olefin selective separation. D. Gorri, R. Zarca, A. Ortiz, I. Ortiz. 20th International Solvent Extraction Conference 2014 (ISEC). Würzburg (Germany). September 2014. *Oral presentation.*

13- Testing the permeability of highly selective ionic liquid/polymer composite membranes for light hydrocarbons. R. Zarca, A. Ortiz, D. Gorri, I. Ortiz. II International Congress of Chemical Engineering of ANQUE (ICCE). Madrid (Spain). July 2014. *Poster.*

14- Highly selective ionic liquid/polymer composite membranes for propylene/propane separation. A. Ortiz, R. Zarca, D. Gorri, I. Ortiz. 2nd International Conference on Ionic Liquids in Separation and Purification Technology (ILSEPT 2014). Toronto (Canada). June 2014. O*ral presentation.*

15- Permeability of propane and propylene in highly selective ionic liquid/polymer composite membranes. R. Zarca, A. Ortiz, D. Gorri, I. Ortiz. IX Ibero-American Conference on Membrane Science and Technology (CITEM 2014). Santander (Spain). May 2014. *Poster and oral presentation.*

A.3 GAMS program used for hybrid process optimization

```
$offlisting
$OFFUPPER
$OFFSYMXREF
$OFFSYMLIST
$Title    Optimization of a Hybrid Membrane-Distillation process
$Stitle   Propene-Propane Distillation at 20 bar


********************************************************************************
*                               COMMON
********************************************************************************

Parameter membcost     membrane unitary cost ($ m-2)                   /200/
          memblife     membrane lifetime (yr)                          /2/
          SF           column service factor                           /0.904/
          daysop       day of operation per year (day)                 /365/
          coolprice    price of cooling water ($ mol-1)                /5.7e-7/
          coolTin      cooling water inlet temperature (K)             /300/
          coolTout     cooling water outlet temperature (K)            /319/
          Cpw          cooling water heat capacity  (J mol-1 K-1)      /75.3/
          steamcost    steamcost ($ mol-1)                             /3.23e-4/
          AHvap        AHvap of saturated steam @150psi (J mol-1)      /35870/
          kWhcost      energy costs ($ kWh-1)                          /0.077/
          compyield    compressors efficiency                          /0.72/
          comp1stages  number of stages of compressor 1                /3/
          comp2stages  number of stages of compressor 1                /1/
          comp1CR      compressor 1 compress. ratio                    /2.72658/
          comp2CR      compressor 2 compress. ratio                    /1.12611/
;

********************************************************************************
*                            MEMBRANE MODULE
********************************************************************************


Sets     a        number of finite elements                /1*20/
         b        number of internal collocation points    /1*3/
* List number of compounds:
         j        components                               /propene,propane/;

Alias   (b,c)
        (j,jb);

Scalar  nfe       number of finite elements                  [-]       /20/
* Problem definition:

        ftp       feed total pressure                      [bar]       /18/
        ptp       permeate total pressure                  [bar]       /1/
        temp      feed temperature                           [K]       /325/

* Define membrane parameters:

        delta     fiber wall thicknes                        [m]       /1e-6/
        conv      Barrer conv. to SI [kmol m bar-1 h-1 Barrer-1]    /1.206e-10/;



* Introduce initial values for feed flowrates:
Parameter ffinit(j) value  [kmol h-1]                   /propene  180
                                                         propane  180/;
* Introduce initial values for permeate flowrates:
Parameter fpinit(j) value  [kmol h-1]                   /propene  0
                                                         propane  0/;


Table   lag(b,b)    Lagrange basis collocation matrix
         1       2       3
      1  1       0       0
      2  0       1       0
      3  0       0       1;


Table  ldot(b,b)  Lagrange basis first derivs collocation matrix
                1                  2                  3
      1  -5.999997202501304  -3.464098384864128  3.464098384864127
      2  6.464099408820847   2.999996178544585   -6.464099408820847
      3  -0.464102206319543  0.464102206319543   3.000001023956719;


Parameter lfinal(b) value   /1  1
                             2  -1.732051615138131
                             3  1.732051615138131/;


Parameter fffinal(j,a)      final molar retentate flowrate
          fpfinal(j,a)      final molar permeate flowrate
          h(a);

h(a) = 1/nfe;

Variables ff(j,a,b)         retentate molar flowrate
          fp(j,a,b)         permeate molar flowrate
          ffdot(j,a,b)      ff first order derivative
          fpdot(j,a,b)      fp first order derivative
          ll(a,b)           fiber lenght
          area              membrane area [*10^-3 m2]
          theta             dimensionless area [-]
          gammap            permeate over feed pressure [-]
;


********************************************************************************
*                            DISTILLATION COLUMN
********************************************************************************
$ontext
          ----------------------------------------------------------------------

                                Section 1
                                Basic Data
                                ___________


        Basic Thermodynamic Data have been taken from
        R.C. Reid, J.M. Prausnitz and B.E. Poling :
        " The Properties of gases and liquids "
        4th Edition, McGraw-Hill (1987)
$offtext



$ontext

        Units:  Pressure : in bars i.e. 0.1 Mpa
                Temperature : in kelvins
                Heat capacity : kJ/kmol K

        Abbreviations :  mm   Molar mass
                         Tb   Normal boiling point
                         Tc   Critical temperature
                         Pc   Critical Pressure
                     Omega    Acentric factor
                   Liq-den    Density of liquid at Tden

$offtext

Table  PRCON (J,*)    Basic Physical Properties
                mm         Tb      Tc         Pc       Omega    Liq-den  Tden
  Propene    42.081     225.4   364.9      46.0      0.142    0.867    293
  Propane    44.097     231.0   369.8      42.4      0.152    0.885    289


Table  VPCON(J,*)    Constants in the wagner equation for vap.pressure
            A            B            C             D          TMIN
 Propene   -6.64231    1.21857      -1.81005       -2.48212     309
 Propane   -6.68770    1.24880      -1.97450       -2.05390     288


Table  CPCON(J,*)  Constants for the isobaric heat capacity equation
              A           B             C           D
 Propene    3.188e1     3.237e-2      3.898e-4   -4.999e-7
 Propane    3.199e1     4.266e-2      4.998e-4   -6.563e-7
```

```
Parameter dhv(j)   Heat of vapourization (kj kmol-1) --- assumed to be constant
             / Propene  18700
               Propane  18800  /   ;

*dhv from Stephenson and Malanowski, 1987.

$Ontext
                                Section 2
                                _________
        In this section, we derive  approximate representations
        for heat capacities and enthalpies for the pure components.
$Offtext

Scalars       Treb    Guess temp. for reboiler
              Tbot    Guess temp. for bottom-most tray
              Ttop    Guess temp. for top-most tray
              Tcon    Guess temp. for condenser  ;
              treb = 330; tbot = 328; ttop = 324; tcon = 322;

Scalar       rg  Universal gas constant  /8.314/ ;
Parameters   cpvu(j),cpvl(j), cplu(j), cpll(j), dcpl(j),dcpv(j)  ;

              cpvu(j) = treb*(cpcon(j,'b') + treb*( cpcon(j,'c')
                         +treb *cpcon(j,'d'))) + cpcon(j,'a')    ;
              cpvl(j) = tcon*(cpcon(j,'b') + tcon*( cpcon(j,'c')
                         +tcon *cpcon(j,'d'))) + cpcon(j,'a')    ;
              cplu(j) = cpvu(j) + rg *( 1.45
                        + 0.45 * (1 - treb/prcon(j,'tc'))**(-1)
                        + 0.25 * prcon(j,'omega') * (17.11
                        + 25.2 *( ( 1 - treb/prcon(j,'tc'))**(1.0/3)) *
                          (treb/prcon(j,'tc'))**(-1) + 1.742 *
                          (1 - treb/prcon(j,'tc'))**(-1) ) )  ;

               cpll(j) = cpvl(j) + rg *( 1.45
                        + 0.45 * (1 - tcon/prcon(j,'tc'))**(-1)
                        + 0.25 * prcon(j,'omega') * (17.11
                        + 25.2 * (( 1 - tcon/prcon(j,'tc'))**(1.0/3)) *
                          (tcon/prcon(j,'tc'))**(-1) + 1.742 *
                          (1 - tcon/prcon(j,'tc'))**(-1) ) )  ;

             dcpl(j) = (cplu(j)-cpll(j))/(treb - tcon) ;
             dcpv(j) = (cpvu(j)-cpvl(j))/(treb - tcon) ;

     display  cpvu ;
     display  cpvl ;
     display  cplu ;
     display  cpll ;
     display  dcpl ;
     display  dcpv ;
$ontext

        Final expressions for enthalpy
        Note: Liquid enthalpy will be computed as
        cpll(j) (t -tcon) + 0.5 * dcpl(j) *(t-tcon)**2
        = hl0(j) + hla(j)*t + hlb(j)* t**2

        Note: Vapour enthalpy will be computed as
        hl0(j) + hla(j)*prcon(j,'tb') + hlb(j) * (prcon(j,'tb')**2)
        + dhv(j)
        + cpvl(j)*(t -prcon(j,'tb')) + 0.5 * dcpv(j)*(t-prcon(j,'tb'))**2
        = hv0(j) + hva(j) *t + hvb(j) * t**2

$offtext

Parameters  hl0(j) ,hla(j), hlb(j)    See description above;
            hl0(j) = tcon *( -cpll(j) + tcon *dcpl(j)/2);
            hla(j) = cpll(j) - dcpl(j)*tcon;
            hlb(j) = dcpl(j)/2;

     display  hl0 ;
     display  hla ;
     display  hlb ;

Parameters  hv0(j),hva(j),hvb(j)    See description above;

            hv0(j) = hl0(j) + hla(j)*prcon(j,'tb') + hlb(j)*(prcon(j,'tb')**2)
                +dhv(j)
                - cpvl(j)*prcon(j,'tb') + 0.5 *dcpv(j)*(prcon(j,'tb')**2) ;
            hva(j) = cpvl(j) - dcpv(j)*prcon(j,'tb') ;
            hvb(j) = dcpv(j)/2 ;

     display  hv0 ;
     display  hva ;
     display  hvb ;

$ontext
                                Section 3
                                _________
        In this section we derive simplified expression for the vapour
        pressure.
        The preferred form is :
        ln( pvap(j)) =  a(j) - b(j)/T  ;  (T  in kelvins)  ;

$offtext

Parameters   vpl(j),vpu(j), av(j), bv(j), xtreb(j), xtcon(j) ;
             xtreb(j) =  1 - treb/prcon(j,'tc');
             xtcon(j) =  1 - tcon/prcon(j,'tc');
             vpu(j)   = log(prcon(j,'pc')) + prcon(j,'tc')/treb *
                       (vpcon(j,'a')*xtreb(j) + vpcon(j,'b')*xtreb(j)**1.5
                      +vpcon(j,'c')*xtreb(j)**3 +vpcon(j,'d')*xtreb(j)**6);
             vpl(j)   = log(prcon(j,'pc')) + prcon(j,'tc')/tcon *
                       (vpcon(j,'a')*xtcon(j) + vpcon(j,'b')*xtcon(j)**1.5
                      +vpcon(j,'c')*xtcon(j)**3 +vpcon(j,'d')*xtcon(j)**6);

            bv(j) = (vpu(j) -vpl(j))/(1/tcon - 1/treb) ;
            av(j) = (vpu(j)*treb - vpl(j)*tcon)/(treb-tcon) ;

  display  vpu , vpl ;
  display  av , bv ;
$ontext
                        Section 4
                        _________
                Thermal condition of the feed stream
$offtext

 Scalars
            tf  temperature of the feed (in kelvins)
            pf  pressure of the feed stream
            vf  vapour fraction in feed(before expansion)
            preb  Pressure in the reboiler
            pbot  Pressure in the bottom-most tray
            ptop  Pressure in the top-most tray
            pcon  Pressure in the condenser   ;

            preb = 20.41 ; pbot = 20.27; ptop = 19.05; pcon = 19.05;
            tf = 323 ;  pf = 20.27 ;

Parameters

           vpf(j)  vapour pressures at feed temperatures ;


Positive Variables

              fdp           Total no. of moles of feed permeate
              fdr           Total no. of moles of feed retentate
              xfp(j)        molefractions in feed-stream permeate
              xfr(j)        molefractions in feed-stream retentate
              Shfp          Specific Enthalpy of feed permeate
              Shfr          Specific Enthalpy of feed retentate
              rebKW         reboiler total duty
              condKW        condenser total duty
              membdev       membrane devaluation
              comp1costyr   permeate recompression total cost
              comp2costyr   retentate recompression total cost
              comp1eleckw   permeate recompression duty
              comp2eleckw   retentate recompression duty
              rebcostyr     reboiler total cost
              condcostyr    condenser total cost
              alpha(j)      selectivity  [-]
              perma         permeability
;
```

```
              vpf(j) = exp ( av(j) - bv(j)/tf) ;


$ontext
                                Section 5
                                _________
                        Modelling Equations

        Note: The enthalpy functions are treated as variables
              in order to eliminate unnecessary differentiations
              in Minos

                       Description of the column

        Note: The stages are numbered bottom upwards (as in the
        floors of a building). Reboiler is stage(tray) no. 1 and the
        condenser is the last tray.

$offtext
Scalar  fst  location of feed stage /2/;

 sets    i           stages    /1*135/
         reb(i)      reboiler
         con(i)      condenser
         col(i)      stages in the col
         top(i)      top-most stage
         abovef(i)   stages above the feed stage
         belowf(i)   feed stage and those below it ;

         reb(i) = yes$(ord(i) eq 1) ;
         con(i) = yes$(ord(i) eq card(i)) ;
         col(i) = yes - (reb(i)+con(i)) ;

         alias (i,ii,iloop);
         abovef(i) = yes $(ord(i) gt fst) ;
         belowf(i) = yes $ (ord(i) le fst ) ;

        display belowf ;
$ontext
--------------------------------------------------------------------------------
   === Adjust pressures in the column according to the total number of the trays
     ***************************************************************************
     *  the presures in condenser and the top-most tray are fixed as the same as
     *  specified by original problem. but that in the bottom-most and reboiler
     *  are adjusted by substract the summation of pressures in dried trays from
     *  the original specified values.
     ***************************************************************************
--------------------------------------------------------------------------------
$offtext

Parameter    p(i)    pressure prevailing in tray i ;

             p(i)$reb(i) = preb ;
             p(i)$con(i)= pcon ;
             p(i)$col(i)  =
             pbot - ((pbot-ptop)/(card(i)-1-2)) * (ord(i)-2)  ;

             display p ;

parameter     pdiff   pressure drop of one tray;
              pdiff = 0;

Positive variables

              pbotm   actual pressure in bottom-most tray
              prebler actual pressure in reboiler;

Equations
          defpbotm
          defprebler;

parameter keq1(i,j);

*------------------------------------------------------------------------------------
 Scalars hllo,hlhi,hvlo,hvhi  limits on enthalpies  ;
   hllo = hl0('propene')+ tcon *(hla('propene') + tcon* hlb('propene')) ;
   hlhi = hl0('propane')+ treb *(hla('propane') + treb* hlb('propane')) ;
   hvlo = hv0('propene')+ tcon *(hva('propene') + tcon* hvb('propene')) ;
   hvhi = hv0('propane')+ treb *(hva('propane') + treb* hvb('propane')) ;


Scalar sigma  feed and reflux deviation parameter;
       sigma = 0.5;

Scalars
        counter  loop counter
              /1/

        purolef purity of propene
              /0.995/
        purpara purity of propane
              /0.95/;


Positive variables
              slack1(i)
              slack2(i)
              dd(i)

              x(i,j)   mole-fraction of j-th component in i-th tray.
              y(i,j)   mole-fraction of j-th component in i-th tray

$ontext
*          -------------------------------------------------------------------
                    This part is for Continuous Variable Optimization
$offtext

              nfp       feed permeate tray location
              ffp(i)    fraction of feed distributed to each tray
              nfr       feed retentate tray location
              ffr(i)    fraction of feed retentate distributed to each tray
              r         reflux ratio
              Nt        reflux tray location
              g(i)      fraction of Reflux distributed to each tray
              rl(i)     fraction of reflux distribution to each tray
              totalrd   total reflux
              rd        portion of total reflux manipulated
              refcom(j) composition of reflux
              refhl     enthalpy of reflux
              rdf       fraction of reflux manipulated
*          -------------------------------------------------------------------
              l(i)     molar flow rate of liquid leaving tray i .(i<n)
              v(i)     molar flow rate of vapour leaving tray i .
              t(i)     temperature of tray i
              ap1      top product rate
              ap2      bottom product rate;

Variables hl(i),hv(i),objective

             A10(i,j)
             A20(i,j)
             A30(i,j)
             A11(i,j)
             A21(i,j)
             A31(i,j)
             K0(i,j)
             K1(i,j)
             Keq(i,j)

 ;
Scalar  smooth;
        SMOOTH = 100;

Positive variables
        GAMMA(I);
Equations

            IFF(j)
            IFP(j)
            ILL
            FECOLff(j,a,b)
            FECOLfp(j,a,b)
            FECOLll(a,b)
            CONff(j,a)
            CONfp(j,a)
            CONll(a)
            ODEff(j,a,b)
            ODEfp(j,a,b)
            GROUP_AREA
            DIM_PRESSURE

             errk(i)          Phase equilibrium error function
             tmb(i)           total material balance for trays in the column
             tmb1(i)          total material balance for reboiler
             tmbn(i)          total material balance for condenser
             defln(i)         definition of l(n)
             defap1(i)        definition of ap1
             cmb(i,j)         component material balance(1<i<n)
             cmb1(i,j)        component material balance(i=1)
             cmbn(i,j)        component material balance(i=n)
             phe(i,j)         phase equilibrium relation
             defhl(i)         definition of hl(i)
             defhv(i)         definition of hv(i)
             eb(i)            enthalpy balance
             ddB(i)
             objpf            penalty objective function
             objs             smoothing objective function
             const1           propene purity constrain
             const2           propane purity constrain
             fluxconect       feed permeate flux conection
             compconect       feed permeate composition conection
             fluxconect2      feed retentate flux conection
             compconect2(j)   feed retentate composition conection
             shfpdef          feed permeate enthalpy definition
             shfrdef          feed retentate enthalpy definition
             distprod         distillate production
             defrebKW         definition of reboiler total duty
             defcondKW        definition of condenser total duty
             defmembdev       definition of membrane devaluation
             defcomp1costyr   definition of permeate compressor total cost
             defcomp2costyr   definition of retentate compressor total cost
             defcomp1eleckw   definition of permeate compressor duty
             defcomp2eleckw   definition of retentate compressor duty
             defrebcostyr     definition of reboiler total cost
             defcondcostyr    definition of condenser total cost
             selectivityfixed fixes alpha propene equal to 1
             tradeoff         permability-selectivity trade-off

             defA10(i,j)
             defA20(i,j)
             defA30(i,j)
             defA11(i,j)
             defA21(i,j)
             defA31(i,j)
             defK0(i,j)
             defK1(i,j)
             defKeq(i,j)


             const2           propane purity constrain
;

 EQUATIONS
             SMTHL(i)      SMOOTHING EQUATION FOR L VALUES
             SMTHL_r(i)    SMOOTHING EQUATION FOR L VALUES
             SMTHL_pf      PENALTY EQUATION FOR L VALUES
             SMTHV(i)      SMOOTHING EQUATION FOR V VALUES
             SMTHV_r(i)    SMOOTHING EQUATION FOR V VALUES
             SMTHV_pf      PENALTY EQUATION FOR V VALUES
*        ------------------------------------------------------------

             feedeqn(i)    feed permeate distribution
             feedeqn2(i)   feed retentate distribution

             refluxeqn     reflux distribution
             deftotrd      define total reflux
             defrd         define portion of total reflux manipulated
             defrefcom(j)  define composition in reflux
;

*****************************MEMBRANE EQUATIONS*********************************

* SELECTIVITY-PERMEABILITY TRADE-OFF

selectivityfixed..   alpha('propene')=e=1;
tradeoff..           alpha('propane')=l=97.507*(perma**(-0.362));
```

```
* LAGRANGE BASIS COLLOCATION

FECOLff(j,a,b)$(ord(b) gt 1).. h(a)*ffdot(j,a,b) =e=
sum(c,ldot(c,b)*ff(j,a,c));

FECOLfp(j,a,b)$(ord(b) gt 1).. h(a)*fpdot(j,a,b) =e=
sum(c,ldot(c,b)*fp(j,a,c));

FECOLll(a,b)$(ord(b) gt 1)..   h(a) =e= sum(c,ldot(c,b)*ll(a,c));

*CONTINUITY ECUATIONS

CONff(j,a)$(ord(a) gt 1)..     ff(j,a,'1') =e=
sum(b, ff(j,a-1,b)*lfinal(b));

CONfp(j,a)$(ord(a) gt 1)..     fp(j,a,'1') =e=
sum(b, fp(j,a-1,b)*lfinal(b));

CONll(a)$(ord(a) gt 1)..       ll(a,'1') =e= sum(b, ll(a-1,b)*lfinal(b));

*ORDINARY DIFFERENTIAL EQUATIONS

ODEff(j,a,b)$(ord(b) gt 1).. ffdot(j,a,b)=e=-theta/alpha(j)*
(ff(j,a,b)/(sum(jb,ff(jb,a,b)))-
fp(j,a,b)/(sum(jb,fp(jb,a,b)))*gammap);

ODEfp(j,a,b)$(ord(b) gt 1).. fpdot(j,a,b)=e=theta/alpha(j)*
(ff(j,a,b)/(sum(jb,ff(jb,a,b)))-
fp(j,a,b)/(sum(jb,fp(jb,a,b)))*gammap);

*ALGEBRAIC EQUATIONS

GROUP_AREA..      theta=e=(area*1e3)*(perma*conv)*ftp/delta;
DIM_PRESSURE..    gammap=e=ptp/ftp;

*INITIAL CONDITIONS

IFF(j)..    ff(j,'1','1')=e=ffinit(j);
IFP(j)..    fp(j,'1','1')=e=fpinit(j);
ILL..       ll('1','1')=e=0;
********************************************************************************


***************************MEMBRANE-COLUMN CONECTIONS***************************

fluxconect..     fdp =e=sum(j,sum(b,lfinal(b)*fp(j,'20',b)));

fluxconect2..    fdr =e=sum(j,sum(b,lfinal(b)*ff(j,'20',b)));

compconect(j)..  sum(b,lfinal(b)*fp(j,'20',b))=e=xfp(j)*
(sum(b,lfinal(b)*sum(jb,fp(jb,'20',b))));

compconect2(j)..  sum(b,lfinal(b)*ff(j,'20',b))=e=xfr(j)*
(sum(b,lfinal(b)*sum(jb,ff(jb,'20',b))));
********************************************************************************



*****************************COLUMN EQUATIONS***********************************

*FEED ENTHALPY

shfpdef..     shfp =e= sum(j,xfp(j)*(hl0(j)+tf*(hla(j)+tf*hlb(j))));
shfrdef..     shfr =e= sum(j,xfr(j)*(hl0(j)+tf*(hla(j)+tf*hlb(j))));
*-------------------------------------------------------------------------------

feedeqn(i)$col(i).. ffp(i) =E= exp(-sqr((ord(i)-nfp)/sigma))/
              sum(ii$col(ii),exp(-sqr((ord(ii)-nfp)/sigma)));

feedeqn2(i)$col(i).. ffr(i) =E= exp(-sqr((ord(i)-nfr)/sigma))/
              sum(ii$col(ii),exp(-sqr((ord(ii)-nfr)/sigma)));

refluxeqn(i)$col(i)..g(i) =E= exp(-sqr((ord(i)-nt)/sigma))/
              sum(ii$col(ii),exp(-sqr((ord(ii)-nt)/sigma)));

* add a intermediate variable to reduce nonlinearity

deftotrd..totalrd - r*ap1 =e= 0;
```

```
defrd..(rd - rdf*totalrd) =e= 0;

* we have to cheat Gmas to get specific values on condenser

defrefcom(j)..refcom(j) =e= sum(ii$(ord(ii) eq card(ii)), x(ii,j));


defpbotm..pbotm =e= pbot - pdiff*(card(i)-nt);

defprebler..prebler =e= preb - pdiff*(card(i) - nt);

*--------------------------------------------------------------------------------

errk(i)..    sum(j,y(i,j)) - sum(j,x(i,j))   =e= 0;


tmb1(i)$reb(i)..               l(i)+v(i)- l(i+1) =e= 0;

*--------------------------------------------------------------------------------

tmb(i)$col(i)..
         l(i) + v(i) - l(i+1) - v(i-1) - ffp(i)*fdp-ffr(i)*fdr - g(i)*rd =e= 0;

tmbn(i)$con(i)..            ( rd + ap1) -  v(i-1) =e= 0;

*--------------------------------------------------------------------------------

defln(i)$con(i)..     l(i) - (totalrd - rd) =e= 0;
defap1(i)$reb(i)..     l(i) - ap2 =e= 0;

*--------------------------------------------------------------------------------

cmb(i,j)$col(i)..
       l(i)*x(i,j) + v(i) *y(i,j) - l(i+1)*x(i+1,j) -v(i-1)*y(i-1,j)
              - ffp(i)*xfp(j)*fdp - ffr(i)*xfr(j)*fdr - g(i)*rd*refcom(j) =e= 0;
*--------------------------------------------------------------------------------
cmb1(i,j)$reb(i)..
       (l(i)*x(i,j) +v(i)*y(i,j)- l(i+1)*x(i+1,j)) =e= 0;

*--------------------------------------------------------------------------------

cmbn(i,j)$con(i)..
        (rd + ap1)*x(i,j) -  v(i-1)*y(i-1,j) =e= 0;

*--------------------------------------------------------------------------------

defhl(i).. hl(i)-sum(j,x(i,j)*(hl0(j)+t(i)*(hla(j)+t(i)*hlb(j))))/hvhi =e= 0;

defhv(i).. hv(i)-sum(j,y(i,j)*(hv0(j)+t(i)*(hva(j)+t(i)*hvb(j))))/hvhi =e= 0;


eb(i)$col(i)..
  l(i)*hl(i) +v(i)*hv(i) - l(i+1)*hl(i+1) - v(i-1)*hv(i-1)
   -  ffp(i)*fdp* shfp/hvhi -  ffr(i)*fdr* shfr/hvhi - g(i)*rd*hl('135') =e=  0;


defA10(i,j)..  A10(i,j)=e=2.18630+(-8.80971)*t(i)/PRCON (J,'TC')+
  10.96486*power(t(i)/PRCON (J,'TC'),2)+(-3.87905)*power(t(i)/PRCON (J,'TC'),3);

defA20(i,j)..  A20(i,j)=e=0.30602+(-0.64992)*t(i)/PRCON (J,'TC')+
   (-0.72423)*power(t(i)/PRCON (J,'TC'),2)+1.64710*power(t(i)/PRCON (J,'TC'),3);

defA30(i,j)..  A30(i,j)=e=(-0.02683)+(-0.28575)*t(i)/PRCON (J,'TC')+
   1.09824*power(t(i)/PRCON (J,'TC'),2)+(-0.90820)*power(t(i)/PRCON (J,'TC'),3);

defA11(i,j)..  A11(i,j)=e=(-3.44761)+14.55943*t(i)/PRCON (J,'TC')+
 (-21.31054)*power(t(i)/PRCON (J,'TC'),2)+11.13279*power(t(i)/PRCON (J,'TC'),3);

defA21(i,j)..  A21(i,j)=e=(-6.40659)+28.27873*t(i)/PRCON (J,'TC')+
 (-39.95181)*power(t(i)/PRCON (J,'TC'),2)+17.62137*power(t(i)/PRCON (J,'TC'),3);

defA31(i,j)..  A31(i,j)=e=0.58201+(-1.28555)*t(i)/PRCON (J,'TC')+
   0.87828*power(t(i)/PRCON (J,'TC'),2)+(-0.80885)*power(t(i)/PRCON (J,'TC'),3);

defK0(i,j)..   K0(i,j)=e=A10(i,j)+A20(i,j)/(p(i)/PRCON (J,'PC'))+
   A30(i,j)*(p(i)/PRCON (J,'PC'));

defK1(i,j)..   K1(i,j)=e=A11(i,j)+A21(i,j)/(p(i)/PRCON (J,'PC'))+
   A31(i,j)*(p(i)/PRCON (J,'PC'));
```

```
defKeq(i,j)..  Keq(i,j)=e=K0(i,j)+(PRCON(j,'omega')-0.193)*K1(i,j);



phe(i,j)..  y(i,j)=e= GAMMA(I)*x(i,j)*Keq(i,j)  ;

DdB(I)..   1 - GAMMA(I) =E= SLACK1(i) - SLACK2(i);

variable btb_smthl, btb_smthv;

SMTHL_pf..  btb_smthl =e= sum(ii,SLACK1(ii)*L(ii)) ;
SMTHV_pf..  btb_smthv =e= sum(ii,SLACK2(ii)*V(ii)) ;

SMTHL(I)..  SLACK1(I)+L(I) =E= SQRT(SQR(L(I)-SLACK1(I))+SQR(1/SMOOTH));
SMTHV(I)..  SLACK2(I)+V(I) =E= SQRT(SQR(V(I)-SLACK2(I))+SQR(1/SMOOTH));

SMTHL_r(I)..  SLACK1(I)*L(I) =l= (1/SMOOTH);
SMTHV_r(I)..  SLACK2(I)*V(I) =l= (1/SMOOTH);


defcomp1eleckw..       fdp*comp1stages*(1.15/0.15)*8.314472*temp*
         ((pf/ptp)**(0.15/(1.15*comp1stages))-1)/3600/compyield-comp1eleckw=e=0;

defcomp2eleckw..       fdr*comp2stages*(1.15/0.15)*8.314472*temp*
         ((pf/ftp)**(0.15/(1.15*comp2stages))-1)/3600/compyield-comp2eleckw=e=0;

defcomp1costyr..         comp1eleckw*365*sf*24*kWhcost-comp1costyr=e=0;
defcomp2costyr..         comp2eleckw*365*sf*24*kWhcost-comp2costyr=e=0;

defrebKW..          v('1')*sum(j,x('1',j)*dhv(j))-3600*rebKW=e=0;
defcondKW..         (totalrd+ap1)*sum(j,refcom(j)*dhv(j))-3600*condKW=e=0;
defmembdev..        membdev-area*1e3*membcost/memblife=e=0;

defrebcostyr.. rebcostyr-rebKW*1000/AHvap*3600*24*sf*daysop*steamcost=e=0;

defcondcostyr.. condcostyr-condKW*1000/(cpw*(coolTout-coolTin))*
                         3600*24*sf*daysop*coolprice=e=0;

objpf..       objective =e= comp1costyr + comp2costyr + rebcostyr +
                  condcostyr + membdev + 1e3*(btb_smthl+btb_smthv);

objs..        objective =e= comp1costyr + comp2costyr + rebcostyr +
                  condcostyr + membdev;

********************************************************************************


********************************MODEL CONSTRAINS********************************

const1..     refcom('propene')=g=purolef;

const2..     x('1','propane')=g=purpara;
********************************************************************************


$ontext
********************************************************************************
                Initialization of membrane variables
********************************************************************************
$offtext

alpha.lo(j)=1;
alpha.l('propane')=20;
perma.lo=1e-5;
perma.up=1e6;
perma.l=100;

ff.lo(j,a,b)=0;    ff.up(j,a,b)=ffinit(j);
fp.lo(j,a,b)=0;    fp.up(j,a,b)=ffinit(j);
ff.l(j,a,b)=ffinit(j);
fp.l(j,a,b)=ffinit(j);
ffdot.l(j,a,b)=1;
fpdot.l(j,a,b)=1;
ll.l(a,b)=1;
area.lo=1e-3; area.l=1;


$ontext
```

```
********************************************************************************
                Initialization of distillation variables
********************************************************************************
$offtext
   ap2.l = 180;
   ap1.l= 180;
*-------------------------------
   xfp.lo(j)=0;
   xfp.up(j)=1;
   xfp.l(j)=0.5;

   xfr.lo(j)=0;
   xfr.up(j)=1;
   xfr.l(j)=0.5;

   fdp.lo=0;
   fdp.up=sum(j,ffinit(j));
   fdp.l=80;

   fdr.lo=0;
   fdr.up=sum(j,ffinit(j));
   fdr.l=20;

   nfr.lo = 2;
   nfr.up = 50;
   nfr.l = 2;

   nfp.lo = nfr.lo+1;
   nfp.up = card(i)-2;
   nfp.l = 54;

   nt.lo = nfp.lo+1;
   nt.up = card(i)-1;
   nt.fx =134;

   g.up(i) = 1;
   g.lo(i) = 0;
   g.l('134')=0.5;

   r.lo = 1;
   r.up = 20;
   r.l = 10;

   ffp.l('80') = 0.8;
   ffr.l('2') = 0.8;
   totalrd.l = r.l*ap1.l;
   totalrd.up = r.up*ap1.l;
   totalrd.lo = r.lo*ap1.l;

   rdf.fx = 1.0;
   rd.up = rdf.lo*totalrd.up;
   rd.lo = rdf.up*totalrd.lo;
   rd.l = rdf.l*totalrd.l;
   l.l(i)$con(i) = totalrd.l - rd.l;
   l.lo(i)$con(i)=0;
   l.up(i)$con(i)= totalrd.up - rd.lo;

*-----------------------------
   dd.lo(i) = 0.0;
   aP1.UP = 360;
   aP2.UP = 360;
   v.l(i) = ((r.l + 1) * ap1.l );
   dd.l(i) = 0.0;

   l.l(i)$reb(i) = ap2.l ;
   l.l(i)$(belowf(i)-reb(i)) = ap1.l * r.l + fdp.l+fdr.l ;
   l.l(i)$abovef(i) = ap1.l * r.l ;

   t.l(i)$reb(i) = treb ;
   t.l(i)$con(i) = tcon ;
   t.l(i)$col(i) = tbot + (ttop -tbot) *(ord(i)-2)/(card(i)-1-2) ;
   t.up(i) = treb+20 ;    t.lo(i) = tcon - 20 ;
   x.l(i,'propene') =0.9 - 0.5 * (ord(i)- card(i))/(1-card(i));
   x.l(i,'propane') = 1 - x.l(i,'propene') ;
   y.l(i,'propene') = 0.999 - 0.8*(ord(i) -card(i))/(1-card(i)) ;
   y.l(i,'propane') = 1 - y.l(i,'propene') ;
   x.up(i,j)  = 1.0 ;  y.up(i,j) = 1.0 ;
   hl.l(i)=sum(j,x.l(i,j)*(hl0(j)+t.l(i)*(hla(j)+t.l(i)*hlb(j))))/hvhi;
   hv.l(i)=sum(j,y.l(i,j)*(hv0(j)+t.l(i)*(hva(j)+t.l(i)*hvb(j))))/hvhi ;
   hl.lo(i) = - 100 ;
   hv.lo(i) = ( 1 - 0.2*sign(hvlo))*hvlo/hvhi ;
   hl.up(i) = ( 1 + 0.2*sign(hlhi))* hlhi/hvhi ;
   hv.up(i)= ( 1 + 0.2*sign(hvhi));


   slack1.l(i) = 0.01;
   slack2.l(i) = 0.01;
   dd.l(i) = 0;



comp1eleckw.l=fdp.l*comp1stages*(1.15/0.4)*8.314472*temp*
                         ((pf/ptp)**(0.15/(1.15*comp1stages))-1)/3600/compyield;

comp2eleckw.l=fdr.l*comp2stages*(1.15/0.4)*8.314472*temp*
                         ((pf/ftp)**(0.15/(1.15*comp2stages))-1)/3600/compyield;

comp1costyr.l=comp1eleckw.l*365*sf*24*kWhcost;
comp2costyr.l=comp2eleckw.l*365*sf*24*kWhcost;


rebKW.l=3e6/3600;
condKW.l=2e6/3600;
membdev.l=-area.l*1e3*membcost/memblife;


rebcostyr.l=rebKW.l*1000/AHvap*3600*24*sf*daysop*steamcost;
condcostyr.l=condKW.l*1000/(cpw*(coolTout-coolTin))*3600*24*sf*daysop*coolprice;

A10.l(i,j)=2.18630+(-8.80971)*t.l(i)/PRCON (J,'TC')+
         10.96486*power(t.l(i)/PRCON (J,'TC'),2)+(-3.87905)*
                         power(t.l(i)/PRCON (J,'TC'),3);

A20.l(i,j)=0.30602+(-0.64992)*t.l(i)/PRCON (J,'TC')+
         (-0.72423)*power(t.l(i)/PRCON (J,'TC'),2)+1.64710*
                         power(t.l(i)/PRCON (J,'TC'),3);

A30.l(i,j)=(-0.02683)+(-0.28575)*t.l(i)/PRCON (J,'TC')+
         1.09824*power(t.l(i)/PRCON (J,'TC'),2)+(-0.90820)*
                         power(t.l(i)/PRCON (J,'TC'),3);

A11.l(i,j)=(-3.44761)+14.55943*t.l(i)/PRCON (J,'TC')+
         (-21.31054)*power(t.l(i)/PRCON (J,'TC'),2)+11.13279*
                         power(t.l(i)/PRCON (J,'TC'),3);

A21.l(i,j)=(-6.40659)+28.27873*t.l(i)/PRCON (J,'TC')+
         (-39.95181)*power(t.l(i)/PRCON (J,'TC'),2)+17.62137*
                         power(t.l(i)/PRCON (J,'TC'),3);

A31.l(i,j)=0.58201+(-1.28555)*t.l(i)/PRCON (J,'TC')+
         0.87828*power(t.l(i)/PRCON (J,'TC'),2)+(-0.80885)*
                         power(t.l(i)/PRCON (J,'TC'),3);

K0.l(i,j)=A10.l(i,j)+A20.l(i,j)/(p(i)/PRCON (J,'PC'))+
                         A30.l(i,j)*(p(i)/PRCON (J,'PC'));

K1.l(i,j)=A11.l(i,j)+A21.l(i,j)/(p(i)/PRCON (J,'PC'))+
                         A31.l(i,j)*(p(i)/PRCON (J,'PC'));

Keq.l(i,j)=K0.l(i,j)+(PRCON(j,'omega')-0.193)*K1.l(i,j);




Model ncp /IFF,IFP,ILL,FECOLff,FECOLfp,FECOLll,CONff,CONfp,CONll,ODEff,ODEfp,
GROUP_AREA,DIM_PRESSURE,fluxconect,fluxconect2,compconect,compconect2,shfpdef,
shfrdef,defpbotm, defprebler, errk, tmb, tmb1, tmbn, defln, defap1,
feedeqn,feedeqn2, refluxeqn, deftotrd, defrd, defrefcom, cmb, cmb1, cmbn, phe,
defhl, defhv, eb, ddB, objs, SMTHL, SMTHV,const1,defrebKW,defcondKW,defmembdev,
defcomp1costyr,defcomp2costyr,defcomp1eleckw,defcomp2eleckw,defrebcostyr,
defcondcostyr,const2,defA10,defA20,defA30,defA11,defA21,defA31,defK0,defK1,
defKeq,tradeoff,selectivityfixed/;


Model reg /IFF,IFP,ILL,FECOLff,FECOLfp,FECOLll,CONff,CONfp,CONll,ODEff,ODEfp,
GROUP_AREA,DIM_PRESSURE,fluxconect,fluxconect2,compconect,compconect2,shfpdef,
shfrdef,defpbotm, defprebler, errk, tmb, tmb1, tmbn, defln, defap1,
feedeqn,feedeqn2, refluxeqn, deftotrd, defrd, defrefcom, cmb, cmb1, cmbn, phe,
defhl, defhv, eb, ddB, objs, SMTHL, SMTHV,const1,defrebKW,defcondKW,defmembdev,
defcomp1costyr,defcomp2costyr,defcomp1eleckw,defcomp2eleckw,defrebcostyr,
defcondcostyr,const2,defA10,defA20,defA30,defA11,defA21,defA31,defK0,defK1,
defKeq,tradeoff,selectivityfixed/;

Model penalty /IFF,IFP,ILL,FECOLff,FECOLfp,FECOLll,CONff,CONfp,CONll,ODEff,
ODEfp,GROUP_AREA,DIM_PRESSURE,fluxconect,fluxconect2,compconect,compconect2,
shfpdef,shfrdef,defpbotm, defprebler, errk, tmb, tmb1, tmbn, defln,
defap1, feedeqn,feedeqn2, refluxeqn, deftotrd, defrd, defrefcom, cmb, cmb1,
cmbn, phe, defhl, defhv, eb, ddB, objpf, SMTHL_pf, SMTHV_pf,const1,defrebKW,
defcondKW,defmembdev,defcomp1costyr,defcomp2costyr,defcomp1eleckw,
defcomp2eleckw,defrebcostyr,defcondcostyr,const2,defA10,defA20,defA30,
defA11,defA21,defA31,defK0,defK1,tradeoff,selectivityfixed,defKeq/;

 penalty.optfile = 1;
 reg.optfile=1;
 option nlp =conopt;
 option decimals = 8;
* option iterlim = 6000;


 option  r:8;


 parameter toluintop;




 smooth = 1.e6;
 solve reg using nlp  minimizing  objective ;

 smooth = 1.e12;
 solve reg using nlp  minimizing  objective ;

 solve penalty using nlp  minimizing  objective ;
 solve penalty using nlp  minimizing  objective ;

 penalty.optfile = 1;
 reg.optfile=1;
 option nlp =oqnlp;
 option decimals = 8;
*   option iterlim = 3000;
 option reslim = 3000 ;

 solve penalty using nlp  minimizing  objective ;


fffinal(j,a)=sum(b,lfinal(b)*ff.l(j,a,b));
fpfinal(j,a)=sum(b,lfinal(b)*fp.l(j,a,b));


Display area.l;
Display fffinal,fpfinal;
Display ll.l,ff.l,fp.l;

keq1(i,j)=y.l(i,j)/x.l(i,j);
display keq1, x.l,y.l;
```

A.4 GAMS program used for multistage process optimization (*two-and-one-half-stages*)

```
$Title: Optimization of a gas separation process with HF-membrane modules

$OFFUPPER
$OFFSYMXREF OFFSYMLIST

* option sysout = off;
* OPTION SOLPRINT = OFF;

* This file implements the optimization of a gas separation process
* using hollow fiber membrane modules.
* Objetive function is minimum net present value cost.
* Decision variables are membrane areas, permeate pressure and carrier loading.
* Constraints are C3H6 and C3H8 product purities.

Sets    i        number of finite elements             /1*100/
        j        number of internal collocation points /1*3/
* List number of compounds and membrane modules:
        comp     number of compounds                   /a,b/
        m        number of membrane modules            /M1,M2,M3/;

Alias (j,k)
      (comp,compb);

Scalar  nfe       number of finite elements                  [-]     /100/
        pi        number pi                                  [-]     /3.141592/
* Problem definition:
        gradeA    minimum purity of A                        [-]     /0.995/
        gradeB    minimum purity of B                        [-]     /0.95/

        ftp       feed total pressure                      [bar]     /18/
        temp      pre-compressor feed temperature            [K]     /325/
* Define membrane parameters:
        permb     permeability of B                     [Barrer]     /20/
        delta     fiber wall thickness                       [m]     /20e-6/
        conv      Barrer conversion [kmol m-1 bar-1 h-1 Barrer-1]    /1.206e-10/
* Define cost parameters:
        ecost     energy cost                          [$ kWh-1]     /0.15/
        MFc       compressor module factor                   [-]     /3.11/
        CEPCI     chem. eng. plant cost index 2016                   /541.7/
        eta       isentropic compressor efficiency           [-]     /0.7/
        CR        compression ratio                                  /2.62071/
        OF        annual operating factor                [h y-1]     /8000/
        r         interest rate                              [%]     /10/
        T         plant lifetime                             [y]     /15/
* Membrane model constants
        EaFC      fixed carrier activation energy      [J mol-1]     /14800/
        pack      modules packing density                    [-]     /0.6/
        Rfib      hollow fiber external radius               [m]     /165e-6/
        Rfibin    hollow fiber internal radius               [m]     /90e-6/
        keq0      reaction constant at 278K           [m3 mol-1]     /0.337/
        AHr       reaction activation energy          [kJ mol-1]     /-11/
        He0       Henrys law constant            [mol bar-1 m-3]     /4.28e-3/
        AHsol     Henrys law activation energy        [kJ mol-1]     /-24.1/
        Dcomp0    Complex diffusivity at 293K           [m2 s-1]     /3.22e-11/
        EaD       Diffusivity activation energy       [kJ mol-1]     /7.13/
        XIL       Ionic liquid fraction                      [-]     /0.2/
        alpha     Fitting parameter               [m2 mol-1 s-1]     /1.35e-11/
        gasR      ideal gas constant               [J K-1 mol-1]     /8.314472/
        kp        Heterogeneous reaction constant        [bar-1]     /0.12/
        Polyload  polymer load per m3 of membrae         [g m-3]     /1.11e6/
        ILload    IL load per m3 of membrane             [g m-3]     /2.76e5/
        Polycost  polymer cost                           [$ g-1]     /0.7/
        Ilcost    IL cost                                [$ g-1]     /0.8/
        Agcost    AgBF4cost                              [$ g-1]     /13/;


* Set initial values for feed flowrates into M1:
Parameter ffinit(comp) value  [kmol h-1]        /a  180
                                                  b  180/;

* Set initial values for permeate flowrates into M1:
Parameter fpinit(comp) value  [kmol h-1]        /a  1e-6
                                                  b  1e-6/;
```

```
Table   l(j,j)    Lagrange basis collocation matrix
         1       2       3
      1  1       0       0
      2  0       1       0
      3  0       0       1;


Table  ldot(j,j)  Lagrange basis first derivs collocation matrix
                1                  2                  3
      1  -5.999997202501304  -3.464098384864128  3.464098384864127
      2  6.464099408820847   2.999996178544585   -6.464099408820847
      3  -0.464102206319543  0.464102206319543   3.000001023956719;


Parameter lfinal(j) value   /1  1
                             2  -1.732051615138131
                             3  1.732051615138131/;


Parameter
          FeedFlow(m)         Module total feed flowrate
          FeedComp(m)         Module feed composition
          RetentateFlow(m)    final molar retentate flowrate
          RetentateComp(m)    Retentate composition
          PermeateFlow(m)     final molar permeate flowrate
          PermeateComp(m)     permeate composition
          fppfinal(m,comp,i)  final partial pressure retentate
          pppfinal(m,comp,i)  final partial pressure permeate
          H2purity            final H2 purity
          H2recovery          final H2 recovery
          compression         total compression work [kW]
          h(i);

h(i) = 1/nfe;

Variables ff(m,comp,i,j)      retentate molar flowrate
          fp(m,comp,i,j)      permeate molar flowrate
          ffdot(m,comp,i,j)   ff first order derivative
          fpdot(m,comp,i,j)   fp first order derivative
          ja(i,m)             propylene transmembrane flux
          jb(i,m)             propylene transmembrane flux
          ll(i,j)             fiber lenght dimension
          Lfib(m)             module fiber length [m]
          Nfib(m)             module fibers
          gamma               permeate over feed pressure [-]
          phi
          NPVcost             net present value cost [M$]
          CAPEX               capital expenses [M$]
          OPEX                operating expenses [M$ y-1]
          H2prod              H2 production [MNm3 y-1]
          compression1        1st stage compressors duty [kW]
          compression2        2nd stage compressors duty [kW]
          NSt                 compression stages
          keq                 reaction constant [m3 mol-1]
          He                  Henrys law constant [mol bar-1 m-3]
          Dcomp               Complex diffusivity  [m2 s-1]
          Ag(m)               silver load          [mol m-3]
          m2cost(m)           membrane cost        [$ m-2]
          area(m)             module total area    [m2]
          vlumen(m,i,j)       linear velocity lumen side [m s-1]
          vshell(m,i,j)       linear velocity shell side [m s-1]
          modcin(m)           module shell diameter [m]
          ptp(m)              permeate total pressure [bar];

Equations   fobj            criterion definition
            compenerg2
            costs
            capcosts
            opcosts
            IFP(m,comp)
            ILL
            FECOLff(m,comp,i,j)
            FECOLfp(m,comp,i,j)
            FECOLll(i,j)
            CONff(m,comp,i)
            CONfp(m,comp,i)
            CONll(i)
            ODEffA(m,i,j)
            ODEfpA(m,i,j)
            ODEffB(m,i,j)
            ODEfpB(m,i,j)
            CON12Feed(comp)
            CON31Feed(comp)
            CON23Feed(comp)
            PURITYA
            PURITYB
            Henry
            VantHoff
            Arrhenius
            MembCost
            areadef
            vlumendef (m,i,j)
            vshelldef (m,i,j)
            modcindef(m)
            equalpressure(m);

*-------------------------------------------------------------------------------
*OBJECTIVE FUNCTION
*-------------------------------------------------------------------------------

fobj..       phi=e=NPVcost;

costs..      NPVcost=e=CAPEX+OPEX*(1-(1+r/100)**(-T))/(r/100);

capcosts..   CAPEX=e=sum(m,m2cost(m)*2*pi*Rfib*Nfib(m)*Lfib(m))/10**6+
             23000*((compression2/Nst/74.57)**0.77)*
             Nst*MFc*(CEPCI/115)/10**6;

opcosts..    OPEX=e=compression2*OF*ecost/10**6+
             0.01*sum(m,m2cost(m)*2*pi*Rfib*Nfib(m)*Lfib(m))/10**6;

compenerg2..
compression2=e=(sum(j,lfinal(j)*sum(compb,fp('M1',compb,'100',j)))+sum(j,lfinal(j)*sum(com
pb,fp('M3',compb,'100',j))))
             *NSt*(1.15/0.15)*(8.314e-2*temp)*(((ftp/ptp('M1'))**(0.15/1.15/NSt))-1)/
             eta/36;

MembCost(m)..   m2cost(m)-delta*(Polyload*Polycost+ILload*ILcost+Ag(m)*194.67*Agcost)=e=0;

areadef(m).. area(m)-2*pi*Rfib*Nfib(m)*Lfib(m)=e=0;


*-------------------------------------------------------------------------------
* HF-MEMBRANE MODULE EQUATIONS
*-------------------------------------------------------------------------------

Henry..       He-He0*exp(-AHsol*1000/gasR/temp)=e=0;
VantHoff..    Keq-Keq0*exp(-AHr*1000/gasR*(1/temp-1/278))=e=0;
Arrhenius..   Dcomp-Dcomp0*exp(-EaD*1000/gasR*(1/temp-1/293))=e=0;


*LAGRANGE BASIS COLLOCATION
FECOLff(m,comp,i,j)$(ord(j) gt 1).. h(i)*ffdot(m,comp,i,j) =e=
sum(k,ldot(k,j)*ff(m,comp,i,k));

FECOLfp(m,comp,i,j)$(ord(j) gt 1).. h(i)*fpdot(m,comp,i,j) =e=
sum(k,ldot(k,j)*fp(m,comp,i,k));

FECOLll(i,j)$(ord(j) gt 1)..        h(i) =e= sum(k,ldot(k,j)*ll(i,k));

*CONTINUITY ECUATIONS
CONff(m,comp,i)$(ord(i) gt 1)..     ff(m,comp,i,'1') =e=
sum(j, ff(m,comp,i-1,j)*lfinal(j));

CONfp(m,comp,i)$(ord(i) gt 1)..     fp(m,comp,i,'1') =e=
sum(j, fp(m,comp,i-1,j)*lfinal(j));

CONll(i)$(ord(i) gt 1)..            ll(i,'1') =e= sum(j, ll(i-1,j)*lfinal(j));

*ORDINARY DIFFERENTIAL EQUATIONS
ODEffA(m,i,j)$(ord(j) gt 1).. ffdot(m,'a',i,j)=e=-2*pi*Lfib(m)*Nfib(m)*Rfib/delta*
(ff(m,'a',i,j)/(sum(compb,ff(m,compb,i,j)))*ftp-
fp(m,'a',i,j)/(sum(compb,fp(m,compb,i,j)))*ptp(m))*
((keq*Ag(m)*He*Dcomp*XIL/(1+keq*ff(m,'a',i,j)/(sum(compb,ff(m,compb,i,j)))*ftp*He))+
(alpha*exp(EaFC/gasR*(1/293-
1/temp))*(Ag(m)/(1+kp*ff(m,'a',i,j)/(sum(compb,ff(m,compb,i,j)))*ftp))*(1-XIL)))*3.6;
```

```
ODEffB(m,i,j)$(ord(j) gt 1).. ffdot(m,'b',i,j)=e=-2*pi*Lfib(m)*Nfib(m)*Rfib/delta*
Permb*conv*(ff(m,'b',i,j)/(sum(compb,ff(m,compb,i,j)))*ftp-
fp(m,'b',i,j)/(sum(compb,fp(m,compb,i,j)))*ptp(m));

ODEfpA(m,i,j)$(ord(j) gt 1).. fpdot(m,'a',i,j)=e=2*pi*Lfib(m)*Nfib(m)*Rfib/delta*
(ff(m,'a',i,j)/(sum(compb,ff(m,compb,i,j)))*ftp-
fp(m,'a',i,j)/(sum(compb,fp(m,compb,i,j)))*ptp(m))*
((keq*Ag(m)*He*Dcomp*XIL/(1+keq*ff(m,'a',i,j)/(sum(compb,ff(m,compb,i,j)))*ftp*He))+
(alpha*exp(EaFC/gasR*(1/293-
1/temp))*(Ag(m)/(1+kp*ff(m,'a',i,j)/(sum(compb,ff(m,compb,i,j)))*ftp))*(1-XIL)))*3.6;

ODEfpB(m,i,j)$(ord(j) gt 1).. fpdot(m,'b',i,j)=e=2*pi*Lfib(m)*Nfib(m)*Rfib/delta*
Permb*conv*(ff(m,'b',i,j)/(sum(compb,ff(m,compb,i,j)))*ftp-
fp(m,'b',i,j)/(sum(compb,fp(m,compb,i,j)))*ptp(m));

*-------------------------------------------------------------------------------
*FLUID DYNAMICS
*-------------------------------------------------------------------------------

modcindef(m)..     modcin(m)-2*rfib*(nfib(m)/pack)**0.5=e=0;

vlumendef(m,i,j).. vlumen(m,i,j)-(sum(comp,fp(m,comp,i,j))*gasR*(1e-
2)*temp/ptp(m))/Nfib(m)/(pi*rfibin**2)/3600=e=0;

vshelldef(m,i,j).. vshell(m,i,j)-(sum(comp,ff(m,comp,i,j))*gasR*(1e-
2)*temp/ftp)/(pi*(modcin(m)/2)**2-nfib(m)*pi*rfib**2)/3600=e=0;


*-------------------------------------------------------------------------------
*CONNECTIONS BETWEEN MEMBRANE MODULES
*-------------------------------------------------------------------------------
CON12Feed(comp).. ff('M2',comp,'1','1')-
                      fp('M1',comp,'100','3')-fp('M3',comp,'100','3')=e=0;

CON31Feed(comp).. ff('M1',comp,'1','1')-
                      ff('M3',comp,'100','3')-ffinit(comp)=e=0;

CON23Feed(comp).. ff('M3',comp,'1','1')-
                      ff('M2',comp,'100','3')=e=0;

*-------------------------------------------------------------------------------
* PROCESS CONSTRAINTS
*-------------------------------------------------------------------------------

PURITYA..            fp('M2','a','100','3')=g=gradeA*
                      sum(compb,fp('M2',compb,'100','3'));

PURITYB..            ff('M1','b','100','3')=g=gradeB*
                      sum(compb,ff('M1',compb,'100','3'));

Equalpressure(m)..   ptp('M1')-ptp('M3')=e=0;


*-------------------------------------------------------------------------------
*INITIAL CONDITIONS
*-------------------------------------------------------------------------------
IFP(m,comp).. fp(m,comp,'1','1')=e=fpinit(comp);
ILL..         ll('1','1')=e=0;



Model Membrane_module /all/;


*-------------------------------------------------------------------------------
*VARIABLE LIMITS AND INITIAL GUESSES
*-------------------------------------------------------------------------------

ff.lo(m,comp,i,j)=0;
fp.lo(m,comp,i,j)=1e-6;
ff.l(m,comp,i,j)=ffinit(comp);
fp.l(m,comp,i,j)=1;
ffdot.l(m,comp,i,j)=1;
fpdot.l(m,comp,i,j)=1;
Lfib.lo(m)=0.1;
Lfib.up(m)=4;
Lfib.l(m)=1;
Nfib.lo(m)=1e3;
Nfib.up(m)=5e6;
Nfib.l(m)=1e5;
He.l=61.1;
Keq.l=0.337;
Dcomp.l=4e-11;
NSt.fx = 3;
Ag.lo(m)=0;
Ag.up(m)=6000;
ptp.lo(m)=1;
ptp.up(m)=15;


*Option nlp=conopt;
Membrane_module.optfile=1;
Option iterlim=3000;
Option reslim=3000;
Option nlp=oqnlp;
option decimals = 8;


Solve Membrane_module minimizing phi using nlp;

RetentateFlow(m)=sum(comp,ff.l(m,comp,'100','3'));
RetentateComp(m)=ff.l(m,'a','100','3')/sum(comp,ff.l(m,comp,'100','3'));

PermeateFlow(m)=sum(comp,fp.l(m,comp,'100','3'));
PermeateComp(m)=fp.l(m,'a','100','3')/sum(comp,fp.l(m,comp,'100','3'));

FeedFlow(m)=sum(comp,ff.l(m,comp,'1','1'));
FeedComp(m)=ff.l(m,'a','1','1')/sum(comp,ff.l(m,comp,'1','1'));

jb.l(i,m)=Permb*conv*(ff.l(m,'b',i,'3')/(sum(compb,ff.l(m,compb,i,'3')))*ftp
-fp.l(m,'b',i,'3')/(sum(compb,fp.l(m,compb,i,'3')))*ptp.l(m))/delta*1000/3600;

ja.l(i,m)=(ff.l(m,'a',i,'3')/(sum(compb,ff.l(m,compb,i,'3')))*ftp-
fp.l(m,'a',i,'3')/(sum(compb,fp.l(m,compb,i,'3')))*ptp.l(m))*
((keq.l*Ag.l(m)*He.l*Dcomp.l*XIL/(1+keq.l*ff.l(m,'a',i,'3')/
(sum(compb,ff.l(m,compb,i,'3')))*ftp*He.l))+(alpha*(Ag.l(m)/
(1+kp*ff.l(m,'a',i,'3')/(sum(compb,ff.l(m,compb,i,'3')))*ftp))*(1-XIL)))/delta;


Display FeedFlow,FeedComp,RetentateFlow,RetentateComp,PermeateFlow,PermeateComp;
Display ll.l,ff.l,fp.l;
Display 'Ja in mol/m2/s',ja.l;
Display 'Jb in mol/m2/s',jb.l;


$ontext

$offtext
```

Agradecimientos

Sirvan estas líneas para mostrar mi más sincero agradecimiento a mis directores de tesis, la profesora Inmaculada Ortiz y el doctor Alfredo Ortiz, por haberme dado la oportunidad de desarrollar mi labor investigadora en el Departamento de Ingenierías Química y Biomolecular y por haberme guiado durante estos años mostrándome su apoyo y confianza.

Al profesor Daniel Gorri por haberme prestado sus conocimientos siempre que los he necesitado, lo que ha constituido una inestimable ayuda durante el desarrollo de esta tesis.

I would also like to offer special thanks to Prof. Larry Biegler and Prof. Chung Tai-Shung for accepting me as visiting researcher in their respective departments, which undoubtedly has contributed to enrich this PhD thesis.

Por último, a mi familia, especialmente a mis padres, a los compañeros y compañeras del departamento y a mis amigos y amigas.